Journal of Research of the National Bureau of Standards Vol. 45, No. 5, November 1950 Research Paper 2145

Recirculating Apparatus for Testing Hygrometers[1]

By Arnold Wexler

An apparatus that was developed for producing atmospheres of known relative humidity is described. It was designed, principally, for research on and calibration of radiosonde hygrometer elements at temperatures above freezing, but is equally useful at temperatures down to −40° C. It operates by saturating air at one temperature and then raising the air temperature sufficiently to give any desired relative humidity. The air is recirculated continuously in a closed system. Four identical, but independent, recirculating systems are employed. Discrete changes in humidity and temperature are obtained by means of a novel pneumatic valve that permits the hygrometers under test to be switched, easily, from system to system. Checks on the performance of the apparatus by means of the gravimetric method of moisture determination and the psychrometric method show an average difference in relative humidity of ±1.2 percent.

I. Introduction

In the meteorological sounding of the upper atmosphere by means of the radiosonde, the device commonly employed for sensing the water vapor content of the air is the electric hygrometer.[2] [3] During a flight, the hygrometer may be subjected to a wide range of temperatures and humidities, as well as to air flows, corresponding to rates of ascent of the balloon, of 1,000 ft/min or more. These conditions of use have created a need for some convenient means of producing and maintaining atmospheres of known relative humidity, at any of the temperatures encountered in a radiosonde flight, for calibration and research purposes.

An apparatus has been developed to fulfill this need. It was designed for operation, principally, at temperatures above 0° C but is equally useful at temperatures down to −40° C. Provision was made for obtaining discrete changes in humidity and temperature and for maintaining given air speeds. It supplements an apparatus of the divided-flow type previously built for use at temperatures below freezing.[4]

II. Theory

A fundamental method for producing an atmosphere of known relative humidity is to saturate a stream of air with water vapor at a given temperature and then to raise the temperature of the air to a specified higher value. If t_s is the temperature of saturation, e_s the saturation pressure of water vapor at temperature t_s, t_t the elevated temperature, and e_t the saturation pressure of water vapor at temperature t_t, then the relative humidity, H, at temperature t_t is

$$H=100\,\frac{e_s}{e_t}. \qquad (1)$$

In eq 1 the assumption is made that the absolute pressure of the air at the elevated temperature, t_t, is the same as the absolute pressure of the air at the saturation temperature, t_s. If these two pressures are not identical, then a pressure correction must be introduced. If P_s is the absolute pressure of the air at t_s, and P_t is the absolute pressure of the air at t_t, then the relative humidity is

$$H=100\,\frac{e_s}{e_t}\,\frac{P_t}{P_s}. \qquad (2)$$

A simplified schematic diagram illustrating how the two-temperature method may be employed in an apparatus is shown in figure 1. By means of a gas pump, air is circulated from a saturator into a test chamber and then back into the saturator. The temperature, t_s, of the saturator and the temperature, t_t, of the test chamber are maintained at their respective desired values by thermostatted baths. Complete saturation is achieved simply, and efficiently by recirculation of air over water in the saturator, in a closed system. The relative humidity, H, in the test chamber is given by eq 2, where the saturation vapor pressures, e_s and e_t, corresponding to temperatures t_s and t_t, are obtained from standard tables, and the absolute pressures, P_s and P_t, are measured values.

The design of a practical system, based on this method, is shown in figure 2. It differs from the elementary design of figure 1 in that the test-chamber temperature is controlled by means of a heater inserted in the air stream rather than by

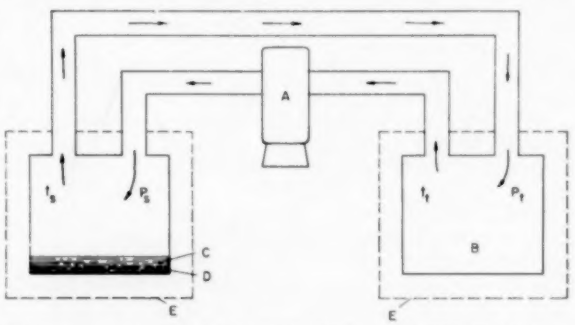

FIGURE 1. *Simplified schematic diagram illustrating the two-temperature recirculating method of relative humidity production.*

A, Gas pump; B, test chamber; C, water; D, saturator; E, thermostatted bath.

[1] This apparatus was developed for the Bureau of Ships, Department of the Navy.
[2] F. W. Dunmore, J. Research NBS **20**, 723 (1938) RP1102.
[3] F. W. Dunmore, J. Research NBS **23**, 701 (1939) RP1265.
[4] A. Wexler, J. Research **40**, 479 (1948) RP1894.

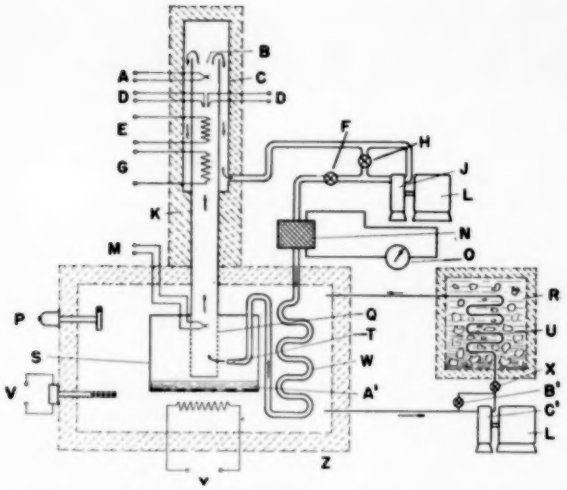

FIGURE 2. *Schematic diagram of a practical two-temperature recirculating humidity apparatus.*

A, Test-chamber thermocouple; B, test chamber; C, reflux tube; D, thermistor; E, intermittent heater; F, control valve (air); G, gross heater; H, bypass valve (air); J, gas pump; K, thermal insulation; L, motor; M, saturator thermocouple; N, flow meter; O, differential pressure gage; P, centrifugal stirrer; Q, screen; R, dry-ice bath; S, saturator; T, nozzle, U, coil (liquid); V, thermoregulator; W, coil (air); X, control valve (liquid); Y, bath heater; Z, thermostatted Varsol bath; A′, water; B′, bypass valve (liquid); C′, circulating pump.

immersing the test chamber in a thermostatted liquid bath. The elimination of a thermostatted bath for the test chamber, with the resultant simplification in design and construction, is made possible by the fact that the saturator must necessarily be maintained at a lower temperature than the test chamber, and hence the only requirement for achieving any desired test-chamber temperature is the introduction of the requisite amount of heat into the air stream. A novel feature of the test-chamber design is the concentric tube arrangement. The air from the saturator flows upward through the inner tube, then reverses its direction and returns downward in the annular space between the inner and outer tubes. The outer tube is thermally insulated. This reflux action contributes to temperature control and a reduction in thermal losses, for it surrounds the test space, which is at the upper end of the inner tube, with air at or near the test-chamber temperature.

The important features of the saturator are its simplicity of design, its adaptability for temperatures below as well as above the freezing point of water, and its effective saturation of air at both high and low flows. These features are achieved in large measure by imparting a centrifugal action to the entrant air stream. The saturator is a cylindrical chamber to which water is added to a convenient depth. Air is discharged through a nozzle into the chamber above the water surface and tangential to the vertical walls and is exhausted through a central port in the top. The centrifugal action creates a whirlpool and thoroughly mixes water vapor with the air. Spray and liquid droplets are forced to the walls by centrifugal force, with the result that there is little tendency for liquid water to emerge through the exit port, except at very low air flows. A multilayer fine wire screen baffle is used at the exit to trap and prevent water from passing out of the saturator at the low flows. As the air does not bubble through the water but only passes over its exposed surface, the water may be frozen without impairing the functioning of the saturator. The saturation pressure of the water vapor in the saturator (for use in eq 2) is taken, then, with respect to ice.

A desirable requirement in a humidity apparatus is a scheme or mechanism whereby the relative humidity may be changed quickly and in discrete steps. Such a scheme is necessary for lag studies on hygrometers. It is achieved in this equipment by utilizing four identical but independent systems that are arranged in such a fashion that their test chambers may be interchanged easily and rapidly. Thus, if a different temperature, t_s, is maintained in each of the four saturators, and if the same temperature, t_t, is maintained in each of the four test chambers, then the relative humidity in each test chamber is different. By interchanging the test chambers, the relative humidities therein undergo discrete changes, as each test chamber now communicates with a different saturator.

The arrangement is shown schematically in figure 3 for two of the four systems. The interchange of test chambers is effected by a special pneumatic switch. It consists of two ground and lapped plates to which the inner and outer tubes are attached and which contain ports through which the air may pass. A quarter turn of the top plate with respect to bottom plate advances each test chamber to a new position and connects each test chamber with a different

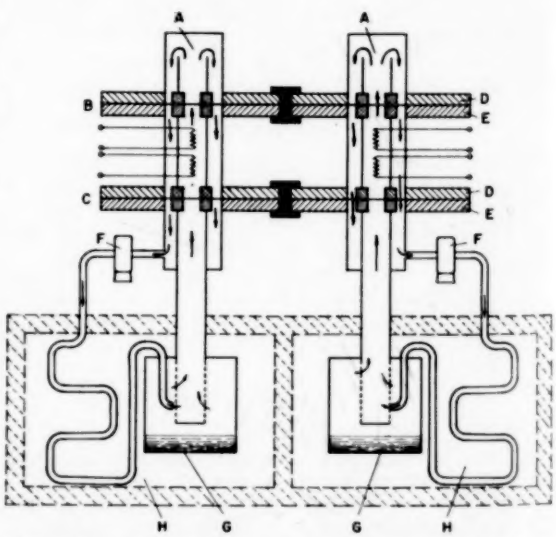

FIGURE 3. *Schematic diagram of pneumatic switches for interchanging test chambers; only two of the four systems are shown.*

A, Test chamber; B, upper switch; C, lower switch; D, top plate; E, bottom plate; F, gas pump; G, saturator; H, thermostatted bath.

saturator. Two such switches are used instead of one for greater convenience and versatility. For lag studies only, the upper switch is used. The speed with which the relative humidity can be changed is of the order of 1 to 2 seconds and depends primarily on the speed with which the switch can be rotated.

III. Design Details

An oil-free impeller-type gas pump is used to circulate air continuously through each system. The flow is controlled by means of a bypass valve, as shown in figure 2, and is measured by a glass-wool linear flowmeter that is calibrated in terms of air speed through the test chamber. The air flows through a copper tube coil, immersed in the same thermostatted liquid bath as the saturator and reaches bath temperature before it passes into the saturator. The cooling coil is essential for satisfactory operation, for unless the air enters the saturator at the bath temperature, an uncertainty in saturation temperature ensues. The saturator is a brass cylinder, 5 in. in diameter and 4 in. deep. The inner tube of the reflux portion of the system is polystyrene with 1¼-in. outside diameter and ⅛-in. wall thickness, while the outer is brass tubing with 2-in. outside diameter and 1/32-in. wall thickness.

The copper tube coil and saturator are immersed in a varsol bath, whose temperature is closely regulated. Varsol is used so that low temperatures may be attained. A bimetal thermoregulator controls a heater through a power relay. The circuit is shown in figure 4. A positive rotary displacement pump

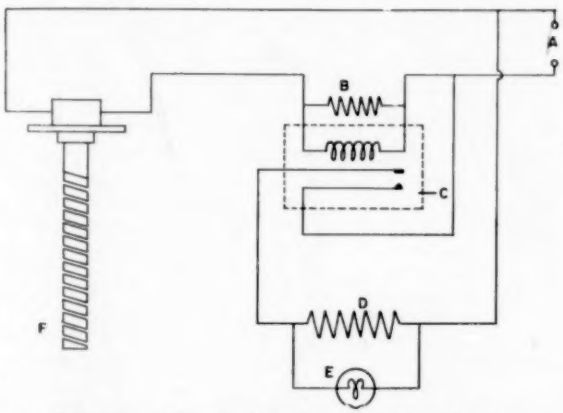

FIGURE 4. *Varsol bath temperature control circuit.*

A, 110-v alternating current; B, shunt resistor; C, power relay; D, bath heater; E, pilot lamp; F, bimetallic thermostat.

withdraws varsol from the bath, circulates it through another cooling coil and discharges it back into the bath. This second cooling coil is maintained at −78° C by crushed dry ice. The cold varsol flow is adjusted, by means of valves, so that the bath temperature will tend to drop very slightly. The heater is arranged to go on when the bath temperature drops below the control point and will go off when the bath temperature is at or above the control point. On-off regulation is thereby achieved. The bath is actively agitated by a centrifugal stirrer.

The temperature of the moving air stream in the test chamber is controlled by two heaters; a gross heater supplies constant heat, the amount manually adjusted, by means of a rheostat, as shown in figure 5; an intermittent heater supplies heat on demand, the amount also manually adjusted by a rheostat and the demand determined by two thermistors acting as the temperature sensitive elements. The gross heater supplies most of the heat, whereas the intermittent heater supplies heat, as required, to raise the temperature to the control point. Figure 6

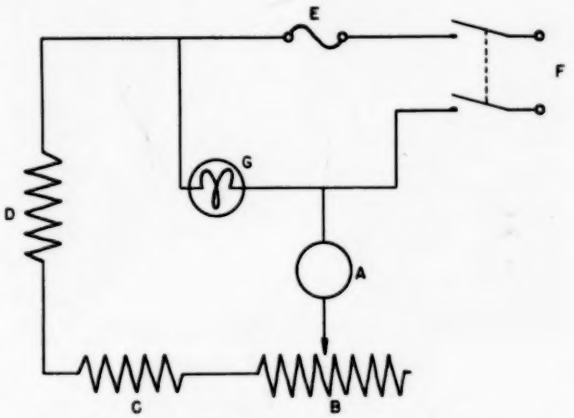

FIGURE 5. *Test-chamber gross-heater circuit.*

A, Ammeter; B, rheostat; C, limiting resistor; D, gross heater; E, fuse; F, 110-v alternating-current regulated supply; G, pilot lamp

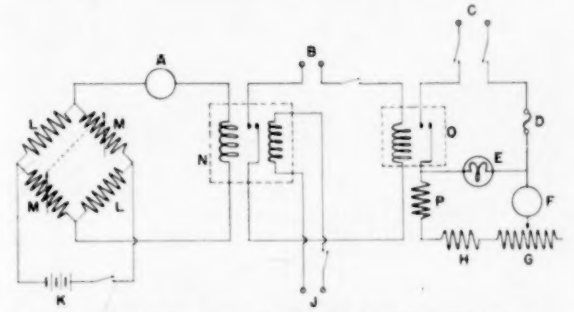

FIGURE 6. *Test-chamber intermittent-heater control circuit.*

A, Microammeter; B, 6-v direct current; C, regulated 110-v alternating current; D, fuse; E, light; F, milliammeter; G, rheostat; H, limiting resistor; J, 28-v pulsing circuit; K, 22½ v; L, thermistor; M, decade resistance box; N, galvanometer relay; O, power relay; P, intermittent heater.

is a circuit diagram of the intermittent heater control circuit. The desired control temperature is established by resistances, *M* (coupled decade resistance boxes) in a Wheatstone bridge circuit containing thermistors, *L*. The bridge balance is sensed by a galvanometer relay. A current of ½ microampere deflects the pointer against a magnetic contact, actuating a power relay and, in turn, the intermittent heater. The operation of an electromagnetic

plunger returns the pointer to a sensing position. If the bridge is balanced, the pointer does not move; if the bridge is unbalanced, the pointer deflects. An electronic pulsing circuit periodically triggers the plunger at a frequency that is adjustable from 2 times a minute to 60 times a minute, so that the galvanometer may sense the balance of the bridge.

The completed apparatus is shown in figure 7. Figure 8 shows the apparatus with the cover raised showing the four thermostatted baths.

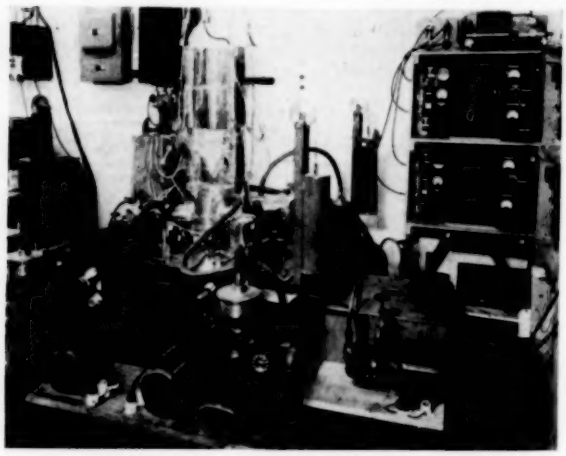

FIGURE 7. *Humidity apparatus.*

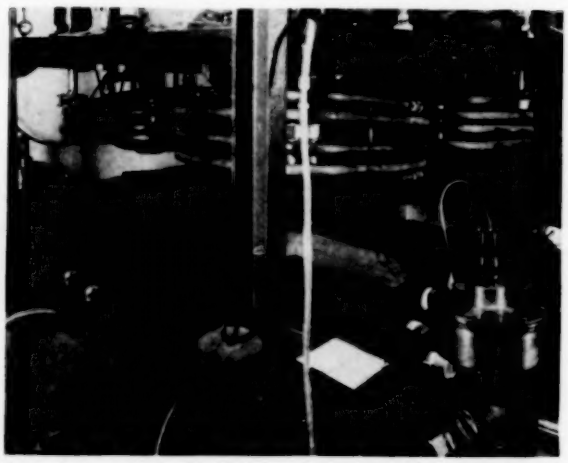

FIGURE 8. *View of apparatus with cover raised showing the four independent thermostatted baths.*

IV. Performance Characteristics

The performance of the apparatus has been investigated to determine the accuracy and the usable temperature and humidity ranges. The gravimetric method of moisture determination (see footnote 4) was used to give an independent check on the relative humidity produced by the apparatus for various saturator and test-chamber temperatures and various speeds of air flow. The results are given in table 1. As an additional check on the accuracy, a thermocouple psychrometer was employed to measure the actual relative humidity in the test chamber. The results are given in table 2. These tests show an average difference in percentage of relative humidity of ± 1.2 percent between the gravimetrically measured relative humidity and the apparatus relative humidity given by eq 2; and an average difference in percentage of relative humidity of ± 0.9 percent between the psychrometric measurements and the apparatus values given by eq 2.

TABLE 1. *Gravimetric calibration*

Run	Date, 1949	Air velocity	Test-chamber temperature	Relative humidity		
				Apparatus	Gravimetric	Difference
		ft/min	*°C*	*Percent*	*Percent*	*Percent*
14	10/28	50	24.52	39.2	39.6	−0.4
15	10/28	250	25.45	37.0	37.8	−.8
16	10/28	500	26.41	34.7	35.8	−1.1
17	10/28	1,000	27.61	32.3	32.6	−0.3
18	11/1	500	−3.85	46.0	47.0	−1.0
19	11/1	500	−3.54	22.8	23.4	−0.6
20	11/4	50	20.53	95.0	95.0	.0
21	11/4	1,000	21.41	87.6	84.7	+2.9
22	11/4	50	17.37	83.9	84.0	−0.1
23	11/4	1,000	17.83	81.1	81.6	−.5
24	11/9	1,000	4.75	88.9	85.1	+3.8
25	11/9	1,000	14.98	44.6	44.5	+0.1
26	11/9	1,000	9.68	97.5	94.6	+2.9
27	11/9	1,000	9.68	97.2	96.3	+0.9
28	11/14	1,000	15.71	89.3	88.7	+.6
29	11/14	1,000	15.71	89.2	86.6	+2.6
30	11/14	1,000	15.68	89.5	88.2	+1.3
Average						±1.3

TABLE 2. *Psychrometric calibration*

(Air velocity=1,000 ft/min)

Test-chamber temperature (°C)	Relative humidity		
	Apparatus	Psychrometer	Difference
	Percent	*Percent*	*Percent*
15.88	88.6	88.8	−0.2
15.90	88.6	88.2	+.4
15.01	65.1	63.8	+1.3
15.05	64.9	65.5	−0.6
5.90	72.1	71.6	+.5
5.83	72.1	72.3	−.2
10.92	51.1	50.1	+1.0
10.71	51.9	51.2	+0.7
10.72	52.1	51.3	+.8
17.22	34.1	33.3	+.8
17.05	34.7	33.7	+1.0
17.12	34.2	32.9	+1.3
21.10	37.2	38.5	−1.3
21.17	37.0	38.5	−1.5
21.08	36.9	38.4	−1.5
21.10	36.9	38.2	−1.3
Average			±0.9

As the precision and accuracy of the apparatus is to a large extent a function of the precision and accuracy of the temperature regulation and measurement of the test chambers and saturators, these temperatures must be adequately controlled and suitably measured. Temperatures are measured

with calibrated copper-constantan thermocouples and a precision potentiometer to a precision of 0.01 deg C. Because of the fair size of the liquid bath, bimetallic regulation is adequate for maintaining saturation temperatures constant to ±0.02 deg C over time intervals of 1 hour and constant to ±0.1 deg C over long time intervals. The thermistor-Wheatstone bridge circuit maintains test chamber temperatures constant to ±0.04 deg C over time intervals of 1 hour and constant to ±0.1 deg C for long time intervals.

The distribution of temperature within the saturator was explored by means of thermocouples located at the inlet, in the water, and at the outlet. The temperature of the air emerging from the saturator is within ±0.04 deg C of the temperature of the air entering the saturator; the temperature of the air entering the saturator is within ±0.06 deg C of the temperature of the water in the saturator; and the temperature of the air emerging from the saturator is within ±0.08 deg C of the temperature of the water. These temperature differentials may account for errors of ±½-percent relative humidity.

The difference in temperature between the saturator and bath was also investigated. The air entering the saturator is within ±0.07 deg C of the bath temperature; the water temperature is within ±0.04 deg C of the bath temperature; and the air emerging from the saturator is within ±0.09 deg C of the bath temperature.

Although the gas pump is capable of producing very high rates of flow, the coupling between motor and pump is set to allow a maximum air speed of 1,500 ft/min in the test chamber. By proper adjustment of the bypass valve, any lesser air speed is obtainable.

The upper relative humidity limit is determined by the saturation temperature, the air velocity and the efficiency of the thermal insulation and refluxing action surrounding the test chamber. The thermal leakage through the insulation is 2.2 cal/min for each degree centigrade temperature difference between the test chamber and room. The maximum relative humidities that may be obtained with air speeds of 50 and 1,000 ft/min for various saturator temperatures and with the apparatus in a room at 30° C are given in table 3. It is apparent that at high air velocities, the thermal leakage does not seriously limit the relative humidity range. At very low air flows, the maximum relative humidity obtainable is seriously limited, especially at the low saturator temperatures. Fortunately, in electric hygrometer calibration and research, high air speeds are used in order to simulate radiosonde flights, hence relative humidities sufficiently high for all practical purposes can be obtained.

TABLE 3. *Computed maximum attainable relative humidities*

Saturator temperature (°C)	Maximum relative humidity at test-chamber air velocity of—	
	50 ft/min.	1,000 ft/min
	Percent	*Percent*
25	93	99
15	86	99
5	77	98
−5	64	97
−20	49	96

For any test chamber temperature, the lowest attainable relative humidity is limited by the lowest attainable saturator temperature, which is about −55°C. It is possible to reduce the relative humidity to about 16 percent at a test-chamber temperature of −40°C, and to lower values at higher test-chamber temperatures.

The saturator temperature must not be permitted to exceed room temperature, for then there is a possibility for the system above the saturator to assume a temperature less than that of the saturator with resultant condensation of water vapor. Equation 2 then would no longer give the relative humidity in the apparatus.

The internal diameter of the test chamber is 1 in. Two standard radiosonde electric hygrometers (4 in.×5/16 in.×1/32 in.) can be inserted into the test chamber. If all four channels or systems of the apparatus are operated simultaneously, then eight elements can be tested at one time.

The ratio of the absolute pressures in the test chamber and saturator, P_t/P_s, used in eq 2, varies somewhat with air velocity and negligibly with temperature. Its variation with velocity may be once determined and then applied as a pressure correction. This correction is very small, and except for the high air velocities may be neglected for most work. Even for an air velocity of 1,000 ft/min, the correction is only of the order of 0.6 percent. The pressure ratio corrections are shown in table 4.

TABLE 4. *Pressure ratio corrections*

Air speed	Pressure ratio corrections, P_t/P_s
ft/min	
0	1.0000
100	1.0000
200	0.9997
400	.9989
600	.9978
800	.9962
1,000	.9938

V. Discussion and Summary

An apparatus particularly suited for research and calibration of electric hygrometers of the Dunmore type has been designed, developed, and constructed. It operates by saturating air at one temperature and then raising the air temperature sufficiently to give any desired relative humidity. The important feature in this method is the continuous recirculation of air in a closed system and the use of a simple and efficient centrifugal saturator that can be used below 0° C, as well as above. Air speeds up to 1,500 ft/min are obtainable. A novel switching mechanism is utilized for giving rapid and discrete changes

in relative humidity. This switching mechanism also is adaptable for giving rapid and discrete changes in temperature.

It is designed to operate at test-chamber temperatures above 0° C, but may readily be used at temperatures as low as −40° C. The low temperatures are achieved, however, at some sacrifice of the maximum attainable relative humidity. For most of the test-chamber temperature range, practically any desired relative humidity may be produced by the apparatus.

Independent checks on the performance of the apparatus by means of the gravimetric method of moisture determination and the psychrometric method show an average agreement in relative humidity of 1.2 percent as measured and as given by the apparatus, eq 2.

The author gratefully acknowledges the assistance of R. A. Baum of the Shop Division in the construction of the apparatus and of E. T. Woolard in the experimental work.

WASHINGTON, August 14, 1950.

Journal of Research of the National Bureau of Standards Vol. 45, No. 5, November 1950 Research Paper 2146

An Improved Apparatus for Determining Moisture in Rubber by Distillation with Toluene

By Max Tryon

An improved apparatus has been developed for the determination of water in rubber by distillation with toluene. The volume of the water collected is measured in a graduated capillary tube, which allows more precise measurement than the tapered tube formerly used. The interior of the trap and condenser is coated with a water-repellent silicone polymer to prevent water droplets from adhering to the walls and to improve the accuracy. This paper describes the construction of the apparatus and a procedure for coating its interior with the silicone polymer. A method for calibration of the trap is included in a general procedure for use of the equipment.

I. Introduction

The water content of certain organic materials can be determined by a method that involves the formation of an azeotrope of an immiscible organic liquid with the water, distillation of the azeotrope, and separation of the water as a separate phase. The volume of water is then measured by the use of a graduated container.

For this purpose there are several devices commercially available for the collection and separation of water distilled with a liquid of low density, such as toluene. Since the time of Dean and Stark [1] [1] there have been a large number of refinements and special applications similar to their original apparatus [2 to 9]. These refinements are essentially attempts to overcome the following shortcomings of the original design. First, there is a tendency for water to adhere to parts of the apparatus rather than to collect in the graduated portion. Second, there is a lack of precision of reading the volume of water collected due to the dimensions and shape of the graduated container. Third, sharp separation of the immiscible liquid and water does not always occur in apparatus with narrow water-collecting tubes, because the immiscible liquid tends to be trapped in the tube by the water. Fourth, the apparatus must be meticulously clean or the water will entrap the immiscible liquid and will not properly fill the measuring tube, regardless of the shape or dimensions of the tube.

[1] Figures in brackets indicate the literature references at the end of this paper.

Subsequent modifications and refinements of the original apparatus have overcome some of these objections to varying degrees. The apparatus described in this paper, however, answers all these objections satisfactorily and also offers a few more advantages.

The procedure and apparatus described in this paper was originally devised in 1947 to determine small amounts of water (about 1% by weight) present in certain types of synthetic rubber [10, 11] that could not be analysed with procedures standard at that time. As a result, this procedure has been accepted as a referee method for determining moisture in all types of synthetic rubbers by the Subcommittee on Test Methods, Reconstruction Finance Corp., Office of Rubber Reserve.

It is felt that this apparatus supplies the need for a rapid, simple, precise method for determining small amounts of water in materials on a routine production basis and furnishes a valuable tool for research.

II. Description of Apparatus

The apparatus is shown schematically in figure 1. The distilling flask, *A*, contains the sample and toluene. This flask is connected to the collecting trap, *T*, by a 24/40 standard taper joint lubricated with silicone stopcock grease. A West condenser equipped with a drip tip is connected to the trap by means of a 24/40 standard taper joint, also lubricated with silicone grease. The tapered portion of the trap

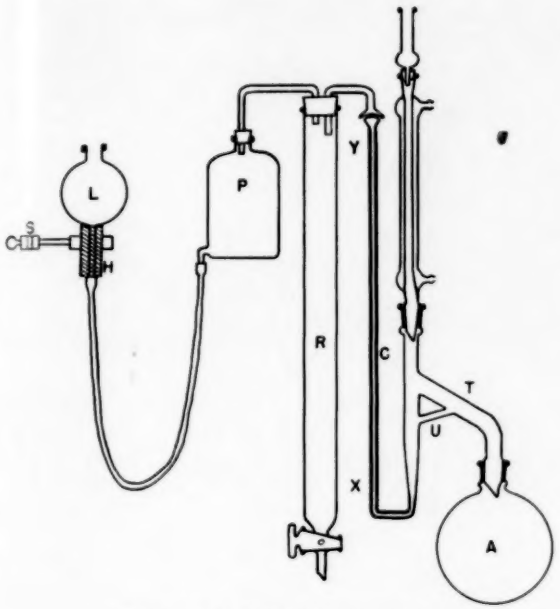

FIGURE 1. *Distillation apparatus.*

has a volume of about 10 ml below the overflow tube, *U*. The overflow tube slopes upward from the tapered portion and so prevents drops of water, falling from the condenser tip, from returning to the distilling flask. A capillary tube, *C*, 56 cm long and of about 1.5-ml volume is sealed to the bottom of the tapered portion of the trap. This capillary is graduated at 1-mm intervals between the points *X* and *Y* (50-cm length) and has a 12/3 ball joint at the top end. This joint, lubricated with silicone grease, serves to connect the capillary to a waste receiver, *R*, which has a drain stopcock at the bottom. The waste receiver is connected by rubber tubing to a bottle of water, *P*, which is in turn connected by rubber tubing to a leveling bulb, *L*. The leveling bulb has both a coarse and a fine adjustment. Raising or lowering the clamp, *S*, affords the coarse adjustment, and the threaded tube, *H*, allows the fine adjustment. Thermometer reading lenses prove very useful for reading the scale on the graduated capillary tube.

The capillary tube, the trap, and the condenser are coated with a thin film of silicone polymer to prevent water droplets from adhering to the walls of the apparatus. The effect of this coating is to reverse the usual water-glass meniscus, and the result is a mercury-type meniscus that is easily seen in the capillary. The silicone coating is applied by pouring a solution, 5 ml of mixed methylchlorosilanes (Drifilm) dissolved in 100 ml of dry toluene, into the clean air-dried apparatus and allowing it to stand in contact approximately 15 min before pouring out the excess solution. It is important that the glassware be air-dry and not oven-dry, as a very thin layer of adsorbed water on the glass surface is essential to form the coating [14]. *Caution: It is recommended that this operation be carried out in a hood, as the methyl chlorosilanes are toxic, flammable, and corrosive.* The apparatus is then air-dried and heated overnight in an oven at 105° C. The apparatus may be used indefinitely and may even be rinsed with acid-dichromate cleaning solution without disturbing the film or the calibration of the capillary. However, the film may be removed by soaking the equipment for 10 to 15 min in alcoholic potassium hydroxide.

The distilling flask may be heated by any suitable heat source, but an electric enveloping heater is recommended for best control of the distillation.

III. Operation of Apparatus

1. Calibration

The capillary is calibrated by adding, progressively, weighed increments of water to the tapered portion of the trap, which has been filled previously with dry toluene up to the overflow tube. After each increment has been added, the water in the trap is raised up into the graduated capillary by lowering the leveling bulb. The fine adjustment affords a simple and quick method for adjusting the bottom of the water column to a zero point on the capillary. The height of the column is noted and the leveling bulb raised to return the water to the tapered portion of the trap. Another weighed increment of water is added and the process repeated. The size and number of the increments to be measured depends on the accuracy and precision desired.

Because toluene is present in the trap, the water column is confined between two columns of toluene while being measured. This prevents evaporation loss and also aids in obtaining a sharp mercury-type meniscus at both ends of the water column. Varying the weight of the water added and measuring the column lengths obtained allows precise calibration of the capillary. If the capillary is uniform, a simple length-to-weight factor is all that is required. However, if the capillary is nonuniform, a simple graphical calibration curve is readily made from such measurements.

2. Distillation of Sample

The sample is weighed to the desired accuracy and placed in the distilling flask with a sufficient amount of toluene to keep the sample covered. The toluene is dried by passing it through a column of activated silica gel. The trap is filled up to the overflow tube with dry toluene and the distilling flask heated slowly until liquid begins to drop from the tip of the condenser. The distillation is continued at the proper rate, depending on the type of sample used, until no more water droplets appear in the distillate dropping into the large part of the trap. Five milliliters of dry toluene is poured in the top of the condenser to wash any water adhering to the condenser down into the trap. The heater is then turned off and the water in the trap allowed to cool to room

temperature, or a beaker with cool water may be lifted around the trap to aid in adjusting the temperature to a predetermined value, dependent on the temperature of the calibration procedure. After cooling, the leveling bulb is lowered to draw the distilled water into the capillary and to adjust the bottom of the water column to the zero point used as a reference in the calibration of the graduated capillary. The length of the water column is read, and then the leveling bulb is lowered further to draw the water and toluene in the trap into the waste receiver. The trap is again filled up to the overflow tube with dry toluene, and the distilling flask is replaced with another flask containing a sample and toluene. This procedure allows another sample to be run almost immediately. Cleaning the trap at intervals by flushing with toluene is accomplished by pouring toluene in the trap through the condenser and lowering the leveling bulb to draw the solvent through the capillary into the waste receiver. The stopcock on the bottom of the waste receiver allows removal of the accumulation of water and toluene.

IV. Accuracy and Precision

Several experiments, designed for statistical analysis, in which a number of possible variables were studied, were used to evaluate the method. The known samples were prepared in batches by taking a 200-g batch of GR–S–10 synthetic rubber and milling it for approximately 5 min., after which it was sheeted out at a setting of 0.02-in. distance between the mill rolls and then placed in a vacuum oven at 90° C for 4 hrs. After the rubber was dried, it was stored in a desiccator overnight. The rubber was then weighed to the nearest milligram and passed through the mill at a 0.02-in. setting several times, taking care that no rubber was lost from the mill. The sample was reweighed to check for loss of rubber. After the rubber was checked for loss in weight, it was banded on the mill, and two 10-ml portions of distilled water were milled into the sample and the mixture thoroughly blended. The sample was next removed from the mill and placed on an electrically grounded sheet of aluminum to cool and discharge the static charge formed during the milling operation. After approximately 10 min., the rubber was weighed. A portion of the rubber was cut into pieces small enough to pass through the opening of the distilling flask and placed as quickly as possible in a weighed tin with an air-tight cover. The remaining portion of the wet rubber was reweighed and stored in an air-tight container. The tin containing the sample was weighed and the sample then removed and placed in the flask containing the toluene. This procedure gave several checks for the weight of the sample, the moisture content by weight, and the possible loss of moisture during handling. Under these conditions the loss of moisture during handling was found to be less than 1 mg.

The data shown in table 1 [11], after statistical analysis, indicated that there was no significant dependence of the precision and accuracy, within the limits of this experiment, on the size of the sample or on the time of distillation after the water drops cease to appear in the distillate. The slope and intercept of each curve shown in figures 2, 3, and 4 indicate

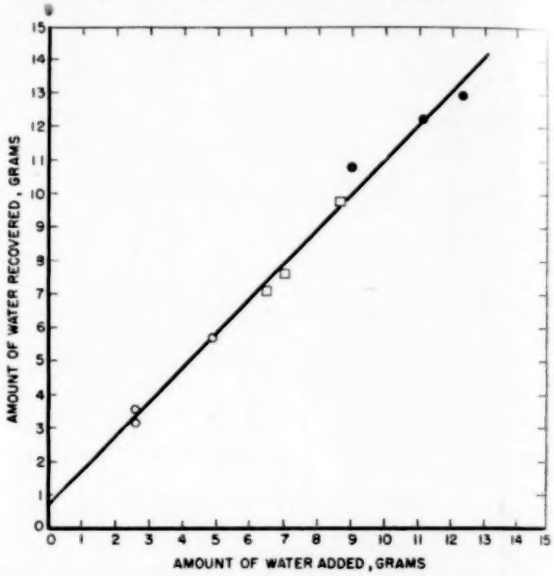

FIGURE 2. *Amount of water recovered versus the amount of water added for untreated drum toluene used directly.*

○, 45-min distillation; □, 90-min distillation; ●, 120-min distillation. Intercept, 0.070 g; slope, 1.03.

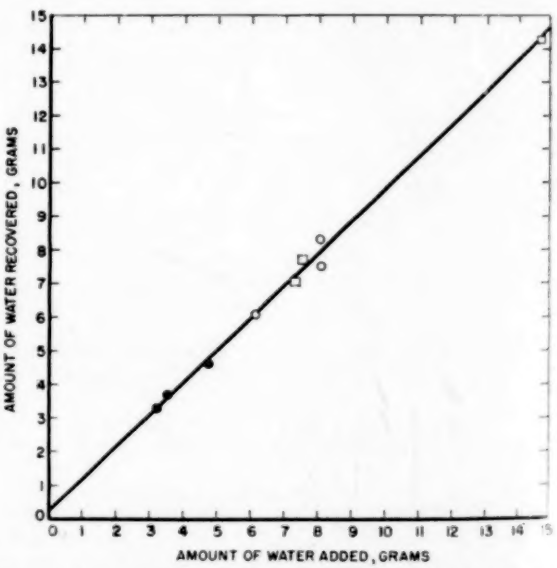

FIGURE 3. *Amount of water recovered versus amount of water added for drum toluene filtered through a 1½-ft column of activated silica gel.*

○, 45-min distillation; □, 90-min distillation; ●, 120-min distillation. Intercept, 0.028 g; slope, 0.957.

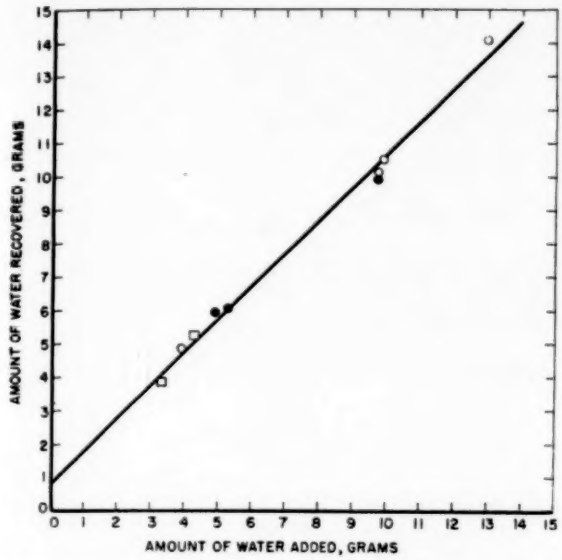

FIGURE 4. *Amount of water recovered versus the amount of water added for drum toluene distilled and the wet forerun removed.*

○, 45-min distillation; □, 90-min distillation; ●120-min distillation. Intercept, 0.085 g; slope, 0.986.

the recovery and correction for water in each of the toluenes listed in table 1. The toluene treated with silica gel showed a recovery significantly less than 100 percent but also showed no significant water correction for the toluene. That the other toluenes did not show a significant difference from 100-percent recovery is probably due to the lower precision in these cases. However, the water correction was appreciable for these two toluenes. Further, the toluene treated with silica gel gave the lowest standard deviation of the three toluenes.

TABLE 1. *Standard deviation, water correction, and recovery as affected by treatment of the toluene*

	Toluene passed through silica gel		Distilled toluene		Untreated toluene	
	Weight of water in rubber	Weight of water recovered	Weight of water in rubber	Weight of water recovered	Weight of water in rubber	Weight of water recovered
	g	*g*	*g*	*g*	*g*	*g*
	1.4685	1.4339	0.9696	0.9888	0.4847	0.5743
	0.4633	0.4650	1.2866	1.4071	.8672	.9748
	.6122	.6058	0.3327	0.3865	.9008	1.0821
	.7511	.7703	.5250	.6070	.2601	0.5564
	.3488	.3714	.4285	.5234	.6991	.7586
	.8064	.8357	.9839	1.0488	1.2306	1.2947
	.7289	.7053	.4896	0.5928	0.2598	0.3159
	.3166	.3316	.9737	1.0135	.6422	.7069
	.8061	.7628	.3887	0.4878	1.1101	1.2188
Std. dev.[a] (g)	0.023		0.035		0.040	
Water (blank) correction (g)	.0282		.0849		.0704	
Recovery (%)	95.66		98.63		103.01	

[a] Single determination.

Comparisons were also made between this method and those involving the mastication of the samples on hot rolls or oven-drying of thin sheets. The data from such a comparison is shown in table 2. The weights of sample used for the water determination in the four methods were quite different, ranging from a few grams for the Mill-oven method to 450 g for the hot-mill method. However, a comparison of the standard deviations of the methods indicates that the distillation method is more precise than either the Goodrich method or the Specification Hot-mill method. The Specification Mill-oven method is more precise than the distillation method, but the operating factors of the mill method are to its disadvantage [12].

TABLE 2. *Comparison of methods for the determination of moisture in synthetic rubbers*

Method	Toluene treatment	Standard deviation of a single determination of water
		Percent
Distillation	Silica gel	0.023
	Distilled	.035
	Untreated	.040
Specification Mill-oven Method (C-1-c) [12]		.008
Specification Hot-mill Method (C-1-a) [12]		.045
Goodrich [12, 13]		.05

The author is very grateful to Patricia Custer Jackson and Aurelia Arnold for making numerous measurements for the purpose of evaluating the improvements in the apparatus, and also to John Mandel for advice and assistance in designing statistical experiments to show quantitatively the value of the improvements.

V. References

[1] E. W. Dean and D. D. Stark, A convenient method for the determination of water in petroleum and other organic emulsions, Ind. Eng. Chem. **12,** 486 (1920).
[2] G. L. Bidwell and W. F. Sterling, Preliminary notes on the direct determination of moisture, Ind. Eng. Chem. **17,** 147 (1925).
[3] J. A. DeLoureiro, An improved technic in the toluene distillation method for the determination of moisture in foodstuffs, J. Assoc. Official Agr. Chem. **21,** 645 (1938).
[4] J. E. Cleland and W. R. Fetzer, Determination of moisture in sugar products, Ind. Eng. Chem. Anal. Ed. **14,** 124 (1942).
[5] W. G. Marskell and J. E. Rayner, An improved apparatus for the determination of water in oils and fuels, Fuel **26,** 49 (1947).
[6] W. Normann, Zur wasserbestimmung in fetten und anderen stoffen, Z. angew. Chem. **38,** 380 (1925).
[7] A. C. Beckel, A. G. Sharp, and R. T. Milner, Apparatus for determining moisture by the distillation method, Ind. Eng. Chem. Anal. Ed. **11,** 425 (1939).
[8] E. R. Caley and L. Gordon, Trap for the determination of water by the distillation method, Anal. Chem. **21,** 749 (1949).
[9] J. Mitchell and D. M. Smith, Aquametry, pp. 4 to 5 (Interscience Publishers, Inc., New York, N. Y., 1948).
[10] M. Tryon and P. Custer, National Bureau of Standards, unpublished report to Office of Rubber Reserve (May 24, 1948).

907877—50——2

[11] M. Tryon, P. C. Jackson, and J. Mandel, National Bureau of Standards, unpublished report to Office of Rubber Reserve (Feb. 28, 1949).
[12] P. Custer, National Bureau of Standards, unpublished report to Office of Rubber Reserve (Feb. 6, 1947).
[13] P. C. Baker, B. F. Goodrich Chemical Co., unpublished report to Office of Rubber Reserve (Aug. 20, 1946).
[14] E. G. Rochow, Introduction to the chemistry of the silicones, p. 32 and 83 to 88 (John Wiley and Sons, Inc., New York, N. Y., 1946).

WASHINGTON, January 24, 1950.

Journal of Research of the National Bureau of Standards Vol. 45, No. 5, November 1950 Research Paper 2147

Porcelains Within the Beryllia Field of the System Beryllia-Alumina-Zirconia

By Stewart M. Lang, Laurel H. Maxwell, and Milton D. Burdick

The general physical properties of practically impervious porcelains within the beryllia (BeO) field of the system beryllia-alumina-zirconia (BeO-Al_2O_3-ZrO_2), whose base compositions approximate that of NBS Body No. 4811C, were found to be: maturing range, 1,500° to 1,600° C; apparent density, 2.9 to 3.4 g/cm³; shrinkage, 17.8 to 20.5 percent; room-temperature compressive strength, 238,000 to 305,000 lb/in.²; room-temperature transverse strength, 17,200 to 34,100 lb/in.²; room-temperature transverse strength after thermal shocking, 17,800 to 31,900 lb/in.²; transverse strength at 1,800° F (982° C), 15,100 to 25,100 lb/in.²; approximate Young's modulus at 1,800° F, 28,000,000 to 38,000,000 lb/in.²; relative thermal shock resistance, good; and Knoop hardness numbers (500-g load), 550 to 830. An admixture of 2 weight percent of calcia (CaO) to the base compositions of these porcelains (without which the specimens would not mature to an impervious structure) caused the appearance of unidentified isotropic phases.

I. Introduction

Because of the advantageous high-temperature strength characteristics of "glass-free" bodies composed of the ceramic oxides, singly or in combination, as compared to similar strength properties of the metallic alloys, many refractory porcelains may be particularly well adapted for diversified uses in such power-plants as the gas-turbine and jet-propulsion engines.

Previous work at this Bureau [1, 2, 3],[1] at the Ohio State University Experiment Station [4], at the University of Illinois [5], and at the Lewis Flight Propulsion Laboratory of the National Adivsory Committee for Aeronautics [6] has shown NBS Body No. 4811C [3], whose composition is within the system beryllia-alumina-zirconia (BeO-Al_2O_3-ZrO_2), to be outstanding in many high-temperature properties when compared with other refractory whitewares. Such comparisons made it seem advisable to investigate and report some of the physical properties of porcelains whose compositions approximate that of body 4811C.

A previous report [3] gives in some detail the phase relations of the system BeO-Al_2O_3-ZrO_2. The failure of these oxide bodies to mature to nonporous structures was discussed in the Bureau report, but it was shown that the addition of small quantities of auxiliary fluxes to the base compositions did permit maturing of the bodies to a practically impervious condition. An addition of 4 percent of magensia to body 4811, whose mole composition ratio is 48 BeO:1Al_2O_3:1ZrO_2, caused the most pronounced effect on the maturing range. Experience has shown that the use of magnesia tends to increase the particle sizes or distort the particle shapes and thereby to decrease the body strength. Considering all of the properties studied, an addition of 2 weight percent of calcia (CaO) produced the most satisfactory 4811 bodies, and this particular body composition is correctly designated as Body No. 4811C. All but one of the porcelain compositions given in this report contain a 2-percent addition of calcia to the base composition; the exception, for comparative purposes, is body 4811M, which contains an addition of 4 percent of magnesia.

[1] Figures in brackets indicate the literature references at the end of this paper.

II. Materials and Equipment

The oxides used in the preparation of the test specimens were commercially available materials of high purity. The beryllia (BeO) was of nominal 99.7-percent purity, and spectrograms showed only traces of copper, iron, and magnesium, and very weak lines of silicon. Ground, washed, and sieved tabular alumina (Al_2O_3) of 99.5-percent purity was supplied through the courtesy of the Champion Spark Plug Co. Commercial zirconia (ZrO_2) of nominal 99-percent purity was recalcined at 1,440° C, after which spectrograms showed medium lines for niobium (columbium) and titanium, and only very weak lines or traces for calcium, copper, iron, magnesium, lead, and silicon. Calcia (CaO) was added as the pure chemically precipitated carbonate. As prepared for use, the materials were, in all instances, sufficiently finely divided to pass the No. 325 U. S. Standard Sieve. Comminution procedures have been given [7].

Firing of the test specimens for the determinations of maturing range and compressive strength was done in the NBS thoria-resistor furnace [8]. Figure 1 is a schematic cut-away drawing of the inner chamber of the furnace and shows three compression-test specimens, the supporting pedestals (thoria, zirconia, alumina, or beryllia), and one of eight heating elements. A Remmey high-temperature gas-fired kiln was used to mature the specimen bars for the thermal shock, transverse strength, and elasticity tests.

The apparatus used for the determination of the moduli of rupture and elasticity in flexure at elevated temperatures was designed by M. D. Burdick and has been described briefly [7]. The test furnace is constructed of lightweight insulating refractory brick, 2,600° F grade, within a shell of transite board. The chamber is 6 in. by 6 in. by 13 in. and is heated by means of six Globar elements. Power is supplied to the top, middle, and bottom pairs of Globars through three separate variable transformers. The specimen bar is supported on porcelain rockers (knife-edges) on dense firebrick of an appropriate thickness to locate the specimen at the center of the furnace chamber. Figure 2 shows the general construction features of the furnace (see also fig. 2 of [7]).

Load is applied to the top of the specimen at the quarter-points of the span through a loading bar and a ceramic yoke that extends through the furnace hearth to a third-order counterweighted lever. This lever was used to exert a downward pressure on the specimen. As it was desired to counterweight the lever to obtain a zero initial load, flexure plates rather than a simple knife edge were used at the fulcrum of the lever system. Flexure plates were used also in attaching the yoke to the lever in order to maintain a constant lever ratio. The calibration of this lever was obtained by using the normal load-point, P (fig. 3, A) as the fulcrum, and determining the ratio of arms A and B by applying known weights at points F and L. If, for example, the ratio of B:A during calibration is found to be 14:1, the lever ratio during use as a third-class lever will be $A+B$:A=15:1. Quarter-point loading results in a bending-moment diagram, as shown by the solid line in figure 3, B. Applying the load at midspan would result in a bending-moment diagram, as shown by the broken line in the same figure. Quarter-point loading was used because, theoretically, the maximum stress is obtained for any fracture occurring between the two points of load application. The relative merits of the two types of loading have been discussed by Bobrowsky [9].

Load was transmitted to the specimen through a knife edge, which is an integral part of the loading

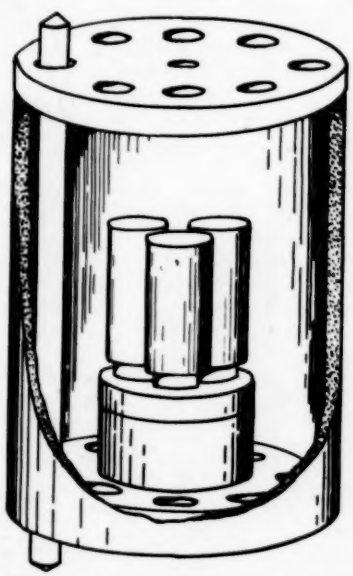

FIGURE 1. *Resistor-furnace chamber.*

This cut-away drawing of the inner chamber of the thoria-resistor furnace shows a typical arrangement for maturing three compression test specimens resting on platinum-rhodium disks. Also shown are the supporting pedestals of either beryllia, thoria, and alumina, and one of the eight thoria-resistor elements.

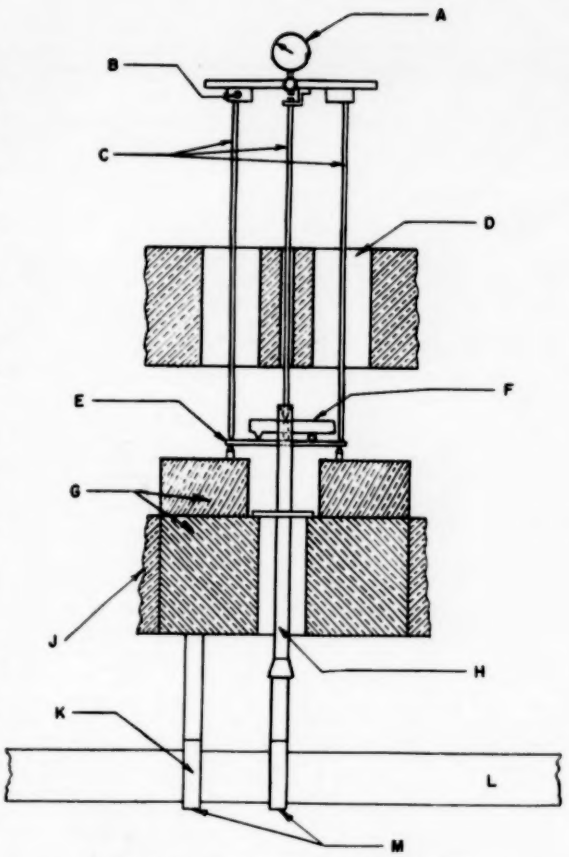

FIGURE 2. *Transverse-strength test furnace.*

This figure shows a section of the bending-strength test furnace indicating the specimen location, the loading arrangement, and the deflection measuring device. A, Dial gage; B, pivot; C, ⅛-in. sapphire rods; D, narrow slot; E, specimen; F, loading bar (load applied at quarter points of span); G, dense fire brick; H, ceramic yoke; J, insulating brick; K, fulcrum; L, lever; M, flexure plates.

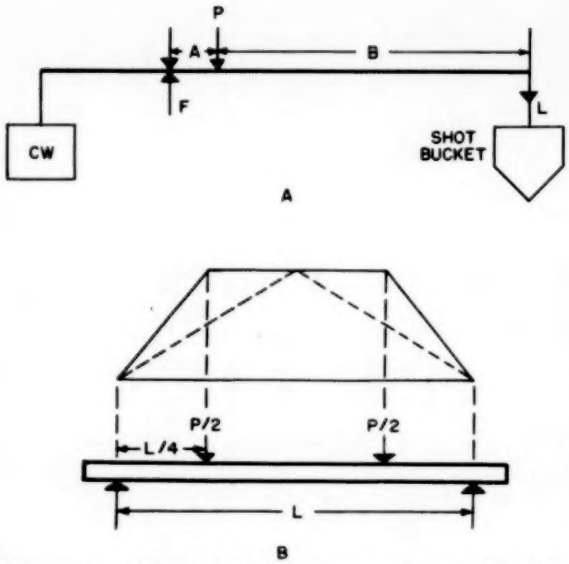

FIGURE 3. *Mechanics of the lever-arm ratio and of quarter-point loading.*

At A is shown the diagram for the calibration of the lever-arm ratio. If the ratio of B to A, during calibration as a first-class lever (fulcrum at P), is found to be 14:1, the lever-arm ratio during use as a third-class lever (fulcrum at F) will be (A+B):A=(1+14):1=15:1. At B is shown the bending-moment diagram resulting from quarter-point loading (solid line) and the bending-moment diagram resulting from single-point (midspan) loading (broken line).

bar, and through a sapphire rod. The rocker-type supports, and the rod and the loading knife edge, permit the use of a single loading bar for specimens of various spans and prevents torsional and axial forces. The deflection of the specimen at midspan is measured by means of a dial gage located directly over the specimen, but outside of the furnace. The gage, clamped to a rigid bar (fig. 2), is supported by two ⅛-in. diameter artificial sapphire rods, the lower ends of which rest on the top of the specimen at the ends of the span. A third sapphire rod is used to actuate the stem of the dial gage. The rod rests on the specimen at midspan, passes through a slot in the loading bar, a hole in the yoke, and a hole in the furnace top. The hot junctions of the base-metal thermocouples are located so that one is above and the other is below the specimen, as near its center as possible.

The apparatus is designed to test specimens at spans of from 3 to 6 in. Slots are provided in the furnace top to permit various spacings between the outer sapphire rods, and one of these rods is attached to the gage-supporting bar through a pivot joint, which permits the bottom end of the rod to follow the shortening of the top of the specimen bar during deflection. A loading bucket is suspended from the end of the long arm of the lever, and lead shot is added to the bucket from a hopper equipped with a solenoid-operated sliding valve for manually starting or stopping the shot flow. In addition, a limit-switch is located under the lever to actuate the solenoid, stopping the flow when the specimen fails.

In order to permit deflection measurements at known stresses, the shot is added by increments rather than continuously. Increments of weight, corresponding to a stress of about 1,500 lb/in.^{2} on the specimen, are added to the lever at 2-min intervals, and the deflection is measured every minute. The values of the moduli of rupture and elasticity are computed from the equations

$$\text{Modulus of rupture}=\frac{3P_1L}{4bd^2}, \quad (1)$$

$$\text{Young's modulus of elasticity}=\frac{P_2a(3L^2-4a^2)}{4\Delta bd^3}, \quad (2)$$

where P_1 is the total load on the specimen at failure; L is the span; b is the width of the specimen; d is the depth of the specimen; a is the point(s) of load application (a fraction of the span L); and Δ is the deflection at midspan corresponding to any load, P_2, below the elastic limit. When a is one-quarter of the span, the modulus of elasticity can be calculated from the equation

$$\text{Modulus of elasticity}=\frac{11P_2L^3}{64\Delta bd^3}. \quad (3)$$

In many instances, the accuracy of the values of Young's modulus reported for ceramic materials has been questioned when testing equipment similar to that described in this report was used. In order to determine whether this equipment would allow duplication of an accepted elasticity value, the Young's modulus of a bar of cold-rolled steel, whose size was almost identical to that of the ceramic specimens used, was determined (at various times) to be 29,400,000 lb/in.^{2} This value is considered to be in good agreement with the accepted value of the modulus of elasticity of cold-rolled steel (30,000,000 lb/in.$^2\pm5\%$).

III. Methods

1. Forming

In order to insure the desired reproducibility of results and to prevent segregation of the batch constituents during preparation of the specimens, the same compounding method was followed as has been described previously [7]. Briefly, the procedure entails weighing the constituent materials on a semi-analytical balance to ±0.005 g, blunging with a laboratory-type variable-speed mixer with distilled water and a wetting agent, drying, sieving, and remixing with a starch binder.

Specimens for the investigation of the maturing range (⅝ in. high by ⅝ in. in diam) and for the compression tests (1¼ in. high by ⅝ in. in diam) were pressed at 9,400 lb/in.^{2} The thermal shock and transverse strength test bars (5/16 in. thick by ¾ in. wide by 6⅛ in. long) were pressed at 6,500 lb/in.^{2} All of the specimens were formed in molds made of case-hardened steel and of oil-hardened nondeforming tool steel. The molds were lightly lubricated with a water-emulsifying oil before each specimen was made.

2. Testing

All of the test methods employed have been described previously [3 and 7] but, for the convenience of the reader, they are given briefly again. Carbon tetrachloride was used for the absorption determinations, and the results were converted to equivalent water absorption values. Matured bodies were considered to be those having less than 0.1 percent of equivalent water absorption. Shrinkage values were calculated from micrometer measurements both before and after heating. Apparent density values were obtained by calculations based on micrometer measurements and the weight of the dry specimens. The ends of the specimens for the compressive-strength tests were ground parallel, so that the length-to-diameter ratio of the test specimens was approximately 2. The test pieces were placed between cold-rolled steel blocks, and the compressive stress was applied at a loading rate of about 31,000 (lb/in.^{2})/min by a 75,000-lb hydraulic press. Ten cycles of quenching from 1,700° F (931° C) to room temperature by an air-blast (20° to 30° C) constituted the thermal shock test, and those bars surviving this quenching were tested for modulus of rupture in bending at room temperature. Comparable values for the modulus of rupture were determined also for specimens that had not been thermally shocked. The moduli of rupture and of elasticity at 1,800° F (982° C) were determined by using the furnace described. When it was noted that the deflection following loading continued after the first minute, it was assumed that permanent deformation, or "plastic flow", was occurring. This deformation could be verified when the test pieces were examined for permanent curvature following rupture. Plastic flow was not reported for body 4811C in a previous study [2] when an older testing furnace was used [10]. In order to investigate further the relative magnitude of the deformation, halves of bars broken in the hot bending tests were reground to about ⅛-in. thickness and the transverse strength test repeated by using a minimum span of 3 in. Loads of 12,000, 15,000, and 18,000 lb/in.^{2} were maintained for 15 min, or until rupture occurred, during which times the deflection was measured at regular intervals.

IV. Results

The base compositions of all of the porcelains studied in this investigation are contained within the beryllia field of the system beryllia-alumina-zirconia. The addition of 2 weight percent of calcia (CaO) to each of the base compositions, except body 4811M, which contains an admixture of 4 weight percent of magnesia (MgO), apparently does not affect primary crystallization to an extent distinguishable by petrographic examination. The base compositions of the bodies are given triaxially in figure 4 and numerically in tables 1 and 2.

It was found that all of the specimens could be matured (an absorption of less that 0.1 %) when heated for 1 hour at temperatures between 1,500° and 1,600° C. Optimum maturity in the electric furnace was obtainable at either 1,500° or 1,550° C, and in the gas-fired furnace at 1,575° C. At optimum maturity the values for absorption were between 0.01 and 0.05 percent, the values for shrinkage were between 18.10 and 20.54 percent, and the apparent density ranged from 2.93 and 3.36 g/cm^3.

It was suspected from the surface appearance of the matured specimens that certain of the porcelains would contain objectionably large grains. Petrographic examination, however, failed to reveal any excessive grain growth in any of the bodies, and the average grain sizes were found to be about 8 to 15 μ for the beryllia crystals, 8 to 15 μ for those of alumina, and from 2 to 8 μ for the zirconia. Occasional grains of beryllia, up to 80 to 100 μ in size, were noted in a few specimens. Although no changes were observed in the component crystal sizes of the 4811M body, a singular difference was noted in the shape of the beryllia crystals. In body 4811M, the BeO invariably occurred as rounded grains, whereas in all of the calcia-containing bodies the BeO was in the form of irregular, lath-shaped crystals.

High compressive strengths at room temperature were exhibited by all of the porcelains. The values ordinarily were about 275,000 lb/in.^{2}, but two bodies, *I* and *J*, have strengths of 302,000 and 305,000 lb/in.^{2}, respectively. Table 1 gives the data for maturing range, properties at maturity, and the compressive strength results determined for the porcelains investigated. Only the compressive strength values of the specimens that broke sharply into small fragments are included in this table. The values for those specimens that had splintered or cracked during the test were discarded. A method of specimen "seating", which practically eliminates splintering, is currently being employed,

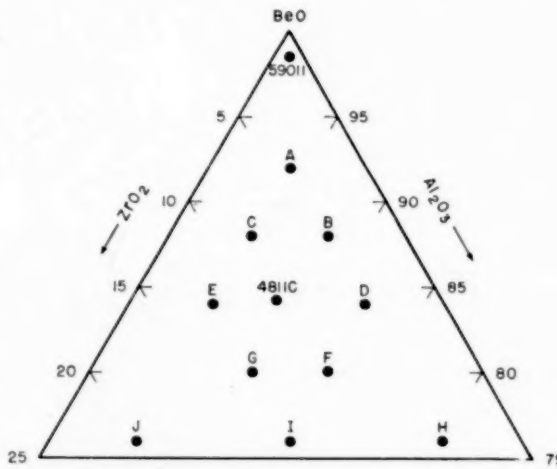

FIGURE 4. *Base compositions of some porcelains within the system* $BeO–Al_2O_3–ZrO_2$.

Shown are the locations of the base composition (in weight percent) of the 13 beryllia porcelains discussed in this report. All but one of the body compositions contained an admixture of 2 weight percent of calcia (CaO); body 4811M contained 4 weight percent of magnesia.

TABLE 1. *Maturing range studies and compressive strength results* [a]

All bodies could be matured to practically imperviousness at temperatures between 1,500° and 1,600° C.

Body	Base composition [b]			Properties at maturity					Properties of compressive strength specimens [c]						
	BeO	Al_2O_3	ZrO_2	Test	Temperature	Shrinkage	Absorption	Apparent density (±0.01)	Test	Temperature	Shrinkage	Absorption	Apparent density (±0.01)	Height/diameter ratio [d]	Strength at room temperature [e] (±5,000 lb./in.²)
	%	%	%		°C	%	%	g/cm³		°C	%	%	g/cm³		lb/in.²
A	92.00	4.00	4.00	599–L	1,550	20.00	0.01	2.99	630–L	1,550	20.16	0.01	3.00	1.98	259×10³
B	88.00	8.00	4.00	599–L	1,550	19.20	.02	3.04	627–L	1,550	19.74	.00	3.03	2.00	276
C	88.00	4.00	8.00	604–L	1,500	19.68	.01	3.07	622–L	1,500	19.58	.01	3.10	2.00	286
D	84.00	12.00	4.00	600–L	1,500	19.36	.02	3.08	625–L	1,500	19.58	.02	3.05	2.00	[f] 272
E	84.00	4.00	12.00	599–L	1,550	20.32	.02	3.18	621–L	1,550	19.58	.00	3.11	1.98	281
F	80.00	12.00	8.00	604–L	1,500	19.20	.01	3.10	631–L	1,500	20.54	.58	3.18	1.99	289
G	80.00	8.00	12.00	600–L	1,500	19.36	.02	3.21	634–L	1,500	20.22	.03	3.21	2.00	281
H	76.00	20.00	4.00	605–L	1,550	18.72	.01	3.10	629–L	1,550	19.10	.01	3.14	1.92	298
I	76.00	12.00	12.00	605–L	1,550	19.20	.01	3.21	628–L	1,550	19.58	.00	3.22	1.94	[f] 302
J	76.00	4.00	20.00	605–L	1,550	20.00	.01	3.30	632–L	1,550	20.54	.00	3.36	2.00	305
59011 [g]	98.50	0.68	0.82						635–L	1,600	19.90	.03	2.91	2.00	240
4811C	84.21	7.15	8.64	599–L	1,550	19.36	.01	3.08		1,550					[h] 251
4811M	84.21	7.15	8.64	536–L	1,600	18.10	.01	3.09	543–L	1,600	17.79	.09	3.16	1.93	238

[a] Values obtained for specimens matured in an electric furnace for 1 hr at the temperatures specified.
[b] All but one of the bodies contain an admixture of 2% of calcia to the base composition; body 4811M contains an admixture of 4% of magnesia.
[c] Unless otherwise indicated, the values given are the averages for three test specimens.
[d] Specimens were about 1 in. high by ½ in. in diameter.
[e] Compression testing was done at a constant loading rate of about 31,250 lb/in.² by using cold-rolled steel blocks for platen protection. The value given is the average of two specimens (three were broken, but one had splintered and the value was discarded).
[f] See footnote e. Value given is for one specimen (three were broken, but two had splintered and the values were discarded).
[g] This body (no admixture to the composition given) reported on by the Battelle Memorial Institute (private communication). See also table 2, footnote f.
[h] R. F. Geller, et al., J. Research NBS **38**, 277, (1946) RP1793.

TABLE 2. *Strength in bending and elasticity values* [a]

All bars survived ten cycles of test for thermal shock resistance (from 1,700° F (931° C) to room temperature by an air blast)

Body	Base composition [b]			Maturing data			Strength in bending (flexure) at— [c]			
							Room temperature		1,800° F (982° C)	
	BeO	Al_2O_3	ZrO_2	Test	Temperature	Absorption	Not thermally shocked	After thermal shocking	(±2,000 lb/in.²)	Young's modulus [d] (±3,000,000 lb/in.²)
	%	%	%		°C	%	lb/in.²	lb/in.²	lb/in.²	lb/in.²
A	92.00	4.00	4.00	33–R	1,575	0.01	31.2×10³	25.8×10³	20.5×10³	30×10⁶
B	88.00	8.00	4.00	33–R	1,575	.01	31.0	25.5	19.0	36
C	88.00	4.00	8.00	33–R	1,575	.01	26.7	23.4	19.6	33
D	84.00	12.00	4.00	33–R	1,575	.02	27.6	26.9	16.8	28
E	84.00	4.00	12.00	31–R	1,575	.01	26.7	25.5	20.7	32
F	80.00	12.00	8.00	35–R	1,575	.02	25.8	25.2	18.2	31
G	80.00	8.00	12.00	35–R	1,575	.02	25.7	23.5	17.3	36
H	76.00	20.00	4.00	31–R	1,575	.03	30.2	25.0	18.9	32
I	76.00	12.00	12.00	32–R	1,575	.25	27.2	26.8	19.9	37
J	76.00	4.00	20.00	32–R	1,575	.04	30.4	29.5	25.1	36
59011 [e]	98.50	0.68	0.82	32–R	1,575	3.5	18.7	19.9?	16.4	31
4811C	84.21	7.15	8.64	35–R	1,575	0.01	34.1	31.9	21.4	36
4811C [f]	84.21	7.15	8.64			about 0.2			18.4	42
4811C [g]	84.21	7.15	8.64			about 0.2	25.2	24.1	13.8	21
4811M	84.21	7.15	8.64	34–R	1,600	1.7	17.2	17.8	15.1	38

[a] Values obtained for specimens matured in a gas-fired furnace for 1 hour at the temperatures specified.
[b] All but one of the bodies contain an admixture of 2% of calcia to the base composition; body 4811M contains an admixture of 4% of magnesia.
[c] Two test bars, about 5½ in. by ¾ in. by ¼ in, of each composition were broken at room temperature, two were thermally shocked and then broken at room temperature, and three were broken for the transverse strength and elasticity tests at 1,800° F (982° C).
[d] The modulus of elasticity values (Young's modulus) are considered as only relative because they were calculated from the curve of the deformation versus load at the lowest part of the curve where the plastic flow was small.
[e] This composition (containing no admixtures) reported on by the Battelle Memorial Institute (private communication) as follows: After heating for 3 hours at 3,100° F (1,740° C), the body showed an apparent porosity of 14%, had a bulk density of 2.56 g/cm³, and showed a room temperature tranverse strength of 18,600 lb/in.²
[f] Specimens of body 4811C prepared for another investigation (foontnote g), but tested for moduli of rupture and elasticity at 1,800° F in the new transverse strength test furnace.
[g] Values given in NACA report W–48 (June 1946), R. F. Geller and M. D. Burdick.

although it was not used for the test specimens of this investigation.

These porcelains are fairly resistant to thermal stresses as evidenced by their ability to withstand 10 cycles of shocking from 1,700° F (931° C) to room temperature by an air blast (20° to 30° C). Their transverse strengths after shocking were usually slightly lower (18,000 to 32,000 lb/in.²) than the values obtained for comparable specimens that had not been shocked (17,000 to 34,000 lb/in.²). Considerably lower strengths in bending (15,000 to 25,000 lb/in.²) were noted for all of the matured

porcelains at 1,800° F (982° C), compared to their strengths at room temperature.

From the viewpoint of transverse strength at room temperature the outstanding body was 4811C, although a loss in strength of 2,000 lb/in.^{2} was noted as the result of thermal shocking. If the effect of heat shock on the transverse strength is chosen as the basis of comparison, the outstanding bodies were 4811M, I, F, D, and J. Only bodies 4811C and J, however, had transverse strengths after heat-shocking of about 30,000 lb/in.^{2}; the other bodies ranged as low as 17,800 lb/in.^{2} The strongest body in the bending tests at 1,800° F (982° C) was J. Its value of 25,000 lb/in.^{2} was about 20 to 25 percent higher than those of the next strongest bodies, 4811C, E, and A.

During the determinations of the moduli of rupture and elasticity at 1,800° F, it was noted that body 4811C and others exhibited plastic deformation. Although the modulus of elasticity values at 1,800° F are reported, they must be considered as only relative, because they were calculated from the curve of the deformation versus load at the lowest part of the curve where plastic flow was relatively small. Table 2 gives the results of the tests of thermal shock, transverse strength at room temperature both before and after heat-shocking, and the moduli of rupture and elasticity at 1,800° F (982° C).

In order to obtain some indirect measure of the deformation-under-load (plastic flow) that occurred during the original tests of rupture and elastic strengths, half-bars of some of the body compositions used for hot transverse strength test (which allowed a minimum 3-in. span) were reground to a thickness of 0.1250±0.0007 in. The deflection was measured at 1,800° F (982° C) at 1-min intervals for 15 min under loads of approximately 12,000, 15,000, and 18,000 lb/in.^{2}, or until rupture had occurred. Figure 5 shows the results of these tests. Table 3 gives the strain-rate data determined from the stress-strain tests and, for correlation purposes, a listing of the hardness, strength, and elastic properties of all of the porcelains of this study is also given.

Examination of table 3 reveals that there is no correlation between the strain rate at 1,800° F and the strength properties of the various porcelains. The very low hardness of body 59011 (whose hardness would be expected to approximate that of BeO) is probably due largely to the porous condition of the test specimen. In addition, considerable difficulty was encountered in obtaining suitably polished surfaces for all of the specimens, and it is con-

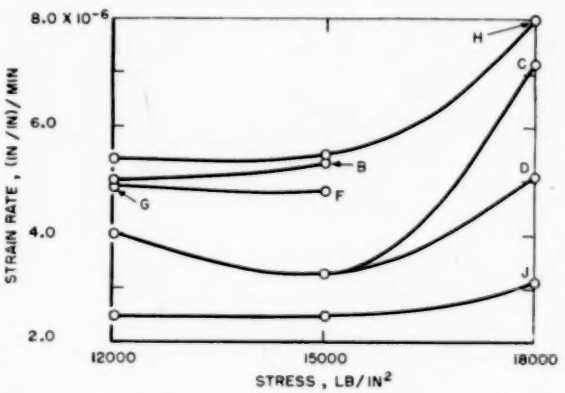

FIGURE 5. *Short-time stress-strain relations of some beryllia porcelains.*

Shown are the strain rates at 1,800° F (982° C) of seven beryllia porcelains when maintained for 15 min at each of three stresses, or until rupture occurred.

TABLE 3. *Strength, stress-strain, and Knoop hardness values*

Strength at room temperature					Strength at 1800° F (982° C) [a]					Strain rates [b]				Knoop hardness [c]		
Compressive strength [d]		Transverse strength [a]			Transverse strength		Young's modulus [e]	Maximum strain at fracture							10 indentions at 500-g load	
Body		Body	Not thermally shocked	After thermal shocking	Body			Calculated [f]	Observed [f]	Body	12,000-lb/in.^{2} stress	15,000-lb/in.^{2} stress	18,000-lb/in.^{2} stress	Body	Average	Range, low to high
	lb/in.^{2}		*lb/in.*^{2}	*lb/in.*^{2}		*lb/in.*^{2}	*lb/in.*^{2}				*(in./in.)/min*	*(in./in.)/min*	*(in./in.)/min*		K_{500}	K_{500}
J	305×10^3	4811C	34.1×10^3	31.9×10^3	J	25.1×10^3	36×10^6	0.70×10^{-3}	21×10^{-3}	H	5.4×10^{-6}	5.5×10^{-6}	8.0×10^{-6}	J	830	700 to 900
I	302	A	31.2	25.8	4811C	21.4	35	.59	18	B	5.0	5.4	.....	F	810	740 to 880
F	289	B	31.0	25.5	E	20.7	32	.65	21	F	4.9	4.8	.....	E	810	760 to 920
C	286	J	30.5	29.5	A	20.5	30	.68	28	G	4.9	.....	.....	H	810	700 to 900
G	281	H	30.2	25.0	I	19.9	37	.54	13	C	4.0	3.3	7.2	4811M	810	710 to 960
E	281	D	27.6	26.9	C	19.6	33	.60	18	D	4.0	3.3	5.1	A	800	760 to 900
B	276	I	27.2	26.8	B	19.0	36	.53	16	J	2.5	2.5	3.1	C	800	700 to 900
D	272	E	26.7	25.5	H	18.9	33	.58	13	.....	.....	.....	.....	B	800	600 to 900
H	268	C	26.7	23.4	F	18.2	31	.58	16	.....	.....	.....	.....	G	790	720 to 880
A	259	F	25.8	25.2	G	17.3	36	.48	15	.....	.....	.....	.....	D	780	710 to 840
4811C	251	G	25.7	23.5	D	16.8	28	.60	20	.....	.....	.....	.....	I	780	670 to 900
59011	240	59011	18.7	19.9?	59011	16.4	31	.53	15	.....	.....	.....	.....	4811C	760	670 to 840
4811M	238	4811M	17.2	17.8	4811M	15.1	38	.40	12	.....	.....	.....	.....	59011	550	420 to 770

[a] The maturing data for the specimens used in these tests are given in columns 5 to 7 of table 2.

[b] One half-bar of each composition from the transverse strength tests at 1,800° F, which allowed a minimum span of 3 in., was reground for this test.

[c] Knoop numbers determined by using a solenoid-operated Tukon tester and a 500-g load. For comparison, a specimen of beryllia (BeO) that had been used as a pedestal in the thoria-resistor furnace had an average Knoop hardness of K_{500}=1,030 (980 to 1,110).

[d] The maturing data and other physical properties of these test specimens are given in columns 11 to 17 of table 1.

[e] Young's modulus values are considered as being only relative because they were calculated from the deformation-load curve at the lowest part where the "plastic flow" was relatively small.

[f] The maximum strain (deformation) at fracture was calculated by dividing the value of the modulus of rupture by that of the modulus of elasticity.

sidered, therefore, that the Knoop hardness values obtained are lower than they should be.

Petrographic examination of the specimens after the bending tests revealed either one or two isotropic phases in all of the test bars, except those of body 4811M. These phases were present also in the test bars made for use in the preliminary study of the tensile and creep properties of porcelains [1]. Unfortunately for identification purposes, these phases appeared as very thin films, usually less than ½μ in thickness, interstitial to and surrounding the beryllia grains. It was possible to identify only their refractive indices, which, in some cases, were considerably above 1.73 and, in others, below 1.71. Reexamination of some of the older specimens and test pieces from the studies of maturing range and compression strength revealed that the isotropic phases were present in the same relative proportions as were noted for the transverse strength specimens. There seemed to be somewhat more of these phases in the bodies matured in the gas-fired furnace than in the bodies matured in the thoria-resistor furnace. Although it was possible to establish the presence of the isotropic phases in the various test specimens, no quantitative correlation between the amounts of the isotropic phases present and the relative order of the strengths of these porcelains (table 3) could be determined. Generally, however, it was found that the order of the bodies according to their estimated content of these phases was H, B, F, G, C, D, E, 4811C, and J. Body H usually contained the most of these phases and, in all instances, none were found in body 4811M.

A number of unsuccessful attempts were made to determine the nature of the isotropic phases. In order to examine the porcelains by reflected light with the metallographic microscope, satisfactorily polished and etched specimen surfaces are required. These surfaces were not obtained by the use of any of the common abrasives, including diamond powders, nor by the use of any of the ordinary etching solutions, including a previously successful electrolytic etching method. The inability to obtain suitably finished surfaces also made it impossible to obtain satisfactory shadowed surface replicas for study with the electrom microscope.

V. Discussion

One of the results of this investigation was the finding that the addition of 2 weight percent of calcia (CaO) to the BeO-Al_2O_3-ZrO_2 porcelains caused one or more isotropic phases to appear in the matured specimens. Whether these phases are crystalline or glassy has not been determined. An admixture of 4 weight percent of magnesia (MgO) to one of the base compositions caused no observable additional phase.

Although no identification of the isotropic phases could be made, there is some basis for speculation as to their probable compositions. Two binary systems, CaO-Al_2O_3 [11] and CaO-BeO [12], contain appreciable areas of complete melting at temperatures below those at which the porcelains of this study were matured. In the first system, CaO-Al_2O_3, isotropic crystalline phases are known to exist [13]. They are the compound $3CaO.Al_2O_3$ with a refractive index of 1.710, the compound $5CaO.3Al_2O_3$ with indices of 1.608 and 1.662 depending upon the crystallization behavior, and an unstable prismatic phase, whose indices are 1.687 and 1.692 (very weak birefringence). A glass of refractive index 1.68, a crystalline phase with an index of 1.684, and an unidentified isotropic phase of index of 1.668 are known for one mixture in the system CaO-Al_2O_3-BeO (42% of CaO, 41% of Al_2O_3, and 17% of BeO). At a temperature of 1,450° C this mixture was completely liquid.

Two isotropic phases were identified in the porcelains investigated in this study. One of these had an index considerably above 1.73 and the other somewhat below 1.71. For the first of these two phases, it is conceivable that either a beryllium calcium zirconate or an aluminum calcium zirconate had been formed, the calcia and zirconia combining first to form a high index cubic zirconia solid solution (n=2.08), and then reacting in the presence of either or both of the other oxides to form an isotropic crystalline phase, an isotropic mixed crystal series, or a glass. The second of the unidentified phases is likely to be one of the isotropic crystalline phases contained within the system CaO-Al_2O_3.

As previously stated, there were not sufficient data available for a study of the correlations that might exist between the amounts of the isotropic phases present and the test values of the various strength properties of these porcelains. Even though an additional boundary phase is present, the strengths of these calcia-containing bodies compare favorably with those of other oxide porcelains, such as the bodies of the systems MgO-BeO-ZrO_2, MgO-BeO-ThO_2, MgO-BeO-Al_2O_3, and BeO-Al_2O_3-ThO_2 (tables 1 and 9 of [7]).

VI. Conclusions

The general physical properties of practically impervious porcelains within the beryllia field of the system BeO-Al_2O_3-ZrO_2, whose base compositions approximate that of NBS Body No. 4811C, were found to be: maturing range, 1,500° to 1,600° C; apparent density, 2.9 to 3.4 g/cm^3; shrinkage, 17.8 to 20.5 percent; room temperature compressive strength, 238,000 to 305,000 lb/in.^{2}; room temperature transverse strength, 17,200 to 34,100 lb/in.^{2}; room temperature transverse strength after thermal shocking, 17,800 to 31,900 lb/in.^{2}; transverse strength at 1,800° F (982° C), 15,100 to 25,100 lb/in.^{2}; approximate Young's modulus at 1,800° F (see discussion), 28,000,000 to 38,000,000 lb/in.^{2}; relative thermal-shock resistance, good; and Knoop hardness numbers (500-g load), 550 to 830.

For an all-ceramic body exhibiting high strengths both at room temperature and at 1,800° F (982° C) and good thermal shock resistance, it is suggested that the possibilities apparent in body J be further investigated. The base composition of this body is

76 percent of beryllia (BeO), 4 percent of alumina (Al_2O_3), and 20 percent of zirconia (ZrO_2), with an admixture of 2 weight percent of calcia (CaO). This body becomes practically impervious at temperatures between 1,500° and 1,600° C in both electric and gas-fired furnaces, with a resultant shrinkage of about 20 percent and an apparent density of about 3.3 g/cm³.

The results of this study indicate that some of the porcelains within the beryllia field of the system beryllia-alumina-zirconia may be of use as components for various heat engines where high strength and some degree of elasticity, rather than the ultimate in refractoriness, are desired.

The authors acknowledge the assistance of L. G. Lambert in the preparation, maturing, and testing of the specimens.

VII. References

[1] M. D. Burdick, R. E. Moreland, and R. F. Geller, NACA Tech. Note 1561 (April 1948).
[2] R. F. Geller and M. D. Burdick, NACA W–48 (June 1946).
[3] R. F. Geller, P. J. Yavorsky, B. L. Steirman, and A. S. Creamer, J. Research NBS **36,** 277 (1946) RP1703.
[4] Ohio State University Reports (Project Ceramics, 210–252–341): No. 36—H. R. Lowers (Dec. 26, 1947); No. 39—A. P. Welch (Jan. 15, 1948); No. 40—E. T. Montgomery (March 4, 1948); and No. 44—H. R. Lowers and A. R. Blackburn (June 23, 1948).
[5] University of Illinois Report No. 26, Contract No. W33–038 ac—14520 (16071) (July 9, 1948).
[6] J. C. Freche and B. W. Sheflin, NACA Research Memor. E8G20 (Sept. 1948), and J. C. Freche, NACA Research Memor. E9L07 (Feb. 1950).
[7] S. M. Lang, L. H. Maxwell, and R. F. Geller, J. Research NBS **43,** 429 (1949) RP2034.
[8] R. F. Geller, J. Research NBS **27,** 555 (1940) RP1443, R. F. Geller and P. J. Yavorsky, J. Research NBS **35,** 87 (1943) RP1662.
[9] A. R. Bobrowsky, Conference on ceramic materials for application to aircraft power plants. Air Matériel Command, Wright-Patterson Air Force Base (May 27 to 28, 1948).
[10] R. A. Heindl and W. L. Pendergast, J. Am. Ceram. Soc., **10,** 524 (1927).
[11] G. A. Rankin and F. E. Wright, Am. Jr. Sci., **39,** 11 (1915).
[12] H. von Wartenburg, H. Reusch, and E. Saran, Z. anorg. allgem. Chem. **230,** 275 (1937).
[13] R. H. Bogue, The chemistry of portland cement (Reinhold Publishing Co. Inc., New York, N. Y., 1947).

WASHINGTON, June 6, 1950.

Journal of Research of the National Bureau of Standards Vol. 45, No. 5, November 1950 Research Paper 2148

Some Electrical Relations in Galvanic Couples[1]

By H. D. Holler

The electrical relations are developed for a galvanic couple (short-circuited cell) with and without polarization by externally applied current. Their significance in the derivation of criteria for cathodic protection is demonstrated. The mechanism of current flow between couples at different potentials is explained. The importance of galvanic-couple theory in governing current distribution over an electrode surface is indicated.

I. Introduction

In the study of electrode processes, an understanding of the electrical relations in galvanic couples and of their behavior toward externally applied current is essential. It has, of course, been known since the time of Galvani and Volta, that a bimetallic junction in contact with an electrolyte is a source of electromotive force and current. While there is some question regarding the exact source of the emf, it can be shown by thermodynamics that the chemical potential of such a system manifests itself as an emf, theoretically capable of delivering current.

In accordance with Nernst's law, it is also well known that an emf may exist between two areas of the same metal, each in different environments, and a galvanic current will flow when they are metallicly connected. Even in the case of a pure metal, in an electrolyte, galvanic currents may flow between its different crystal faces, from cracks in its surface to surrounding areas, or between areas in different states of oxidation. As a result, the conditions favoring the existence of galvanic couples in the phase boundary are nearly always fulfilled whenever a metal comes into contact with an electrolyte. In connection with the "local-cell" theory of corrosion, some of the electrical relations governing these currents have been derived by Müller, Akimow, and Thomasow, and others [1].[2] There are galvanic circuits of all magnitudes ranging from those of molecular dimensions to those of great size existing underground. They are present, to some extent, on the electrodes in practically all electrochemical processes. Systems of several electrodes have been studied by many workers including Brown and Mears, Landau and Petrocelli [2].

While thermodynamics defines the driving force of an electrochemical reaction, the rate of the latter is controlled by irreversible factors, represented by polarization, as defined in its broadest sense; that is, including resistive potential differences also. Sometimes, as in electric batteries, it is desirable that the polarization resulting from delivery of current to an

[1] The term "galvanic couple" or "couple" is used in this paper for the sake of brevity and means a galvanic cell having its electrodes metallicly connected through an external resistance that may be negligibly small.

[2] Figures in brackets indicate the literature references at the end of this paper.

external circuit be kept at a minimum. However, in these same batteries, the polarization of any galvanic couples on the surfaces of the individual electrodes should be a maximum, in order to reduce the "self-discharge" of the electrode. This may be accomplished by the proper choice of pure materials, the use of inhibitors, or by other means.

In other electrochemical processes, such as electroplating, the reaction at the electrode may be selectively determined by its polarization. For example, when the dissolution of a metal anode with high current-efficiency is desired, additions to the electrolyte may be made for the reduction of polarization. At the cathode, the control of polarization by chemical or electrical means may determine the proportions of elements deposited and their distribution. Thus, the "throwing power" of an electroplating solution is a function of the rate of change of polarization with current [3].

In corrosion mitigation, it is fortunate when, through self-polarization of the galvanic couples, the galvanic currents become negligible. This is the basis of the mechanism of passivity developed by Mears and Brown [4]. The presence of such galvanic couples and their polarization may thereby explain why some metals do not corrode, as well as why others do corrode. The protection of a metal by a coating of another metal depends largely upon the electrical characteristics of the galvanic couples involved and the principles of cathodic protection. An understanding of these principles also requires a derivation of the relations among the electrode potentials, currents, and resistances involved in a galvanic cell on closed circuit. Since opening this circuit is usually impossible, only a few electrical measurements can be made. The most important of these is the potential of the couple with reference to another electrode of constant potential. Unfortunately, this measurement by itself is usually of limited value in ascertaining the corrosion status.

However, if an external current be applied to the couple, any change in the relation of its potential to the applied current may supply valuable information. Before such information may be correctly interpreted, an elementary analysis of the electrical relations is required.

II. Derivation of Basic Electrical Relations

Let figure 1, *A* represent a galvanic couple consisting of separate electrodes where e_a and e_c are the polarized anode and cathode potentials,[3] respectively. The term "polarized potential" means that the potential is a function of current. This results from the electrochemical effects of current at the interface. We shall assume that the anode and cathode are each free from local couples. Since the effect of time will not be considered here, e_a and e_c are momentary values. Then by Ohm's law

$$(e_a - e_c) - i_o\,(r_a + r_c) = 0, \tag{1}$$

where r_a and r_c are the resistances, mainly ionic, associated with the anode and cathode, respectively, and i_o is the momentary value of the galvanic current. The external resistances R_a and R_c between e_a and e_c are neglected here and throughout this paper, as their omission makes no difference in the argument. The potential difference $(E_G - E_s)$ between the terminal G and an electrode having a constant potential E_s may be measured with a potentiometer and expressed by the following equations:

$$(E_G - E_s) - (e_a - E_s) + i_o r_a = 0 \tag{2}$$

and

$$-(E_G - E_s) + (e_c - E_s) + i_o r_c = 0. \tag{3}$$

If now a potential difference E_t be applied by closing k_B in figure 1, B, a current I will be superposed on

[3] "Potential" as used in this paper is a potential level referred to some electrode of constant value in the same electrolyte.

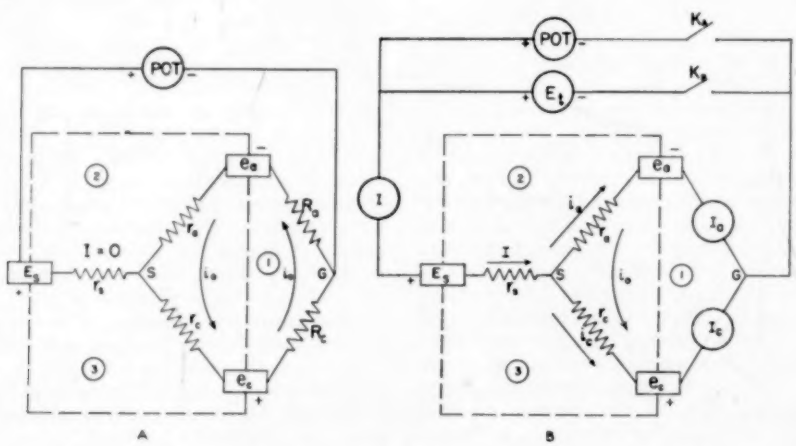

FIGURE 1. *Electrical relations between a galvanic couple and reference electrode.*

POT is a high-resistance voltage indicator. A, Without external current; B, with external current.

the galvanic couple if $E_t \neq (E_G - E_s)$. It will flow internally from E_s toward the couple if $E_t > (E_G - E_s)$. We shall consider E_s to be unpolarized, that is, its potential is not changed by current I. Let r_s be the ionic resistance between E_s and the point S where I divides into two components, i_a through r_a and i_c through r_c. Then

$$I_a = i_a - i_o \text{ and } I_c = i_c + i_o, \tag{4}$$

I_a and I_c being measurable.

At the instant of closing the switch k_B, we shall assume that e_a and e_c as well as r_a and r_c, are unchanged by current I. As a result the momentary value of i_o is the same as in figure 1, *A*, and eq 1, 2, and 3 still hold. We shall consider the distribution of I_a and I_c such that each electrode is either wholly anodic, or wholly cathodic.

Taking meshes 1 and 2 in figure 1, *B* clockwise, then by Kirchoff's laws:

$$(e_a - e_c) + (i_a - i_o)r_a - (i_c + i_o)r_c = 0. \tag{5}$$

Likewise

$$E_t - (e_a - E_s) - (i_a - i_o)r_a - Ir_s = 0. \tag{6}$$

Now let

$$E_t - Ir_s = E, \tag{7}$$

where E = that portion of the potential difference E_t that is applied directly to the couple between the junction point S and the terminal G.

Rewriting eq 5 and 6

$$(i_a - i_o)r_a - (i_c + i_o)r_c = -(e_a - e_c), \tag{8}$$

$$-(i_a - i_o)r_a = -[E - (e_a - E_s)] \tag{9}$$

and solving

$$i_a - i_o = \frac{-r_c[E - (e_a - E_s)]}{-r_a r_c} = \frac{E - (e_a - E_s)}{r_a} = I_a. \tag{10}$$

Likewise

$$i_c + i_o = \frac{-r_a[E - (e_a - E_s)] - r_a(e_a - e_c)}{-r_a r_c} =$$

$$\frac{E - (e_c - E_s)}{r_c} = I_c. \tag{11}$$

In eq 10 and 11, it is seen that for given values of e_a and e_c the relative magnitude of E determines the direction of the current through each electrode. For example, no current flows to the anode unless $E > (e_a - E_s)$.
Then $i_a > i_o$ and $I_a > 0$.

Now let us derive additional equations evaluating the same currents. Again, by Kirchoff's laws, we have

$$(i_a - i_o) + (i_c + i_o) = I, \tag{12}$$

$$(i_a - i_o)r_a - (i_c + i_o)r_c = -(e_a - e_c), \tag{8}$$

and solving

$$i_a - i_o = \frac{-Ir_c + (e_a - e_c)}{-r_c - r_a} = -\frac{(e_a - e_c)}{(r_a + r_c)} + \frac{Ir_c}{(r_a + r_c)} = I_a, \tag{13}$$

and

$$i_c + i_o = \frac{-(e_a - e_c) - Ir_a}{-r_c - r_a} = \frac{(e_a - e_c)}{(r_a + r_c)} + \frac{Ir_a}{r_a + r_c} = I_c. \tag{14}$$

In eq 13 and 14 it is seen that, since from eq 1

$$\frac{e_a - e_c}{r_a + r_c} = i_o, \tag{15}$$

$$i_a = \frac{Ir_c}{r_a + r_c} \text{ and } i_c = \frac{Ir_a}{r_a + r_c}. \tag{16}$$

Before switch k_B was closed, the emf $(E_G - E_s)$ of the galvanic couple followed from eq 2 and 3. Thus,

$$(E_G - E_s) = (e_a - E_s) - i_o r_a \tag{17a}$$

$$= (e_c - E_s) + i_o r_c \tag{17b}$$

On closing k_B the applied potential difference E_t is opposed by emf, $(E_G - E_s)$.

Thus

$$E_t - (E_G - E_s) - Ir_s - IR_G = 0, \tag{18}$$

where R_G is the resistance of the couple.

Introducing E, as defined in eq 7

$$\frac{E - (E_G - E_s)}{I} = R_G. \tag{19}$$

To evaluate R_G, let us proceed by equating the two expressions for $i_a - i_o$ given in eq 10 and 13. Thus,

$$i_a - i_o = \frac{E - (e_a - E_s)}{r_a} = \frac{Ir_c}{(r_a + r_c)} - \frac{(e_a - e_c)}{(r_a + r_c)} = I_a. \tag{20}$$

Since $(e_a - e_c)/(r_a + r_c) = i_o$, eq 20 becomes

$$E - (e_a - E_s) = \frac{Ir_a r_c}{r_a + r_c} - i_o r_a, \tag{21}$$

and since eq 17a may be written

$$E_G = e_a - i_o r_a, \tag{22}$$

eq 21 becomes

$$E - (E_G - E_s) = I\,\frac{r_a r_c}{r_a + r_c}, \tag{23}$$

then from eq 19 and 23 we obtain

$$R_G = \frac{r_a r_c}{r_a + r_c}. \tag{24}$$

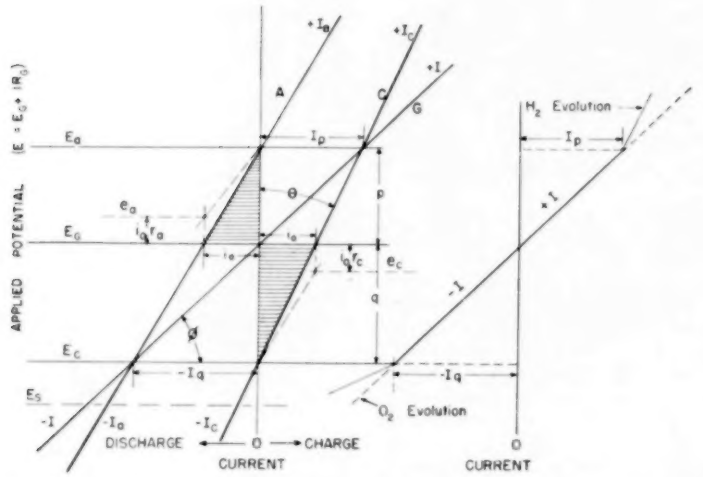

FIGURE 2. *Polarization curves for anode A, cathode C, and galvanic couple G, showing possible discontinuities at I_p and I_q.*

III. Polarization of a Galvanic Couple

In order to understand more clearly the potential-current relations resulting from the application of current to a galvanic couple, let us synthesize the diagram in figure 2, where all quantities indicated may be measured directly or calculated from experimental data. It comprises three polarization curves, one for the anode A, one for the cathode C, and one for the galvanic couple G. Consider two separate electrodes, A and C, having open-circuit potentials E_a and E_c, and a reference electrode at potential level E_s, all three being in the same electrolyte. Beginning with zero current, let us polarize the electrode potential represented by E_c, cathodically, that is, pass current I_c from the electrolyte to the electrode. In order to do this, a potential difference E greater than E_c is required. The relation E/I_c represents the cathode polarization curve, and when I_c becomes equal to I_p, the cathode potential is equal to E_a. Next, beginning with zero current, let us polarize anodically the electrode whose "open-circuit" potential is represented by E_a, that is, pass current, I_a from electrode to electrolyte. This requires a potential difference E less than E_a. The relation $E/-I_a$ represents the anode polarization curve, and when $-I_a$ becomes equal to $-I_q$, the anode potential is equal to E_c.

After these polarization curves have been separately constructed, let the two electrodes be electrically connected. Then when the potential, E, is equal to E_G, no external current I enters or leaves the couple, and $-I_a=I_c=i_o$. If now we polarize the couple G cathodically by increasing I in the "charge" direction the applied potential required is $E=E_G+IR_G$ where R_G is the resistance of the couple.

When $E=E_G$, $I=0$; when $E=E_a$, $I_a=0$, and when $E=E_c$, $I_c=0$. The conditions for cathodic protection are $I_a=0$, $E=E_a$ and $I=I_c=I_p=$the protective current.

Then, from eq 13 we have

$$\frac{e_a-e_c}{r_a+r_c}=Ip\,\frac{r_c}{r_a+r_c} \tag{25}$$

likewise, when $I_c=0$, $-I=I_a=I_q$, and from eq 14 we have

$$-\frac{e_a-e_c}{r_a+r_c}=Iq\,\frac{r_a}{r_a+r_c} \tag{26}$$

then

$$\frac{e_a-e_c}{r_c}=Ip \text{ and } \frac{e_a-e_c}{r_a}=Iq \tag{27}$$

and

$$\frac{I_p\cdot I_q}{I_p+I_q}=\frac{e_a-e_c}{r_a+r_c}=i_o. \tag{28}$$

It also follows from eq 27 that

$$\frac{I_p}{I_q}=\frac{r_a}{r_c}. \tag{29}$$

Equation 28 may also be derived from the trigonometry of figure 2 as follows:

$$\tan\theta=\frac{i_o}{q}=\frac{I_p}{p+q} \tag{30}$$

$$\tan\phi=\frac{q}{I_q}=\frac{p+q}{I_p+I_q}. \tag{31}$$

Rearranging and combining

$$i_o=\frac{I_p\cdot q}{p+q}=\frac{I_p\cdot I_q}{I_p+I_q}. \tag{32}$$

If, therefore, it be possible to estimate I_p and I_q from changes in the E/I relation as indicated in figure 2, the magnitude of galvanic current i_o may be evaluated from eq 28 and 32; and the ratio of the electrode resistances r_a/r_c may be obtained from eq 29. The measurement of I_q, and particularly I_p, by any means, direct or indirect, is therefore of prime importance in evaluating the characteristics of a galvanic couple.

IV. Partition of the Applied Current

The partition of I into its anodic and cathodic components may be interpreted either from eq 10 and 11 or from eq 13 and 14, and figure 1 *B*.

Since

$$\frac{i_a - i_o}{i_c + i_o} = \frac{I_a}{I_c}, \tag{33}$$

the term "partition" is ambiguous unless defined as i_a/i_c or I_a/I_c. If the measurable ratio be used, then

$$\frac{I_a}{I_c} = \frac{[E-(\epsilon_a - E_s)]\cdot r_c}{[E-(\epsilon_c - E_s)]\cdot r_a} \tag{34}$$

or

$$\frac{I_a}{I_c} = \frac{\dfrac{\epsilon_a - \epsilon_c}{r_a + r_c} + \dfrac{Ir_c}{r_a + r_c}}{\dfrac{\epsilon_a - \epsilon_c}{r_a + r_c} + \dfrac{Ir_a}{r_a + r_c}} = \frac{-i_o + \dfrac{Ir_c}{r_a + r_c}}{i_o + \dfrac{Ir_a}{r_a + r_c}}. \tag{35}$$

If $\epsilon_a = \epsilon_c$, $i_o = 0$, and both eq 34 and 35 become

$$\frac{I_a}{I_c} = \frac{r_c}{r_a}. \tag{36}$$

When ϵ_a and ϵ_c are not equal, partition of current I_a/I_c is determined by the product of the emf-difference ratio $E-(\epsilon_a - E_s)/E-(\epsilon_c - E_s)$ and the resistance ratio r_c/r_a as in eq 34.

The partition of current may also be expressed by an equation, including a term that expresses the rate of change of polarization of the anode with current; and also a similar one for the cathode.

Thus, from eq 10 and 11, and still assuming E_s to be constant, we have by elimination of E,

$$\frac{I_a}{I_c} = \frac{r_c + \dfrac{(\epsilon_c - E_s)}{I_c}}{r_a + \dfrac{(\epsilon_a - E_s)}{I_a}}. \tag{37}$$

Taking the partial derivative of eq 10 with respect to I_a, we have

$$\frac{\partial E}{\partial I_a} = r_a + \frac{\partial}{\partial I_a}(\epsilon_a - E_s),\ r_a \text{ constant}, \tag{37a}$$

similarly from eq 11 we have

$$\frac{\partial E}{\partial I_c} = r_c + \frac{\partial}{\partial I_c}(\epsilon_c - E_s),\ r_c \text{ constant}, \tag{37b}$$

and dividing 37b by 37a we have

$$\left.\frac{\partial E}{\partial I_c}\right/\frac{\partial E}{\partial I_a} = \frac{\partial I_a}{\partial I_c} = \frac{r_c + \dfrac{\partial}{\partial I_c}(\epsilon_c - E_s)}{r_a + \dfrac{\partial}{\partial I_a}(\epsilon_a + E_s)},$$

where $\partial(\epsilon_c - E_s)/\partial I_c$ and $\partial(\epsilon_a - E_s)/\partial I_a$ represent the rates of change in counter emfs ϵ_c and ϵ_a with currents, I_c and I_a respectively.

Equation 37 is a general expression of the potential-current relations, which govern the current distribution over any electrode. For example, in electroplating, the current is opposed not only by resistance but also by the emf of polarization, which tends to divert the current to more remote areas and thereby exhibit "throwing power". Also, in cathodic protection a high rate of change of counter emf with current tends to divert more current to remote areas than if current partition were controlled entirely by resistance.

V. Measurement of E_G

As previously indicated, the chief measurable characteristic of a "closed circuit" galvanic cell is its potential E_G with reference to a standard electrode E_s.

Equations 17 represent the value of the emf $(E_G - E_s)$, which is indicated graphically in figure 3, *A* and *B*. When an external emf E_t is applied, (k_B closed, fig. 1 *B*) and $E > (E_G - E_s)$, the resistive components indicated in eq 38 are added to eq 17, giving eq 39.

$$IR_G = i_a r_a = i_c r_c \tag{38}$$

$$(E_G - E_s) + IR_G = (\epsilon_a - E_s) - i_o r_a + i_a r_a \tag{39a}$$

$$= (\epsilon_c - E_s) + i_o r_c + i_c r_c \tag{39b}$$

or, using the real currents, I_a and I_c,

$$(E_G - E_s) + IR_G = (\epsilon_a - E_s) \pm I_a r_a \tag{40a}$$

$$= (\epsilon_c - E_s) + I_c r_c \tag{40b}$$

I_a is positive if $E > (\epsilon_a - E_s)$ and negative if $E < (\epsilon_a - E_s)$ as in figure 3*B*. With current I flowing (k_A and k_B closed) through the couple, the potential difference $E_t = (E_G - E_s) + Ir_s + IR_G$ is measured directly, by using a potentiometer.

In order to determine $(E_G - E_s)$ during passage of external current I, it is necessary to cancel the resistive component $Ir_s + IR_G$ from the above potentiometer measurement. Two methods of doing this are briefly as follows: first, if k_A, figure 1, *B*, be closed immediately after opening k_B, $E_G - E_s$ may be observed by a suitable voltage indicator, POT. This of course may be done manually if E_G is the same whether I is on or off. However, if E_G is appreciably affected by I, then it must be observed a-

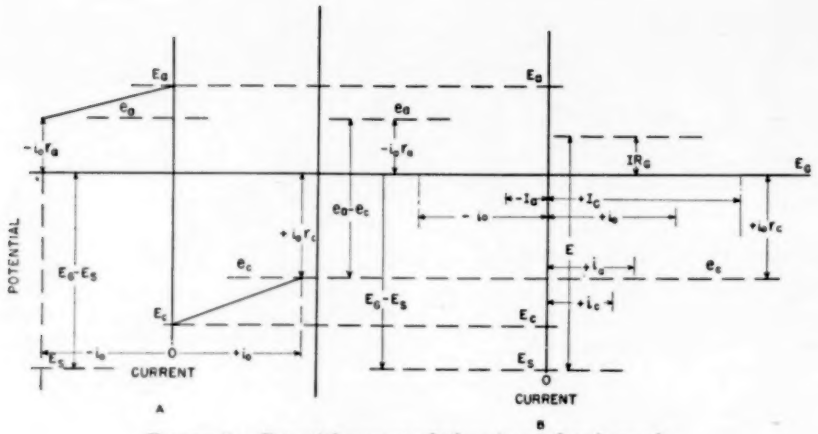

FIGURE 3. *Potential-current relations in a galvanic couple.*

A, Without external current; B, with external current.

the instant of current interruption. This may be done by a suitable commutator [5], which opens k_B for short periods in succession, during which k_A is momentarily closed, The voltage indicator will then give an average value of E_G during the periods when $I=0$. By using the proper commutator speed, period of interruption, and indicator, the observed average can be made approximately equal to the true value of E_G during the flow of current I. The use of an electronic interruptor [6] and amplifier with high-speed recorder or oscillograph [7], permits the measurement of emf, free of ir drop, with high precision.

A second method of cancelling the ir components, Ir_s+IR_G from the measurement of (E_G-E_s) is based on the Wheatstone bridge principle [8]. To balance the bridge, having an emf in one arm, use is made of a short interruption of current I, or a part of I, by touching a key. After the balance, the values of (E_G-E_s) and also of (r_s+R_G) are directly observed.

Let us now suppose that through electrochemical effects resulting from flow of current, the emf, (e_a-e_c) be changed to $(e'_a-e'_c)$. Then the galvanic current will also be changed from i_o to i'_o in accordance with Ohm's law. Thus

$$i'_o=\frac{e'_a-e'_c}{r_a+r_c}. \tag{41}$$

From the new values in eq 41, a new value for the galvanic couple potential is also obtained. Thus, eq 2 and 3 are written

$$(E'_G-E_s)=(e'_a-E_s)-i'_o r_a \tag{42a}$$

$$=(e'_c-E_s)+i'_o r_c \tag{42b}$$

The emf (E'_G-E_s) may be observed by either of the above methods. For each increment in applied current new sets of values for i'_o, e'_a, e'_c and E'_G are obtained, depending upon the length of time of application.

Their substitution in eq 10, 11 and 13, 14 give the following:

$$i'_a-i'_o=\frac{E-(e'_a-E_s)}{r_a}=I'_a, \tag{43a}$$

$$i'_c+i'_o=\frac{E-(e'_c-E_s)}{r_c}=I'_c, \tag{43b}$$

$$i'_a-i'_o=\frac{e'_a-e'_c}{r_a+r_c}+I'\frac{r_c}{r_a+r_c}=I'_a, \tag{44a}$$

$$i'_c+i'_o=\frac{e'_a-e'_c}{r_a+r_c}+I'\frac{r_a}{r_a-r_c}=I'_c. \tag{44b}$$

Each new set of values of I'_a and I'_c, if plotted according to figure 2 will give a succession of corresponding diagrams, each with a new E''_G level.

VI. Conditions for Cathodic Protection

From eq 43a and 44a, it follows that when

$i'_a=i'_o$ *or* $E=(e'_a-E_s)$,
$I'_a=0$,

which is the "current" criterion for cathodic protection. Then also $e'_a=E_a$, and therefore $E=(E_a-E_s)$, which is the "potential" criterion for cathodic protection.

The diagram used in figure 2 for expressing the electrical characteristics of a galvanic couple has the practical advantage that it may be constructed from results of polarization measurements on individual electrodes. However, in the case of a galvanic cell on closed circuit, the only measurable emf component is (E'_G-E_s). Let us consider what relation it bears to the criteria for cathodic protection. From eq 40a, we have

$$(E'_G-E_s)+I'R_G=(e'_a-E_s)\pm I'_a r_a.$$

When cathodic protection is achieved,

$$(E'_G - E_s) + I'R_G = (E_a - E_s). \qquad (45)$$

If the measured value of $(E'_G - E_s)$ becomes equal to $(E_a - E_s)$, the applied potential exceeds the criterion for cathodic protection by the amount $I'R_G$. A method of measuring R_G (independently of Ir_s) is not yet available. If R_G is negligibly small, the equality $(E_a - E_s) = (E_G - E_s)$ is an accurate criterion of cathodic protection. If R_G is relatively high, the observed value of $(E_G - E_s)$ is not an accurate criterion. This fact indicates the need for a technique by which R_G may be measured.

The relation of E to I (fig. 2) will now be considered. First, if E be increased from $E = E_G$ to $E = E_a$, the liberation of hydrogen may be expected to increase in proportion to the increase in I_c. If E be further increased, $I_a > 0$ and liberation of hydrogen may then be expected to increase in proportion to the increase in $(I_a + I_c)$. If I_a is sufficiently large, the increased rate of evolution of hydrogen above I_p may manifest itself as a discontinuity in the E/I relation. If, instead of hydrogen evolution, some other reduction process occurs, such as reduction of oxygen, of a film, or of some other depolarizer, there may be no evidence of a discontinuity in the E/I relation.

Second, if E be decreased from $E = E_G$ to $E = E_c$, the liberation of hydrogen should decrease in proportion to the decrease in I_c. When I becomes equal to $-I_q$, $I_c = 0$, and liberation of hydrogen should entirely cease. If $-I$ be further increased in the negative direction, either metal will be dissolved or oxygen will be liberated in proportion to $-(I_a + I_c)$. If liberation of oxygen occurs, a discontinuity, even more abrupt than that due to liberation of hydrogen, may be observed.

The effect of any change in values of r_a or r_c may be interpreted from figure 3, *A*. For example, if $(e_a - e_c)$ remains constant, and r_c decreases, then i_a, according to eq 1 must increase. This will increase the numerical value of $-i_a r_a$, and, consequently, E_G will be lowered. If, on the other hand, the cathodic resistance is increased by the presence of a hydrogen film, the accompanying change in resistive potential is in the same direction as an increase in the emf component, e_c, and i_a must decrease. An increase in r_a would result in a lowering of E_G and conversely. It can therefore be seen that an increment or decrement in E (also in E_G) may occur when $E > E_a$, or $E > E_c$, not only as the result of liberation of hydrogen, but also if the anodic or cathodic resistance changes.

VII. Multiple Galvanic Couples

Let us now consider the electrical relations between two galvanic couples (*R*) and (*O*) having different potentials with reference to E_s. For example, in figure 4, E_{GR} may represent the reducing potential and E_{GO}, the oxidizing potential. Such conditions exist on iron in a wet clay where one area is poorly aerated (*O*) and the other is well aerated (*R*). Then

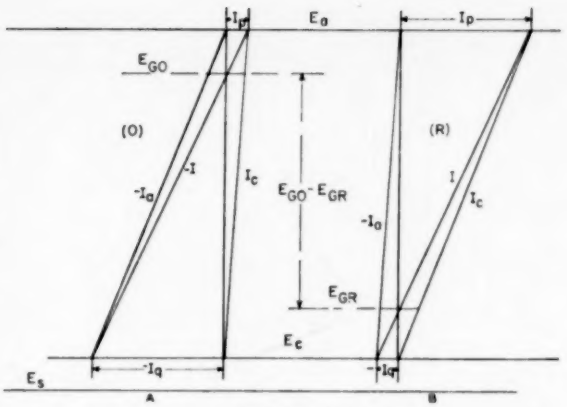

FIGURE 4. *Multiple galvanic couples.*

A, One at oxidizing potential, E_{GO}; B, one at reducing potential, E_{GR}.

$$E_{GO} - E_{GR} = I'(R_{GO} + R_{GR} + r), \qquad (46)$$

where

R_{GO} = the resistance of couple E_{GO}.
R_{GR} = the resistance of couple E_{GR}.
r = internal resistance of the path of current I between the couples (external resistance being neglected).
I' = current supplied by the anodic couple (*O*) to the cathodic couple (*R*).

Couple (*R*) is therefore receiving some cathodic protection at the expense of couple (*O*). Such protection is complete only if I' becomes equal to the I_p, required by the cathodic (*R*) couple.

In this illustration, complete cathodic protection without external current is impossible because it would require the protective current I_p to flow to the potential level E_a, which is higher than that of the current source. Such relations also apply in the field of metal coatings, where the coating may behave like a galvanic couple. If it is anodic toward the base metal, which itself also has a potential level depending on its galvanic-couple properties, then figure 4, shows that cathodic protection is not complete when the coating is perforated. For example, couple (*O*) might represent a zinc coating on iron as the basis metal represented by (*R*).

When an external potential difference E_t is applied to multiple couples, the current distribution to them depends upon their E_G values and the resistances r between them and the auxiliary electrode. Thus, in figure 5, where a metal is represented as having a reducing (*R*) and an oxidizing area (*O*), local currents i flow from the anodes *a* to the cathodes *c*, in each area. In addition, a "long-line" current I′ may flow from the local anodes in the oxidizing area to the local cathodes in the reducing area. If now E_t be gradually increased from zero, current i_{CR} will begin to flow first to the area of lowest potential, that is, to

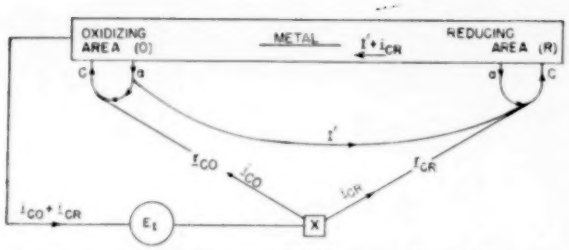

FIGURE 5. *External potential difference, E_t, and current applied to multiple galvanic couples.*

the cathodes of the reducing area. When

$$E_{GR}+i_{CR}\,r_{CR}=E_{GO}, \tag{47}$$

I' becomes zero, and current i_{CO} will begin flowing to the oxidizing area. Consequently, if $r_{CR}\gg r_{CO}$, it may be possible to polarize the oxidizing area (O) to the potential E_a, and achieve cathodic protection there, before it is possible at the reducing area, where a much higher value of E_t may be required for complete cathodic protection. That is, even though the rate of corrosion may be less in the reducing area, a higher value of E_t may be required there for complete protection, than in the oxidizing area. However, it is fortunate that protection in the oxidizing area, where it may be needed most, is the more easily accomplished.

Conversely, if $r_{CR}\ll r_{CO}$, a very high value of i_{CR} may be required to meet the condition represented by eq 47. This is unfortunate, if corrosion is more severe in the oxidizing area.

VIII. Summary

The electrical theory of galvanic couples has been outlined as a basis for an understanding of the polarization of electrodes. It applies to most electrochemical processes including those in batteries, electrodeposition of metals and other electrolytic processes, and corrosion. By the technique of separated electrodes, some of the electrical quantities, which together comprise the characteristics of the galvanic couples, may be measured or computed. In the usual galvanic couple, which is a galvanic cell on closed circuit, electrical measurement is practically limited to determining its potential E_G in reference to an electrode of constant potential E_a. The relations of E_G to applied current I, and applied potential difference E, is developed for a couple having resistance R_G. From these, both "current" and "potential" criteria for cathodic protection are derived. The theory is also applied to multiple galvanic couples at different potentials.

IX. References

[1] W. J. Müller, Korrosion u Metallschutz **13,** 144 (1937).
W. J. Müller, Trans. Electrochem. Soc. **76,** 167 (1939).
G. W. Akimow, Korrosion u Metallschutz **8,** 201 (1932).
G. W. Akimow and N. D. Tomaschow, Korrosion u Metallschutz **13,** 114 (1937).
[2] R. H. Brown and R. B. Mears, Trans. Electrochem. Soc. **81,** 455 (1942).
R. Landau and C. S. Oldach, Trans. Electrochem. Soc. **81,** 521 (1942).
R. Landau, Trans. Electrochem. Soc. **81,** 559 (1942).
J. V. Petrocelli and A. Phillips, Trans. Electrochem. Soc. **85,** 257 (1944).
[3] H. E. Haring and W. Blum, Trans. Electrochem. Soc. **44,** 313 (1923).
T. P. Hoar and J. N. Agar, Faraday Society, Electrode processes, Discussion No. 1, p. 162 (1947).
[4] R. B. Mears, J. Electrochem. Soc. **95,** 1 (1949).
R. B. Mears and R. H. Brown, J. Electrochem. Soc. **97,** 75 (1950).
[5] A. L. Ferguson, Trans. Electrochem. Soc. **76,** 113 (1939).
[6] A. Hickling, Trans. Faraday Soc. **33,** 1540 (1937).
[7] E. Newbury, et al., Trans. Faraday Soc. **43,** 123 (1947).
E. Newbury, Trans. Faraday Soc. **43,** 127 (1947).
[8] H. D. Holler, J. Electrochem. Soc. **97,** 271 (1950).

WASHINGTON, June 1, 1950.

Journal of Research of the National Bureau of Standards Vol. 45, No. 5, November 1950 Research Paper 2149

Study of the System Barium Oxide-Aluminum Oxide-Water at 30° C

By Elmer T. Carlson, Thomas J. Chaconas, and Lansing S. Wells

A study has been made of the action of water and of barium hydroxide solutions on the following compounds: $BaO.Al_2O_3$, $3BaO.Al_2O_3$, $BaO.Al_2O_3.H_2O$, $BaO.Al_2O_3.2H_2O$, $BaO.Al_2O_3.4H_2O$, $BaO.Al_2O_3.7H_2O$, $7BaO.6Al_2O_3.36H_2O$, $2BaO.Al_2O_3.5H_2O$, and $Al_2O_3.3H_2O$. From this, together with a study of precipitation from supersaturated barium aluminate solutions, a diagram of phase equilibria (stable and metastable) at 30° C has been drawn. All the barium aluminates are hydrolyzed by water. The stable solid phases in the system BaO-Al_2O_3-H_2O at 30° C are $Al_2O_3.3H_2O$ (gibbsite), $Ba(OH)_2.8H_2O$, and, over a narrow range, probably $2BaO.Al_2O_3.5H_2O$. With the exception of the two lowest hydrates, all the hydrated barium aluminates possess a range of metastable solubility.

I. Introduction

Although the calcium aluminates, because of their relationship to hydraulic cements, have been the subject of numerous investigations here and elsewhere during recent years, the barium aluminates have been somewhat neglected. The latter, at present, are of limited practical importance. They have been used to some extent in water softening [1],[1] and they may be formed as intermediate products in the conversion of barium minerals to other compounds [2, 3]. It has been shown [4] that $BaO.Al_2O_3$ possesses binding properties. Hunt and Temin [5] reported some experiments with barium aluminate relative to its suitability as a wall plaster for protection against X-rays, but no details as to preparation or composition of the aluminate were given. Attempts have also been made to prepare barium cement, analogous to portland cement, by substituting barium carbonate, in whole or in part, for calcium carbonate in the raw mix. It has recently been reported by Gallo [17] and by Braniski [19] that such substitution is feasible, and that the resulting cement is particularly resistant to sea water and to sulfate waters.

The purpose of the present investigation was twofold. First, to study the hydration of the barium aluminates; and second, to discover what analogies, if any, exist between the aluminates of barium and those of calcium, in the hope that this might aid in clarifying some aspects of the hydration of the calcium aluminates that are not completely understood.

A number of anhydrous barium aluminates are reported in the literature, but only three may be considered definitely established, namely, $3BaO.Al_2O_3$, $BaO.Al_2O_3$, and $BaO.6Al_2O_3$ [6, 7, 8, 9]. The last is believed to be analogous to β-alumina [10, 11], and its exact composition appears to be somewhat in doubt [8]. It was not included in the present study.

The various barium aluminate hydrates have been described in a previous paper [12]. No evidence of any hydrate more basic than $2BaO.Al_2O_3.5H_2O$ was found in the present study, although Beckmann [13] and Maekawa [14, 15] have reported the preparation of a tribarium aluminate hydrate. Neither optical properties nor X-ray diffraction data, however, were given. Malquori [16] has published a phase equilibrium diagram of the system BaO-Al_2O_3-H_2O at 20° C.

The present investigation includes a study of the action of water and of barium hydroxide solutions on the various aluminates and a diagram of phase equilibria in the system at 30° C.

II. Preparation of Compounds

1. Raw Materials

The alumina used in the preparation of the various aluminates was a commercial preparation of gibbsite ($Al_2O_3.3H_2O$) used in the manufacture of glass. It contained about 0.30 percent of Na_2O; other impurities were negligible. Barium was obtained in the form of the carbonate, the hydroxide, and (for a few experiments) the nitrate. These were reagent quality chemicals meeting ACS standards.

2. $BaO.Al_2O_3$

Barium carbonate and gibbsite were blended in the correct proportions, made up to a thin paste with water containing a few drops of a dispersing agent, and thoroughly mixed. The paste was then dried and heated in a platinum dish at 1,400° C for 1 hr. The product was shown by petrographic examination and X-ray diffraction analysis to be essentially monobarium aluminate ($BaO.Al_2O_3$). Treatment with hydrochloric acid left a residue amounting to 0.7 percent, probably consisting of corundum. Attempts to improve the product by grinding and reheating were unsuccessful. Lower burning temperatures were found to be unsatisfactory; for example, a batch heated for 1 hr at 1,300° had an insoluble residue of 8.5 percent.

3. $3BaO.Al_2O_3$

Tribarium aluminate was prepared in the manner described above for monobarium aluminate, with the appropriate change in proportion of raw materials. The mixture was heated in a refractory crucible, as experience showed that platinum was strongly

[1] Figures in brackets indicate the literature references at end of this paper.

attacked. A temperature of 1,300° was found to be adequate to reduce the insoluble residue to 0.1 percent. For some of the tests, the product was subsequently fused in an oxygen blast.

4. $BaO.Al_2O_3.H_2O$

The compound to which the formula $BaO.Al_2O_3.H_2O$ is assigned was prepared hydrothermally. Gibbsite and barium hydroxide were mixed in the required proportion, with added water, and placed in platinum dishes that were then stacked in a bomb-type autoclave and heated in an oven at about 260° C for 7 days. The product in each of the dishes consisted of a hard crust of the desired hydrate surrounding a core of softer material. The latter was shown by X-ray analysis to consist of boehmite ($Al_2O_3.H_2O$). Despite this evidence of the presence of excess alumina, the molar ratio of BaO to Al_2O_3 in the aluminate ranged from 1.10 to 1.14, in agreement with the findings previously published [12]. It appears likely that the actual formula should be $8BaO.7Al_2O_3.7H_2O$ or $9BaO.8Al_2O_3.8H_2O$, but it would be impossible to establish either formula on the basis of present data. All preparations of this hydrate, regardless of changes in raw materials and in conditions of heating, have been more or less contaminated with minute inclusions of some unknown material in the crystals.

5. $BaO.Al_2O_3.2H_2O$

Monobarium aluminate dihydrate, $BaO.Al_2O_3.2H_2O$, was prepared by the method described above for $BaO.Al_2O_3.H_2O$, except that the temperature was held at about 215° C, and the duration of heating was 4 days. The product consisted of well-formed crystals, ranging up to 3 mm in size. Apparently there was a small amount of uncombined alumina, as the molar ratio, $BaO:Al_2O_3:H_2O$, was found to be 0.95:1:1.95, and a slight turbidity remained when the crystals were dissolved in hydrochloric acid.

6. $BaO.Al_2O_3.4H_2O$

Several small batches of monobarium aluminate tetrahydrate, $BaO.Al_2O_3.4H_2O$, prepared by various means, were used in the solubility studies. Some were prepared by allowing $BaO.Al_2O_3.7H_2O$ to stand, in contact with barium aluminate solution, for several months at 30° C. The usual procedure, however, was to raise the temperature to 50° C, whereby the transition period was shortened to a few days. In all cases, the analysis of the products was very close to the theoretical.

7. $BaO.Al_2O_3.7H_2O$ and $7BaO.6Al_2O_3.36H_2O$

Monobarium aluminate heptahydrate ($BaO.Al_2O_3.7H_2O$) and the compound $7BaO.6Al_2O_3.36H_2O$ are close together in composition but quite dissimilar in optical properties. In a previous publication [12], the latter compound was designated $1.1BaO.Al_2O_3.6H_2O$. They were prepared by precipitation from supersaturated solutions. These solutions were prepared in various ways, the most satisfactory being agitation of anhydrous $BaO.Al_2O_3$ with $Ba(OH)_2$ solution for 1 hr, followed by filtration. By this method, solutions containing as high as 35 g of Al_2O_3 per liter were obtained. Solutions of lower concentration were prepared somewhat more conveniently by the action of boiling barium hydroxide solution on gibbsite. Best results were obtained by using 75 g of gibbsite, 125 g of $Ba(OH)_2.8H_2O$, and 1 liter of water, boiling for 1½ hrs, filtering at once, and allowing to cool. Concentrations ranging from 11 to nearly 19 g of Al_2O_3 per liter were obtained by this method.

The course of precipitation varied somewhat with concentration. From highly concentrated solutions, $7BaO.6Al_2O_3.36H_2O$ began to separate almost at once, while from more dilute solutions the start of precipitation was sometimes delayed several days. After a period ranging from a few days to 4 mos, the solid phase underwent a transformation to $BaO.Al_2O_3.7H_2O$, probably by means of re-solution and reprecipitation, as no intermediate forms were observed. This phase change occurred when the concentration of alumina had been lowered to a rather poorly established range indicated by the dotted line in figure 10. $7BaO.6Al_2O_3.36H_2O$ appears to be progressively more stable as the BaO concentration is increased. Solutions having initial concentrations below or only slightly above the dotted line in figure 10 yielded $BaO.Al_2O_3.7H_2O$ as the primary crystalline phase.

Considerable work was done in an effort to establish the composition of these hydrates. In the case of $BaO.Al_2O_3.7H_2O$, analysis of numerous preparations gave values ranging from 6 to 7 moles of H_2O per mole of Al_2O_3. The following experiment throws some light on the question. A preparation of the hydrate was filtered, washed lightly with water, and divided into two portions, one of which was stored in a desiccator over calcium chloride, the other over a saturated solution of ammonium chloride (relative humidity about 79%). After 11 days, both samples had reached constant weight. The molar ratio $H_2O:Al_2O_3$ was 6.25 in the sample dried over calcium chloride, 6.96 in the one dried at the higher humidity. It is inferred that the formula is $BaO.Al_2O_3.7H_2O$, and that 1 molecule of water is so loosely bound that it is easily given off in dry air. The hydrate is completely broken down at 120° C [12].

In the case of the hydrate previously designated $1.1BaO.Al_2O_3.6H_2O$[12], the chief uncertainty is in the ratio of BaO to Al_2O_3. Analysis of numerous preparations gave ratios ranging from 1.12 to 1.16, with no apparent trend toward higher values from solutions richer in BaO (as would be the case if it were a question of solid solution). On the basis of these analyses the formula $7BaO.6Al_2O_3.36H_2O$ has been tentatively assigned to this compound.

8. $2BaO.Al_2O_3.5H_2O$

The most basic of the barium aluminate hydrates found in this study is $2BaO.Al_2O_3.5H_2O$. Several

small batches of this were prepared by boiling a mixture of gibbsite and barium hydroxide solution until crystallization commenced, then filtering the solution and concentrating the filtrate by further boiling. The compound separated out in coarsely crystalline form and was readily washed by decantation. In all cases the analyses were close to the theoretical composition. Attempts to prepare a more basic hydrate were unsuccessful.

III. Reactions with Water and with Barium Hydroxide Solutions

1. General Procedure

Preliminary experiments were performed to ascertain the quantities of the various compounds that might be expected to go into solution. A moderate excess of solid material was then used in subsequent experiments. The compound being studied was ground, if necessary, to 100-mesh or finer, and placed in an Erlenmeyer flask of appropriate size, and the flask was then nearly filled with water or with barium hydroxide solution of the desired strength. The flask was then tightly stoppered, shaken frequently until there was no longer any danger of "setting", and then stored in a cabinet maintained at 30° C. The cabinet was equipped with a recording thermometer. No provision was made for cooling the air, so that in summer the temperature regularly exceeded 30° C. This deviation did not materially affect the experiments described below but of course could not be tolerated for the equilibrium determinations described in section III, 11. Consequently, the latter tests were made during cooler weather. The normal fluctuation in temperature of the air in the cabinet was about ±0.2° C, but it was undoubtedly much less within the flasks.

The flasks were shaken at intervals. From time to time, samples of the clear liquid (5 or 10 ml) were pipetted out and analyzed for Al_2O_3 and BaO by standard analytical methods. Alumina was precipitated by ammonium hydroxide, BaO by sulfuric acid. At the same time, in most cases, a drop of the liquid containing particles of the solid phase or phases present was removed by means of a small pipette, placed on a slide, and examined under the microscope. In this way, phase changes were readily detected.

In experiments dealing with the anhydrous aluminates the reactions were very rapid at first, and the intervals between samplings were too brief to permit clarification by settling. It was therefore necessary to filter off portions of the solutions for analysis. The liquid was filtered through a fritted glass crucible by means of suction and caught in a small test tube inside the filter flask. In this way, the solution was exposed to the air only very briefly, and carbonation was negligible.

In the tables that follow, it will be noted that the values for BaO are given to the nearest tenth of 1 percent, although those for Al_2O_3 are carried to hundredths. In the majority of cases this results in three significant figures, which is believed to be the limit of precision in sampling with a 10-ml pipette. Initial concentration values enclosed in parentheses were calculated from mixing proportions, rather than determined by analysis.

2. $BaO.Al_2O_3$

The results of a series of experiments with monobarium aluminate ($BaO.Al_2O_3$) are given in table 1 and figure 1. Experiments 1-1, 1-2, and 1-3 were designed to show the action of water on the aluminate. To avoid confusion, 1-1 and 1-3 are not included in figure 1. In experiment 1-1, table 1, 15 g of the dry aluminate was shaken with 300 ml of water. The data show that it dissolved rather rapidly, attaining a concentration of 17.40 g of Al_2O_3 per liter at 1 hr. This is equivalent to roughly 85 percent of the material originally present. Precipitation of amorphous hydrated alumina was appreciable at 1 hr, slightly greater at 1 day, and very pronounced at 3 days, as shown by the sharp drop in Al_2O_3 concentration, while the BaO remained practically constant.

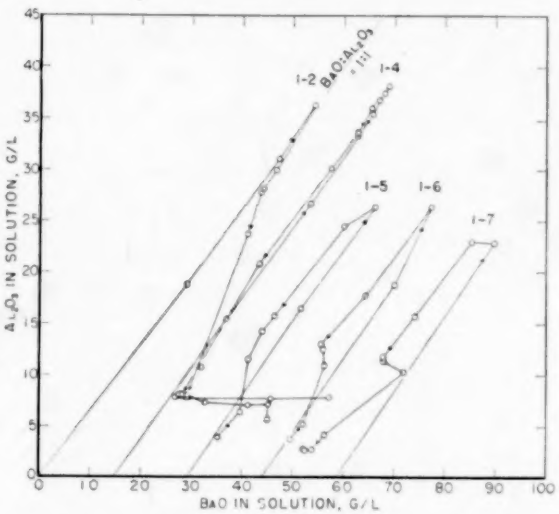

FIGURE 1. *Solubility of* $BaO.Al_2O_3$ *in water and in barium hydroxide solutions at 30° C.*

For the rest of the experiments, the proportion of the anhydrous aluminate was increased to 25 or 30 g/300 ml of water (or solution). In No. 1-2, maximum concentration was reached in 1 hr. The ascending curve in figure 1 has a slope corresponding closely to a molar $BaO:Al_2O_3$ ratio of 1:1, and reaches a point in excess of 36 g of Al_2O_3 per liter. Examination of the table shows that not one but three separate maxima were found, at 1, 2, and 6 hours, respectively. For the sake of clarity some of these points are omitted from the graph in figure 1. The concentration fluctuated up and down, very close to the 1:1 ratio line, during this period. By way of confirma-

TABLE 1. *Solubility of $BaO.Al_2O_3$ in water and in barium hydroxide solutions at 30° C*

Time	Concentration of solution		Solid phases present
	Al_2O_3	BaO	
	g/liter	*g/liter*	
Experiment 1-1 *			
0	0	0	$BaO.Al_2O_3$.
1 hr	17.40	26.5	$BaO.Al_2O_3$+hyd. Al_2O_3.
4 hr	17.65	27.5	
1 day	17.40	27.8	Hyd. Al_2O_3.
3 days	7.30	28.0	Do.
14 days	4.25	27.9	Do.
1 mo	3.80	28.0	Do.
3 mo	3.40	28.2	Do.
Experiment 1-2			
0	0	0	$BaO.Al_2O_3$.
20 min	18.80	29.0	$BaO.Al_2O_3$+hyd. Al_2O_3.
40 min	31.12	47.3	Do.
60 min	36.30	54.4	Do.
80 min	26.62	41.0	Do.
2 hr	30.00	46.7	Do.
3 hr	28.22	44.2	Do.
4 hr	27.10	42.5	Do.
6 hr	27.78	43.7	Do.
1 day	23.70	41.1	Do.
2 days	8.02	29.2	Hyd. Al_2O_3+$BaO.Al_2O_3.7H_2O$.
8 days	7.30	32.8	Do.
1 mo	7.00	41.3	Do.
2 mo	7.10	45.1	Do.
4 mo	5.70	45.1	Hyd. Al_2O_3.
Experiment 1-3 *			
0	0	0	$BaO.Al_2O_3$.
40 min	25.90	39.7	Do.
50 min	27.90	43.0	Do.
60 min	26.70	40.6	Do.
70 min	30.82	46.5	Do.
80 min	29.54	44.1	$BaO.Al_2O_3$+hyd. Al_2O_3.
90 min	30.62	45.5	Do.
100 min	29.38	44.5	Do.
2 hr	28.34	43.2	Do.
3 hr	30.70	46.8	Do.
7 hr	28.36	45.2	Do.
1 day	16.76	32.1	Hyd. Al_2O_3+$BaO.Al_2O_3.7H_2O$.
7 days	7.20	32.5	Do.
1 mo	7.60	41.3	Do.
4 mo	6.10	47.9	Hyd. Al_2O_3+$BaO.Al_2O_3.4H_2O$.
Experiment 1-4			
0	0	14.7	$BaO.Al_2O_3$.
15 min	15.50	36.9	Do.
30 min	26.70	53.4	Do.
45 min	33.30	62.7	Do.
60 min	35.46	65.7	Do.
75 min	36.80	66.9	Do.
90 min	37.50	67.9	Do.
105 min	37.60	67.7	Do.
120 min	36.90	67.0	Do.
150 min	38.20	68.9	Do.
190 min	35.96	65.4	$BaO.Al_2O_3$+$7BaO.6Al_2O_3.36H_2O$.
280 min	33.50	63.0	Do.
330 min	33.70	62.8	Do.
390 min	30.10	57.3	Do.
450 min	20.80	43.4	$7BaO.6Al_2O_3.36H_2O$.
1 day	10.80	31.9	$BaO.Al_2O_3.7H_2O$.
4 days	8.05	28.2	Do.
8 days	8.00	27.4	Do.
19 days	7.78	26.8	Do.
1 mo	7.75	29.3	Do.
2 mo	7.65	45.7	Do.
3 mo	7.85	57.1	$BaO.Al_2O_3.7H_2O$+hyd. Al_2O_3.
Experiment 1-5			
0	0	(29.2)	$BaO.Al_2O_3$.
15 min	16.50	51.7	
30 min	26.40	66.2	$7BaO.6Al_2O_3.36H_2O$.
1 hr	24.50	60.0	Do.
2 hr	15.80	46.4	Do.
4 hr	14.30	44.0	Do.
3 days	11.50	41.2	Do.
10 days	6.30	39.6	$BaO.Al_2O_3.4H_2O$+hyd. Al_2O_3.
1 mo	3.95	35.3	Do.

* Not plotted in figure 1.

TABLE 1. *Solubility of $BaO.Al_2O_3$ in water and in barium hydroxide solutions at 30° C*—Continued

Time	Concentration of solution		Solid phases present
	Al_2O_3	BaO	
	g/liter	*g/liter*	
Experiment 1-6			
0	0	(43.9)	$BaO.Al_2O_3$.
15 min	18.84	70.1	
30 min	26.40	77.3	$7BaO.6Al_2O_3.36H_2O$.
1 hr	17.90	64.3	
2 hr	13.10	55.5	$7BaO.6Al_2O_3.36H_2O$.
4 hr	12.50	55.9	
3 days	10.86	56.2	$7BaO.6Al_2O_3.36H_2O$+$BaO.Al_2O_3.4H_2O$.
10 days	5.25	52.0	$BaO.Al_2O_3.4H_2O$.
1 mo	3.81	49.5	Do.
Experiment 1-7			
0	0	(58.5)	$BaO.Al_2O_3$.
15 min	22.86	89.7	
30 min	23.00	85.3	$7BaO.6Al_2O_3.36H_2O$.
1 hr	15.70	74.0	
2 hr	11.80	67.9	$7BaO.6Al_2O_3.36H_2O$.
4 hr	11.40	67.8	
3 days	10.34	71.9	$BaO.Al_2O_3.4H_2O$+$7BaO.6Al_2O_3.36H_2O$.
10 days	4.23	56.3	$BaO.Al_2O_3.4H_2O$+$Ba(OH)_2.8H_2O$.
1 mo	2.85	53.8	Do.
2 mo	2.77	52.5	
4 mo	2.88	52.0	$BaO.Al_2O_3.4H_2O$.
5 mo	2.75	52.3	Do.

tion of this unexpected finding, the experiment was repeated, with samples taken at shorter intervals (experiment No. 1-3 in table 1). This time four maxima were found, at 50, 70, and 90 min., and 3 hr, respectively, and again the concentration varied up and down along the 1:1 line. Although the actual mechanism of this process could not be determined, a partial explanation may be advanced. When the anhydrous aluminate is agitated with water it dissolves rapidly at first, but the rate of solution decreases as the concentration rises and the amount of undissolved solid diminishes. Precipitation of a new solid phase, or phases, commences as soon as a sufficiently high concentration has been reached and proceeds at an increasing rate for some time. Eventually the point is reached at which the two processes of solution and precipitation are equal. For some reason, in these experiments, they failed to remain in balance; instead, first one and then the other predominated. The fact that the concentration moved downward as well as upward along the 1:1 ratio line suggests that the precipitating phase must have been $BaO.Al_2O_3.7H_2O$. None of this phase was actually observed at this stage, but the undissolved grains of $BaO.Al_2O_3$ were seen to be coated with a thin layer of extremely fine birefringent crystals, too small for identification. It is assumed that these were $BaO.Al_2O_3.7H_2O$. The subsequent departure from the 1:1 line is reflected in an increase in the proportion of hydrated Al_2O_3 in the precipitate. The sudden break in the direction of high BaO indicates that some of the precipitated $BaO.Al_2O_3.7H_2O$ has been hydrolyzed, with precipitation of hydrated Al_2O_3. This process continued for 2 mo or longer until no $BaO.Al_2O_3.7H_2O$ remained. The final vertical portion of the curve indicates that Al_2O_3 was still coming

out of solution when the experiment was terminated.

Experiments 1-4 to 1-7 in this series were designed to determine the action of barium hydroxide solutions on monobarium aluminate. By referring to the table and the figure it may be seen that the aluminate went into solution in the 1:1 molar ratio in all cases, and that the first new phase to be precipitated was $7BaO.6Al_2O_3.36H_2O$. This compound, because of its needle-like crystalline habit, formed a voluminous precipitate with the result that the contents of the flasks acquired a thick, mushy consistency. In their subsequent behavior, these preparations differed. In experiment 1-4, the precipitate was transformed to $BaO.Al_2O_3.7H_2O$ within 1 day. This, in turn, showed evidence of hydrolysis after 3 mos. It may be noted parenthetically, that in this experiment, as in 1-2, more than one maximum was observed, also that some of the points in the table have been omitted from the graph for the sake of clarity. In 1-5 and 1-6, the precipitate was transformed to $BaO.Al_2O_3.4H_2O$, without intermediate formation of the heptahydrate. There is also evidence of a shift in concentration of the solution in the direction of increasing BaO, corresponding to the liberation of excess BaO as the 7:6:36 hydrate was converted to the 1:1:4. Experiment 1-7 followed a similar course, but with the addition of another precipitated phase, $Ba(OH)_2.8H_2O$, first noted after 10 days. The curve in this case shifts toward the left, as would be expected.

A close study of the curves in figure 1 reveals that the ascending branch does not indicate a molar ratio of exactly 1:1, although it is very close to that value in the case of No. 1-2. The others become progressively steeper as we go toward the high BaO side of the diagram, reaching the $BaO:Al_2O_3$ ratio of 0.91:1 for No. 1-7. This is due to the fact that the samples for analysis were measured volumetrically, and that no correction was made for the increase in volume of the barium hydroxide solution resulting from addition of the solid aluminate. This increase was found to be of the right order of magnitude to account for the departures from the theoretical 1:1 slope.

The process of solution to form a supersaturated solution, followed by precipitation of a different solid phase, is characteristic of binding agents, such as portland cement and gypsum plaster. Other investigators [4] have reported that monobarium aluminate is capable of setting, and this fact was confirmed during the course of the present study. Some of the aluminate was mixed with sufficient water to make it workable, molded into a briquet, and allowed to stand in a moist closet. A moderate amount of heat was evolved shortly after molding. After 5 hr, the briquet was firm enough to be removed from the mold. After standing moist overnight and then being allowed to dry, the specimen was quite hard, but did not have enough strength to permit an actual test to be made. The material expanded about 10 percent during setting. The set product contained considerable isotropic material, probably hydrated alumina. X-ray analysis [2] showed the presence of a small amount of $BaO.Al_2O_3.7H_2O$. These observations, together with the fact that the set material is readily attacked by water, make it appear unlikely that monobarium aluminate, in itself, would have any value as a cementitious material.

3. $3BaO.Al_2O_3$

Tribarium aluminate, $3BaO.Al_2O_3$, reacts violently with water with the evolution of considerable heat. The course of solution and precipitation when 50 g of this compound was shaken with 300 ml of water is shown in figure 2 and table 2. It may be seen that the maximum concentration was reached in 4 min. At this time, barium hydroxide ($Ba(OH)_2.8H_2O$) precipitated out, followed shortly by

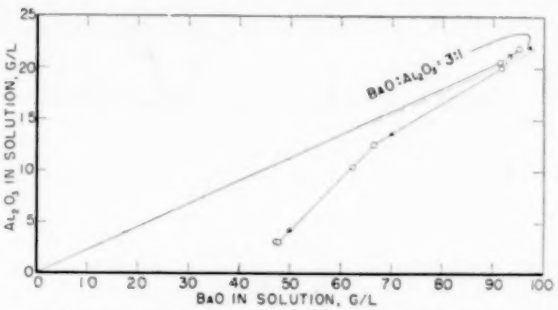

FIGURE 2. *Solubility of* $3BaO.Al_2O_3$ *in water at 30° C.*

$7BaO.6Al_2O_3.36H_2O$. Eventually, the predominant solid phase was found to be $2BaO.Al_2O_3.5H_2O$ in a very finely divided form not hitherto observed. These results were confirmed by two similar experiments, in one of which the tribarium aluminate previously had been heated to the fusion point and reground. The results differed in minor details, but were in essential agreement. The fused material reacted slightly less rapidly than did the anhydrous aluminate burned at 1,300°.

TABLE 2. *Solubility of* $3BaO.Al_2O_3$ *in water at 30° C*

Time	Concentration of solution		Solid phases present
	Al_2O_3	BaO	
Experiment 2-1			
	g/liter	*g/liter*	
0	0	0	$3BaO.Al_2O_3$.
1 min	20.60	91.3	
4 min	21.90	95.1	$3BaO.Al_2O_3+Ba(OH)_2.8H_2O$.
8 min	20.04	91.6	
1 hr	12.60	66.4	$7BaO.6Al_2O_3.36H_2O+Ba(OH)_2.8H_2O$.
1 day	10.35	62.2	$7BaO.6Al_2O_3.36H_2O+2BaO.Al_2O_3.5H_2O$.
1 mo	3.15	47.8	$2BaO.Al_2O_3.5H_2O$.
4 mo	3.10	47.2	

[2] X-ray diffraction patterns referred to in this paper were made by Barbara Sullivan, of the Constitution and Microstructure Section of this Bureau.

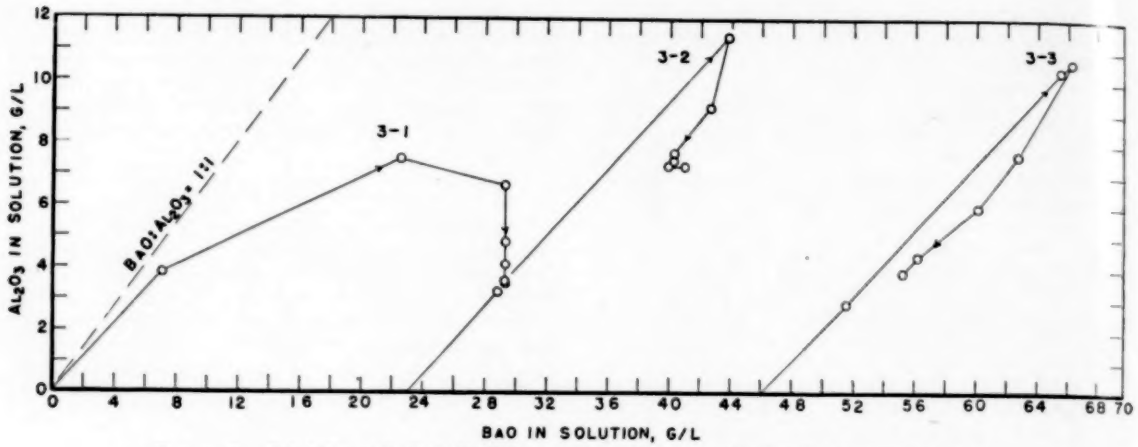

FIGURE 3. *Solubility of* $BaO.Al_2O_3.H_2O$ *in water and in barium hydroxide solutions at 30° C.*

Inasmuch as the solution of this aluminate in water rapidly reaches a concentration at which barium hydroxide is precipitated, it appeared that little could be learned by studying its reaction with barium hydroxide solutions; hence no tests of this kind were made.

The capacity of tribarium aluminate for absorbing moisture is illustrated by the following experiment. A 5-g sample of the freshly burned aluminate was placed in a crucible and confined over water in a covered glass jar at room temperature and weighed at intervals. In 6 days it took up moisture equivalent to 13 moles of H_2O per mole of $3BaO.Al_2O_3$. From then on the increase in weight proceeded more slowly, but when the test was terminated at the end of 5 mo, the total water that had been taken up was equivalent to 43 moles of H_2O per mole of $3BaO.Al_2O_3$. This is considerably more than would be required to hydrolyze the compound completely to $Ba(OH)_2.8H_2O$ and $Al_2O_3.3H_2O$.

4. $BaO.Al_2O_3.H_2O$

A series of three tests was made with $BaO.Al_2O_3.H_2O$, using pure water and half-saturated and saturated solutions of barium hydroxide. The results are given in table 3 and plotted in figure 3. Ten grams of the crystalline hydrate, ground to pass a No. 100 sieve, was added to 200 ml of solution. The rate of solution is seen to be relatively slow. After 5 days, the material in No. 3-1 had been converted to hydrated alumina, and the others to $7BaO.6Al_2O_3.36H_2O$. Further phase changes occurred on longer standing, as indicated in the table, and it may be assumed that if the mixtures had been kept still longer their behavior would have been essentially similar to that described below for solutions of comparable concentrations.

TABLE 3. *Solubility of* $BaO.Al_2O_3.H_2O$ *in water and barium hydroxide solutions at 30° C.*

Time	Concentration of solution		Solid phases present
	Al_2O_3	BaO	
Experiment 3-1			
	g/liter	*g/liter*	
0	0	0	$BaO.Al_2O_3.H_2O$.
5 hr	3.85	7.1	$BaO.Al_2O_3.H_2O$+hyd. Al_2O_3.
5 days	7.50	22.5	Hydrated Al_2O_3.
13 days	6.57	29.3	Do.
24 days	4.85	29.3	Do.
1 mo	4.13	29.3	Do.
2 mo	3.60	29.3	Do.
3 mo	3.45	29.3	Do.
Experiment 3-2			
0	0	(23)	$BaO.Al_2O_3.H_2O$.
5 hr	3.27	28.8	
5 days	11.45	43.8	$7BaO.6Al_2O_3.36H_2O$.
13 days	9.20	42.6	$BaO.Al_2O_3.7H_2O$.
24 days	7.75	40.3	Do.
1 mo	7.48	40.3	$BaO.Al_2O_3.7H_2O$+$BaO.Al_2O_3.4H_2O$.
2 mo	7.30	39.9	Do.
3 mo	7.30	41.0	Do.
Experiment 3-3			
0	0	(46)	$BaO.Al_2O_3.H_2O$.
5 hr	2.85	51.6	
5 days	10.33	65.5	$7BaO.6Al_2O_3.36H_2O$.
13 days	10.63	66.2	$7BaO.6Al_2O_3.36H_2O$+$BaO.Al_2O_3.4H_2O$.
24 days	7.65	62.7	$BaO.Al_2O_3.4H_2O$.
1 mo	6.01	60.1	Do.
2 mo	4.40	56.2	Do.
3 mo	3.85	55.2	$BaO.Al_2O_3.4H_2O$+hyd. Al_2O_3.

5. $BaO.Al_2O_3.2H_2O$

A series of three experiments parallel to those described in the previous section was made with the dihydrate. The results are shown in table 4 and figure 4. Again we find that the rate of solution

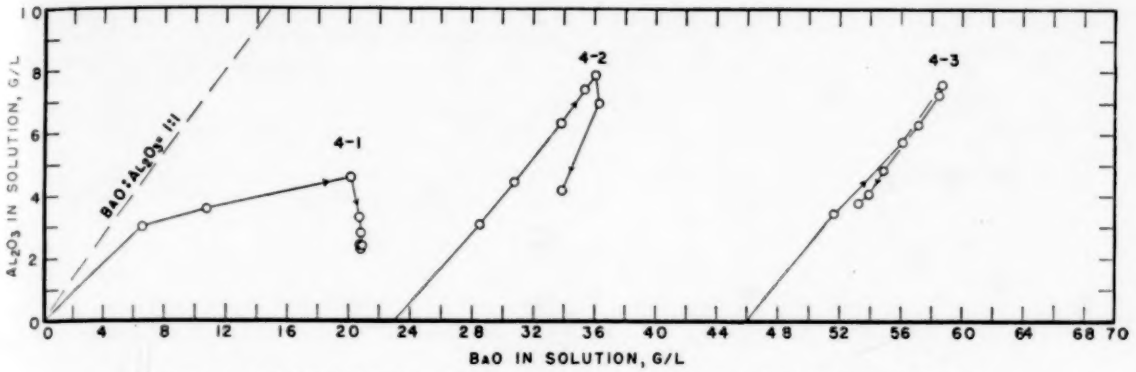

FIGURE 4. *Solubility of* $BaO.Al_2O_3.2H_2O$ *in water and in barium hydroxide solutions at 30° C.*

was relatively slow, and that the sample mixed with pure water eventually precipitated hydrated alumina. Sample 4-2, however, went into solution slowly, and no new phase was observed until after 2 mo had elapsed. Then the tetrahydrate appeared, and gradually increased at the expense of the dihydrate. Sample No. 4-3 dissolved somewhat more rapidly, and the original material had all disappeared within 1 mo, with precipitation of the tetrahydrate. A small amount of hydrated alumina was observed at the later ages in experiments 4-2 and 4-3.

TABLE 4. *Solubility of* $BaO.Al_2O_3.2H_2O$ *in water and in barium hydroxide solutions at 30° C*

Time	Concentration of solution		Solid phases present
	Al_2O_3	BaO	
Experiment 4-1			
	g/liter	*g/liter*	
0	0	0	$BaO.Al_2O_3.2H_2O$.
5 hr	3.00	6.6	Do.
5 days	3.55	10.8	Do.
13 days	4.58	20.1	$BaO.Al_2O_3.2H_2O$+hyd. Al_2O_3.
24 days	3.25	20.7	Hydrated Al_2O_3.
1 mo	2.75	20.8	Do.
2 mo	2.40	20.7	Do.
3 mo	2.40	20.9	Do.
4 mo	2.28	20.8	Do.
Experiment 4-2			
0	0	(23)	$BaO.Al_2O_3.2H_2O$.
5 hr	3.05	28.5	Do.
5 days	4.45	30.8	Do.
13 days	6.30	33.8	Do.
24 days	7.40	35.3	Do.
1 mo	7.75	35.9	Do.
2 mo	7.85	36.0	$BaO.Al_2O_3.2H_2O$+$BaO.Al_2O_3.4H_2O$.
3 mo	7.00	36.3	Do.
4 mo	4.18	33.9	$BaO.Al_2O_3.4H_2O$+hyd. Al_2O_3.
Experiment 4-3			
0	0	(46)	$BaO.Al_2O_3.2H_2O$.
5 hr	3.43	51.7	Do.
5 days	5.73	56.1	Do.
13 days	7.58	58.7	Do.
24 days	7.25	58.4	$BaO.Al_2O_3.4H_2O$+$BaO.Al_2O_3.2H_2O$.
1 mo	6.32	57.1	$BaO.Al_2O_3.4H_2O$.
2 mo	4.85	54.9	$BaO.Al_2O_3.4H_2O$+hyd. Al_2O_3.
3 mo	4.07	53.9	Do.
4 mo	3.78	53.2	$BaO.Al_2O_3.4H_2O$+hyd. Al_2O_3.

6. $BaO.Al_2O_3.4H_2O$

Preliminary experiments showed that $BaO.Al_2O_3.4H_2O$, unlike the compounds previously discussed, exists as a stable or metastable phase in the system BaO-Al_2O_3-H_2O at room temperature. A larger number of mixtures was therefore made, in order to ascertain the location of the solubility curve. The results obtained with this hydrate are given in table 5 and plotted in figure 5. The rate of solution of this hydrate was relatively slow. The sample in contact with distilled water showed evidence of hydrolysis at 1 day, and hydrated alumina was observed after 2 days. After about a month, all of the BaO was in solution. Precipitation of hydrated alumina continued, accompanied by a drop in concentration of alumina in solution.

TABLE 5. *Solubility of* $BaO.Al_2O_3.4H_2O$ *in water and in barium hydroxide solutions at 30° C*

Time	Concentration of solution		Solid phases present
	Al_2O_3	BaO	
Experiment 5-1			
	g/liter	*g/liter*	
0	0	0	$BaO.Al_2O_3.4H_2O$.
1 day	1.05	2.3	Do.
2 days	1.73	5.1	$BaO.Al_2O_3.4H_2O$+hyd. Al_2O_3.
5 days	2.00	8.5	Do.
12 days	2.40	12.4	
19 days	2.50	14.5	
26 days	2.48	15.1	$BaO.Al_2O_3.4H_2O$+hyd Al_2O_3.
40 days	2.05	15.5	Hyd. Al_2O_3.
2 mo	1.98	15.5	Do.
3 mo	1.90	15.7	Do.
4 mo	1.70	15.1	Do.
5 mo	1.55	14.9	Do.
7 mo	1.40	14.6	Do.
Experiment 5-2			
0	0	(7.6)	$BaO.Al_2O_3.4H_2O$.
1 day	0.30	8.3	Do.
2 days	1.15	9.5	Do.
5 days	1.70	10.3	$BaO.Al_2O_3.4H_2O$+hyd. Al_2O_3.
12 days	2.73	11.9	
19 days	3.00	12.5	$BaO.Al_2O_3.4H_2O$+hyd. Al_2O_3.
26 days	3.03	12.6	Do.
40 days	2.81	13.5	Do.
2 mo	2.89	14.5	Do.
3 mo	3.00	17.4	Do.
4 mo	2.80	19.4	Do.
5 mo	2.70	21.2	Do.
7 mo	2.60	23.4	Hyd. Al_2O_3.
9 mo	2.00	22.9	Do.

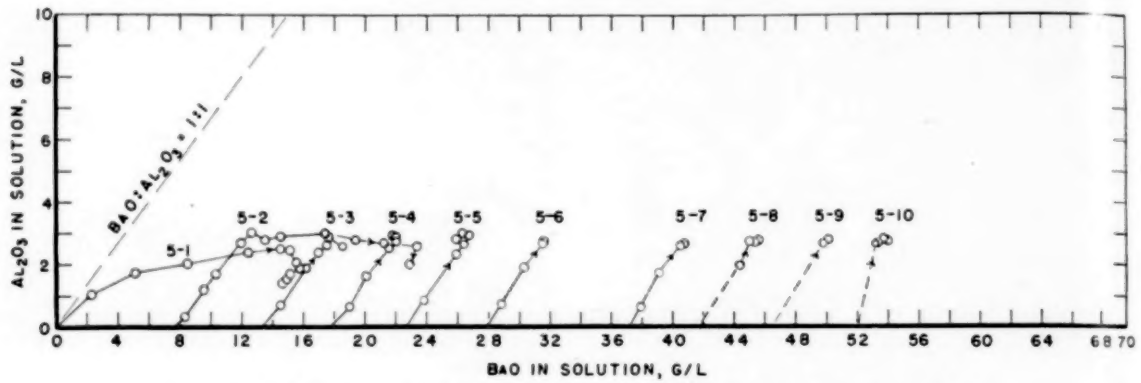

FIGURE 5. *Solubility of* $BaO.Al_2O_3.4H_2O$ *in water and in barium hydroxide solutions at 30° C.*

TABLE 5. *Solubility of* $BaO.Al_2O_3.4H_2O$ *in water and in barium hydroxide solutions at 30° C*—Continued

Time	Concentration of solution		Solid phases present [a]
	Al_2O_3	BaO	
Experiment 5-3			
	g/liter	*g/liter*	
0	0	(13.3)	$BaO.Al_2O_3.4H_2O$.
1 day	0.67	14.5	Do.
6 days	1.75	15.9	Do.
15 days	2.40	17.0	Do.
1 mo	2.60	17.5	Do.
2 mo	2.85	17.6	$BaO.Al_2O_3.4H_2O$+hyd. Al_2O_3.
3 mo	2.87	17.5	Do.
4 mo	2.85	17.6	Do.
5 mo	2.75	17.7	Do.
8 mo	2.90	17.9	Do.
14 mo	2.51	18.5	Hyd. Al_2O_3.
Experiment 5-4			
0	0	(17.7)	$BaO.Al_2O_3.4H_2O$.
1 day	0.64	19.0	Do.
6 days	1.65	20.1	Do.
15 days	2.50	21.6	Do.
1 mo	2.75	22.0	Do.
2 mo	2.80	22.0	$BaO.Al_2O_3.4H_2O$+hyd. Al_2O_3.
3 mo	2.82	22.1	Do.
4 mo	2.82	22.0	Do.
5 mo	2.75	22.0	Do.
8 mo	2.85	21.8	
14 mo	2.85	22.0	$BaO.Al_2O_3.4H_2O$+hyd. Al_2O_3.
Experiment 5-5			
0	0	(22.7)	$BaO.Al_2O_3.4H_2O$.
1 day	0.85	23.8	Do.
2 days	2.00		Do.
12 days	2.35	25.9	Do.
19 days	2.65	26.4	Do.
26 days	2.77	26.5	$BaO.Al_2O_3.4H_2O$+hyd. Al_2O_3.
33 days	2.90	26.5	Do.
40 days	2.95	26.7	Do.
2 mo	3.06	26.3	Do.
3 mo	2.80	26.6	Do.
4 mo	2.90	26.4	Do.
6 mo	2.83	25.8	$BaO.Al_2O_3.4H_2O$+hyd. Al_2O_3.
7 mo	2.85	25.9	Do.
Experiment 5-6			
0	0	(27.9)	$BaO.Al_2O_3.4H_2O$.
1 day	0.73	28.8	Do.
6 days	1.92	30.3	Do.
15 days	2.70	31.5	Do.
1 mo	2.75	31.6	Do.
2 mo	2.75	31.6	$BaO.Al_2O_3.4H_2O$+hyd. Al_2O_3.
3 mo	2.77	31.6	Do.

TABLE 5. *Solubility of* $BaO.Al_2O_3.4H_2O$ *in water and in barium hydroxide solutions at 30° C*—Continued

Time	Concentration of solution		Solid phases present [a]
	Al_2O_3	BaO	
Experiment 5-7			
	g/liter	*g/liter*	
0	0	(37.2)	$BaO.Al_2O_3.4H_2O$.
1 day	0.65	37.9	Do.
6 days	1.74	39.1	Do.
15 days	2.60	40.5	Do.
1 mo	2.70	40.8	Do.
2 mo	2.68	40.7	$BaO.Al_2O_3.4H_2O$+hyd. Al_2O_3.
3 mo	2.75	40.7	Do.
Experiment 5-8			
0	0	(41.7)	$BaO.Al_2O_3.4H_2O$.
1 day	0.73	[a] 42.7	
6 days	2.00	44.4	$BaO.Al_2O_3.4H_2O$.
15 days	2.70	45.3	Do.
1 mo	2.75	45.6	Do.
2 mo	2.75	45.5	$BaO.Al_2O_3.4H_2O$+hyd. Al_2O_3.
3 mo	2.70	45.4	Do.
4 mo	2.80	45.3	Do.
5 mo	2.75	45.0	Do.
Experiment 5-9			
0	0	(46.5)	$BaO.Al_2O_3.4H_2O$.
1 day	0.81	[a] 42.0	
6 days	2.00	[a] 47.8	$BaO.Al_2O_3.4H_2O$+$Ba(OH)_2.8H_2O$.
15 days	2.70	49.8	Do.
1 mo	2.80	50.1	Do.
2 mo	2.70	49.9	Do.
3 mo	2.75	49.9	Do.
Experiment 5-10			
0	0	[a] (52.0)	$BaO.Al_2O_3.4H_2O$.
1 day	0.96	[a] 42.2	
7 days	2.20	[a] 50.1	$BaO.Al_2O_3.4H_2O$+$Ba(OH)_2.8H_2O$.
16 days	2.90	52.7	Do.
1 mo	2.70	53.3	Do.
2 mo	2.68	53.1	$BaO.Al_2O_3.4H_2O$+$Ba(OH)_2.8H_2O$+hyd. Al_2O_3.
3 mo	2.86	53.7	Do.
4 mo	2.78	54.0	Do.

[a] Prepared when room temperature was below 30°, resulting in some precipitation of $Ba(OH)_2.8H_2O$ which redissolved very slowly. These points are not plotted in figure 5.

In test No. 5-2, the material appeared to dissolve congruently at first, but hydrated alumina was observed after 5 days. After about a month, maximum concentration of Al_2O_3 in solution was attained. Thereafter, BaO continued to dissolve, leaving a residue of hydrated alumina. In many cases the original form of the crystals was maintained, but the gradual disappearance of birefringence and the

loss of transparency gave evidence of the decomposition. After 7 mo none of the original crystalline material was observed.

All of the other samples went into solution in a molar ratio of 1:1 ($BaO:Al_2O_3$), attaining an apparently stable condition of equilibrium. Nevertheless, hydrated alumina appeared eventually in all the flasks, indicating progressive hydrolysis. As would be expected, this reaction occurred more rapidly in the less basic solutions, but it was apparent even in those in contact with solid barium hydroxide. This will be discussed further in section III, 13.

7. $BaO.Al_2O_3.7H_2O$

Although less stable than the tetrahydrate, the heptahydrate lasts long enough to permit a determination of its metastable solubility, and numerous tests were made for this purpose. The results obtained from some of these are given in table 6 and figure 6. In water (No. 6-1) this compound hy-

TABLE 6. *Solubility of* $BaO.Al_2O_3.7H_2O$ *in water and in barium hydroxide solutions at 30° C*

Time	Concentration of solution		Solid phases present
	Al_2O_3	BaO	
Experiment 6-1			
	g/liter	*g/liter*	
0	0	0	$BaO.Al_2O_3.7H_2O$.
30 min	1.82	2.74	Do.
2 hr	2.80	4.14	Do.
17 hr	2.60	6.37	$BaO.Al_2O_3.7H_2O$+hyd. Al_2O_3.
2 days	3.30	17.2	Hyd. Al_2O_3.
5 days	2.31	17.3	Do.
13 days	1.90	17.1	Do.
2 mo	1.63	17.2	Do.
3 mo	1.45	16.3	Do.
6 mo	1.30	15.7	Do.
Experiment 6-2			
0	0	9.7	$BaO.Al_2O_3.7H_2O$.
10 min	4.20	15.4	Do.
1 day	6.60	19.1	Do.
2 days	7.10	19.5	Do.
4 days	7.46	19.8	Do.
7 days	7.42	20.2	
16 days	7.00	27.3	Hyd. Al_2O_3.
1 mo	3.60	27.6	Do.
2 mo	2.85	27.8	Do.
3 mo	2.55	27.4	Do.
4 mo	2.45	27.8	Do.

TABLE 6. *Solubility of* $BaO.Al_2O_3.7H_2O$ *in water and in barium hydroxide solutions at 30° C*—Continued

Time	Concentration of solution		Solid phases present
	Al_2O_3	BaO	
Experiment 6-3			
	g/liter	*g/liter*	
0	0	18.5	$BaO.Al_2O_3.7H_2O$.
10 min	5.15	25.4	Do.
1 hr	5.75	26.1	Do.
1 day	6.80	27.5	Do.
4 days	7.00	27.4	Do.
13 days	7.15	28.3	
1 mo	7.16	27.8	$BaO.Al_2O_3.7H_2O$+hyd. Al_2O_3.
2 mo	7.05	29.6	
3 mo	3.70	33.0	Hyd. Al_2O_3.
4 mo	3.27	33.0	Do.
Experiment 6-4			
0	0	25.3	$BaO.Al_2O_3.7H_2O$.
15 min	2.70	28.3	
1 day	4.35	30.2	
2 days	6.65	33.6	
6 days	6.70	33.5	
15 days	7.45	34.5	$BaO.Al_2O_3.7H_2O$+hyd. Al_2O_3.
2 mo	7.28	34.5	Do.
3 mo	7.25	34.3	$BaO.Al_2O_3.7H_2O$+hyd. Al_2O_3+$BaO.Al_2O_3.4H_2O$.
Experiment 6-5			
0	0	32.3	$BaO.Al_2O_3.7H_2O$.
10 min	5.64	39.2	Do.
1 hr	6.42	40.9	Do.
1 day	7.45	41.6	Do.
6 days	7.55	41.3	Do.
15 days	7.35	41.2	
1 mo	7.70	41.5	$BaO.Al_2O_3.7H_2O$.
3 mo	7.20	41.6	$BaO.Al_2O_3.7H_2O$+$BaO.Al_2O_3.4H_2O$.
Experiment 6-6			
0	0	(40.0)	$BaO.Al_2O_3.7H_2O$.
5 days	6.70	49.7	Do.
1 mo	7.10	50.1	Do.
2 mo	7.30	50.5	Do.
3 mo	7.14	50.5	Do.
4 mo	7.00	50.2	Do.
5 mo	7.00	50.3	Do.
6 mo	7.08	50.2	Do.
Experiment 6-7			
0	0	47.1	$BaO.Al_2O_3.7H_2O$.
1 hr	4.35	52.0	Do.
1 day	4.86	52.7	Do.
6 days	7.22	54.1	Do.
15 days	7.75	55.1	Do.
1 mo	7.60	55.4	Do.
4 mo	7.60	54.5	Do.

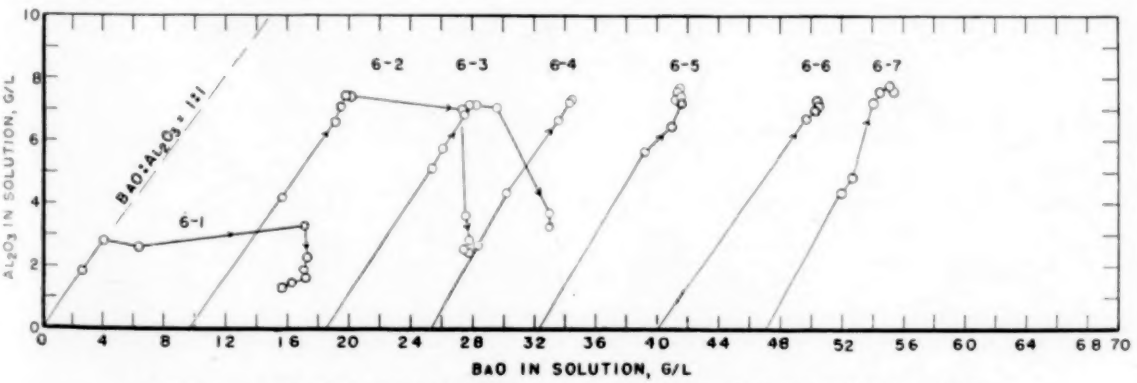

FIGURE 6. *Solubility of* $BaO.Al_2O_3.7H_2O$ *in water and in barium hydroxide solutions at 30° C.*

drolyzed rapidly, with precipitation of hydrated alumina. The approximately horizontal portion of the curve indicates that solution and precipitation proceeded simultaneously until the hydrate was exhausted.

In experiment 6-2, the least basic of the barium hydroxide solutions used, hydrolysis was not apparent until after 7 days. The concentration, meanwhile, had remained approximately constant for several days, and this concentration was taken as the metastable solubility of $BaO.Al_2O_3.7H_2O$ at this point. The subsequent behavior of the mixture was similar to that of 6-1. Experiment 6-3 followed the pattern of 6-2, except that the hydrolysis in this case did not proceed rapidly until after 2 mo. All the mixtures in the more basic region reached a condition of equilibrium that persisted until the experiment was terminated. It will be shown below, however, that this equilibrium is actually metastable, and that $BaO.Al_2O_3.7H_2O$ is not the final reaction product.

8. $7BaO.6Al_2O_3.36H_2O$

The results of experiments with $7BaO.6Al_2O_3.36H_2O$ are given in table 7 and figure 7. In general, this compound behaves much as does the heptahydrate, but it is more soluble and considerably less stable. In experiment 7-1, the hydrate dissolved almost completely in water within 10 min, with simultaneous precipitation of amorphous hydrated alumina. The latter process continued at a diminishing rate, and equilibrium was not reached even after several months. In 7-2 the hydrolysis was much slower, and some of the original hydrate was still present after 4 days. At 8 days, however, the remainder of the hydrate was found to have been transformed into $BaO.Al_2O_3.7H_2O$. The latter phase soon disappeared, and for some time the precipitation of alumina continued, as evidenced by the vertical portion of the curve. At 3 mo., $BaO.Al_2O_3.4H_2O$ was first observed as a solid phase, and there is an accompanying break in the curve toward the left.

TABLE 7. *Solubility of* $7BaO.6Al_2O_3.36H_2O$ *in water and in barium hydroxide solutions at 30° C*

Time	Concentration of solution		Solid phases present
	Al_2O_3	BaO	
Experiment 7-1			
	g/liter	*g/liter*	
0	0	0	$7BaO.6Al_2O_3.36H_2O$.
10 min	8.80	16.6	$7BaO.6Al_2O_3.36H_2O$+hyd. Al_2O_3.
2 hr	9.30	17.5	Hyd. Al_2O_3.
1 day	9.30	19.4	Do.
2 days	6.60	19.4	Do.
9 days	3.80	19.4	Do.
19 days	3.00	19.1	Do.
1 mo	2.75	19.0	Do.
2 mo	2.43	18.6	Do.
3 mo	2.35	18.6	Do.
4 mo	2.20	18.8	Do.
5 mo	1.95	18.5	Do.
7 mo	1.95	18.4	Do.
Experiment 7-2			
0	0	7.8	$7BaO.6Al_2O_3.36H_2O$.
13 min	9.40	24.7	
2 hr	11.40		$7BaO.6Al_2O_3.36H_2O$+hyd. Al_2O_3.
1 day	11.80	29.5	Do.
4 days	10.86	29.6	Do.
8 days	9.00	29.8	$BaO.Al_2O_3.7H_2O$+hyd. Al_2O_3.
18 days	6.60	29.4	Hyd. Al_2O_3.
1 mo	5.40	29.5	Do.
2 mo	4.35	28.5	Do.
3 mo	3.75	28.0	Hyd. Al_2O_3+$BaO.Al_2O_3.4H_2O$ (trace).
4 mo	3.55	29.1	Do.
5 mo	3.30	29.0	Do.
7 mo	3.00	28.8	Hyd. Al_2O_3.
Experiment 7-3			
0	0	15.2	$7BaO.6Al_2O_3.36H_2O$.
10 min	6.34	25.7	Do.
1 hr	8.90	29.2	Do.
1 day	12.10	34.3	Do.
2 days	12.20	35.2	Do.
5 days	12.60	36.7	
14 days	7.93	34.4	$BaO.Al_2O_3.7H_2O$+hyd. Al_2O_3.
1 mo	7.05	36.6	Do.
2 mo	6.75	41.8	Hyd. Al_2O_3+$BaO.Al_2O_3.4H_2O$ (trace).
3 mo	5.00	42.3	Do.
4 mo	4.30	42.1	Do.
6 mo	3.95	41.7	Do.

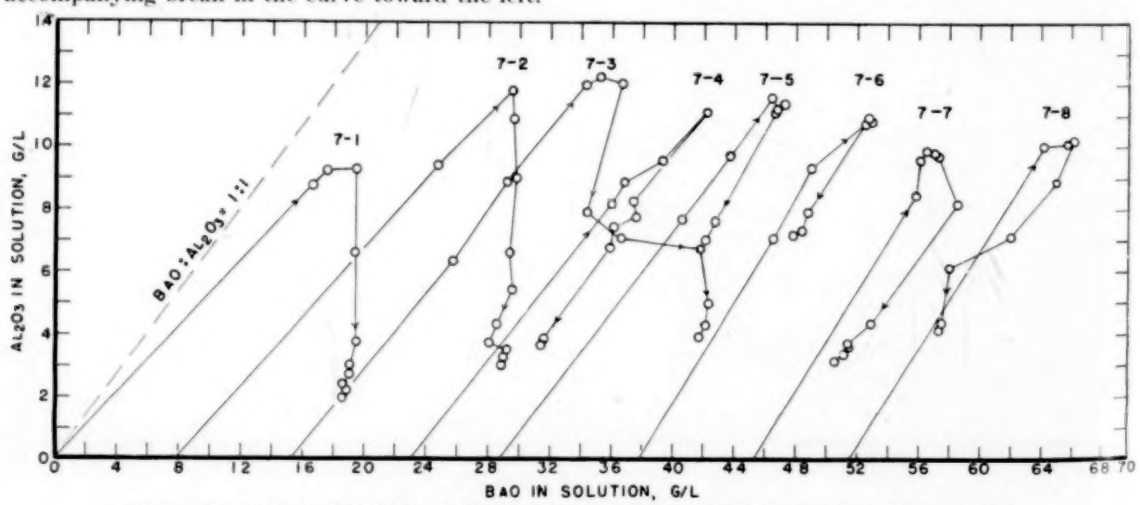

FIGURE 7. *Solubility of* $7BaO.6Al_2O_3.36H_2O$ *in water and in barium hydroxide solutions at 30° C.*

TABLE 7. *Solubility of* $7BaO.6Al_2O_3.36H_2O$ *in water and in barium hydroxide solutions at 30° C*—Continued

Time	Concentration of solution		Solid phases present
	Al_2O_3	BaO	
Experiment 7-4			
	g/liter	*g/liter*	
0	0	23.0	$7BaO.6Al_2O_3.36H_2O$.
10 min	8.20	36.0	
2 hr	8.90	36.8	
1 day	9.60	39.3	$7BaO.6Al_2O_3.36H_2O$.
4 days	11.14	42.1	Do.
18 days	8.30	37.4	$BaO.Al_2O_3.7H_2O+BaO.Al_2O_3.4H_2O$.
1 mo	7.80	37.6	Do.
2 mo	7.45	36.1	$BaO.Al_2O_3.4H_2O$+hyd. Al_2O_3.
3 mo	6.80	35.9	Do.
6 mo	3.90	31.6	Do.
7 mo	3.65	31.4	Do.
Experiment 7-5			
0	0	28.7	$7BaO.6Al_2O_3.36H_2O$.
10 min	7.70	40.6	Do.
1 hr	9.76	43.7	Do.
1 day	11.60	46.4	Do.
2 days	11.26	46.8	Do.
5 days	11.40	47.3	
14 days	11.10	46.6	$BaO.Al_2O_3.7H_2O$.
1 mo	7.65	42.8	Do.
2 mo	6.95	41.8	Do.
4 mo	7.05	42.1	$BaO.Al_2O_3.7H_2O+BaO.Al_2O_3.4H_2O$.
Experiment 7-6			
0	0	37.8	$7BaO.Al_2O_3.36H_2O$.
10 min	7.10	46.5	Do.
1 hr	9.36	49.0	Do.
1 day	10.80	52.6	Do.
2 days	10.90	52.7	Do.
5 days	10.84	52.9	
15 days	11.00	52.7	$7BaO.Al_2O_3.36H_2O+BaO.Al_2O_3.7H_2O$.
1 mo	7.95	48.8	$BaO.Al_2O_3.7H_2O$.
2 mo	7.35	48.4	Do.
4 mo	7.20	47.8	Do.
Experiment 7-7			
0	0	45.3	$7BaO.6Al_2O_3.36H_2O$.
10 min	8.50	55.8	Do.
30 min	9.60	56.1	Do.
1 day	9.90	56.5	Do.
2 days	9.80	57.0	Do.
5 days	9.70	57.3	$7BaO.6Al_2O_3.36H_2O+BaO.Al_2O_3.4H_2O$.
9 days	8.20	58.5	Do.
1 mo	4.38	52.9	$BaO.Al_2O_3.4H_2O$.
2 mo	3.70	51.4	$BaO.Al_2O_3.4H_2O$+hyd. Al_2O_3.
3 mo	3.60	51.4	Do.
4 mo	3.37	51.1	Do.
5 mo	3.15	50.5	Do.
Experiment 7-8			
0	0	51.5	$7BaO.6Al_2O_3.36H_2O$.
1 day	10.04	64.2	$7BaO.6Al_2O_3.36H_2O+Ba(OH)_2.8H_2O$.
4 days	10.10	65.7	Do.
7 days	10.20	66.1	$7BaO.6Al_2O_3.36H_2O+BaO.Al_2O_3.4H_2O$ $+Ba(OH)_2.8H_2O$.
10 days	8.90	65.0	$BaO.Al_2O_3.4H_2O+Ba(OH)_2.8H_2O$.
17 days	7.10	62.0	Do.
1 mo	6.15	58.0	Do.
3 mo	4.40	57.5	Do.
4 mo	4.15	57.3	Do.

Mixtures in the more basic region reached a maximum concentration that persisted long enough (5 to 15 days) to permit the plotting of an approximate metastable solubility curve in this range. The data and curve for experiment 7-3 show that it resembled 7-2, except that in the more basic solution the intermediate phase, $BaO.Al_2O_3.7H_2O$, persisted longer. Experiment 7-3 shows another peculiarity in that the heptahydrate formed was subsequently hydrolyzed, with a corresponding increase in basicity of the solution. Experiments 7-4, 7-5, and 7-6, in solutions progressively more basic, are characterized by greater stability of the intermediate phase, $BaO.Al_2O_3.7H_2O$, and by a decrease in the amount of hydrated alumina precipitated. In 7-7 and 7-8, the heptahydrate no longer appears as an intermediate phase, the original hydrate being transformed directly into the tetrahydrate. In 7-8, $Ba(OH)_2.8H_2O$ also appears as a solid phase. The reverse kink in the curve for this mixture reflects a temporary failure of the temperature control, which permitted the temperature to fall about 1 deg, resulting in precipitation of more barium hydroxide.

9. $2BaO.Al_2O_3.5H_2O$

Results of solubility experiments with $2BaO.Al_2O_3.5H_2O$ are given in table 8 and figure 8. This hydrate dissolved in water without any precipitation at first, so that the molar ratio of BaO to Al_2O_3 in solution remained approximately 2:1. Precipitation of hydrated alumina was first observed after 26 days. The remaining crystalline material thereupon went into solution as alumina continued to separate out.

TABLE 8. *Solubility of* $2BaO.Al_2O_3.5H_2O$ *in water and in barium hydroxide solutions at 30° C*—Continued

Time	Concentration of solution		Solid phases present
	Al_2O_3	BaO	
Experiment 8-1			
	g/liter	*g/liter*	
0	0	0	$2BaO.Al_2O_3.5H_2O$.
1 day	3.42	10.4	
5 days	5.05		$2BaO.Al_2O_3.5H_2O$.
12 days	5.50	16.8	Do.
19 days	6.10	18.4	Do.
26 days	6.15	19.7	$2BaO.Al_2O_3.5H_2O$+hyd. Al_2O_3.
33 days	5.60	20.8	Hyd. Al_2O_3.
40 days	4.55	20.9	
2 mo	3.40	21.1	Hyd. Al_2O_3.
3 mo	2.70	20.6	Do.
4 mo	2.55	20.6	Do.
6 mo	2.15	20.3	Do.
10 mo	1.87	19.9	Do.
Experiment 8-2			
0	0	(8.5)	$2BaO.Al_2O_3.5H_2O$.
1 day	2.18	14.9	
5 days	3.55		$2BaO.Al_2O_3.5H_2O$.
12 days	3.98	20.3	Do.
19 days	4.60	21.9	Do.
26 days	4.90	22.6	$2BaO.Al_2O_3.5H_2O$+hyd. Al_2O_3.
33 days	5.15	23.1	Do.
40 days	5.48	24.3	
2 mo	5.52	24.1	$2BaO.Al_2O_3.5H_2O$+hyd. Al_2O_3.
3 mo	5.35	24.2	Hyd. Al_2O_3.
4 mo	5.35	24.2	Do.
6 mo	4.60	23.6	Do.
10 mo	3.05	23.5	Do.
Experiment 8-3			
0	0	(17.0)	$2BaO.Al_2O_3.5H_2O$.
1 day	1.85	23.0	
5 days	3.20		$2BaO.Al_2O_3.5H_2O$+hyd. Al_2O_3.
12 days	4.00	29.3	Do.
19 days	4.70	31.2	Do.
26 days	5.00	32.0	Do.
33 days	5.15	32.3	Do.
40 days	5.25	32.9	
2 mo	5.25	32.4	$2BaO.Al_2O_3.5H_2O$+hyd. Al_2O_3.
3 mo	5.12	32.8	Do.
4 mo	5.30	32.5	Do.
6 mo	5.15	32.0	Do.

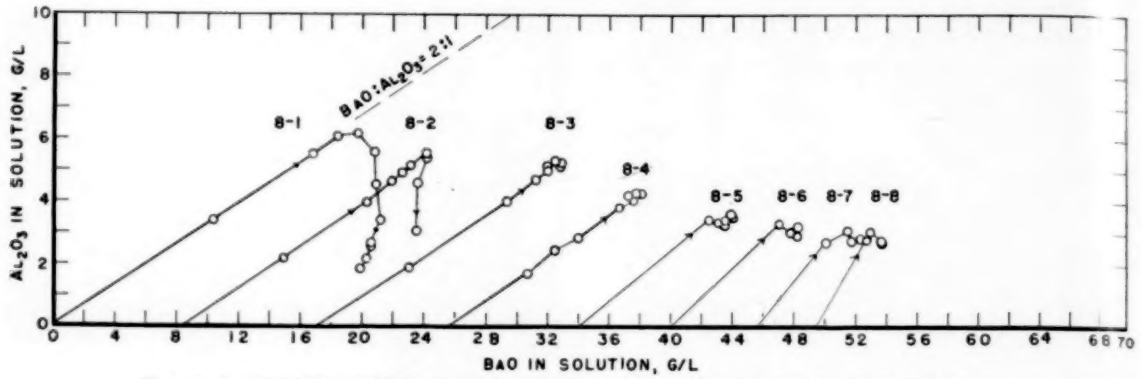

FIGURE 8. *Solubility of* $2BaO.Al_2O_3.5H_2O$ *in water and in barium hydroxide solutions at 30° C.*

TABLE 8. *Solubility of* $2BaO.Al_2O_3.5H_2O$ *in water and in barium hydroxide solutions at 30° C*—Continued

Time	Concentration of solution		Solid phases present
	Al_2O_3	BaO	
Experiment 8-4			
	g/liter	*g/liter*	
0	0	(25.7)	$2BaO.Al_2O_3.5H_2O$.
1 day	1.70	30.7	Do.
2 days	2.45	32.5	$2BaO.Al_2O_3.5H_2O$+hyd. Al_2O_3.
5 days	2.85	34.0	Do.
12 days	3.80	36.7	
19 days	4.20	37.8	
26 days	4.30	37.8	
40 days	4.15	38.0	$2BaO.Al_2O_3.5H_2O$+hyd. Al_2O_3.
2 mo	4.25	38.1	Do.
3 mo	4.40	37.9	Do.
4 mo	4.20	37.3	Do.
5 mo	4.05	37.6	Do.
Experiment 8-5			
0	0	(34.2)	$2BaO.Al_2O_3.5H_2O$.
9 days	3.40	42.5	$2BaO.Al_2O_3.5H_2O$+hyd. Al_2O_3.
22 days	3.40	43.6	Do.
36 days	3.60	43.9	Do.
2 mo	3.25	43.5	Do.
3 mo	3.35	43.1	Do.
4 mo	3.35	43.8	Do.
5 mo	3.40	44.0	Do.
Experiment 8-6			
0	0	(39.9)	$2BaO.Al_2O_3.5H_2O$.
9 days	3.30	47.0	$2BaO.Al_2O_3.5H_2O$+hyd. Al_2O_3.
22 days	3.02	48.0	Do.
36 days	3.20	48.2	Do.
2 mo	2.90	48.2	Do.
3 mo	3.02	47.8	Do.
4 mo	2.99	48.2	Do.
5 mo	2.95	48.1	Do.
Experiment 8-7			
0	0	45.6	$2BaO.Al_2O_3.5H_2O$.
9 days	2.70	50.1	$2BaO.Al_2O_3.5H_2O$+$Ba(OH)_2.8H_2O$.
22 days	3.00	*47.0	$2BaO.Al_2O_3.5H_2O$+$Ba(OH)_2.8H_2O$+hyd. Al_2O_3.
36 days	3.05	51.5	Do.
2 mo	2.78	51.7	Do.
3 mo	2.85	52.1	Do.
4 mo	2.80	52.3	$2BaO.Al_2O_3.5H_2O$+hyd. Al_2O_3.
Experiment 8-8			
0	0	(49.4)	$2BaO.Al_2O_3.5H_2O$.
12 days	2.80	52.7	
22 days	2.88	*48.4	$2BaO.Al_2O_3.5H_2O$+$Ba(OH)_2.8H_2O$+hyd. Al_2O_3.
36 days	3.05	52.9	Do.
2 mo	2.80	*50.0	Do.
3 mo	2.70	53.7	Do.
4 mo	2.75	53.7	Do.

* Fluctuations in BaO concentration reflect temporary failure of temperature control.

In barium hydroxide solutions, the course of solution was similar, but the original hydrate appeared to be more stable as the concentration of barium hydroxide increased. Although small amounts of hydrated alumina were formed in all cases, much of the crystalline material remained even after 5 mo, except in 8-2, the least basic of these mixtures.

10. Precipitation From Supersaturated Solutions

In any study of phase equilibria in aqueous solutions, it is desirable to approach equilibrium from both sides, that is, from supersaturation as well as undersaturation. This is particularly true when reactions are slow and when metastable phases may be formed. In the present study, it was found that precipitation from supersaturated solution gave results that were not always reproducible and that often were difficult to interpret. This phase of the investigation, the first actually to be undertaken, yielded information vital to an understanding of the various solid phases and their formation, but it did not furnish a clear picture of the equilibrium relationships in the system. The solubility experiments described in the preceding sections proved to be essential to a clarification of these relationships.

Supersaturated solutions for the precipitation experiments were prepared as described in section II, 7. These were kept in the 30° C cabinet with occasional shaking, and samples of the solutions were pipetted out from time to time for analysis. Small samples of the solid phases that precipitated were also taken for microscopic examination. Out of a large number of such solutions prepared at various times, a few have been selected as typical of the group, and the results are presented in table 9 and figure 9.

Examination of the curve for Experiment 9-1 shows that the precipitation followed a straight line, aside from slight irregularities that may be attributed to experimental errors. The last two analyses indicate a slight but definite shift toward a lower concentration of BaO. This is probably due to crystallization of $Ba(OH)_2.8H_2O$ on the wall of the flask above the level of the liquid, a phenomenon observed in a number of the flasks after standing for

TABLE 9. *Precipitation from supersaturated barium aluminate solutions at 30° C*

Time	Concentration of solution		Solid phases present
	Al_2O_3	BaO	
Experiment 9-1			
	g/liter	*g/liter*	
0	17.80	27.8	None.
1 day	16.38	27.1	Hyd. Al_2O_3.
2 days	8.08	26.1	Do.
5 days	5.58	25.8	Do.
13 days	3.90	25.5	Do.
20 days	3.50	26.0	Do.
29 days	3.45	26.1	Do.
47 days	3.20	26.0	Do.
2 mo	2.95	23.8	Do.
3 mo	2.65	25.6	Do.
4 mo	2.45	24.8	Do.
6 mo	2.45	24.7	Do.
Experiment 9-2			
0	19.24	35.6	None.
1 day	18.92	34.9	Hyd. Al_2O_3.
2 days	17.66	34.9	Do.
5 days	9.12	32.2	Hyd. Al_2O_3+$BaO.Al_2O_3.7H_2O$.
13 days	6.70	32.5	Do.
20 days	5.60	33.6	Hyd. Al_2O_3.
29 days	5.00	33.7	Do.
47 days	4.40	33.7	Do.
2 mo	3.93	33.8	Do.
3 mo	3.50	33.4	Do.
4 mo	3.30	33.1	Do.
6 mo	3.10	32.8	Do.
Experiment 9-3			
0	19.40	43.8	None.
1 day	19.34	43.5	$7BaO.6Al_2O_3.36H_2O$.
2 days	14.36	36.6	$7BaO.6Al_2O_3.36H_2O$+$BaO.Al_2O_3.7H_2O$.
5 days	10.16	30.8	$BaO.Al_2O_3.7H_2O$.
13 days	8.14	28.0	$BaO.Al_2O_3.7H_2O$+hyd. Al_2O_3.
20 days	7.70	27.6	Do.
47 days	7.46	26.9	Do.
2 mo	7.32	26.7	Do.
3 mo	6.86	25.7	Do.
4 mo	6.80	25.6	Do.
6 mo	7.00	25.4	Do.
7 mo	7.10	38.8	
8 mo	7.25	42.9	
Experiment 9-4			
0	14.10	37.8	None.
5 mo	7.48	30.7	$BaO.Al_2O_3.7H_2O$.
7 mo	6.60	37.4	Hyd. Al_2O_3.
9 mo	4.66	37.1	Do.
12 mo	4.05	36.9	Do.
15 mo	3.40	36.8	Do.
18 mo	3.20	36.5	Do.
Experiment 9-5			
	g/liter	*g/liter*	
0	20.04	51.5	None.
1 day	19.30	51.0	$7BaO.6Al_2O_3.36H_2O$.
2 days	11.90	40.5	$7BaO.6Al_2O_3.36H_2O$+$BaO.Al_2O_3.7H_2O$.
5 days	9.20	36.8	$BaO.Al_2O_3.7H_2O$.
13 days	7.40	34.6	Do.
30 days	7.30	34.2	Do.
47 days	7.10	33.8	Do.
2 mo	7.05	33.6	Do.
3 mo	7.23	33.6	Do.
4 mo	7.25	33.5	Do.
6 mo	7.12	32.9	Do.
Experiment 9-6			
0	17.65	51.7	None.
1 day	17.39	51.1	$7BaO.6Al_2O_3.36H_2O$.
4 days	13.29	43.5	Do.
7 days	11.41	40.2	Do.
11 days	10.78	42.6	$BaO.Al_2O_3.7H_2O$.
15 days	8.75	39.4	Do.
2 mo	7.43	38.0	Do.
7 mo	7.24	36.6	Do.
11 mo	5.18	47.4	$BaO.Al_2O_3.4H_2O$+hyd. Al_2O_3.
15 mo	3.86	45.2	Do.
18 mo	3.40	44.5	Do.

TABLE 9. *Precipitation from supersaturated barium aluminate solutions at 30° C*—Continued

Time	Concentration of solution		Solid phases present
	Al_2O_3	BaO	
Experiment 9-7			
	g/liter	*g/liter*	
0	20.20	59.4	None.
1 day	16.46	54.2	$7BaO.6Al_2O_3.36H_2O$.
2 days	13.42	49.5	Do.
5 days	11.30	47.2	$7BaO.6Al_2O_3.36H_2O$+$BaO.Al_2O_3.7H_2O$.
9 days	8.47	44.5	$BaO.Al_2O_3.7H_2O$.
15 days	7.90	43.3	Do.
20 days	7.30	42.4	Do.
47 days	7.00	41.8	Do.
2 mo	7.00	41.4	Do.
Experiment 9-8			
0	17.74	64.3	None.
1 day	17.52	62.7	$7BaO.6Al_2O_3.36H_2O$.
2 days	15.28	59.8	Do.
5 days	11.22	54.3	$7BaO.6Al_2O_3.36H_2O$+$BaO.Al_2O_3.7H_2O$.
9 days	8.70	51.7	$BaO.Al_2O_3.7H_2O$.
13 days	7.74	50.0	Do.
20 days	7.60	49.7	Do.
47 days	7.30	49.3	Do.
2 mo	7.05	48.5	Do.
Experiment 9-9			
0	14.16	59.2	None.
6 days			$BaO.Al_2O_3.7H_2O$+$7BaO.6Al_2O_3.36H_2O$ (slight amt.).
10 days	11.44	54.9	$BaO.Al_2O_3.7H_2O$.
3 mo	7.68	50.3	$BaO.Al_2O_3.7H_2O$+$BaO.Al_2O_3.4H_2O$.
7 mo	4.00	44.1	$BaO.Al_2O_3.4H_2O$+hyd. Al_2O_3.
11 mo	3.38	43.2	Do.
13 mo	3.30	43.2	Do.
15 mo	3.30	43.2	Do.
Experiment 9-10			
0	11.10	60.8	None.
5 mo	7.80	55.9	$BaO.Al_2O_3.7H_2O$+$BaO.Al_2O_3.4H_2O$.
7 mo	6.00	53.8	$BaO.Al_2O_3.4H_2O$+hyd. Al_2O_3.
9 mo	5.20	52.5	Do.
12 mo	4.32	51.3	Do.
15 mo	4.00	50.5	Do.
18 mo	3.75	50.4	Do.
Experiment 9-11			
0	12.10	68.1	$Ba(OH)_2.8H_2O$.
10 days	11.75	67.6	
1 mo	8.00	63.2	$Ba(OH)_2.8H_2O$+$BaO.Al_2O_3.4H_2O$.
2 mo	6.00	59.3	
3 mo	4.85	58.0	$Ba(OH)_2.8H_2O$+$BaO.Al_2O_3.4H_2O$.

several months. Disregarding these two points, the average slope of the line indicates a molar ratio, $BaO:Al_2O_3=0.10:1$, in the precipitate. Analysis of the precipitate after 7 mo gave a molar ratio, $BaO:Al_2O_3:H_2O=0.07:1:3.27$.

The precipitate was bulky, and under the microscope appeared as extremely fine, irregular, isotropic grains, with refractive index about 1.57, close to the median index of gibbsite ($Al_2O_3.3H_2O$). The X-ray diffraction pattern showed the stronger lines of gibbsite, superimposed on a broad band indicative of amorphous material. It is inferred that the precipitate originally was amorphous, and that crystallization to gibbsite occurred progressively on aging. The BaO present may be assumed to be adsorbed.

Experiment 9-2 followed a similar course, except that a small amount of $BaO.Al_2O_3.7H_2O$ appeared as an intermediate product and persisted for several

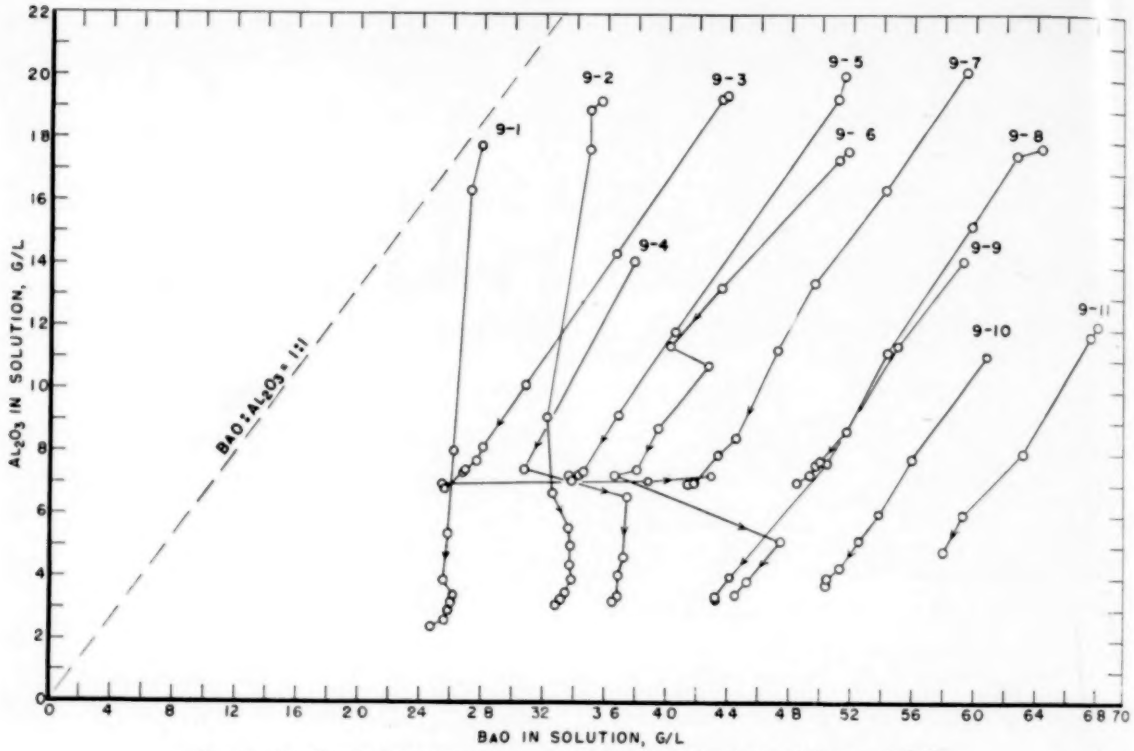

FIGURE 9. *Precipitation from supersaturated barium aluminate solutions at 30° C.*

days. Its subsequent re-solution is reflected in an inflection toward the right in the curve.

Solutions more basic than No. 9-2 behaved differently. Experiments 9-3, 9-5, 9-6, 9-7, and 9-8 precipitated $7BaO.6Al_2O_3.36H_2O$ as the initial solid phase, followed by simultaneous disappearance of this phase and precipitation of $BaO.Al_2O_3.7H_2O$. In 9-4, 9-9, and 9-10, the latter hydrate was the initial phase to separate out. It will be noted that in this latter group the initial concentration of Al_2O_3 was below 15 g/liter in each case. No. 9-6 is exceptional in that the inversion from $7BaO.6Al_2O_3.36H_2O$ to $BaO.Al_2O_3.7H_2O$ was accompanied by an abrupt change in direction of the concentration curve. For some unknown reason, the other members of the series failed to show this break, though 9-7 and 9-8 do show a more gradual change in slope, which may be attributed to the same reaction.

Experiment 9-4 is of interest in that it exhibits complete hydrolysis of the $BaO.Al_2O_3.7H_2O$ first formed, with a corresponding change in concentration of the solution. The same is true of No. 9-3, except that in this case the hydrolosis was still incomplete when the experiment was terminated after 8 mos. Experiment 9-6 underwent an analogous change in concentration, but in this case $BaO.Al_2O_3.4H_2O$ was precipitated along with the alumina. In 9-9 and 9-10 these two phases were also coprecipitated, but the hydrated alumina was present only in small amount, insufficient to cause any deflection of the concentration curve. Experiments 9-3, 9-5, 9-7, and 9-8 appear to have reached equilibrium at about 7 g of Al_2O_3 per liter, but it will be noted that these experiments were terminated after 7 mos or less. This group was started as the investigation was nearing completion, and their study was necessarily abbreviated. It should be clear from the previous discussion, however, that this apparent equilibrium is metastable, and it may reasonably be assumed that on longer standing, this group would have behaved as did the other members of the series.

Experiment 9-11 contained an excess of $Ba(OH)_2.8H_2O$ present as a solid phase. The first new phase observed was $BaO.Al_2O_3.4H_2O$, rather than the heptahydrate. It is worthy of note that even in contact with excess barium hydroxide, the hydrate that was first precipitated was a monobarium compound.

The results of the above experiments and of a number of others involving precipitation from supersaturated solution may be generalized as follows: (1) Solutions containing less than 36 g of BaO per liter (approximately) precipitate amorphous hydrated alumina, together with some adsorbed BaO. The rate of precipitation from the more concentrated solutions is fairly rapid, but from solutions less concentrated it may be extremely slow. The stable product is gibbsite. (2) Solutions containing more than 36 g of BaO per liter (approximately) precipitate one of

the hydrated barium aluminates. In this more basic region the concentration of alumina determines which aluminate precipitates first. Above 15 g of Al_2O_3 per liter (very roughly) the first phase to appear is $7BaO.6Al_2O_3.36H_2O$; below that concentration the initial solid phase is $BaO.Al_2O_3.7H_2O$. (3) $7BaO.6Al_2O_3.36H_2O$ is relatively unstable and soon disappears with the formation of either hydrated alumina, $BaO.Al_2O_3.7H_2O$, or $BaO.Al_2O_3.4H_2O$, depending on the concentration of BaO in the solution. (4) $BaO.Al_2O_3.7H_2O$ is metastable and eventually disappears with formation of either hydrated alumina or $BaO.Al_2O_3.4H_2O$ or both.

11. Phase equilibria in the system BaO-Al_2O_3-H_2O at 30° C

From the data given in the preceding sections, it is possible to construct the greater part of the phase equilibrium diagram for the system BaO-Al_2O_3-H_2O at 30° C. The equilibrium concentrations and the corresponding solid phases are listed in table 10. In order to complete the diagram, it was necessary to study the solubilities of two additional compounds, namely, gibbsite ($Al_2O_3.3H_2O$) and barium hydroxide octahydrate ($Ba(OH)_2.8H_2O$). Gibbsite was treated with barium hydroxide solutions in the manner previously described in connection with the aluminates. Analyses were made at intervals for a period of 8 to 9 mos, at the end of which time the concentrations had remained substantially constant for 3 mos. The barium hydroxide curve was established in part by experiments described above. Two additional points were obtained by determining the solubility of recrystallized barium hydroxide octahydrate in water and in a barium aluminate solution containing 1.42 g of Al_2O_3 per liter. In these experiments equilibrium was attained quickly, but because of the high temperature coefficient of solubility and the lack of high-precision temperature control it was necessary to make repeated analyses and use average values. The equilibrium data obtained in these two series of experiments are included in table 10.

TABLE 10. *Concentration of barium aluminate solutions in stable or metastable equilibrium with solid phases at 30° C*

Experiment	Concentration of solution		Solid phases present	Direction of approach to equilibrium
	Al_2O_3	BaO		
	g/liter	*g/liter*		
10-1	0.20	4.8	$Al_2O_3.3H_2O$	From undersaturation.
10-2	.39	9.7	do	Do.
10-3	.70	14.2	do	Do.
10-4	.88	19.0	do	Do.
10-5	1.06	23.9	do	Do.
10-6	1.40	29.1	do	Do.
10-7	1.69	34.2	do	Do.
10-8	2.00	38.8	do	Do.
10-9	2.56	44.7	do	Do.
10-10	2.69	49.6	do	Do.
10-11	3.08	55.4	$Al_2O_3.3H_2O+Ba(OH)_2.8H_2O$	Do.
5-2	3.00	12.5	$BaO.Al_2O_3.4H_2O$+hyd. Al_2O_3	Do.
5-3	2.83	17.6	do	Do.
5-4	2.79	22.0	do	Do.
5-5	2.90	26.4	do	Do.
5-6	2.74	31.6	do	Do.

TABLE 10. *Concentration of barium aluminate solutions in stable or metastable equilibrium with solid phases at 30°C*—Continued

Experiment	Concentration of solution		Solid phases present	Direction of approach to equilibrium
	Al_2O_3	BaO		
	g/liter	*g/liter*		
10-21	3.11	33.3	$BaO.Al_2O_3.4H_2O$+hyd. Al_2O_3	From supersaturation.
10-22	3.08	35.2	do	Do.
10-23	3.25	37.5	do	Do.
5-7	2.68	40.7	do	From undersaturation.
9-9	3.33	45.2	do	From supersaturation.
5-8	2.74	45.4	do	From undersaturation.
5-9	2.74	49.9	$BaO.Al_2O_3.4H_2O$	Do.
10-12	2.86	55.6	$BaO.Al_2O_3.4H_2O+Ba(OH)_2.8H_2O$	Do.
8-3	5.20	32.4	$2BaO.Al_2O_3.5H_2O$+hyd. Al_2O_3	Do.
8-4	4.20	37.8	do	Do.
8-5	3.35	43.6	do	Do.
8-6	2.95	48.1	do	Do.
8-7	2.80	52.0	do	Do.
8-8	2.75	53.7	do	Do.
10-13	2.70	55.4	$2BaO.Al_2O_3.5H_2O+Ba(OH)_2.8H_2O$.	Do.
6-2	7.44	20.0	$BaO.Al_2O_3.7H_2O$	Do.
10-14	7.42	22.8	do	Do.
9-3	6.89	25.6	do	From supersaturation.
6-3	7.12	27.8	do	From undersaturation.
9-4	7.48	30.7	do	From supersaturation.
9-5	7.20	33.3	do	Do.
6-4	7.33	34.4	do	From undersaturation.
9-6	7.24	36.6	do	From supersaturation.
10-15	7.20	37.3	do	From undersaturation.
6-5	7.45	41.4	do	Do.
9-7	7.10	41.9	do	From supersaturation.
10-16	7.16	43.6	do	From undersaturation.
10-24	6.95	46.3	do	From supersaturation.
9-8	7.32	49.2	do	Do.
6-6	7.10	50.3	do	From undersaturation.
10-25	7.16	54.2	do	From supersaturation.
6-7	7.78	55.3	do	From undersaturation.
10-17	7.65	57.7	do	Do.
10-18	7.80	62.2	$BaO.Al_2O_3.7H_2O+Ba(OH)_2.8H_2O$.	Do.
7-2	11.80	29.5	$7BaO.6Al_2O_3.36H_2O$+hyd. Al_2O_3.	Do.
7-3	12.20	35.2	$7BaO.6Al_2O_3.36H_2O$	Do.
7-4	11.14	42.1	do	Do.
7-5	11.60	46.4	do	Do.
7-6	11.00	52.7	$7BaO.6Al_2O_3.36H_2O+BaO.Al_2O_3.7H_2O$.	Do.
7-7	9.90	56.5	$7BaO.6Al_2O_3.36H_2O$	Do.
7-8	10.20	66.1	$7BaO.6Al_2O_3.36H_2O+BaO.Al_2O_3.4H_2O+Ba(OH)_2.8H_2O$.	Do.
10-19	(0)	52.9	$Ba(OH)_2.8H_2O$	Do.
10-20	1.42	54.1	do	Do.

Also included are a number of points representing equilibrium (metastable) approached from supersaturation rather than undersaturation. These points are shown as filled triangles in figure 10, in order to distinguish them from the others. It will be noted that there is fair agreement between the two methods of approach in the case of $BaO.Al_2O_3.7H_2O$. In the case of the tetrahydrate, however, the values obtained from the precipitation experiments are erratic and are generally higher than those obtained from solution experiments. The reason for this is not known. No corresponding figures are given for $7BaO.6Al_2O_3.36H_2O$, as there was no arrest in concentration during precipitation in this range. Further, there are no precipitation data for $2BaO.Al_2O_3.5H_2O$ because this phase was not obtained by precipitation at 30°.

No attempt was made to determine the solubility curve of amorphous hydrated alumina, partly because it is difficult to prepare this material free of interfering ions, and partly because it was believed

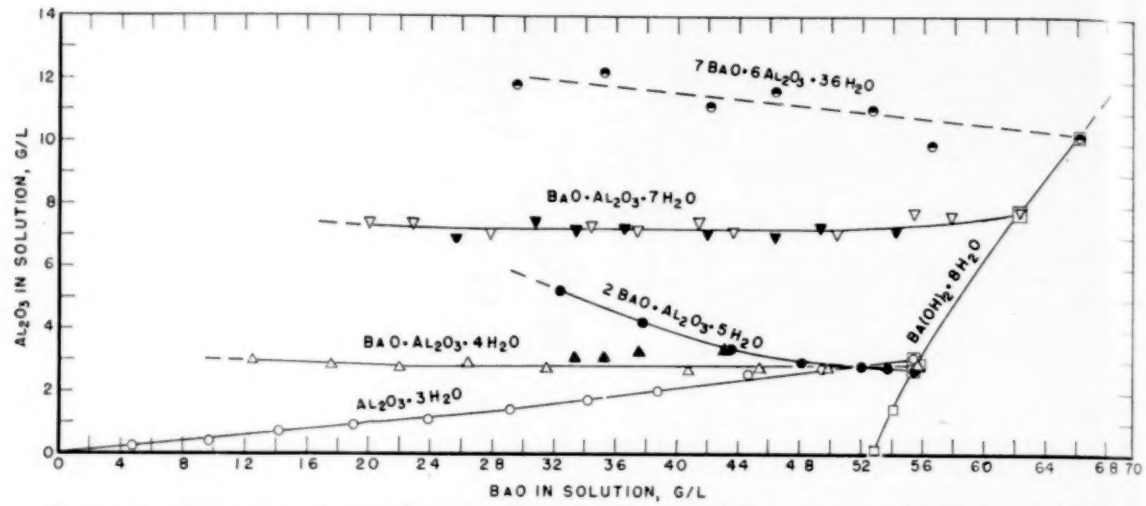

FIGURE 10. *Concentration of barium aluminate solutions in stable or metastable equilibrium with solid phases at 30° C.*

Symbols represent solid phases present, as follows: ◓, $7BaO.6Al_2O_3.36H_2O$; ▽, ▼, $BaO.Al_2O_3.7H_2O$; △, ▲, $BaO.Al_2O_3.4H_2O$; ●, $2BaO.Al_2O_3.5H_2O$; ○, $Al_2O_3.3H_2O$ (gibbsite); □, $Ba(OH)_2.8H_2O$. Combination of two symbols indicates coexistence of two solid phases. Filled triangles represent equilibrium approached from supersaturation. Other points represent equilibrium approached from undersaturation.

that such a curve would be dependent on the mode of preparation, hence not very significant. No tests were made with any of the crystalline forms of hydrated alumina other than gibbsite, and, as mentioned above, no work was done on the compound $BaO.6Al_2O_3$.

Solubility curves for $BaO.Al_2O_3.H_2O$ and $BaO.Al_2O_3.2H_2O$ are likewise missing. As shown in section III, 4 and III, 5, these hydrates, both of which were prepared hydrothermally, are unstable in contact with barium hydroxide solutions at 30° C, and hence cannot be said to possess solubility curves at this temperature.

Figure 10 is the phase equilibrium diagram of the system BaO-Al_2O_3-H_2O at 30° C, complete except as noted above. The stable phases are gibbsite and barium hydroxide octahydrate, and possibly, over a narrow range, $2BaO.Al_2O_3.5H_2O$ or $BaO.Al_2O_3.4H_2O$. The other phases for which curves are shown are metastable throughout their entire range. Nevertheless, because of the slowness of transition from one phase to another, it is possible to trace a definite solubility curve for each of the solid phases, except $7BaO.6Al_2O_3.36H_2O$ and amorphous hydrated alumina. A dotted curve has been drawn to represent the approximate solubilities of the former.

It is apparent from figure 10 that there is some uncertainty as to what is the stable solid phase over a short range (50 to 56 g of BaO per liter, approximately). On the basis of the data given, it appears that there is a point at 2.8 g of Al_2O_3 and 52.0 g of BaO per liter at which gibbsite and $2BaO.Al_2O_3.5H_2O$ are in equilibrium, and another point at 2.7 g of Al_2O_3 and 55.6 g of BaO per liter at which $2BaO.Al_2O_3.5H_2O$ and $Ba(OH)_2.8H_2O$ are the stable solid phases. However, the solubilities of the three aluminous phases are so close together in this area, and the reactions leading to equilibrium are so slow, that the stability relations here indicated cannot be considered definitely established. Additional experiments a few degrees above and below 30° C might assist in clarifying the question.

12. Equilibria at Other Temperatures

A few experiments were conducted at temperatures other than 30° C. In particular, sufficient work was done on the solubilities of $BaO.Al_2O_3.7H_2O$ and $Ba(OH)_2.8H_2O$ at 25° C to establish at least a portion of the curves for these compounds. As might be expected, they are parallel to the curves at 30° C, but at lower concentrations. The solubility of $Ba(OH)_2.8H_2O$ was found to be equivalent to 42.7 g of BaO per liter at 25° C, and the point at which the two solid phases coexist was placed approximately at 6.8 g of Al_2O_3 and 52.0 g of BaO per liter. The solubility of $Ba(OH)_2.8H_2O$ at 50° C, expressed in terms of BaO, was found to be about 102 g/liter. This figure is not exact, as the temperature control was probably no closer than 1 deg, but is given merely to indicate the magnitude of the temperature coefficient of solubility. At this temperature $BaO.Al_2O_3.7H_2O$ is rapidly converted to $BaO.Al_2O_3.4H_2O$. No equilibrium measurements were made for the tetrahydrate at temperatures other than 30° C.

As mentioned in the introduction, a diagram of phase equilibria in this system at 20° C has been published by Malquori [16]. With due allowance for the difference in temperature, it still is difficult to reconcile his diagram with that given in figure 10. In particular, Malquori shows only two barium aluminate hydrates, $2BaO.Al_2O_3.5H_2O$ and one that he designates $BaO.Al_2O_3.6H_2O$. The latter, which we may assume to be identical with the compound referred to herein as the heptahydrate, is indicated to be the stable phase along a curve extending approx-

imately from 2 g of Al_2O_3 and 12 g of BaO to 6 g of Al_2O_3 and 22 g of BaO per liter. This is considerably above the curve shown in figure 10 for gibbsite ($Al_2O_3.3H_2O$), and the latter very probably would be found to have a lower solubility at 20° than at 30°. It is believed, therefore, that Malquori's curve does not represent stable equilibrium.

13. Effect of Impurities

As is well known, barium hydroxide solutions rapidly absorb carbon dioxide from the air, with the formation of barium carbonate. Preliminary experiments indicated that this reaction would not seriously affect the results obtained in this study. The carbonate formed is practically insoluble in barium hydroxide, and thus would be expected to have no effect on equilibrium relations. Samples for analysis generally were taken with a pipette, leaving little chance for carbonation during sampling. Any carbonate formed on the microscope slide was readily distinguished from other phases by its high birefringence. Periodic opening of flasks for sampling resulted in visible carbonation, but the total amount was negligible, as evidenced by the constancy of concentration of the solution after attainment of equilibrium.

More serious contamination was introduced by the solvent action of the barium hydroxide solutions on the glass containers. In order to estimate the extent of the attack, a large number of silica determinations were made on reaction mixtures that had stood for varying periods of time. The amount of silica found in solution was invariably small, usually about 2 or 3 mg/liter. The amount of silica in the solid residue, however, was considerable in flasks that had been standing a long time, but there was no apparent uniformity as to amount. For example, the molar ratio of SiO_2 to Al_2O_3 was found to be 0.03 in the precipitate from one solution (not listed above), and 0.84 in the precipitate from another of very nearly the same concentration. Both had stood 2 yr, and in both cases the total quantity of solid was slight, having precipitated from relatively dilute solution. In most cases the amount of precipitate was much greater and the percentage of SiO_2 correspondingly smaller. For example, the residue from mixture 9-1, filtered off after 6 mo, contained 0.01 mole of SiO_2 per mole of Al_2O_3. The silica was found to be present in the amorphous phase, not in the crystalline $BaO.Al_2O_3.4H_2O$, which was in most cases the other phase present in the precipitate after long standing. This was shown in a number of cases by separation of the precipitate into fine and coarse fractions, followed by analysis of each. This fact may be significant in connection with the observed presence of the amorphous phase in even the most basic mixtures, in the region where the equilibrium diagram indicates that one of the crystalline hydrates should be the stable phase. It is probable that in this case the observed amorphous material (always small in amount) is either a barium silicate hydrate or a barium aluminosilicate hydrate, in either case relatively insoluble.

The presence of silica in the precipitate is positive evidence of the solvent action of the solutions on the glass containers. It must be assumed, therefore, that the other constituents of the glass, chiefly soda and boron trioxide, likewise were present as contaminants. No tests, however, were made for these constituents. It is reasonable to suppose that the soda would remain in solution and that it might therefore have some effect on the equilibrium concentrations. From the fact that no progressive change in equilibrium concentration with time was observed, it is believed that this factor was of negligible significance.

IV. Comparison of Barium and Calcium Aluminates

It was brought out in section III, 2 that anhydrous monobarium aluminate possesses the property of setting to a hard mass after being mixed with water. The same phenomenon was observed with anhydrous tribarium aluminate as well. It was also shown that both of these compounds, when mixed with water, form solutions that are highly supersaturated with respect to certain hydrated products. This is in agreement with the well-known theory of Le Chatelier [18] that "the crystallization which accompanies the set of all of the bodies hardening upon contact with water results from the previous production of a supersaturated solution". Le Chatelier and later investigators have shown that this is true of the calcium aluminates, so that in this respect it may be said that there is a similarity in behavior between the aluminates of barium and of calcium. There is a further similarity in that both $3BaO.Al_2O_3$ and $3CaO.Al_2O_3$ react very vigorously with water, whereas the corresponding 1:1 aluminates react much more slowly. Beyond this, however, it is immediately apparent that the aluminates of barium are quite different from those of calcium. The former are much more soluble and form an entirely different series of hydration products. As is well known, the calcium aluminates produce an isometric hydrate, $3CaO.Al_2O_3.6H_2O$, as well as a crystalline product consisting of hexagonal plates in which the ratio of CaO to Al_2O_3 is either 2:1 or 4:1 or an intermediate value. Neither type of product was observed with the barium aluminates. These, on the other hand, yield a series of hydrates in which the ratio of BaO to Al_2O_3 is 1:1, or nearly so, together with a single more basic hydrate, $2BaO.Al_2O_3.5H_2O$, which in no way resembles the dicalcium aluminate hydrate. Only in the least basic region of the phase diagram are the systems $BaO-Al_2O_3-H_2O$ and $CaO-Al_2O_3-H_2O$ similar. Here, over a short range in the latter system, and over a much longer range in the former, gibbsite is the stable solid phase.

V. Summary

On the basis of the experiments described above, and subject to the experimental conditions, the following conclusions are presented:

1. Monobarium aluminate is hydrolyzed by water, with precipitation of hydrated alumina.

907877—50——4

2. Monobarium aluminate dissolves in barium hydroxide solutions with precipitation first of $7BaO.6Al_2O_3.36H_2O$, subsequently of $BaO.Al_2O_3.7H_2O$ in the less basic and $BaO.Al_2O_3.4H_2O$ in the more basic solutions.

3. Tribarium aluminate is rapidly hydrolyzed by water, with precipitation of $Ba(OH)_2.8H_2O$, $BaO.Al_2O_3.7H_2O$, and, subsequently, $2BaO.Al_2O_3.5H_2O$.

4. All the hydrated barium aluminates dissolve in water and are hydrolyzed, with precipitation of hydrated alumina.

5. The hydrated barium aluminates dissolve in barium hydroxide solutions with eventual precipitation of the equilibrium solid phases, but frequently with preliminary separation of metastable intermediate solid phases.

6. The stable solid phases in the system BaO-Al_2O_3-H_2O at 30° C are: (a) gibbsite ($Al_2O_3.3H_2O$) over a range from approximately zero concentration to about 52 g of BaO and 2.8 g of Al_2O_3 per liter; (b) $Ba(OH)_2.8H_2O$ from 52.9 g of BaO and zero Al_2O_3 to about 55.5 g of BaO and 2.7 g of Al_2O_3 per liter; (c) probably $2BaO.Al_2O_3.5H_2O$ (but possibly $BaO.Al_2O_3.4H_2O$ or gibbsite) over the short range from 52 BaO and 2.8 Al_2O_3 to 55.5 BaO and 2.7 Al_2O_3.

7. $7BaO.6Al_2O_3.36H_2O$ is a metastable phase, not sufficiently stable to permit an accurate determination of its solubility.

8. $BaO.Al_2O_3.7H_2O$ is also metastable, but it may exist in contact with solution for several months.

9. $BaO.Al_2O_3.4H_2O$ is likewise metastable over the greater part, if not all, of its range, but its stability is greater than that of the higher hydrates.

10. $2BaO.Al_2O_3.5H_2O$ resembles $BaO.Al_2O_3.4H_2O$ in its degree of stability in the metastable range.

11. No hydrate more basic than $2BaO.Al_2O_3.5H_2O$ was found.

VI. References

[1] R. Stumper, Chimie & industrie **22,** 1067 to 83 (1929).
[2] G. Grube and G. Heintz, Z. Electrochem. **41,** 797 (1935).
[3] K. Akiyama, Z. Kajima, and H. Aiba, J. Soc. Chem. Ind. (Japan) **41,** 218 (1938), and **42,** 145 (1939); abstr. in Chem Abstr. **33,** 325 and 7497 (1939).
[4] V. F. Zhuravlev, Tsement **1939,** No. 8, 41; abstract in Chem. Abstr. **35,** 595 (1941).
[5] F. L. Hunt and M. Temin, Radiology (Feb. 1927).
[6] G. W. Morey, U. S. Patent 1,688,054 (1928).
[7] H. V. Wartenburg and H. J. Reusch, Z. anorg. allgem. Chem. **207,** 1 (1932).
[8] S. Wallmark and A. Westgren, Arkiv. Kemi, Mineral, Geol. **12B,** No. 35 (1937).
[9] N. A. Toropov, Compt. rend. acad. sci. URSS **1935,** 150.
[10] N. A. Toropov and M. M. Stukalova, Compt. rend. acad. sci. URSS, **24,** 459 (1939).
[11] N. A. Toropov and M. M. Stukalova, Compt rend. acad. sci. URSS, **27,** 974 (1940).
[12] E. T. Carlson and L. S. Wells, J. Research NBS **41,** 103 (1948) RP1908.
[13] E. Beckman, J. prakt. Chem. [2] **26,** 385 and 474; **27,** 126 (1883).
[14] G. Maekawa, J. Soc. Chem. Ind. (Japan) **44,** 912 (1941); abstr. in Chem. Abstr. **42,** 2536 (1948).
[15] G. Maekawa, J. Soc. Chem. Ind. (Japan) **45,** 130 (1942).
[16] G. Malquori, Gazz. chim. ital. **56,** 51 (1926).
[17] G. Gallo, Ind. ital. del cemento **17,** 123 (1947).
[18] H. Le Chatelier, Experimental researches on the constitution of hydraulic mortars (1887) (Translated by J. L. Mack, 1905).
[19] A. Braniski, Rev. matériaux construction trav. publ. (Ed. C), No. 404, 154 (1949).

WASHINGTON, June 2, 1950.

Journal of Research of the National Bureau of Standards Vol. 45, No. 5, November 1950 Research Paper 2150

Permeability of Glass Wool and Other Highly Porous Media[1]

By Arthur S. Iberall

An elementary treatment is developed for the permeability of fibrous materials of high porosities, based on the drag of the individual filaments. It is believed that the same treatment is valid for other highly porous media. A brief historical review is given of theories relating the permeability to the structure of porous media. The applicability of the currently accepted permeability theory, based on the hydraulic radius, only to media of low porosities is discussed. Both approaches may be extended to permit approximate correlation for intermediate porosities. For fibrous materials of high porosity, it is shown that the effect of fluid inertia results in a permeability that varies with flow even at low Reynolds number. The permeability to gaseous flow is also shown to vary with the absolute gas pressure. This variation is appreciable when the molecular mean free path is of the same order of magnitude as the separation between filaments or particles in the medium. Data suitable for the design of linear flowmeters utilizing fibrous materials of high porosity are given, including data on the useful porosity range of fibrous media.

I. Introduction

During the war there arose a need in the Bureau of Aeronautics, Department of the Navy, for rapid procurement of equipment suitable for field tests of diluter-demand oxygen regulators, which are used by flight personnel at high altitudes. Due to difficulties in procurement, and certain disadvantages in the convenient use of commercially available flowmeters for the measurement of gaseous flow, the development of a suitable flowmeter was undertaken. After some preliminary consideration, efforts were centered on the development of a constant-resistance flowmeter utilizing a porous medium as the flow-

[1] This paper is a theoretical abstract of a report to the Bureau of Aeronautics, Navy Department [1]. Figures in brackets indicate the literature references at the end of this paper.

resistance element. The major advantage of the constant-resistance (or constant-permeability) flowmeter is that its pressure drop is an indication of and proportional to the volume rate of flow, so that an instrument with linear response can be obtained.

Glass wool appeared to be a suitable porous medium because it is relatively inactive chemically, relatively nonhygroscopic, its fibers are strong and elastic, making in bulk a resilient mass that will retain its characteristics; and the fibers can be made in an almost unlimited range of sizes. A wide range of permeability is therefore obtainable that is absolutely essential for latitude in the design of flowmeters. In addition, the wool is inexpensive and easy to procure.

The development of these flowmeters included an investigation into the general flow characteristics of porous media, with particular reference to a medium consisting of randomly arrayed filaments. The primary concern in this paper is with the theoretical aspects of the permeability of highly porous media of this type.

II. Permeability of Porous Media

1. Historical Review

The characteristic law of fluid flow through a porous medium, for sufficiently low flows, is given by

$$\frac{\Delta p}{L}\frac{A}{Q}=c\mu, \tag{1}$$

where

A = cross-sectional area of a cylindrical plug of a porous medium.
L = length of the plug.
Q = volumetric rate of flow of fluid through the plug.
μ = absolute viscosity of the fluid.
Δp = pressure drop between the ends of the plug.
c = a constant (used indiscriminately throughout this paper). In eq 1 it is a factor characteristic of each particular medium. It is approximately a constant, increasing at high flows, and for gases, decreasing at low absolute pressures.

It is the elucidation of the principal dependence of the factor c on the structure of the medium and its incidental dependence on the properties of the fluid that is the principal object in this paper. It will be useful to define the quantity $A\Delta p/LQ$ as the resistivity of the medium for a given fluid, and its reciprocal $LQ/A\Delta p$ as the permeability. The quantity c may then be referred to as the coefficient of resistivity of the porous medium, or its reciprocal $1/c$ as the coefficient of permeability.

D'Arcy's experiments (in 1856) on the flow of water through sands led him to establish eq 1, and it is commonly referred to as D'Arcy's equation.

Dupuit (in 1863) extended it to partially include dependence on the porosity of the medium. The porosity ϵ is defined as the ratio of the volume occupied by voids available to the fluid in a porous medium to the total volume. He argued that the apparent velocity Q/A in a porous medium was less than the actual average velocity in the pore spaces. His expression was thus equivalent to

$$\frac{\Delta p}{L}\frac{A}{Q}=c\frac{\mu}{\epsilon}. \tag{2}$$

Slichter (in 1897) considered a granular bed as an equivalent system of capillary tubes. On this basis he derived the equation

$$\frac{\Delta p}{L}\frac{A}{Q}=c\frac{\mu}{d^2F(\epsilon)}, \tag{3}$$

where

d = dimension characteristic of the structure of the medium. In this instance, it is the diameter of the granule.
$F(\epsilon)$ = empirical function of the porosity.

Many investigators have subsequently attempted to obtain a generally applicable form of the porosity function.

The valuable methods of Stanton and Pannell (in 1914) of correlating data on flow through smooth circular pipes on the basis of the Reynolds number and other dimensionless groups, were followed by the concept of Schiller (in 1923) of a mean hydraulic radius that permitted correlating flow data on noncircular pipes. The mean hydraulic radius r may be defined as the ratio of the volume of a medium filled with a fluid to the surface within the medium in contact with the fluid. Blake (in 1922) utilized the idea of a mean hydraulic radius in graphically correlating data on flow through granular beds in terms of a Reynolds number and other dimensionless groups. The results of Blake's work and the theoretical exposition of Kozeny (in 1927) on granular beds may be summarized in the formula

$$\frac{\Delta p}{L}\frac{A}{Q}=c\frac{\mu s^2}{\epsilon^3}, \tag{4}$$

in which s is the surface per unit volume of a porous medium in contact with the fluid ($s=\epsilon/r$).

The Kozeny, or hydraulic radius, theory (eq 4) is intended to have general applicability to all porous media, because the only properties of the medium that remain buried in the constant c involve the detailed structure of the medium, such as factors that take into account the shape and configuration of the fluid path or the shape and orientation of the material particles. In fact, experiments where this theory is definitely applicable show only moderate variation of this constant for a variety of shapes.

An extensive list of references, complete up to 1938, and more complete exposition of the problem can be found in reference [2].

In 1938 and 1939 [3], eq 4 was modified by Carman to the form

$$\frac{\Delta p}{L}\frac{A}{Q}=c\frac{\mu s_o^2(1-\epsilon)^2}{\epsilon^3}, \tag{5}$$

in which s_o is the "specific" surface exposed to the fluid (surface exposed to the fluid per unit volume of solid material).

The value of c in eq 5 was found to be about 5 for granular materials of low porosities.

Equation 5 was applied to fibrous materials by Wiggins, Campbell, and Maass [4], and by Fowler and Hertel [5]. A clear exposition of the hydraulic radius theory leading to eq 5 may be also found in reference [4].

The latest modification of the hydraulic radius theory [6] involves the introduction of an orientation factor O, which is defined as the averaged value of the square of the sine of the angle between a normal to the particle, fiber, or wall forming the microscopic flow channel and the macroscopic direction of flow. The resulting formula is

$$\frac{\Delta p}{L}\frac{A}{Q}=\frac{\mu K_o s_o^2}{O}\frac{(1-\epsilon)^2}{\epsilon^3}. \tag{6}$$

K_o is a shape factor that should be the same for all channels of the same geometric shape and that should not vary markedly from shape to shape.

The Kozeny, or hydraulic radius, theory (from eq 4 onward) has thus been carried to a high degree of refinement. Many investigators, however, have not felt justified in using any relationship more complicated than the D'Arcy formula (eq 1), in which an empirical constant $1/c$ (the coefficient of permeability) is obtained experimentally for each medium investigated.

A theory developed from a different point of view—which may be referred to as the drag theory—has existed for some time without attracting much recognition or support. Emersleben (in 1925) attempted a mathematical solution of the hydrodynamic problem of the viscous drag of a fluid on a special array of parallel fibers. Burke and Plummer (in 1928) used the drag on spheres to obtain a law for the dependence of permeability of a porous medium on its porosity. The drag theory leads to a different expression for the dependence of resistivity on porosity than that given by the hydraulic radius theory. As existing data at that time and later, particularly on flow through sands, appeared to be consistent with the hydraulic radius theory, little attention has been given to the drag theory.

Actually, it appears that neither the hydraulic radius theory nor the drag theory can be entirely correct, but that each will have a range of application. This concept is implicit in Emersleben's solution. Indeed, data on fibrous materials obtained by Sullivan in 1942 indicated that the hydraulic radius theory broke down at high porosities, where one may expect an elementary viscous drag theory to apply most satisfactorily.

It can be easily understood why there is a separate range of applicability of these two theories by considering the extreme cases. For an array of fibers or particles of large separation, the resistance to flow can be computed as the sum of the fluid drags on each element. As the elements are brought closer together, adjacent elements will modify the flow pattern surrounding a particular element. In principle, if account could be taken of the effect of the mutual interference between particles, the drag theory should be applicable to all porosities. However, in practice, this is beset by mathematical difficulties. Thus an elementary drag theory should fail when applied to low porosities.

In the hydraulic radius theory, the estimate of the resistance offered by a connected network of flow channels is based on the product of the area of solid surface in contact with fluid and an "equivalent" shearing stress acting on this area. The equivalent shearing stress is assumed to be that obtained from the normal velocity gradient that would exist at the walls of an equivalent channel formed between two parallel plates [4]. When the separation between the drag surfaces is small (more exactly, when the separation is small compared to the radius of curvature of a surface), a valid estimate is obtained. However, as the separation increases (higher porosities), the velocity gradient normal to the surface depends more and more on the ratio of the radius of curvature at the surface to the separation rather than on the distance to an adjacent wall. This is readily seen in the case of two concentric tubes with axial flow between them. With small separation, the hydraulic radius theory gives a true account of the flow resistance in the annulus. As the inner tube is shrunk, this is no longer true. Thus it turns out that the hydraulic radius theory is best applicable at low porosities and the drag theory at high porosities.

In the present investigation, expressions for the resistivity of fibrous materials have been derived from elementary consideration of the viscous drag of individual elements and were found to be moderately successful experimentally. This might be expected, as, in general, fibrous materials under moderate packing will still have rather high porosity. It is thus proposed that the same method of attack is suitable for all materials of high porosity.

The problem of intermediate porosities will be left untouched. It is possible, by semiempirical methods, to find expressions that may be expected to fit approximately the entire range of porosities, or, by perturbation methods, to extend the range of applicability of each theory individually, or finally, it may be possible by great effort, to find one single mathematical solution that is applicable at all porosities.

2. Drag Theory of Permeability

We will undertake to account for the permeability of a random distribution of circular cylindrical fibers of the same diameter on the basis of the drag on individual elements.

It will be assumed that the flow resistivity of all random distributions of the same fibers per unit volume will not differ, and that it will be the same as that obtained with an equipartition of fibers in three perpendicular directions, one of which is alon

the direction of macroscopic flow. It will be further assumed that the separation between fibers, and the length of individual fibers are both large compared to the fiber diameter (high porosities), and that the disturbance due to adjacent fibers on the flow around any particular fiber is negligible.

If it be assumed that fluid inertial forces are negligible (low local Reynolds number) an equation can be derived by equating the pressure at two planes perpendicular to the direction of macroscopic flow to the viscous drag force on all elements between the planes. It is assumed that the pressure drop necessary to overcome the viscous drag is linearly additive for the various fibers, whether parallel or perpendicular to the flow.

It was estimated from Emersleben's paper [7] that the drag force per unit length of a single fiber surrounded by similar fibers all oriented along the direction of flow and with moderate separations is approximately given by

$$f=4\pi\mu v, \tag{7}$$

where

f=drag force per unit length of fiber.
v=velocity of the fluid stream distant from the filament.

If it be assumed that there are n filaments per unit volume, and that $n/3$ filaments are arrayed in each of the three perpendicular directions, the total drag force in a unit volume due to the $n/3$ filaments parallel to the flow can be equated to the pressure drop per unit length, so that

$$\frac{\Delta p}{L}=\frac{4\pi n}{3}\mu v. \tag{8}$$

It is estimated from Oseen's solution for a cylinder perpendicular to a stream that partially takes into account fluid inertia (see Lamb's "Hydrodynamics") that the drag force for such filaments is given by

$$f=\frac{4\pi}{2-ln\ R}\mu v. \tag{9}$$

in which

$\ln R$=natural logarithm of the local Reynolds number.
R=Reynolds number, defined as $dv\rho/\mu$.
d=fiber diameter.
ρ=fluid density.

The drag force on each of the two sets of $n/3$ filaments per unit volume, arrayed perpendicular to the fluid flow, can be equated to the pressure drop per unit length, giving

$$\frac{\Delta p}{L}=\frac{4\pi n}{3(2-ln\ R)}\mu v. \tag{10}$$

Linear superposition or simple addition of the three sets of pressure drops necessary to overcome the drag of the three sets of filaments results in the total pressure gradient of

$$\frac{\Delta p}{L}=\frac{4\pi n}{3}\frac{4-ln\ R}{2-ln\ R}\mu v. \tag{11}$$

The number of fibers n per unit volume, which is also equal to the total fiber length per unit volume, may be eliminated, as the apparent density of a fibrous pack in vacuum σ_p is equal to the product of the fiber volume and the fiber density σ_f, or

$$\sigma_p=\frac{\pi}{4}d^2 n\sigma_f. \tag{12}$$

Eliminating n, eq 11 reduces to

$$\frac{\Delta p}{L}=\frac{16\mu v}{3}\frac{\sigma_p}{\sigma_f d^2}\frac{4-ln\ R}{2-ln\ R}. \tag{13}$$

The velocity profile between fibers is assumed to be sufficiently flat for high porosities so that the velocity may be taken as constant. The velocity v is therefore related to the volumetric rate of flow Q and the macroscopic cross sectional area of a plug A by the relation

$$v=\frac{Q}{\epsilon A} \tag{14}$$

It follows from the definition of the porosity ϵ that

$$1-\epsilon=\frac{\sigma_p}{\sigma_f}. \tag{15}$$

With the use of these two relations, eq 13 may be put in the form

$$\frac{\Delta p}{L}\frac{A}{Q}=\frac{16\mu}{3}\frac{1-\epsilon}{\epsilon d^2}\frac{4-ln\ R}{2-ln\ R},$$

$$=\frac{16\mu}{3}\frac{\sigma_p}{(\sigma_f-\sigma_p)d^2}\frac{4-ln\ R}{2-ln\ R}. \tag{16}$$

Although the derivation, as given, assumed an incompressible fluid, it can be readily shown that the derived equations are unchanged for a compressible fluid, flowing isothermally, if the volumetric flow at the arithmetic mean pressure Q_m is used in eq 16. It is therefore applicable to both liquids and gases. However, it will be shown later, that an additional correction must be made to eq 16 for gases at low absolute pressures.

If eq 6 is compared with eq 16 and their ratio is interpreted in terms of the shape factor of the hydraulic radius theory, it is possible to predict the general variation of the shape factor K_o at high porosity. At low porosities, K_o is constant, but at high porosities it should become asymptotic to

$$K_o=\frac{c}{1-\epsilon} \tag{17}$$

where c is a constant.

This prediction is qualitatively compatible with the data given in reference [6].

Another significant implication in eq 16 is that the resistivity (or permeability) is not a constant but varies slowly with Reynolds number. The theoretical variation of the resistivity is shown in table 1.

TABLE 1. *Theoretical variation of resistivity with Reynolds number for a porous plug of randomly arrayed fibers*

Reynolds number, $\frac{dQ_p}{\mu A \epsilon}$	Factor proportional to resistivity, $\frac{16}{3}\frac{4-\ln R}{2-\ln R}$
0	5.3
10^{-5}	6.1
10^{-4}	6.3
10^{-3}	6.5
10^{-2}	6.9
10^{-1}	7.8
1	10.7

This slow variation of resistivity with flow is quite characteristic of many elements in which the flow is nominally viscous and was immediately found experimentally in the first glass wool flowmeters that were studied. While in general it is reasonable to assume that this effect is associated with fluid inertia, it is often difficult to account for it precisely. In fact, a common method of separating the resistance into two additive components, one proportional to the viscous resistance, and the other proportional to a kinetic energy loss, often fails in securing added precision in describing experimental results with linear flow elements.

In eq 16, it is noteworthy that the effect has been associated with an intrinsic variation of drag with Reynolds number. An extremely interesting mathematical interpretation of eq 16 is possible. The slow variation of a logarithmic expression, as that give in eq 16, can be closely approximated by an exponential form.

$$\frac{\Delta p}{Q} = cQ^x. \tag{18}$$

This type of relation is often successfully used for linear flow elements without apparent theoretical justification. At least in the case of highly porous fibrous media it has been shown to have theoretical validity.

The quantity Q^x represents to a high degree the point variation of Reynolds number, where the best value of x depends on the Reynolds number.

For the resistance law given by eq 16, the best value of x is

$$x = \frac{2}{(2-\ln R)(4-\ln R)}. \tag{19}$$

In reference [1], eq 16 was used for comparison with experimental data on glass wool and fair agreement found, so that its essential validity appears established. While it is apparent that eq 16 was derived from elementary considerations, to which many refinements are possible, particularly as to the statistical distribution function for drag and second-order effects of porosity, lack of extensive experimental data make these refinements dubious. As an illustration of the possible accuracy of eq 16, some selected data of fair accuracy obtained subsequent to the issue of reference [1] permitted close fitting by the formula

$$\frac{\Delta p}{L}\frac{A}{Q} = 9.4\mu \frac{\sigma_p}{(\sigma_f - \sigma_p)d^2}\frac{2.4-\ln R}{2-\ln R}. \tag{20}$$

Although at first sight, the change in numerical constants appears drastic, it can be shown to represent moderately reasonable changes in the amount and relative weighting of the parallel and perpendicular fiber drags.

The main conclusion from all the experimental data obtained is that the coefficient of the resistivity function always fell in the approximate range of 5 to 10, and that the variation of resistivity with Reynolds number is less than given by eq 16, but not as small as given by eq 20.

3. Limits of Linearity

It is well known that a laminar flow regime does not persist around elements producing drag in a fluid stream at Reynolds numbers much greater than 1. Even at Reynolds numbers less than 1, the drag force will not remain strictly proportional to the velocity. Furthermore, even when drag is almost proportional to velocity for an indivdual element, this may not necessarily hold true for an array of similar elements, even though widely spaced.

The value of the resistivity given by eq 16 may therefore not be expected to apply for Reynolds numbers much greater than 1. However, experimental data indicated no inconsistencies up to a value of Reynolds number even as great as 1.2. Therefore, as a round measure of the limit of flow linearity, a Reynolds number of 1 may be assumed.

The resistance of a given porous plug used as a flowmeter may therefore be expressed as

$$\frac{\Delta p}{Q} = \left(\frac{\Delta p}{Q}\right)_{\max}\left(\frac{4-\ln R_{\max}-\ln Q/Q_{\max}}{2-\ln R_{\max}-\ln Q/Q_{\max}}\right)\left(\frac{2-\ln R_{\max}}{4-\ln R_{\max}}\right). \tag{21}$$

where the subscript max refers to the values of quantities at the maximum or full scale flow.

4. Pressure Variation of Resistivity at Low Pressure for Gases

At low absolute pressures, the flow of gas along a tube does not obey Poiseuille's law, the flow being somewhat larger for a given pressure drop than predicted by this law. At low gas pressures the resistance to flow in a tube may be derived by the methods of statistical mechanics [8].

The essential idea is that at low pressures, where the separation between walls is of the order of the mean free path, molecules will suffer few collisions with each other, and therefore should be capable of being urged to drift, or "flow", by an infinitesimal pressure gradient. However, there will be a loss of momentum suffered by molecules that collide with a stationary boundary (the tube wall). This loss of momentum is computed by assuming that, with a finite pressure gradient, the velocity of a molecule consists of its drift, or flow, velocity, superimposed on its Maxwellian thermal velocity; and that as a result of collisions with a wall, the molecule will be diffusely reflected, that is, it will give up its drift velocity and be reflected with some random Maxwellian velocity. The average velocity profile for gas flowing at low absolute pressures in a tube will therefore consist of a flat portion between the walls of constant velocity equal to the drift velocity, and a portion near the walls that falls very rapidly to zero, so that the velocity profile looks essentially flat-topped. This represents the model for molecular "drift" flow in a tube. At high pressures, viscosity is used to account for the flow resistance.

Knudsen found that, for a given pressure gradient at any absolute pressure, a large fraction of the drift velocity can be added to the "viscous" velocity to obtain a composite velocity in good agreement with experiment. The fraction of the computed drift velocity was semiempirically determined to range from 0.81 to 1, depending on the ratio of mean free path to wall separation. The effect of this superposition leads to a result that encompasses the entire pressure range. One term, the Knudsen term, becomes predominant at low pressures, while the other term, the Poiseuille term, becomes predominant at high pressures. In the intermediate pressure range (above 1 mm Hg absolute pressure), although small, the Knudsen term is not negligible.

Application of the same theory to porous media of a random filament nature leads to the result that the molecular drift flow at low pressure Q'_m is approximately given by

$$Q'_m=\left(\frac{8}{9\pi}\right)^{1/2}\frac{A\Delta p}{L}\frac{d(1-\sigma_p/\sigma_f)^2\sigma_f}{\sigma_p}\left(\frac{p}{\rho}\right)_o^{1/2}\left(\frac{1}{p_o}\right)\frac{p_o}{p_m}, \quad (22)$$

where subscript m refers to conditions at the mean pressure, and

p_o=arbitrary reference pressure, chosen as 1 atmosphere.

$(p/\rho)_o$=pressure to density ratio for the gas at the mean plug temperature.

Following Knudsen, 0.81 of the drift flow is simply added to the viscous flow of eq 16, so that the total flow at mean conditions is

$$Q_m=\frac{1}{5.3}\,\frac{2-\ln R}{4-\ln R}\,\frac{(\sigma_f-\sigma_p)d^2}{\sigma_p}\,\frac{A\Delta p}{\mu_m L}$$
$$\left[1+(.81)(10)\left(\frac{8}{9\pi}\right)^{1/2}\frac{\sigma_f-\sigma_p}{\sigma_f d}\left(\frac{p}{\rho}\right)_m^{1/2}\frac{\mu_m}{p_o}\,\frac{p_o}{p_m}\right]. \quad (23)$$

The approximate value 10 was chosen for the resistivity function in the Knudsen term in the bracket.

The form of eq 23 is thus

$$Q_m=c\left(1+b\,\frac{p_o}{p_m}\right)\Delta p, \quad (24)$$

where b is the coefficient of the Knudsen term.

Experimentally, a linear variation of permeability $Q_m/\Delta p$ with the reciprocal mean pressure ratio p_o/p_m was always obtained. In fact, fair agreement was found with the theoretically computed cofficient b in practically all cases, although this result may have been purely fortuitous.

III. Range of Useful Porosities of Fibrous Materials

The following section, largely based on speculative considerations, is irrelevant to the development of the theory of permeability of porous media. However, it is of utility in the design of flowmeters. In a flowmeter, it is desirable to pack the fibrous material to such a density that it will remain relatively rigid under vibration, shock, or differential pressure overload.

The following theoretical and experimental conclusions, while tentative, furnish a rough guide in determining usable porosity limits for design purposes:

1. The upper limit to the porosity of a fibrous material is obtained with a free pack and is approximately 0.98. The minimum ratio of free pack to fiber density σ_p/σ_f is thus approximately 0.02. The usable upper limit of porosity is set by other design considerations.

2. The lower limit to the porosity of a fibrous material is approximately 0.50.

3. To a crude approximation, the compressibility of all fibrous materials is the same, and equals 0.0021 lb/in.^{3} of pack per pounds per square inch of pressure load.

4. Fibrous materials have fairly reproducible and constant compressibility characteristics on increasing load but show erratic hysteresis with decreasing load. Therefore all packing adjustments on fibrous plugs should be made with increasing load.

The approximate constancy of the free-pack density, it is believed, is related to the geometric-mechanical problem of the minimum number of filaments that must be introduced into a given volume to bind and form a stable pack.

The lower limit to the porosity of fibrous materials may be estimated by considering a close packed array of fibers perpendicular to each other in three directions. The porosity for such an array was computed to be 0.41. Experimentally, porosities as low as 0.5 were obtained. While lower porosities can be obtained, it is believed that serious compression of the material rather than fiber bending would take place.

The approximate constancy of compressibility of various materials is probably related to the similar small variation in the ratio of elastic modulus to

density for many elastic materials. Various models for the compressibility of a fibrous pack demonstrate the dependence of pack compressibility on this parameter.

In lieu of any other information, the variation of pack density with pressure loading for increasing load may be taken as

$$\sigma_p = 0.02\sigma_f + 0.0021P, \tag{25}$$

where

σ_p = pack density.
σ_f = density of the fiber (in the same units).
P = pressure loading. The constant 0.0021 has the units lb/in.^{3}/psi.

The theoretical range of pack density ratio is approximately 0.02 to 0.50. The practical range of pack density ratio for flowmeter design is probably 0.1 to 0.3.

IV. Design of Linear Flowmeters

A convenient procedure is outlined in this section for designing a linear flowmeter on the basis of the theory developed in section II. It is assumed that the basic problem is to design a linear flowmeter that will possess a desired resistance $\Delta p/Q$, which is constant within given limits over a desired flow range $O - Q_{max}$ for a given fluid. To meet these requirements, compromise choices must be made of fiber diameter, cross-sectional area of the flow-metering plug, plug density, and plug length.

A scheme, involving the use of a simple chart, has been evolved for design purposes. In the interests of clarity, the theory by which the design chart was devised will be sketched.

Equation 23 sets forth the law of isothermal gas flow for a fibrous plug as

$$Q_m = \frac{1}{5.3}\,\frac{2-\ln R}{4-\ln R}\,\frac{(\sigma_f-\sigma_p)\,d^2}{\sigma_p}\,\frac{A\Delta p}{\mu_m L}\left[1+(.81)\,(10)\left(\frac{8}{9\pi}\right)^{1/2}\frac{\sigma_f-\sigma_p}{\sigma_f d}\left(\frac{p}{\rho}\right)_m^{1/2}\frac{\mu_m}{p_o}\,\frac{p_o}{p_m}\right]. \tag{23}$$

The same equation holds for liquids, except that the bracketed expression has the value unity.

As it is assumed that this law holds only for high porosities, the small correction term in the bracket may be evaluated for a porosity of unity so that eq 23, for gases, becomes

$$Q_m = \frac{1}{5.3}\,\frac{2-\ln R}{4-\ln R}\,\frac{\sigma_f-\sigma_p}{\sigma_p}\,d^2\,\frac{A}{\mu_m L}\left[1+\frac{4.3}{d}\left(\frac{p}{\rho}\right)_m^{1/2}\frac{\mu_m}{p_o}\,\frac{p_o}{p_m}\right]\Delta p. \tag{26}$$

It will be convenient, in this section, to drop the subscript m, which denotes mean isothermal conditions, leaving it understood.

From the definition, the Reynolds number is

$$R = \frac{d\rho Q\sigma_f}{\mu A(\sigma_f-\sigma_p)}. \tag{27}$$

These equations may be regrouped by the following definitions:

$$L_o = L\,\frac{\sigma_p}{\sigma_f-\sigma_p} = L\,\frac{1-\epsilon}{\epsilon}, \tag{28}$$

where

L = actual plug length.
L_o = fictitious plug length (length of plug if compressed to a porosity of 0.50).

$$M_o = \frac{M_{max}}{R_{max}}\,\frac{\sigma_f}{\sigma_f-\sigma_p} = \frac{M_{max}}{R_{max}}\,\frac{1}{\epsilon}, \tag{29}$$

in which

M = mass flow ($M = \rho Q$).
M_{max} = maximum mass flow for which the flowmeter is to be used.
R_{max} = corresponding maximum Reynolds number.
M_o = fictitious flow (mass flow at which the Reynolds number is unity if the medium had unit porosity).

$$\left.\begin{aligned}\left(\frac{Q}{\Delta p}\,L_o\right)_o &= \frac{1}{5.3}\,\frac{(\mu A)^3}{(\mu M_o)^2},\\ &= \frac{1}{5.3}\left(\frac{d}{\mu}\right)^3\mu M_o\end{aligned}\right\}. \tag{30}$$

The quantity $(QL_o/\Delta p)_o$ is a fictitious value for the flow per unit pressure gradient (the value for a Reynolds number of zero). It is closely related to the true value by the relation

$$\frac{QL_o}{\Delta p} = \frac{2-\ln R}{4-\ln R}\left(\frac{Q}{\Delta p}\,L_o\right)_o\left[1+\left(\frac{4.3}{p_o}\right)\left(\frac{p}{\rho}\right)^{1/2}\left(\frac{\mu}{d}\right)\frac{p_o}{p}\right]. \tag{31}$$

The definitions, eq 27 through 30, and eq 31 contain the desired solution.

Equation 30 may be plotted as a generalized chart applicable to all fluids, or, by choice of fluid parameters, as a design chart suitable for a specific fluid. It is presented in generalized form in figure 1 as a logarithmic plot of $(Q/\Delta p)L_o$ against μM_o for constant values of μA and d/μ respectively. The use of figure 1 or eq 30 leads to values of A, L, and d for a porous plug that nominally will have the desired resistance $\Delta p/Q$. The best choice of these parameters depends upon the deviations from constant resistance that may be tolerated.

As the permeability theory developed has only nominal certainty, it is not to be expected that a desired resistance will be experimentally obtained with any great accuracy, so that in general, a moderate amount of resistance adjustment will be found necessary. (Illustratively, this may be accomplished by variation of the weight of glass wool used.) Therefore little distinction need be made as to the nominal design value of $\Delta p/Q$. The value $(\Delta p/Q)_o$ may thus be regarded as the resistance at full scale,

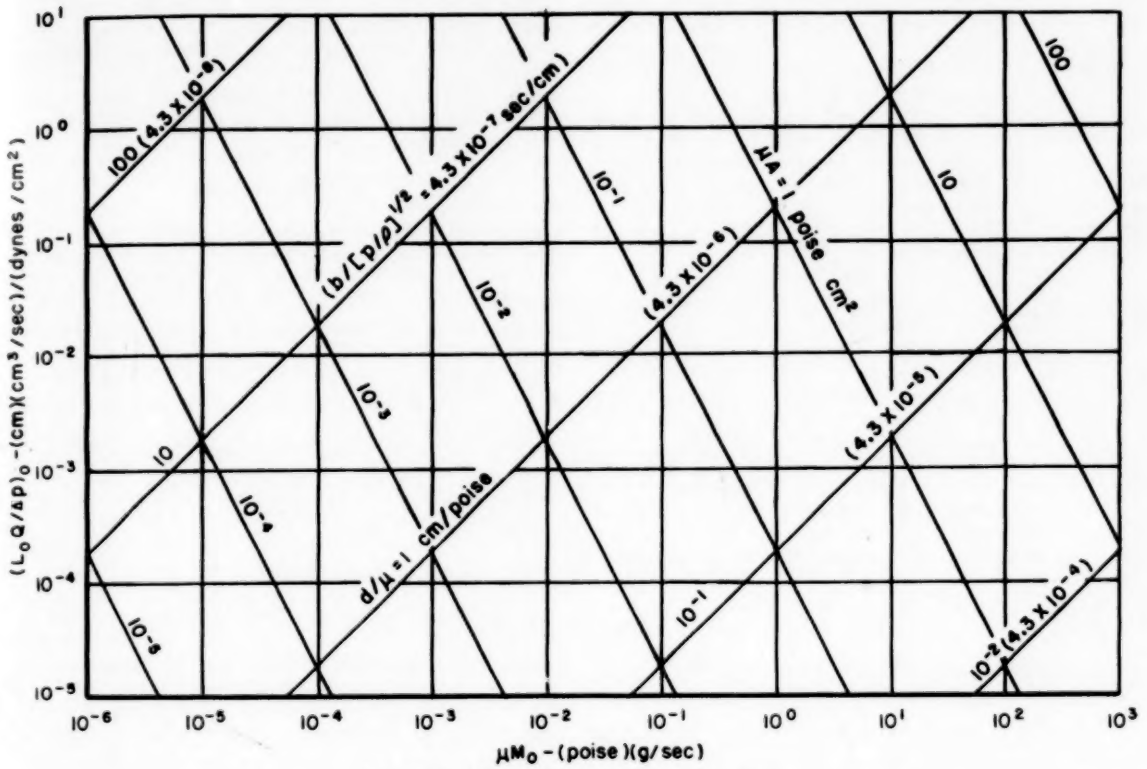

FIGURE 1. *Design chart for linear flowmeters*

(See text for explanation of its use.)

establishing a nominal straight line calibration for the flowmeter. The variation of $(2-1nR)/(4-1nR)$ with flow may be regarded as determining the expected deviation from linearity, which may be characterized by its maximum value as either a quadratic deviation, or, more accurately, as an exponential deviation. The maximum deviation from a straight line fitted to the maximum flow and pressure drop is given in table 2, computed on the basis of eq 16. Any desired degree of linearity therefore determines a maximum value of Reynolds number to use for design purposes.

TABLE 2. *Theoretical maximum deviation from linearity for a fibrous plug flowmeter*

Reynolds number at full scale flow, R_{max}	Maximum difference between true flow and linear approximation	Location of maximum
	Percentage of full scale flow	*Percentage of full scale flow*
1	6.5	48
10^{-1}	2.2	43
10^{-2}	1.1	41
10^{-3}	0.7	40
10^{-4}	.5	40
10^{-5}	.3	40
10^{-6}	.3	39

For gases, eq 31 indicates a change in resistance with absolute pressure, which depends on the fiber diameter d. Any desired degree of uniformity in the resistance over a range of absolute pressures can be secured by proper selection of d.

Finally, practical consideration of size and the usable porosity range of 0.7 to 0.9 determine the length L and cross-sectional area A.

For purposes of clarity, a design procedure is given in some detail below:

1. Determine the following constants of the fluid to be metered: μ, ρ, p/ρ (for gases).

2. Decide upon the maximum flow Q_{max} to be metered, the desired resistance $\Delta p/Q$, the maximum amount of nonlinear deviation that may be tolerated, and in the case of gases, the absolute pressure range in which the flowmeter is to be used, and the corresponding range of resistance $\Delta p/Q$ that may be tolerated.

3. Decide upon the maximum practical range that may be used for A, L, and d.

4. From table 2, choose the maximum value of R_{max} that will give the desired linearity. Smaller values of R_{max} will give better linearity but may require such large plug areas as to be impractical. A rough empirical criterion is to consider a design band 1 decade wide. Compute minimum and maxi-

mum values of M_o (eq 29) assuming minimum and maximum values for both R_{max} and ϵ. The range of ϵ may be taken as 0.7 to 0.9. Compute the corresponding values for μM_o and mark out the vertical band corresponding to these limits in figure 1.

5. For the maximum and minimum limits assumed for both L and ϵ, compute the corresponding limits for L_o (eq 28). Compute the corresponding values of $QL_o/\Delta p$ and mark out the horizontal band corresponding to these limits in figure 1. Steps (4) and (5) result in a design rectangle on figure 1 within which a solution is possible.

6. Further limit this design rectangle by excluding regions of figure 1 representing greater and lesser area A (really μA) than desired.

7. For gas flow, compute the maximum tolerable value of the coefficient of the Knudsen term b and the corresponding minimum value of fiber diameter d. Exclude regions of figure 1 representing smaller values of d (really d/μ). One may then choose design parameters corresponding to any point in the design region that has not been excluded.

8. When the flowmeter is built and tested, adjustment of the resistivity can then be made by the principal technique of changing the weight of glass wool used.

Financial support for this investigation was provided by the Office of Naval Research under a project on Basic Instrumentation of Scientific Research. Grateful acknowledgement is also due W. A. Wildhack, at whose suggestion and under whose supervision the development of the glass wool flowmeter was carried on.

V. References

[1] National Bureau of Standards Report to the Bureau of Aeronautics, Navy Department, Washington, D. C., entitled, Linear pressure drop flowmeters for oxygen regulator test stands, reference 6.2/6211–2885 (Sept. 25, 1947).
[2] P. C. Carman, Trans. Institution Chem. Engrs. **15,** 151 (1937); **16,** 168 (1938).
[3] P. C. Carman, J. Soc. Chem. Ind. **57,** 225 (1938); **58,** 1 (1939).
[4] E. Wiggin, W. Campbell, O. Maass, Can. J. Research **17,** 318 (1939).
[5] J. Fowler and K. Hertel, J. App. Phys. **12,** 503 (1941).
[6] R. Sullivan, J. App. Phys. **12,** 503 (1941); **13,** 725 (1942).
[7] O. Emersleben, Physik. Z. **26,** 601 (1925).
[8] R. Tolman, Statistical mechanics with applications to physics and chemistry (Chemical Catalogue Co., New York, N. Y., 1927).

WASHINGTON, April 6, 1950.

Journal of Research of the National Bureau of Standards Vol. 45, No. 5, November 1950 Research Paper 2151

Density, Refractive Index, Boiling Point, and Vapor Pressure of Eight Monoolefin (1-Alkene), Six Pentadiene, and Two Cyclomonoolefin Hydrocarbons[1]

By Alphonse F. Forziati,[2] David L. Camin,[3] and Frederick D. Rossini[3]

Density (at 20°, 25°, and 30° C), refractive index (at seven wavelengths at 20°, 25°, and 30° C), vapor pressure, and boiling point (from 48 to 778 mm Hg) of 16 highly purified samples of hydrocarbons of the API–NBS series were measured for 8 monoolefin (1-alkene), 6 pentadiene, and 2 cyclomonoolefin hydrocarbons.

The data on refractive index were adjusted by means of modified Cauchy and Hartmann equations, and values of the constants are given for each compound.

The data on vapor pressure were adjusted by means of the method of least squares and the three-constant Antoine equation. The values of the constants are given for each compound.

Values were calculated for the specfic dispersions, $(n_F-n_C)/d$ and $(n_s-n_D)/d$.

As a cooperative investigation of the National Bureau of Standards, the U. S. Office of Rubber Reserve, and the American Petroleum Institute Research Project 6, measurements of density, refractive index, vapor pressure, and boiling point were made on highly purified samples of eight monoolefin (1-alkene), six pentadiene, and two cyclomonoolefin hydrocarbons of the API–NBS series.

The compounds measured were made available through the American Petroleum Institute Research Project 44 on the "Collection, calculation, and compilation of data on the properties of hydrocarbons." The samples were purified by the American Petroleum Institute Research Project 6 on the "Analysis, purification, and properties of hydrocarbons," from material supplied by the following laboratories:

1-Pentene, by the Phillips Petroleum Co., Bartlesville, Okla.

1-Hexene, 1-heptene, 1-nonene, 1-undecene, and 1,4-pentadiene, by the American Petroleum Institute Research Project 45, at the Ohio State University, Columbus, Ohio.

[1] This investigation was performed at the National Bureau of Standards as part of the work of the American Petroleum Institute Research Project 6 on the "Analysis, purification, and properties of hydrocarbons."
[2] Formerly Research Associate on the American Petroleum Institute Research Project 6.
[3] Present address: Carnegie Institute of Technology, Pittsburgh 13, Pa.

1-Octene, 1-decene, 1-dodecene, 2-methyl-1,3-butadiene, and cyclohexene, by the American Petroleum Institute Research Project 6.

1,2-Pentadiene and 2,3-pentadiene, by the Hydrocarbon Laboratory, Pennsylvania State College, State College, Pa.

1,*cis*-3-Pentadiene and 1,*trans*-3-pentadiene, by the Office of Rubber Reserve, Washington, D. C.

Cyclopentene, by the Atlantic Refining Co., Philadelphia, Pa., and the American Petroleum Institute Research Project 45 at the Ohio State University, Columbus, Ohio.

The purification and determination of purity and freezing point of these compounds are described in references [1 to 5].[4]

It is believed that in each case the impurity was of such nature and present in such small amount that the properties measured were not affected beyond the indicated limits of uncertainty.

The measurements of density were made at 20°, 25°, and 30° C with a density balance, the assembly, calibration, and operation of which has been previously described [6]. The experimental results on density are given in table 1. Individual measurements were reproducible within ± 0.00003 g/ml. The accuracy of the tabulated values, including the effect of impurities, is estimated to be ± 0.00005 to ± 0.00010 g/ml for the 10 monoolefins and ± 0.00008 to ± 0.00015 g/ml for the 6 pentadienes.

The refractive index was measured by means of the same apparatus and procedure previously described [7]. The calculations and correlations were also made in the same manner as in [7]. Table 2 gives the values of the constants of the modified Cauchy and Hartmann equations for each of the 16 compounds. The fifth and last columns of the table give the root-mean-square value of the deviations of the observed from the calculated points. Table 3 gives the adjusted values of refractive index at each of seven wavelengths (from 6,678 to 4,358 Angstrom units) at 20°, 25°, and 30° C. Figure 1 is a plot of the values of the constants n_∞ and C of the modified Hartmann equation, as a function of the number of carbon atoms in the normal alkyl radical of the series of 1-alkenes. Table 4 gives the values of the specific dispersions $10^4(n_F - n_C)/d$ and $10^4(n_g - n_D)/d$ calculated from the values of refractive index in table 3 and of density in table 1.

[4] Figures in brackets indicate the literature references at the end of this paper.

TABLE 1. *Values of density*

Compound	Formula	Density [a]			Temperature coefficient of density at 25° C
		20° C	25° C	30° C	
		g/ml	*g/ml*	*g/ml*	*g/ml °C*
1-Pentene	C_5H_{10}	0.64050	0.63533		[b] 0.001034
1-Hexene	C_6H_{12}	.67317	.66848	0.66374	.000943
1-Heptene	C_7H_{14}	.69398	.69267	.68815	.000883
1-Octene	C_8H_{16}	.71492	.71085	.70658	.000834
1-Nonene	C_9H_{18}	.72922	.72531	.72134	.000788
1-Decene	$C_{10}H_{20}$	.74081	.73693	.73304	.000777
1-Undecene	$C_{11}H_{22}$	.75032	.74655	.74276	.000756
1-Dodecene	$C_{12}H_{24}$	.75836	.75474	.75103	.000733
1,2-Pentadiene	C_5H_8	.69257	.68760	.68260	.000997
1,*cis*-3-Pentadiene	C_5H_8	.69102	.68592	.68082	.001020
1,*trans*-3-Pentadiene	C_5H_8	.67603	.67102	.66592	.001011
1,4-Pentadiene	C_5H_8	.66076			
2,3-Pentadiene	C_5H_8	.69502	.69000	.68479	.001023
2-Methyl-1,3-butadiene	C_5H_8	.68095	.67587	.67076	.001019
Cyclopentene	C_5H_8	.77199	.76653	.76124	.001075
Cyclohexene	C_6H_{10}	.81096	.80609	.80141	.000955

[a] For air-saturated hydrocarbon in the liquid state at 1 atm.
[b] This value at 22.5° C.

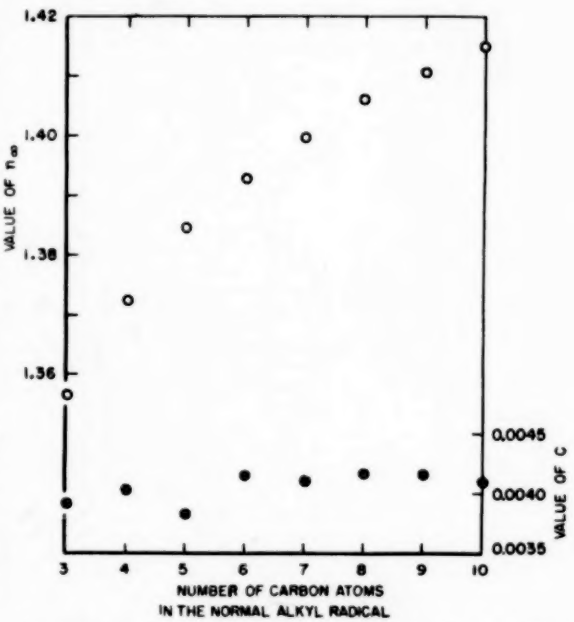

FIGURE 1. *Values of the constants, n_∞ and C, of the modified Hartmann equation, as a function of the number of carbon atoms in the normal alkyl radical for the series of 1-alkenes.*
○=n_∞; ●=C.

TABLE 2. *Values of the constants of the modified Cauchy and Hartman equations*

Compound	Formula	Constants in the equation [a] $\Delta n = a + b/\lambda^3$			Constants in the equation $n_\lambda = n_\infty + C/(\lambda - \lambda^*)^{1.6}$ at 25° C			
		$a \times 10^3$	$b \times 10^3$	$\rho \times 10^3$	n_∞ ;	C	λ^*	$\rho \times 10^3$
1-Pentene	C_5H_{10}	2.998	0.0471	7.44	1.35600	0.003924	0.10060	4.11
1-Hexene	C_6H_{12}	2.773	.0308	4.30	1.37241	.004022	.09976	3.25
1-Heptene	C_7H_{14}	2.560	.0382	3.18	1.38474	.003835	.10874	1.60
1-Octene	C_8H_{16}	2.408	.0334	6.47	1.39311	.004271	.09260	5.07
1-Nonene	C_9H_{18}	2.309	.0284	5.76	1.40048	.004103	.09942	1.65
1-Decene	$C_{10}H_{20}$	2.244	.0285	4.10	1.40616	.004169	.09725	2.54
1-Undecene	$C_{11}H_{22}$	2.176	.0295	4.43	1.41081	.004185	.09737	2.07
1-Dodecene	$C_{12}H_{24}$	2.121	.0292	3.96	1.41490	.004111	.10033	1.14
1,2-pentadiene	C_5H_8	3.053	.0433	5.92	1.40119	.004885	.12273	5.31
1,*cis*-3-Pentadiene	C_5H_8	3.218	.0737	4.24	1.41010	.006167	.14772	2.10
1-*trans*-3-Pentadiene	C_5H_8	3.192	.0690	3.42	1.40386	.006289	.14256	3.74
1,4-Pentadiene	C_5H_8				[b] 1.37404	[b] .004320	[b] .12451	[b] 4.47
2,3-Pentadiene	C_5H_8	3.194	.0462	5.19	1.40728	.005353	.11758	1.73
2-Methyl-1,3-butadiene	C_5H_8	3.225	.0694	8.02	1.39722	.005967	.13783	5.54
Cyclopentene	C_5H_8	2.972	.0293	2.00	1.40550	.004350	.10549	1.03
Cyclohexene	C_6H_{10}	2.672	.0326	2.03	1.42947	.004429	.10859	1.57

[a] $\Delta n = \frac{n_{20} - n_{30}}{2}$.

[b] These values at 20° C.

TABLE 3. *Values of refractive index at seven wavelengths and three temperatures*

Wavelength	Spectral line	Index of refraction at—											
		20° C	25° C	30° C	20° C	25° C	30° C	20° C	25° C	30° C	20° C	25° C	30° C
		1-Pentene, C_5H_{10}			1-Hexene, C_6H_{12}			1-Heptene, C_7H_{14}			1-Octene, C_8H_{16}		
A													
6678.1	He_{red}	1.36883	1.36573	.....	1.38519	1.38235	1.37951	1.39711	1.39446	1.39181	1.40594	1.40346	1.40098
6562.8	Hc	1.36916	1.36605	.....	1.38552	1.38268	1.37984	1.39744	1.39479	1.39214	1.40629	1.40380	1.40131
5892.6	Na_D	1.37148	1.36835	.....	1.38788	1.38502	1.38216	1.39980	1.39713	1.39446	1.40870	1.40620	1.40370
5460.7	Hg_e	1.37348	1.37032	.....	1.38991	1.38703	1.38415	1.40183	1.39914	1.39645	1.41077	1.40825	1.40573
5015.7	He_{blue}	1.37614	1.37295	.....	1.39261	1.38971	1.38681	1.40455	1.40184	1.39913	1.41351	1.41097	1.40843
4861.3	Hf	1.37725	1.37405	.....	1.39373	1.39083	1.38793	1.40569	1.40297	1.40025	1.41465	1.41210	1.40955
4358.3	Hg_g	1.38183	1.37858	.....	1.39837	1.39543	1.39249	1.41042	1.40766	1.40490	1.41933	1.41675	1.41417
		1-Nonene, C_9H_{18}			1-Decene, $C_{10}H_{20}$			1-Undecene, $C_{11}H_{22}$			1-Dodecene, $C_{12}H_{24}$		
6678.1	He_{red}	1.41208	1.41061	1.40824	1.41870	1.41639	1.41408	1.42332	1.42108	1.41884	1.42727	1.42508	1.42289
6562.8	Hc	1.41332	1.41095	1.40858	1.41904	1.41673	1.41442	1.42366	1.42142	1.41918	1.42761	1.42542	1.42323
5892.6	Na_D	1.41572	1.41333	1.41094	1.42146	1.41913	1.41680	1.42609	1.42383	1.42157	1.43002	1.42782	1.42562
5460.7	Hg_e	1.41778	1.41538	1.41298	1.42352	1.42118	1.41884	1.42816	1.42589	1.42362	1.43210	1.42988	1.42766
5015.7	He_{blue}	1.42052	1.41810	1.41568	1.42627	1.42391	1.42155	1.43093	1.42864	1.42635	1.43486	1.43262	1.43038
4861.3	Hf	1.42167	1.41924	1.41681	1.42741	1.42505	1.42269	1.43208	1.42978	1.42748	1.43601	1.43377	1.43153
4358.3	Hg_g	1.42639	1.42393	1.42147	1.43213	1.42974	1.42735	1.43682	1.43449	1.43216	1.44077	1.43850	1.43623
		1,2-Pentadiene, C_5H_8			1,*cis*-3-Pentadiene, C_5H_8			1,*trans*-3-Pentadiene, C_5H_8			1,4-Pentadiene, C_5H_8		
6678.1	He_{red}	1.41724	1.41409	1.41094	1.43103	1.42765	1.42427	1.42483	1.42148	1.41813	1.38550	.....	.....
6562.8	Hc	1.41709	1.41454	1.41139	1.43168	1.42829	1.42490	1.42547	1.42212	1.41877	1.38591	.....	.....
5892.6	Na_D	1.42091	1.41773	1.41455	1.43634	1.43291	1.42948	1.43008	1.42669	1.42330	1.38876	.....	.....
5460.7	Hg_e	1.42372	1.42052	1.41732	1.44046	1.43699	1.43352	1.43415	1.43073	1.42731	1.39125	.....	.....
5015.7	He_{blue}	1.42750	1.42428	1.42106	1.44612	1.44261	1.43910	1.43972	1.43625	1.43278	1.39461	.....	.....
4861.3	Hf	1.42910	1.42586	1.42262	1.44854	1.44501	1.44148	1.44209	1.43861	1.43513	1.39603	.....	.....
4358.3	Hg_g	1.43579	1.43251	1.42923	1.45887	1.45526	1.45165	1.45219	1.44863	1.44507	1.40199	.....	.....
		2,3-Pentadiene, C_5H_8			2-Methyl-1,3-butadiene, C_5H_8			Cyclopentene, C_5H_8			Cyclohexene, C_6H_{10}		
6678.1	He_{red}	1.42450	1.42120	1.41790	1.41708	1.41370	1.41032	1.41947	1.41643	1.41339	1.44344	1.44069	1.43794
6562.8	Hc	1.42498	1.42168	1.41838	1.41768	1.41429	1.41090	1.41984	1.41680	1.41376	1.44383	1.44108	1.43833
5892.6	Na_D	1.42842	1.42509	1.42176	1.42194	1.41852	1.41510	1.42246	1.41940	1.41634	1.44654	1.44377	1.44100
5460.7	Hg_e	1.43140	1.42805	1.42470	1.42570	1.42224	1.41878	1.42472	1.42165	1.41858	1.44888	1.44610	1.44332
5015.7	He_{blue}	1.43542	1.43204	1.42866	1.43081	1.42731	1.42381	1.42773	1.42464	1.42155	1.45201	1.44921	1.44641
4861.3	Hf	1.43711	1.43372	1.43033	1.43300	1.42948	1.42596	1.42900	1.42590	1.42280	1.45333	1.45052	1.44771
4358.3	Hg_g	1.44415	1.44071	1.43727	1.44221	1.43862	1.43503	1.43423	1.43110	1.42797	1.45877	1.45593	1.45309

TABLE 4. *Calculated values of the specific dispersion*

Temperature (°C)	$10^4(n_F - n_C)/d$	$10^4(n_g - n_D)/d$	$10^4(n_F - n_C)/d$	$10^4(n_g - n_D)/d$	$10^4(n_F - n_C)/d$	$10^4(n_g - n_D)/d$	$10^4(n_F - n_C)/d$	$10^4(n_g - n_D)/d$
	1-Pentene		1-Hexene		1-Heptene		1-Octene	
20	126.31	161.59	121.96	155.83	118.37	152.37	116.94	148.69
25	125.92	161.02	121.92	155.73	118.09	152.02	116.76	148.41
30			121.89	155.63	117.85	151.71	116.62	148.18
	1-Nonene		1-Decene		1-Undecene		1-Dodecene	
20	114.51	146.32	112.98	144.03	112.22	143.01	110.77	141.75
25	114.30	146.14	112.90	143.98	111.98	142.79	110.63	141.51
30	114.09	145.98	112.82	143.92	111.75	142.58	110.51	141.27
	1,2-Pentadiene		1,*cis*-3-Pentadiene		1,*trans*-3-Pentadiene		1,4-Pentadiene	
20	164.75	214.85	243.99	326.04	245.85	327.06	153.18	200.25
25	164.63	214.95	243.76	325.84	245.75	326.96		
30	164.52	215.06	243.53	325.64	245.68	326.92		
	2,3-Pentadiene		2-Methyl-1,3-butadiene		Cyclopentene		Cyclohexene	
20	174.53	226.32	224.98	297.67	118.65	152.46	117.15	150.81
25	174.49	226.38	224.75	297.39	118.72	152.64	117.11	150.85
30	174.51	226.49	224.52	297.13	118.75	152.78	117.04	150.86

The measurements and calculations of vapo pressures and boiling points were made as previously described [8, 9], except that the samples were introduced into the apparatus without contact with air. Table 5 gives the experimental data on the temperatures and pressures of the liquid-vapor equilibrium for the 16 compounds. Table 6 gives the values of the three constants of the Antoine equation, the normal boiling point at 760 mm Hg, the pressure coefficient of the boiling point at 760 mm Hg, and the range of measurement, in pressure and in temperature. The last column of table 6 gives the root-mean-square value of the ratios of the deviations of the observed points from the Antoine equation to the expected standard deviation [9]. Figure 2 is a plot of the values of the constants B and C of the Antoine equation, as a function of the number of carbon atoms in the normal alkyl radical of the series of 1-alkenes.

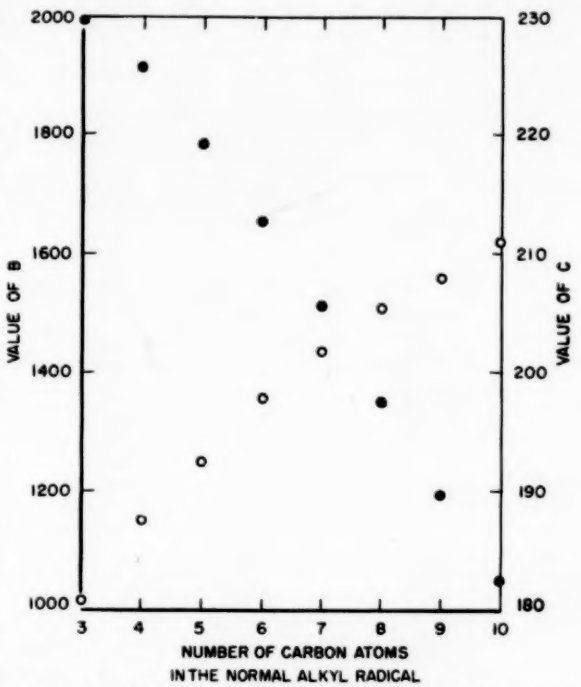

FIGURE 2. *Values of the constants, B and C, of the Antoine equation, as a function of the number of carbon atoms in the normal alkyl radical for the series of 1-alkenes.*

○=*B*; ●=*C*.

TABLE 5. *Experimental data on the temperatures and pressures of the liquid-vapor equilibrium*

t	P	t	P	t	P	t	P	t	P	t	P	t	P	t	P
1-Pentene		1-Hexene		1-Heptene		1-Octene		1-Nonene		1-Decene		1-Undecene		1-Dodecene	
°C	mm Hg	°C	mm Hg	°C	mm Hg	°C	mm Hg	°C	mm Hg	°C	mm Hg	°C	mm Hg	°C	mm Hg
30.723	779.98	64.311	780.03	94.531	780.08	122.223	780.21	147.860	780.22	171.605	780.26	193.742	780.26	214.472	780.36
30.289	768.46	63.837	768.49	94.022	768.53	121.685	768.62	147.289	768.62	171.012	768.65	193.130	768.66	213.826	768.75
29.756	755.52	63.299	755.54	93.444	755.56	121.075	755.64	146.653	755.63	170.345	755.67	192.441	755.69	213.125	755.81
29.362	744.27	62.827	744.29	92.941	744.31	120.539	744.38	146.091	744.38	169.762	744.42	191.832	744.43	212.497	744.57
28.900	732.40	62.323	732.42	92.391	732.44	119.967	732.50	145.488	732.50	169.134	732.53	191.179	732.55	211.823	732.62
24.584	628.21							139.859	628.33			185.091	628.38	205.542	628.45
18.468	501.02	50.914	501.03	80.179	501.05	106.997	501.09	131.881	501.09	154.939	501.12	176.462	501.13	196.624	501.21
12.834	402.81	44.763	402.82	73.563	402.82			124.521	402.84	147.265	402.86	168.501	402.87	188.406	402.97
		38.993	325.27	67.366	325.27	93.428	325.27	117.622	325.26	140.063	325.22	161.031	325.28	180.699	325.41
		33.399	262.04			87.053	262.03	110.935	262.03			153.780	262.05	173.214	262.14
		28.762	217.44	56.384	217.43	81.779	217.44			127.265	217.44	147.780	217.45	167.019	217.54
		23.720	176.15	50.970	176.13	76.022	176.13	99.341	176.13	120.995	176.14	141.240	176.14	160.266	176.24
		19.950	149.61	46.923	149.60	71.736	149.60	94.829	149.60	116.283	149.64	136.350	149.65	155.208	149.72
		15.890	124.85	42.564	124.84	67.096	124.84	89.942	124.84	111.213	124.86	131.081	124.86	149.773	124.95
				38.281	103.85	62.557	103.84	85.202	103.85	106.223	103.87	125.902	103.87	144.428	103.97
				34.525	87.91	58.557	87.91	81.001	87.92	101.844	87.93	121.355	87.94	139.736	88.03
						55.581	77.48	77.861	77.49	98.604	77.51	117.997	77.51	136.258	77.59
				28.768	67.44	52.410	67.46	74.517	67.46	95.134	67.48	114.388	67.48		
				25.492	57.69	48.975	57.68	70.874	57.69	91.308	57.71	110.423	57.72	128.424	57.78
				21.609	47.89	44.863	47.87	66.607	47.89	86.774	47.98	105.866	47.99	123.703	48.02

TABLE 5. *Experimental data on the temperatures and pressures of the liquid-vapor equilibrium*—Continued

1,2-Pentadiene		1,*cis*-3-Pentadiene		1,*trans*-3-Pentadiene		1,4-Pentadiene		2,3-Pentadiene		2-Methyl-1,3-butadiene		Cyclopentene		Cyclohexene	
°C	mm Hg	°C	mm Hg	°C	mm Hg	°C	mm Hg	°C	mm Hg	°C	mm Hg	°C	mm Hg	°C	mm Hg
45.631	780.27	44.846	780.28	42.810	780.28	26.714	780.26	49.041	780.26	34.834	780.29	45.024	780.13	83.852	780.14
45.191	768.66	44.403	768.68	42.367	768.67	26.287	768.66	48.602	768.66	34.399	768.69	44.576	768.58	83.353	768.59
44.690	755.71	43.902	755.73	41.866	755.72	25.806	755.70	48.101	755.70	33.903	755.74	44.071	755.64	82.791	755.66
44.252	744.47	43.461	744.49	41.423	744.48	25.384	744.46	47.658	744.46	33.469	744.51	43.624	744.41	82.292	744.42
43.778	732.52	42.989	732.54	40.952	732.53	24.931	732.51	47.183	732.51	33.006	732.55	43.146	732.46	81.757	732.47
39.373	628.37	38.578	628.39	36.538	628.39	20.699	628.36	42.781	628.36	28.661	628.40	38.678	628.25	76.766	628.26
33.126	501.13	32.326	501.15	30.282	501.15	14.706	501.12	36.541	501.12	22.506	501.16	32.340	501.09	69.708	501.10
27.374	402.89	26.566	402.91	24.514	402.90			30.803	402.88	16.836	402.92	26.506	402.86	63.200	402.87
21.971	325.32	21.161	325.35	19.109	325.34			25.402	325.31			21.028	325.34	57.107	325.35
16.702	262.08	15.917	262.10									15.718	262.07	51.191	262.07
12.361	217.48											11.325	217.47	46.302	217.48
														40.976	176.20
														36.996	149.70
														32.702	124.89
														28.490	103.94
														24.794	88.01
														22.063	77.59
														19.137	67.55
														15.920	57.82
														12.236	48.13

TABLE 6. *Summary of the results of the correlation of the experimental data with the Antoine equation for vapor pressure*

Compound	Formula	Constants of the Antoine equation $\log_{10}P=A-B/(C+t)$, or $t=B/(A-\log_{10}P)-C$ (P in mm Hg; t in °C)			Normal boiling point at 760 mm Hg	Pressure coefficient dt/dP at 760 mm Hg	Range of measurement		Measure of precision
		A	B	C			Pressure	Temperature	
					°C	°C/mm Hg	mm Hg	°C	ρ
1-Pentene	C_5H_{10}	6.78568	1014.294	229.783	29.968	0.03801	402 to 780	12.8 to 30.7	0.63
1-Hexene	C_6H_{12}	6.86573	1152.971	225.849	63.485	.04149	124 to 780	15.9 to 64.3	.06
1-Heptene	C_7H_{14}	6.90069	1257.505	219.179	93.643	.04447	48 to 780	21.6 to 94.5	.62
1-Octene	C_8H_{16}	6.93262	1353.486	212.764	121.280	.04711	48 to 780	44.8 to 122.2	.78
1-Nonene	C_9H_{18}	6.95389	1435.359	205.535	146.868	.04944	48 to 780	66.6 to 147.9	.97
1-Decene	$C_{10}H_{20}$	6.96936	1501.872	197.578	170.570	.05157	48 to 780	86.7 to 171.6	1.61
1-Undecene	$C_{11}H_{22}$	6.96662	1562.469	189.743	192.671	.05348	48 to 780	105.8 to 193.7	.55
1-Dodecene	$C_{12}H_{24}$	6.97522	1619.862	182.271	213.357	.05522	48 to 780	123.7 to 214.4	.49
1,2-Pentadiene	C_5H_8	7.01099	1154.420	234.652	44.856	.03867	217 to 780	12.3 to 45.6	.76
1,*cis*-3-Pentadiene	C_5H_8	6.94179	1118.371	231.327	44.068	.03875	262 to 780	15.9 to 44.8	.16
1,*trans*-3-Pentadiene	C_5H_8	6.92257	1108.937	232.338	42.032	.03879	325 to 780	19.1 to 42.8	.22
1,4-Pentadiene	C_5H_8	6.84880	1025.016	232.354	25.967	.03720	501 to 780	14.7 to 26.7	.12
2,3-Pentadiene	C_5H_8	6.88603	1086.636	223.040	48.265	.03871	325 to 780	25.4 to 49.0	.49
2-Methyl-1,3-butadiene	C_5H_8	6.90335	1080.996	234.668	34.067	.03818	402 to 780	16.8 to 34.8	.20
Cyclopentene	C_5H_8	6.92066	1121.818	233.446	44.242	.03928	217 to 780	11.3 to 45.0	.46
Cyclohexene	C_6H_{10}	6.88617	1229.973	224.104	82.979	.04781	48 to 780	12.2 to 83.9	.54

[1] A. R. Glasgow, Jr., E. T. Murphy, C. B. Willingham, and F. D. Rossini, J. Research NBS **37,** 141 (1946) RP1734.

[2] A. J. Streiff, E. T. Murphy, V. A. Sedlak, C. B. Willingham, and F. D. Rossini, J. Research NBS **37,** 331 (1946) RP1752.

[3] A. J. Streiff, E. T. Murphy, J. C. Cahill, H. F. Flanagan, V. A. Sedlak, C. B. Willingham, and F. D. Rossini, J. Research NBS **38,** 53 (1947) RP1760.

[4] A. J. Streiff, E. T. Murphy, J. C. Zimmerman, L. F. Soule, V. A. Sedlak, C. B. Willingham, and F. D. Rossini, J. Research NBS **39,** 321 (1947) RP1833.

[5] A. J. Streiff, J. C. Zimmerman, L. F. Soule, M. T. Butt, V. A. Sedlak, C. B. Willingham, and F. D. Rossini, J. Research NBS **41,** 323 (1948) RP1929.

[6] A. F. Forziati, B. J. Mair, and F. D. Rossini, J. Research NBS **35,** 513 (1945) RP1685.

[7] A. F. Forziati, J. Research NBS **44,** 373 (1950) RP2085.

[8] C. B. Willingham, W. J. Taylor, J. M. Pignocco, and F. D. Rossini, J. Research NBS **35,** 219 (1945) RP1670.

[9] A. F. Forziati, W. R. Norris, and F. D. Rossini, J. Research NBS **43,** 555 (1949) RP2049.

WASHINGTON JULY 3, 1950.

Journal of Research of the National Bureau of Standards Vol. 45, No. 5, November 1950 Research Paper 2152

A Study of the Determination of the Heat of Hydration of Portland Cement

By Edwin S. Newman

Three relatively inexperienced operators made six determinations each of the heat of hydration of a sample of portland cement. The results of their measurements were calculated by the method described in Federal Specification SS–C–158b and by two simpler reduced-observation methods. By statistical analysis, no significant differences were found among either operators or methods. The precision (standard deviation of a single determination) of the heat-of-hydration measurements was about 3 calories per gram at 7 days and 2 calories per gram at 28 days. Somewhat better precision can be expected from experienced operators.

I. Introduction

The heat-of-solution procedure for determining the heat of hydration of portland cement has been a part of the federal specification [1] [1] for a number of years. More recently, the method has been accepted by the American Society for Testing Materials [2]. Excepting a paper by Shartis and Newman [3], there has been little published on its precision.

The method depends upon the determination of the heat of solution in acid of a cement and of a hardened paste made therefrom. The difference between these values is approximately the heat evolved during the preparation and hardening of the paste and is very nearly equal to the true heat of hydration of the cement.[2] Auxiliary determinations of the ignition losses of the cement and of the hardened paste are required to determine the quantity of ignited cement represented by a weighed amount of the hardened paste. Heats of solution and hydration are given in this paper on the basis of the weight of ignited cement.

For low apparatus cost and for simplicity in operation, the calorimeter chosen for the routine acceptance testing of cement [4] consisted of a 1-pint vacuum flask and a Beckmann thermometer with a reading lens, together with a motor-driven stirrer. This calorimeter was to be operated in an ordinary laboratory with only superficial protection from changes in the ambient temperature. The difficulties that exist in making determinations with this calorimeter arise in large part from the fact that there is in the cork and the glass of the flask considerable material with a low thermal conductivity and a relatively large heat capacity. This material is at an indeterminate temperature between that of the room and that within the calorimeter, and when the liquid temperature is suddenly changed several degrees, as in a heat-of-solution determination, the lag caused by its presence in the path of heat flow interferes with the determination of the amount of heat lost to or gained from the surroundings. This interference has led to some doubt that the application of methods of precise calorimetry embodied in the specification procedure is entirely valid.

The original method for the heat-of-solution determination was somewhat oversimplified [4]. The precision necessary in this test is somewhat greater than appears at first glance. It is required to determine the heat of solution of a dry cement, amounting to approximately 600 cal/g, and the heat of solution of the corresponding hardened paste, 520 to 550 cal/g, with such precision that their difference, the heat of hydration of the cement, can be considered reliable to a few calories per gram. If a precision (standard deviation) of 2.0 cal/g, not an impressive value, is desired in the heat-of-hydration determination, a precision of 1.4 cal/g ($2.0/\sqrt{2}$) is required in each of the individual heat-of-solution tests. This amounts to a precision of approximately 0.25 percent, a value not easily reached consistently in routine calorimetry with relatively crude apparatus.

In an effort to improve the precision, and partly as a result of work at the Bureau [3], the original method was revised [1], primarily to allow more time for the calorimeter to establish constant operating conditions during the test and also to introduce a correction allowing for the time required to dissolve the sample. The effect of the revision was to substantially extend the time required for the test and to demand somewhat more attention by the operator. The procedure requires the recording of time-temperature data during two rating periods, one before and one after the period during which the sample is being dissolved. The temperature of the surroundings is assumed constant, and the thermal-leakage constant is calculated from these data taken when the rates of temperature change of the calorimeter depend only on the flow of heat to or from the room and on the energy of stirring. Besides the readings at 5-min intervals required by the original method, four additional readings are taken at 1-min intervals during the first part of the solution period. These data permit the approximate correction of the observed temperature rise of the calorimeter for the energy received from the surroundings and for the

[1] Figures in brackets indicate the literature references at the end of this paper.
[2] The heat of hydration defined as the difference between the two heats of solution ignores the heat of solution of the water contained in the paste, amounting to approximately 0.1 cal/g of cement. The effect of the absorption of CO_2 during the grinding of the paste is also ignored.

energy of stirring and evaporation. These details are in accordance with precision calorimetry in which an isothermal jacket is employed.

It has been suggested that some of these revisions could be omitted without seriously affecting the value of the calorimetric test. From an examination of routine test data, it appeared to the author that excluding all the observations taken during the solution period from the calculations would cause a systematic error of possibly +1 cal/g in the value for the heat of hydration. The precision of 2.0 cal/g suggested in an earlier paragraph implies that one-third of the tests will differ by more than 2 cal/g from the true (unknown) value. In other words, with an acceptance value of 80 cal/g, one-third of the samples with an actual heat of hydration of 82 cal/g will be accepted, and one-third of the samples with a heat of hydration of 78 cal/g will be rejected. Only when the true heat of hydration is below 75 cal/g will the cement be almost certain to pass the acceptance test. Only when the true value is above 85 cal/g will the cement be almost certain to be rejected. In the light of this uncertainty it would appear that a systematic error of +1 cal/g could be permitted. The test could then be considerably simplified, although the time required for its performance could not safely be shortened.

If this apparent systematic error can be tolerated, it is possible to eliminate the preliminary 5-min rating period (distinct from the preliminary 20-min stirring period), to reduce the number of observations, and to avoid much of the calculation. In this suggested procedure only three readings of time and temperature are required, one at the end of the preliminary stirring period just before the introduction of the sample, one at the end of the solution period, and one subsequently to establish the final rate of temperature change. It is necessary to extend the solution period sufficiently to insure the calorimeter's return to a steady state, after complete solution of the sample, before the second temperature is recorded. The time between the second and third readings of the temperature is the rating period. If the solution and rating periods are of the same length, the calculation of the corrected temperature is simple. The difference between the first two readings is the uncorrected rise. The difference between the second and third readings is the correction to be added or subtracted according to whether the calorimeter temperature falls or rises during the rating period. If the two periods differ in length, the observed correction is adjusted to correspond to the duration of the solution period. During the interval between readings, the operator's time can be utilized to operate a second calorimeter, or for any other purpose not requiring undivided attention. The reduced-observation method was used in the investigation reported by Shartsis and Newman [3]. The temperature of the calorimeter was recorded at 0, 20, and 40 min for the determinations presented in their paper. It is this author's belief that 20 min may sometimes be too short for a solution period, and it is suggested that the reduced-observation method be performed by taking readings at the end of the preliminary stirring period and twice thereafter at intervals of 25 min. A comparison of reduced-observation methods with the specification method of performing the heat-of-hydration test is a purpose of this paper.

II. Materials, Apparatus, and Procedure

A calorimeter meeting the requirements of the Federal Specification [1] was used. Three operators were available: A, with a moderate amount of experience; B, with a small amount; and C, with a few days. Approximately 50 liters of 2.00 N HNO_3 were prepared and standarized. This quantity was sufficient for the entire series of tests, and thereby uncertainties were avoided that might be introduced by the use of different batches of acid.

Three kilograms of Type 2 cement (moderate heat of hardening) were mixed for several hours in a laboratory ball mill containing a few pebbles, divided into three portions, and stored in tightly closed Mason jars. The portions were numbered 1, 2, and 3, and each portion was assigned to an operator. Each operator mixed a paste from each portion according to the procedure described in the Federal Specification [1].

The three operators each determined the heat capacity [1] of the calorimeter three times. In addition, during the time before the 7-day heat-of-solution test, each operator made a single determination of the heat of solution of each of the three portions of dry cement. At 7 days and again at 28 days, each operator determined the heat of solution of the three hydrated pastes made from the one portion of cement assigned to him. Thus each operator determined the heat of solution of paste samples prepared from one portion of cement by himself and by each of the other operators. This entire series of tests was repeated, so that each determination was made twice. The entire elapsed time during the tests was about 6 weeks.

III. Results and Discussion

The results of the heat-capacity and heat-of-solution tests are given in table 1, calculated as described in the specification [1]. In addition, the calorimetric observations were used in calculating the test results by two reduced-observation methods. Table 1 also shows these values as calculated from temperature readings taken at 0, 20, and 40 min and at 0, 25, and 50 min, respectively. Throughout the tables and the paper these reduced-observation methods will be called 0–20–40 and 0–25–50 methods. The heat capacities appearing in the table and used in calculation of the heats of solution were calculated in the same manner as the heat-of-solution values for which they were used.

TABLE 1. *Heat capacity of the calorimeter and heats of solution and hydration of a sample of portland cement*

[The average heat capacity of the three values determined by each operator during a round was used to calculate that operator's heats of solution for that round]

Paste mixed by	Calorimeter operator	Specification method [a]					0-20-40 method [b]					0-25-50 method [c]				
		Heat capacity	Heat of solution			Heat of hydration [d]	Heat capacity	Heat of solution			Heat of hydration [d]	Heat capacity	Heat of solution			Heat of hydration [d]
			Dry cement	7-day paste	28-day paste	7-day / 28-day		Dry cement	7-day paste	28-day paste	7-day / 28-day		Dry cement	7-day paste	28-day paste	7-day / 28-day
		cal/degC	*cal/g*	*cal/g*	*cal/g*	*cal/g* / *cal/g*	*cal/degC*	*cal/g*	*cal/g*	*cal/g*	*cal/g* / *cal/g*	*cal/degC*	*cal/g*	*cal/g*	*cal/g*	*cal/g* / *cal/g*
ROUND 1																
a	a	394.3	598.0	533.9	522.0	64.1 / 76.0	394.3	598.1	534.9	523.0	63.2 / 75.1	393.5	598.9	534.9	523.0	64.0 / 75.9
	b	395.9	594.9	539.8	518.9	55.1 / 76.0	394.3	594.6	539.6	518.7	55.0 / 75.9	395.0	595.4	538.7	519.8	56.7 / 75.6
	c	396.9	596.2	541.8	519.3	54.4 / 76.9	396.2	595.0	540.7	518.2	54.3 / 76.8	396.4	595.6	540.9	517.3	54.7 / 78.3
b	a	393.6	599.7	536.4	519.1	63.3 / 80.6	394.1	600.6	537.4	520.0	63.2 / 80.6	394.1	600.6	538.5	520.0	62.1 / 80.6
	b	395.1	596.4	540.7	518.9	55.5 / 77.5	394.5	596.1	540.7	518.7	55.4 / 77.4	395.1	596.0	541.9	519.2	54.1 / 76.8
	c	398.4	596.0	537.7	520.3	58.3 / 77.7	394.8	594.8	536.6	519.2	58.2 / 75.6	394.8	595.1	535.8	519.3	59.3 / 75.8
c	a	396.5	598.3	538.2	519.1	60.1 / 79.2	395.6	599.4	539.2	520.0	60.2 / 79.4	396.5	599.4	539.2	518.8	60.2 / 80.6
	b	396.9	596.8	539.1	519.5	57.7 / 77.3	396.2	596.5	539.0	519.4	57.5 / 77.1	396.9	597.3	539.7	520.6	57.6 / 76.7
	c	395.2	598.9	542.2	523.5	56.7 / 75.4	394.7	597.7	541.1	522.3	56.6 / 75.4	394.7	597.8	541.3	522.6	56.5 / 75.2
ROUND 2																
a	a	395.3	595.8	536.8	517.3	59.0 / 78.5	394.9	596.0	537.1	516.9	58.9 / 79.1	394.1	596.0	537.1	516.9	58.9 / 79.1
	b	395.0	599.9	539.0	515.6	60.9 / 84.3	394.7	599.6	538.7	514.9	60.9 / 84.7	394.9	599.8	539.1	515.6	60.7 / 84.2
	c	393.0	597.7	536.2	515.6	61.5 / 82.1	394.6	600.6	535.5	517.6	65.1 / 83.0	394.6	600.3	536.0	517.3	64.3 / 83.0
b	a	394.5	596.3	535.2	521.9	61.1 / 74.4	394.1	596.7	537.5	521.6	59.2 / 75.1	394.9	598.3	533.3	521.6	65.0 / 76.7
	b	395.2	595.1	535.7	520.5	59.4 / 74.6	395.4	596.6	537.1	520.1	59.5 / 76.5	395.9	596.0	536.2	520.2	59.8 / 75.8
	c	395.3	597.3	536.0	519.2	61.3 / 78.1	395.5	598.5	536.7	519.3	61.8 / 79.2	394.8	598.2	536.5	519.0	61.7 / 79.2
c	a	395.0	599.2	540.7	518.2	58.5 / 81.0	394.6	595.7	542.3	519.3	53.4 / 76.4	394.6	599.1	541.0	518.3	58.1 / 80.8
	b	396.3	598.4	538.3	518.1	60.1 / 80.3	394.6	598.3	538.5	517.8	59.8 / 80.5	394.7	598.6	538.4	518.3	60.2 / 80.3
	c	394.8	598.5	533.5	517.7	65.0 / 80.8	393.1	599.6	533.9	517.5	65.7 / 82.1	393.1	599.3	535.5	517.0	63.8 / 82.3

[a] Heat of solution calculated according to Federal Specification SS-C-158b.
[b] Heat of solution calculated from the temperature of the calorimeter at zero time, 20 min, and 40 min.
[c] Heat of solution calculated from the temperature of the calorimeter at zero time, 25 min, and 50 min.
[d] Calculated from differences in the heats of solution of corresponding dry cements and hydrated pastes.

The data were subjected to a complete analysis of variance. Information was sought as to the reproducibility of the methods of test, the variation among the operators, and the deviations introduced by the reduced-observation methods.

The uncertainty of an individual determination of the heat of solution is shown in table 2. There is evidence [3] to suggest that the heat of solution of dry cement changes when the container is opened even briefly. To eliminate the possible influence of this phenomenon on the correlation of the heats of solution of the hydrated pastes, the data were arranged in groups of three in the order shown in table 1. Each member of a set of three was determined on pastes mixed on a single day. From the data of table 1 the standard deviations of individual determinations of the heats of solution of the dry cement and of the 7- and 28-day hydrates were calculated and are shown in table 2. It will be noted that the uncertainty of the determination made with the 7-day hydrated paste is distinctly larger than either of the others. This is possibly due to a more rapid gain of CO_2 from the atmosphere and loss of water through evaporation by this paste during grinding.

TABLE 2. *Reproducibility of heat-of-solution tests*

Method	Standard deviation [a] of an individual test		
	Dry cement	7-day paste	28-day paste
	cal/g	*cal/g*	*cal/g*
Specification [b]	1.5	2.7	1.4
0-20-40 [c]	1.1	2.5	1.5
0-25-50 [c]	1.4	2.3	1.6

[a] Standard deviation, σ,

$$= \sqrt{\frac{\sum_{(1)}^{(6)} \sum_{1}^{3} (X-\overline{X})^2}{6}},$$

where the summation (1) to (6) refers to mixes by A, B, and C in rounds 1 and 2, and the summation 1 to 3 refers to the individual determinations within a mix by A, B, etc. X is the value of the single determination, and $\overline{X}$ is the average value of the group of three.

[b] Heat of solution calculated by the method described in Federal Specification SS-C-158b.

[c] These are reduced-observation methods of calculating the heat of solution from readings taken at zero time, 20 min, and 40 min, and at zero time, 25 min, and 50 min, respectively.

From the standard deviations of the heat-of-solution determinations in table 2, a predicted value can be calculated for the uncertainty of the heat of hydration. In table 3 are shown predicted values and actual values of the standard deviation of the heat of hydration. The predicted and the observed values are generally in good agreement. An exception is to be noted in the observed value for 7-day pastes calculated by the 0–20–40 method. The precision is somewhat less than that assumed earlier for purposes of discussion. It is apparent from table 2 that the variability of the 7-day determination is responsible.

TABLE 3. *Predicted and observed reproducibility of heat-of-hydration measurements of portland cement*

Tested at—	Standard deviation		
	Method [a]	Predicted [b]	Observed [c]
		cal/g	*cal/g*
7 days	Specification	3.1	3.2
	0–20–40	2.7	3.9
	0–25–50	2.7	3.2
28 days	Specification	2.1	2.0
	0–20–40	1.9	2.3
	0–25–50	2.1	2.2

[a] The method of calculation of the heats of solution were according to the Federal Specification 88–C–158b: and from the temperature readings taken at zero time, 20 min, and 40 min; and at zero time, 25 min, and 50 min, respectively.

[b] Calculated from the values given in table 2 for the standard deviations of the individual tests by the formula:

$$\text{standard deviation (predicted)} = \sqrt{\sigma^2_{\text{dry}} + \sigma^2_{\text{hydrated}}}.$$

[c] Calculated from the individual differences between the heats of solution of the dry cements and the hydrated pastes given in table 1 by the formula:

$$\text{standard deviation (observed)} = \sqrt{\frac{\sum_{(1)}^{(6)} \frac{\sum_{1}^{3} (X-\overline{X})^2}{2}}{6}},$$

where the summation (1) to (6) refers to mixes by A, B, and C in rounds 1 and 2 and the summation 1 to 3 refers to the individual determinations within a mix. X is the value for a single determination, and $\overline{X}$ is the average of the mix.

The operators can be compared accurately only on the results obtained with dry cement and during calibrations, as each operator had a different paste for the tests with hydrated cement. In table 4 are shown the standard deviations calculated for the individual operators and for the test when considering all operators. To facilitate comparison, the coefficients of variation have also been calculated. The heat-capacity determinations are slightly less precise than the heat-of-solution measurements, as judged from the coefficients of variation. The differences shown in table 4 are insignificant, but it was expected that any difference would be in favor of the calibrations. The zinc oxide, of analytical-reagent quality, is freshly heated before each determination, whereas the dry cement is subject to attack by whatever moisture and CO_2 enters the container during removal of test samples or between tests. In table 5 are shown the averages of six determinations by each operator on dry cement and on hydrated pastes at 7 and 28 days. There is, in tables 4 and 5, no indication of significant differences among the operators either in bias or precision. The agreement among the results is as close as would be expected if all the determinations had been made by the same operator. This is true in spite of the differences in the operators' experience.

TABLE 4. *Comparison of operator's precision*

Operator	Standard deviation [a]			Coefficient of variation [b]		
	Specification	0–20–40	0–25–50	Specification	0–20–40	0–25–50
HEAT CAPACITY MEASUREMENTS						
	cal/deg C	*cal/deg C*	*cal/deg C*	%	%	%
a	1.1	0.6	1.2	0.28	0.15	0.30
b	0.8	.8	0.9	.20	.20	.23
c	1.4	1.0	.9	.35	.25	.23
All [c]	1.1	0.8	1.0	.28	.20	.25
HEAT OF SOLUTION OF DRY CEMENT						
	cal/g	*cal/g*	*cal/g*			
a	1.4	0.7	1.3	0.23	0.12	0.22
b	1.9	1.3	1.5	.32	.22	.25
c	1.2	1.4	1.3	.20	.23	.22
All [c]	1.5	1.1	1.4	.25	.20	.23

[a] Standard deviation, σ_r,

$$= \sqrt{\frac{\sum_{1}^{3}(X_1-\overline{X}_1)^2}{2} + \frac{\sum_{1}^{3}(X_2-\overline{X}_2)^2}{2}},$$

where the summation 1 to 3 refers to determinations by the operator in a single round, the subscript refers to round 1 or round 2, X indicates individual determinations, and $\overline{X}$ indicates the average value of the determination for the round and operator indicated.

[b] The coefficient of variation is the ratio of the standard deviation to the average value of the determinations involved, expressed as percentage.

[c] The standard deviation for all of the operators is equal to

$$\sqrt{\frac{\sigma_a^2+\sigma_b^2+\sigma_c^2}{3}}.$$

TABLE 5. *Heat capacities and heats of solution and hydration*

[Average of six determinations by each operator]

Operator	Method		
	Specification [a]	0–20–40 [b]	0–25–50 [b]
HEAT CAPACITY OF THE CALORIMETER			
	cal/deg C	*cal/deg C*	*cal/deg C*
a	394.8	394.6	394.6
b	395.8	395.0	395.4
c	395.5	394.8	394.8
Range	1.0	0.4	0.8
Expected range [c]	1.1	0.8	1.0
HEAT OF SOLUTION, DRY CEMENT			
	cal/g	*cal/g*	*cal/g*
a	597.9	597.9	598.7
b	596.9	597.0	597.2
c	597.4	597.7	597.7
Range	1.0	0.9	1.5
Expected range [c]	1.6	1.1	1.4
HEAT OF SOLUTION, 7-DAY PASTE			
a	536.9	537.8	537.3
b	538.8	538.9	539.1
c	537.9	537.4	537.7
Range	1.9	1.5	1.8
Expected range [c]	2.8	2.6	2.4
HEAT OF SOLUTION, 28-DAY PASTE			
a	519.6	520.1	519.8
b	518.6	518.3	519.0
c	519.3	519.0	518.8
Range	1.0	1.8	1.6
Expected range [c]	1.5	1.6	1.7
HEAT OF HYDRATION AT 7 DAYS			
a	61.0	59.7	61.4
b	58.1	58.0	58.2
c	59.5	60.3	60.0
Range	2.9	1.7	3.2
Expected range [c]	3.3	4.0	3.3
HEAT OF HYDRATION AT 28 DAYS			
a	78.3	77.6	79.0
b	78.4	78.7	78.2
c	78.5	78.7	79.0
Range	0.2	1.1	0.8
Expected range [c]	2.1	2.4	2.3

[a] Calculated according to Federal Specification SS–C–158b.

[b] These are reduced-observation methods of calculating the heat of solution from calorimeter-temperature readings taken at zero time, 20 min, and 40 min, and at zero time, 25 min, and 50 min.

[c] Expected range for the average of six is equal to $2.534\frac{\sigma}{\sqrt{6}}$, where σ is the standard deviation of an individual determination (given in table 2 for heat of solution tests, in table 4 for heat capacities, and in table 3 for observed heats of hydration).

By regrouping the data in table 1, the effect of different operators as mixers can be tested. This was done, and table 6 shows the results. The averages are in good agreement, showing that the differences between mixers are not significant.

TABLE 6. *Heats of solution of hydrated cement pastes*

[Average of six specimens prepared by each mixer]

Mixer	Method		
	Specification [a]	0–20–40 [b]	0–25–50 [b]
HEATS OF SOLUTION, 7-DAY PASTES			
	cal/g	*cal/g*	*cal/g*
a	537.9	537.7	537.8
b	537.0	537.4	537.0
c	538.7	539.0	539.3
Range	1.7	1.6	2.3
Expected range [c]	2.8	2.6	2.4
HEATS OF SOLUTION, 28-DAY PASTES			
a	518.1	518.2	518.3
b	520.5	519.8	519.9
c	519.3	519.4	519.3
Range	2.4	1.6	1.6
Expected range [c]	1.5	1.6	1.7

[a] Heat of solution calculated according to Federal Specification SS–C–158b.

[b] Heat of solution calculated from calorimeter temperature readings made at zero time, 20 min, and 40 min; and at zero time, 25 min, and 50 min; respectively.

[c] From table 5.

It was found unexpectedly that the heats of solution of the pastes determined during the second round were lower than those determined during the first. For round one, cement was taken from the containers on July 7, 8, and 14, to mix the pastes. For round two, the dates were July 20, 21, and 22. The dry-cement determinations were made on July 12, 13, and 21 for the first round and on July 22, 25, and 26 for the second. At these times the containers were opened.

In table 7 are shown the results of calculations made on the tests grouped by rounds. In every case

TABLE 7. *Heats of solution*

[Average for all operators for separate rounds]

	Method [a]								
	Specification			0–20–40			0–25–50		
	Dry cement	7-day paste	28-day paste	Dry cement	7-day paste	28-day paste	Dry cement	7-day paste	28-day paste
	cal/g	*cal/g*	*cal/g*	*cal/g*	*cal/g*	*cal/g*	*cal/g*	*cal/g*	*cal/g*
Round 1	597.2	538.9	520.1	597.1	538.8	519.9	597.3	539.0	520.1
Round 2	597.6	536.8	518.2	597.9	537.3	518.3	598.4	537.1	518.2
Difference (round 1—round 2)	−0.4	2.1	1.9	0.8	1.5	1.6	−1.1	1.9	1.9
Standard deviation of difference [b]	.5	0.9	0.5	.4	0.8	0.5	0.5	0.8	0.5
t [c]	.8	*2.3	*3.8	2.0	1.9	*3.2	2.2	*2.4	*3.8

[a] Heats of solution calculated according to Federal Specification; from calorimeter temperatures at zero time, 20 min, and 40 min; and from calorimeter temperatures at zero time, 25 min, and 50 min; respectively.

[b] Standard deviation of the difference is equal to:

$$\frac{\sqrt{2}}{\sqrt{18}}\sigma;\ \sigma \text{ from table 2.}$$

[c] t = difference divided by the standard deviation of the difference. The 5-percent level of significance is 2.2. Differences exceeding this value are marked with an asterisk.

the average heat of solution of the hardened paste is less for the second round of tests than for the first. With one exception, this difference appears to be real for each age and for each method of calculation. The average value of the heat of solution of the dry cement was higher for the second round than for the first, the difference in one case approaching significance. This difference is in the wrong direction to be the effect of CO_2 and H_2O, apparently the only available agents, and must be considered accidental.

Up to this point, the determination of the ignition residues of the cement and cement pastes has not been discussed. Every heat-of-solution determination depends on a companion determination of the ignition residue of the calorimeter sample. When the hardened paste is removed from the sealed vial and ground, part of the water is lost, and CO_2 is absorbed from the atmosphere. The extent of these changes depends on the temperature, humidity, and CO_2 content of the air as well as on the length of time the sample is exposed during grinding. The loss of water affects mainly the ignited weight of the calorimeter sample, but the absorption of CO_2 results in a reduction in the heat of solution, as the heat of solution of $CaCO_3$ is markedly less than that of $Ca(OH)_2$. Carlson and Forbrich [5] have discussed the drying and carbonation of the hydrated paste in considerable detail.

The ignition-residue data obtained in these tests were analyzed in the same manner as the heat-of-solution data. The average ratios of ignited residue to sample taken were 0.9807, 0.7218, and 0.7189 for the dry cement, the 7-day paste, and the 28-day paste, respectively. The standard deviation of a single determination for the corresponding samples was 0.0008, 0.0050, and 0.0029. The theoretical ratio for the pastes mixed from this cement is 0.7005. Experiment has shown that there is negligible loss of water from the pastes while stored in the sealed vials. It is apparent that appreciable water was lost during mixing or grinding. The statistical analysis shows no significant differences among the operators either in mixing the paste or in determining the ignition residue of the dry cement. There were differences, perhaps significant, among the values obtained by the operators on the hydrated pastes. The largest difference, however, was between the average residue at 7 days found in the first round and that found in the second. The average values were 0.7179 and 0.7256, respectively, and the *t*-value (see table 7, footnote c) was calculated to be 4.5. At 28 days it was only 0.9. This indicates that there was a real and significant difference in the grinding of the pastes for rounds 1 and 2, although there was perhaps none at 28 days.

When the heats of solution of the 7-day second-round hydrates were being determined, the room temperature rose from 30° to 34° C during the working days. This occurred at a comparatively uniform rate of about 0.5 deg C/hr. When the heats of solution of the 7-day first-round hydrates were being determined, the daily temperature range was from 27° to 30° C on the first two days and from 30° to 32° C on the third. During the determination of the heats of solution of the 28-day hydrates the room temperature varied between 24° and 26° C. The higher average temperature for the second-round hydrates probably caused greater loss of water during grinding and hence the higher values for the residue on ignition. This difference in water loss and room temperature may have caused the lower heats of solution of the 7-day pastes in the second round, although no such difference in either room temperature or ignited residue occurred in the 28-day tests, in which the first-round heats of solution also exceeded those of the second round by a significant amount.

There appears to be no significant difference in the values obtained for the heats of solution whether calculated by the specification method or from the same data by either of the reduced-observation methods. From an examination of the tables, it seems also clear that on the basis of precision there is no choice among the three methods of calculation. Either of the shorter methods of calculation should give acceptable results. Because of the possibility that some cements may dissolve more slowly than that used in this study, there may be an advantage

TABLE 8. *Heats of hydration of routine samples*

Brand	Bin	At 7 days			At 28 days		
		Method [a]					
		Specification	0–20–40	0–25–50	Specification	0–20–40	0–25–50
		cal/g	*cal/g*	*cal/g*	*cal/g*	*cal/g*	*cal/g*
A	1	58	53	58	78	73	78
		58	54	58	78	74	78
		58	53	58	82	71	75
B	1	51	56	56	73	74	74
		50	51	51	66	66	67
		52	54	54	68	69	69
		54	54	54	72	72	72
		56	58	57	76	76	75
B	2	56	56	56	72	72	73
		59	61	59	74	74	74
		63	64	62	79	79	78
		58	55	53	75	76	75
		61	61	60	76	78	77
		63	64	63	78	80	78
C	1	60	58	59	76	76	75
		59	56	60	75	71	73
		61	60	61	76	77	77
		64	63	63	77	77	76
		57	60	58	74	78	76
		60	58	60	76	77	77
		62	60	63	79	78	80
D	1	61	62	62	77	74	73
		58	59	60	73	70	69
		60	60	61	79	75	75
		57	68	58	76	75	75
		60	58	58	78	76	74
		58	59	58	76	75	72
		61	60	60	80	76	76
		52	58	56	77	74	73
		62	63	63	78	75	74
		58	59	58	80	76	76
		57	59	59	77	76	76
Average		58.2	58.6	58.6	76.0	74.7	74.6
Average difference from specification		.....	2.3	1.2	.....	2.1	2.0

[a] Heats of solution were calculated (a) according to Federal Specification SS–C–158b, (b) from the calorimeter temperature at zero time, 20 min, and 40 min., and (c) from the calorimeter temperature at zero time, 25 min, and 50 min.

in using the method having observations made at 25 or 50 min after the beginning of the solution test.

In table 8 are shown the heats of hydration determined in the routine testing of five bins of cement of four different brands. The average heat of hydration of thirty two samples is 0.4 cal/g lower at 7 days and about 1 cal/g higher at 28 days when calculated by the specification method than when calculated by either of the others. At 7 days the average deviation (without regard to sign) of the 0–25–50 method from the specification method is about half of the 0–20–40 method. At 28 days the average deviations are about the same, for either of the reduced-observation methods, about 2 cal/g. A difference in the behavior of the cement or in the operation of the calorimeter is evidenced by the much larger deviations for the fourth brand.

IV. Summary

A study was made of the precision of the heat-of-solution test for determining the heat of hydration of portland cement. Three operators participated in making six determinations each of the heat of hydration of a single portland cement sample. The results of their measurements were calculated by the specification method and by two reduced-observation methods, and a complete analysis was made of the variance of the data. It was found that there were no significant differences among these measurements obtained by three operators and that the reduced-observation methods each gave acceptable results in these special tests. The agreement among the methods of calculation was somewhat poorer when they were applied to routine tests. The special tests indicate that the heat of hydration of portland cement can be determined by the heat-of-solution method with a precision of about 3 cal/g at 7 days and about 2 cal/g at 28 days. Somewhat better precision may be attained by experienced operators.

The heat-of-solution tests were made by R. B. Peppler, E. D. West, and J. V. Gilfrich. The statistical analysis was performed by W. J. Youden and J. M. Cameron, who also assisted in designing the experiment. The author is deeply indebted to them for their interest and assistance in this project.

V. References

[1] Federal Specification for cements, hydraulic; general specifications (methods for sampling, inspection, and testing) SS–C–158b (May 20, 1946).

[2] Standard method of test for heat of hydration of portland cement. American Society for Testing Materials Designation C–186–47 (Oct. 15, 1947).

[3] L. Shartsis and E. S. Newman, A study of the heat-of-solution procedure for determining the heat of hydration of portland cement, Proc. Am. Soc. Testing Materials **43,** 905 (1943).

[4] Federal Specification for cements, hydraulic; general specifications (methods for sampling, inspection, and testing) SS–C–158 (Sept. 30, 1936).

[5] R. W. Carlson and L. R. Forbrich, Correlation of methods of measuring heat of hydration of cement, Ind. Eng. Chem. **10,** 382 (1938).

Washington, June 1, 1950.

Journal of Research of the National Bureau of Standards Vol. 45, No. 5, November 1950 Research Paper 2153

pH Standards of High Acidity and High Alkalinity and the Practical Scale of pH

By Roger G. Bates, Gladys D. Pinching, and Edgar R. Smith

The practical scale of pH is defined in terms of the electromotive force of the galvanic cell

Pt; H_2 (*g*), solution | satd. KCl | standard, H_2 (*g*); Pt.

This potential is usually obtained as the difference of two electromotive force values for a cell with glass and calomel electrodes, one of which is a calibration with a standard of known pH. Appropriate corrections must be applied if the glass electrode does not respond to changes in hydrogen-ion activity in exactly the same manner as the hydrogen electrode. However, there is no simple means of correcting pH measurements for the potential differences at the junctions of the solution and the standard with the solution of potassium chloride. These errors are sufficiently large in highly acid and highly alkaline solutions to render uncertain the interpretation of measured pH in these regions, in spite of the fact that reasonably accurate standards of hydrogen-ion activity are available at intermediate pH values.

The purpose of this study was twofold: (a) to determine the extent of aberration of the practical pH scale near its ends, and (b) to select new standards that might improve the accuracy of pH measurements and facilitate their interpretation over the entire practical scale, with particular attention to the regions of high acidity and high alkalinity. The results indicate that pH obtained by adjustment of the meter with the present standards (phthalate, pH 4.01 at 25° C; phosphate, pH 6.86; borax, pH 9.18) will usually be low by at least 0.02 to 0.05 unit above pH 11, while errors as great as 0.03 unit, either positive or negative, are not uncommon below pH 2.5. The following additional standards were selected to supplement the three presently available: (1) 0.01–*M* potassium tetroxalate—pH 2.15 at 25° C; (2) potassium hydrogen tartrate (saturated at room temperature)—pH 3.56; (3) 0.025–*M* sodium acid succinate, 0.025–*M* sodium succinate—pH 5.40; (4) 0.025–*M* sodium bicarbonate, 0.025–*M* sodium carbonate—pH 10.02; and (5) 0.01–*M* trisodium phosphate—pH 11.72. The choice was based on a comparison of pH derived from cells with and without liquid junction in a study of 41 promising standard solutions. The pH on the practical scale was determined at 25° C, and electromotive force measurements of hydrogen-silver chloride cells without liquid junction were made at 0°, 10°, 25°, and 38° C.

I. Introduction

Recent demands for methods and standards for the accurate measurement of acidity and alkalinity have stimulated interest in the meaning of the pH scale so widely used today. The pH may be regarded on the one hand as a measurable property of many diverse materials, a property capable of adequate measurement by one of the commercially available electrometric instruments. From the point of view of the physical chemist, however, the pH value is usually regarded as conveying some information concerning the effective concentration or activity of hydrogen ions, a_H, in the solution in question. Carried to extremes, the first point of view reduces pH to an empirical number the quantitative interpretation of which is unimportant, if not impossible. The second approach creates a pH unit with meaning but offers no simple method of measuring acidity in terms of it. The conflict between pH as an empirical number in routine control and as a significant concept in research work has caused much confusion.

Fortunately, a compromise between the two extreme views is possible. Although the need for a practical scale demands that pH be defined from the operational point of view [1 to 4],[1] it is certainly desirable that this scale be adjusted in any way necessary to endow the measured pH numbers with a certain amount of significance in terms of hydrogen ion. To see how this can be accomplished, let us consider the practical determination of pH.

Commercial pH instruments almost universally employ a cell composed of a glass electrode (with inner reference) and a calomel electrode, together with a bridge solution saturated with potassium chloride:

(glass, inner ref.), solution | satd. KCl, Hg_2Cl_2; Hg, (I)

where the vertical line indicates a boundary between two different solutions. The hydrogen, quinhydrone, or antimony electrode may replace the glass electrode. The calomel serves as a reference electrode for the measurement of the potential of the glass electrode, which is a function of the hydrogen-ion activity. Reference electrodes other than calomel are rarely used. Although the hydrogen gas electrode is the primary standard for hydrogen-ion measurements, the versatile glass electrode serves satisfactorily when the corrections necessary in alkaline solutions (and to a lesser degree in strongly acid solutions) are applied.

Unfortunately, no known cell can furnish an exact practical measurement of either the activity or the concentration of hydrogen ion. Furthermore, the usual forms of the convenient glass and calomel

[1] Figures in brackets indicate the literature references at the end of this paper.

electrodes are not sufficiently reproducible and constant in potential to permit the same relationship between emf and pH to be used for long periods of time. This latter difficulty is readily circumvented by frequent calibration of the instrument with standards of known or assigned pH. The actual potential of the glass-calomel cell is then unimportant. The difference of potential, $E-E_s$, resulting from replacement of the standard S (the pH of which is designated pH_s) by the unknown solution is of sole concern. Hence, the practical definition of pH is formulated as follows,

$$pH = pH_s + \frac{(E-E_s)\boldsymbol{F}}{2.3036RT}, \qquad (1)$$

where $\boldsymbol{F}$ is the faraday, 96,496 abs coulombs per equivalent [5]; R is the gas constant, 8.3144 abs j deg^{-1} $mole^{-1}$ [5]; and T is the temperature on the absolute, or Kelvin, scale, (° C+273.16). At 25° C, $2.3026RT/\boldsymbol{F}$ is 0.059154.

The validity of eq 1 rests upon two assumptions. First, it is implied that replacement of the standard by the unknown causes no change in either the sign or magnitude of the potential difference across the boundary between the saturated solution of potassium chloride and the solution in contact with it. Second, eq 1 assumes that the potential of the electrode reversible to hydrogen ion (the glass electrode in cell I) changes by $2.3026RT/\boldsymbol{F}$ v/pH unit, as does the standard hydrogen electrode. If this is not the case, corrections must be applied for the imperfect response of the electrode. The sodium-ion error of the glass electrode in alkaline solutions provides a common example of departure from the theoretical response. The hydrogen electrode is usually chosen for standardization work in order to obviate the necessity of applying these empirical and often approximate corrections.

Evidently $E-E_s$ is independent of the reference electrode employed. Indeed, if the potential of the glass electrode changes by the same amount as does the hydrogen electrode for a given change of hydrogen-ion activity, $E-E_s$ represents the electromotive force of the cell

$$\text{Pt; } H_2\ (g),\ \text{solution} \left| \begin{matrix}\text{satd.} \\ \text{KCl}\end{matrix} \right| \text{standard, } H_2\ (g);\ \text{Pt,} \qquad \text{(II)}$$

in which a saturated solution of potassium chloride is interposed directly between the solutions of known and unknown pH.

As has already been indicated, the pH cannot be interpreted with exactness. The meaning of the values furnished by eq 1 rests upon the adequacy of the relationship between $pH-pH_s$ and $E-E_s$, and the meaning of the pH number, pH_s, assigned to the standard. Corrections for liquid-junction potentials, which might effect some improvement of eq 1, are inaccurate and laborious, and hence out of the question for practical measurements. However, the utility of this scale is not impaired by assignment of pH values that represent as closely as possible the presumed hydrogen-ion activity in the standard solution, and by this means the interpretation of the measured pH may be somewhat clarified.

In order to avoid some of the troublesome features of the hydrogen-calomel cell, it is logical to turn to a cell without liquid junction for the important task of establishing standards. That composed of hydrogen and silver–silver-chloride electrodes is probably the most suitable. For the purpose at hand, this cell can be represented

$$\text{Pt; } H_2\ (g,\ 1\ \text{atm}),\ \text{solution, KCl}\ (m),\ \text{AgCl; Ag.} \qquad \text{(III)}$$

The emf, E, is a function of the temperature and of the activities of hydrogen and chloride ions in the solution surrounding the two electrodes. It is convenient to define a quantity pwH, the value of which is readily obtained from emf measurements of cell III [6]:

$$\text{pwH} \equiv -\log\,(f_{\text{H}} f_{\text{Cl}} m_{\text{H}}) = \frac{(E-E^\circ)\boldsymbol{F}}{2.3026RT} + \log\, m_{\text{Cl}}, \qquad (2)$$

where m is molality, f an activity coefficient on the molal scale, and E° the standard potential of the hydrogen–silver-chloride cell [7]. Values of E° and $2.3026RT/\boldsymbol{F}$ in absolute volts are tabulated in an earlier publication [8]. The formal relationship between pwH and pH_s is simple:

$$pH_s \equiv \log\,(1/\boldsymbol{a}_{\text{H}}) = \text{pwH} + \log f_{\text{Cl}}. \qquad (3)$$

The pH of a chloride-free buffer solution can be writen similarly

$$pH_s = \text{pwH}^\circ + \log f_{\text{Cl}}^\circ, \qquad (3a)$$

where pwH° and f_{Cl}° are the limits of pwH and f_{Cl} as the molality of potassium chloride is reduced to zero.

The indeterminate character of the potential at the liquid junction precludes the exact calculation of hydrogen-ion activity from the emf of a cell in which a liquid junction is present. When the cell without liquid junction is chosen, it is necessary to evaluate the activity coefficient of a single ionic species in order to compute the activity, and this coefficient, like the liquid-junction potential, is not amenable to measurement. For standardization purposes, however, the latter method has a very real advantage, for the uncertainty diminishes with decreasing ionic strength. Thus the pH_s values obtained from the cell without liquid junction become increasingly accurate as the concentration of dissolved electrolyte decreases [6, 9]. On the other hand, the only recognized means of assuring the reduction of the residual liquid-junction potential to a negligible value appears to be the employment, in the preparation of the buffer solutions, of an artificial solvent medium containing a neutral salt in high concentration. This device has been used successfully to determine the concentrations of hydrogen

ions in buffer solutions [10, 11, 12], but the estimation of a_H for a buffer solution in such a medium is very difficult.

Ionic activity coefficients are often computed by the Debye-Hückel equation[13] for the variation of f_i with ionic strength, μ, in the form that allows for the restriction of attraction between ions due to their finite size:

$$\log f_i = -Az_i^2\sqrt{\mu}/(1+Ba_i\sqrt{\mu}), \qquad (4)$$

where A and B depend on the temperature and dielectric constant of the solvent, z_i is the valence of the ion i and a_i is an adjustable parameter with the dimension of distance and order of magnitude of the ionic diameter. Equation 4 is often valuable as an interpolation and extrapolation formula. When it is tested with the mean activity coefficients of uni-univalent strong electrolytes at ionic strengths below 0.1, the mean ionic diameter is usually found to lie between 7 and 3.5 A, the Bjerrum lower limit for complete dissociation [14]. For example, when a_i is 6 and z_i is 1, the calculated logarithm of the mean activity coefficient of hydrochloric acid differs from the observed value by 0.001 at 0.02 m, 0.002 at 0.05 m, 0.000 at 0.1 m, and 0.006 at 0.2 m. The usefulness of the equation can be extended to concentrations as high as 3 m by adding a term $\beta\mu$, where β is a second adjustable parameter [15]. But at the lower concentrations there is nothing to be gained in the estimation of f_{Cl} by introducing an empirical term linear in ionic strength.

Although an equation of the form of eq 4 doubtless expresses the variation of f_{Cl} with ionic strength at low concentrations, it is impossible to ascertain the proper value of a_i. Various reasonable methods of estimating this parameter lead to results differing by more than 0.01 unit in $\log f_{Cl}^{\circ}$ and pH_s when the ionic strength exceeds 0.1 [6]. The safest procedure is to choose standard buffer solutions of as low concentration as is consistent with an adequate buffer capacity. Under these conditions any reasonable value of a_i will yield pH_s values with uncertainties less than the arbitrary tolerances of about 0.01 to 0.02 unit.

From measurements of the emf of cells of type III, pH values from 0° to 60° have been assigned by the National Bureau of Standards to three buffer standards: acid potassium phthalate, pH about 4; a mixture of potassium dihydrogen phosphate and disodium hydrogen phosphate, pH about 7; and borax, pH about 9. These solutions serve to calibrate pH equipment for use in the range pH 3 to 11. In this intermediate region of acidities, the potential at the junction between saturated potassium chloride and a variety of buffer solutions is believed to be fairly uniform. This conclusion is affirmed by the fact that other semithermodynamic pH scales based upon the emf of hydrogen-calomel cells with liquid junction [16, 17] furnish almost the same values for the three NBS standards as were assigned from measurements of hydrogen-silver-chloride cells without liquid junction. But with solutions that contain appreciable amounts of strong acids or bases the highly mobile hydrogen and hydroxyl ions cause the liquid-junction potential to be altered.

The object of the present study was twofold. The first purpose was to examine a series of promising standards for the ranges of high acidity and high alkalinity with a view to selecting the most suitable materials to fix the practical pH scale at one or more points below pH 4 and above pH 9. The second purpose was to demonstrate the extent of the error in practical measurements at the ends of the pH scale that results from variation of the liquid-junction potential as one standard buffer solution is replaced by another or by an unknown. solution. To accomplish this object, differences of pH were calculated from measurements of the cell without liquid junction and compared with the result afforded by the usual cell with liquid junction.

Studies were made at 25° C of 41 promising standard solutions with pH from 1.1 to 13.3. Twenty-one of these solutions were investigated at 0°, 10°, 25°, and 38° C, and one at 25° and 38° alone, by emf measurements of hydrogen-silver-chloride cells without liquid junction. The data for 24 solutions are used to elucidate the extent of aberration of the practical pH scale at its extremes. The results suggest that solutions of the following materials are suitable standards for pH: Potassium tetroxalate dihydrate, potassium hydrogen tartrate, a mixture of sodium acid succinate and sodium succinate, a mixture of sodium bicarbonate and sodium carbonate, and trisodium phosphate.

II. Apparatus and Procedure

The determination of pH on the practical scale is based upon two or more measurements of a cell such as type I. One measurement must be a calibration with a standard buffer solution. The practical scale overlooks possible changes in the liquid-junction potential, but any failure of the glass electrode to respond to hydrogen-ion activity in the manner of the standard hydrogen electrode must be allowed for by application of appropriate corrections. Hence, cell II is the basis for the determination of pH values. The direct measurement of the emf of this cell is probably the most accurate means of studying the practical scale and of determining the pH of secondary standards.

The cell vessel illustrated in figure 1 was designed expressly for the determination of the emf, $E-E_s$, of cells of type II. It consists essentially of a reservoir, a, of saturated potassium chloride solution; a double mercury-calomel electrode, b, of the saturated type; and two hydrogen-electrode compartments, c and c′. The liquid junctions are formed in the bulbs e and e′, and each is protected from the disturbing effect of the bubbling hydrogen by a glass bead that forms an imperfect closure at the top. This arrangement has been used by Hitchock and Taylor [16]. The calomel electrode is unnecessary when the reference is a hydrogen electrode in a standard buffer solution. Therefore, the calomel

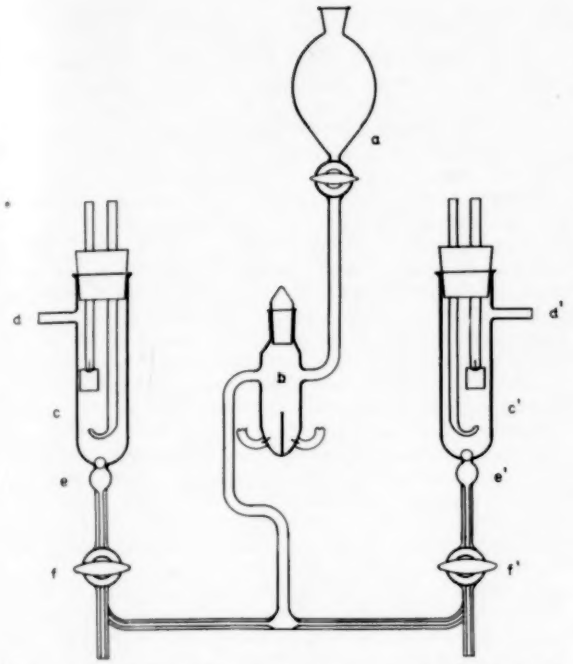

FIGURE 1. *Cell vessel for emf measurements of cells of type* II.
a, Reservoir of saturated KCl; b, calomel electrode; c, c', hydrogen electrodes.

electrode was omitted in the construction of one of the two cells used in this study. It was found useful in the first cell, however, to determine the time required for the hydrogen electrodes to reach equilibrium and to observe the stability of the reference buffer. The 0.025-*M* phosphate solution with pH near neutrality was used as the standard in all measurements of cell II.

The saturated solution of potassium chloride was formed by dissolving the bromide-free fused salt [18] in water at 60° to 70° C and cooling to room temperature. A few drops of a solution of the sodium salt of methyl red were added to aid in making the junctions visible. The calomel electrodes were prepared by grinding calomel, pure mercury, and crystals of pure potassium chloride with a small amount of the saturated solution of potassium chloride and transferring the thick paste to compartment b, each leg of which contained a little mercury.

Fresh hydrogen electrodes were prepared daily by electrolysis of the platinum foils for about 2 min at 300 ma in a 3-percent solution of chloroplatinic acid containing 80 mg of lead acetate trihydrate in each 100 ml. The foils were coated with palladium for use in the phthalate solutions [19]. The purified hydrogen was not usually saturated with water vapor before entering the cell. However, the gas that was led into the carbonate solutions had been passed through a presaturator containing some of the same solution. Hydrogen escaped from the cell through d and d'. To equalize the pressure in the two electrode compartments, these led to a T-tube and a common exit.

The cell was rinsed twice with each solution and drained through the three-way stopcocks f and f' before it was filled and the solutions adjusted to approximately the same level in each arm. The cell was then placed in the constant-temperature bath and the flow of hydrogen started. After ½ to 1 hr it was removed in order that the liquid junctions could be formed. The following procedure was adopted to avoid disturbance of the junctions resulting from slight differences of solution level. The stopcock at a was opened and potassium chloride solution brought about halfway up the capillary tubes above f and f'. With both f and f' open, the junctions were brought simultaneously to the center of the bulbs e and e' by admitting potassium chloride solution through a. Stopcocks f and f' were closed while the cell was being returned to the bath but were opened immediately thereafter and measurements begun. The hydrogen electrodes usually reached equilibrium in 10 to 20 min thereafter. The emf, $E-E_s$, which represents the difference of potential between the hydrogen electrodes, was often constant as soon as the junctions were made and remained so within ±0.1 to 0.2 mv for 30 to 90 min.

The cells without liquid junction (type III) have been described previously [20]. For the measurements of carbonate solutions, the hydrogen was passed, before entering the cell, through a presaturator of three chambers each containing cell solution [8]. The electrode supports and the interior of the cells and solution flasks were coated with paraffin for most of the measurements of solutions of sodium hydroxide and trisodium phosphate, with some improvement in the constancy of the emf. The silver–silver-chloride electrodes were prepared by forming approximately 150 mg of silver on platinum helices by thermal decomposition of a paste of well-washed silver oxide at 550°. These silver electrodes were then chloridized by electrolysis for 45 min at a current of 7 ma in a 1-*M* solution of distilled hydrochloric acid. Each cell contained two hydrogen electrodes and two silver–silver-chloride electrodes. The recorded emf is thus the mean of two observed values.

In order to obtain data which would furnish an accurate value of pwH°, the limit of pwH (eq 2) as the chloride concentration approaches zero, emf measurements were made on three portions of each buffer solution, to which different amounts of potassium chloride had been added. The molalities of chloride selected for this purpose were 0.015, 0.01, and 0.005. The temperature measurements were made with a platinum resistance thermometer and bridge or with a calibrated mercury thermometer.

907877—50——5

III. Material

The 41 solutions chosen for a study of the practical pH scale and for examination as to their suitability for use as standards are listed approximately in order of increasing pH in the tables of the following sections. The same order will be observed here.

The hydrochloric acid solution was prepared from a distilled sample and was analyzed gravimetrically. The emf found with a 0.0993-*M* solution was corrected by 0.18 mv to obtain the emf of the 0.1-*M* solution. The mixture of hydrochloric acid and potassium chloride was prepared by dilution of the 0.0993-*M* solution of acid and addition of bromide-free potassium chloride.

A commercial sample of anhydrous sulfamic acid, NH_2-SO_3H was used without further purification. The composition was unchanged by drying at 105°, as shown by titration with standard alkali.

Some difficulty was experienced in obtaining potassium tetroxalate dihydrate of the theoretical composition by recrystallization from water and drying in air. However, a procedure was ultimately found that yielded a pure product. Reagent-grade salt was crystallized twice from water, the two components being taken in such amounts that no crystals separated above 50°. The mixture was cooled to 10°, and the crystals were collected on a sintered-glass funnel. The product was finely ground and dried overnight at 58°.

The anhydrous citric acid was furnished by Chas. Pfizer & Co., Inc.

Two samples of potassium hydrogen tartrate were employed. The first was reagent-grade material. The second was obtained by recrystallization of the first and appeared to be of identical composition.

Potassium dihydrogen citrate was prepared as described elsewhere [21]. The total acidity of the product was found to be somewhat too low. The necessary amount of citric acid was therefore added, and the salt precipitated from aqueous solution by the addition of ethanol and by cooling. The salt was dried below 80° and its titration value determined.

The potassium acid phthalate was NBS Standard Sample 185.

The acetic acid was purified by three fractional freezings. The acetic acid-sodium acetate buffer solutions were prepared by adding the required amount of a standardized solution of carbonate-free sodium hydroxide to a solution of the acid.

Preparation of the sodium hydrogen succinate and sodium succinate has been described [22].

NBS Standard Sample 187 of borax was used.

Lithium carbonate, which has a negative temperature coefficient of solubility, was prepared by adding a hot solution of lithium chloride to a vigorously stirred hot solution of potassium carbonate. It was washed by decantation with hot water until the washings gave no further test for chloride. The salt was heated to 450° before use.

Potassium and sodium bicarbonate of reagent grade were found sufficiently pure without further treatment, as was sodium carbonate after heating at 270° to 300°.

Preliminary studies of calcium and barium hydroxides indicated that the saturated solutions of these substances would not be suitable as alkaline standards of readily reproducible pH. Hence, the composition of the reagent-grade materials was not determined.

Attempts to prepare a pure carbonate-free sample of trisodium phosphate were unsuccessful. The commercial material contained about 2.5 mole percent of free alkali and about 8 moles of water per mole of salt. Although precipitation with ethanol removed the excess alkali with partial success, it appeared that a stable product with a definite water content between 0 and 12 moles per mole of salt would be difficult or impossible to obtain. The attempts were therefore abandoned in favor of forming the substance in solution from disodium hydrogen phosphate, NBS Standard Sample 186 II b, and a carbonate-free solution of sodium hydroxide.

The sodium hydroxide solution was made by dilution of a 50-percent solution from which the precipitated carbonate had been removed by centrifuging. Its concentration was determined by titration of samples of potassium acid phthalate, NBS Standard Sample 84c. The diluted solution gave a negative test for carbonate by the method suggested by Kolthoff and Sandell [23].

The reference 0.025-*M* phosphate buffer solution was prepared by dissolving 3.401 g (air weight) of potassium dihydrogen phosphate, Standard Sample 186 I b, and 3.548 g (air weight) of disodium hydrogen phosphate, Standard Sample 186 II b, in sufficient water to make a liter of solution.

Freshly boiled water, protected from atmospheric carbon dioxide while cooling, was used for all the solutions. The pH of the water was 6.8 to 7.2.

The results of the analyses of materials are summarized in table 1. The titrations with acid and alkali were performed by weight methods. Endpoints were determined with suitable indicators. Phenol red was used in the titration of sulfamic acid to pH 7.5. Citric acid and potassium dihydrogen citrate were titrated to pH 9.0 with the aid of thymol blue. The endpoint in the titration of tetroxalate and tartrate was taken to be pH 8.4, with phenolphthalein as the indicator. Phenolphthalein was also

TABLE 1. *Results of analyses*

Material	Purity	Method
	Percent	
Sulfamic acid	99.77	Alkali titration.
Potassium tetroxalate.$2H_2O$	100.00	Do.
Citric acid	100.03	Do.
Potassium hydrogen tartrate	100.05	Do.
Potassium dihydrogen citrate	100.01	Do.
Sodium hydrogen succinate	100.03	Do.
Sodium succinate	99.99	Ignition to Na_2CO_3.
Sodium bicarbonate	100.01	Acid titration.
Potassium bicarbonate	99.99	Do.
Lithium carbonate	99.95	Do.
Sodium carbonate	100.00	Do.

used to titrate the acid succinate salt to pH 8.7. Bromcresol green was used in determining the purity of the bicarbonates and carbonates [23].

IV. Results

1. Cells with liquid junction, type II

Table 2 is a summary of $E-E_s$ at 25° and the pH values computed therefrom by eq 1. Each entry is the mean of the measurements of at least two cells. The pH given by Hitchcock and Taylor (H) [16] and MacInnes, Belcher, and Shedlovsky (M) [17] is noted in the last column. Kiehl and Loucks [24] have determined the pH of four of the alkaline solutions at 30° by measurement of the emf of a hydrogen-calomel cell. Their values have been corrected to 25° with the aid of temperature coefficients of pH derived from measurements of cell III. The results, given in the last column of table 2, are identified by K.

TABLE 2. *Electromotive force of cell* II *and* pH *from cells with liquid junction at 25°*

No.	Solution	$E-E_s$	pH	
		v		
1	HCl, 0.1 *M*	−0.34094	1.096	1.085 (H)
2	HCl, 0.01 *M*; KCl, 0.09 *M*	−.28320	2.073	2.078 (H)
3	Sulfamic acid, 0.1 *M*	−.33263	1.237	
4	Sulfamic acid, 0.05 *M*	−.31819	1.481	
5	Sulfamic acid, 0.01 *M*	−.28101	2.110	
6	$KH_3(C_2O_4)_2$, 0.1 *M*	−.31820	1.481	1.480 (H)
7	$KH_3(C_2O_4)_2$, 0.05 *M*	−.30842	1.646	
8	$KH_3(C_2O_4)_2$, 0.025 *M*	−.29622	1.852	
9	$KH_3(C_2O_4)_2$, 0.01 *M*	−.27855	2.151	
10	Citric acid, 0.05 *M*	−.27448	2.220	
11	Citric acid, 0.01 *M*	−.25158	2.607	
12	KH tartrate, satd. 25°	−.19516	3.561	
13	KH tartrate, 0.03 *M*	−.19471	3.569	3.567 (H)
14	KH_2 citrate, 0.1 *M*	−.18565	3.722	3.719 (H)
15	KH_2 citrate, 0.02 *M*	−.17869	3.839	
16	KH phthalate, 0.05 *M*	−.16893	4.004	4.008 (H); 4.000 (M)
18	Acetic acid, 0.05 *M*; NaAc, 0.05 *M*	−.12965	4.668	
19	Acetic acid, 0.01 *M*; NaAc, 0.01 *M*	−.12696	4.714	4.714(H);4.700(M)
21	NaHsuccinate, 0.025 *M*; Na_2Suc, 0.025 *M*	−.08655	5.397	
8	KH_2PO_4, 0.025 *M*; Na_2HPO_4, 0.025 *M*	0	6.860	6.857 (H)
23	$Na_2B_4O_7$, 0.01 *M*	+.13721	9.180	9.180 (H)
28	$NaHCO_3$, 0.025 *M*; Na_2CO_3, 0.025 *M*	.18599	10.004	
30	Na_2CO_3, 0.01 *M*	.24351	10.977	
31	Na_2CO_3, 0.025 *M*	.25302	11.137	
33	Na_3PO_4, 0.01 *M*	.28604	11.696	
34	Na_3PO_4, 0.05 *M*	.30597	12.032	12.00 (K)
35	Na_3PO_4, 0.1 *M*	.31060	12.116	12.09 (K)
36	NaOH, 0.01 *M*	.29799	11.898	
37	NaOH, 0.02 *M*	.31440	12.175	
38	NaOH, 0.05 *M*	.33765	12.568	12.52 (K)
39	NaOH, 0.1 *M*	.35187	12.808	12.80 (K)
40	$Ca(OH)_2$, satd. 25°	0.329 to 0.334	12.42 to 12.52	
41	$Ba(OH)_2$, satd. 25°	0.379, 0.381	13.27, 13.30	

The pH of the reference 0.025-*M* phosphate buffer (pH_s) was taken to be 6.860 at 25°, the value derived from emf measurements of cells without liquid junction [25]. This agrees closely with 6.857 obtained from the emf of the hydrogen-calomel cell [16].

Six different phosphate solutions, designated by the letters A to F, were prepared during the course of the study, and each was used for a period of 2 to 5 weeks. The reference solution was kept in a glass-stoppered Pyrex bottle. Hitchcock and Taylor found the emf of phosphate and borax solutions reproducible to 0.1 mv only when the solutions were freshly prepared [16]. Although the variation of E_s, the emf of the hydrogen-calomel cell containing phosphate solution, was slightly greater than 0.1 mv in this investigation, no trend in one or the other direction with age of the solution was observed. The values of $E-E_s$ appeared more reproducible than E_s alone. This observation suggests that the variations were caused, in part at least, by hysteresis of the calomel electrode, which was not kept at constant temperature between measurements. The potential of the calomel electrode is of no concern in discussions of cell II. As a matter of interest, however, the average E_s for each buffer solution and the corresponding potentials, $E^{\circ\prime}+E_j$ [6], of the calomel electrode are listed in table 3. The liquid-junction potential between phosphate and saturated potassium chloride is included in $E^{\circ\prime}+E_j$. These data are in absolute volts and are to be compared with 0.2442 from the study of Hitchcock and Taylor [16] and 0.2447 found by MacInnes, Belcher, and Shedlovsky [17].

TABLE 3. *E_s for six 0.025-M phosphate solutions and $E^{\circ\prime}+E_j$, the potential of the saturated calomel electrode at 25°*

Phosphate solution	Number of Measurements	E_s	$E^{\circ\prime}+E_j$
		v	v
A	16	0.65052 ±0.00012	0.2447
B	12	.65051 ±0.00025	.2447
C	15	.65064 ±0.00013	.2448
D	12	.65047 ±0.00006	.2447
E	16	.65043 ±0.00004	.2446
F	15	.65018 ±0.00011	.2444

2. Cells Without Liquid Junction, Type III

The emf at 0°, 10°, 25°, and 38° of cells of type III is given in tables 4 and 5. Each figure is the mean potential between two separate pairs of electrodes in the same cell, corrected to a partial pressure of 1 atm of hydrogen. The pwH value calculated by eq 2 from each value of E at 0°, 25°, and 38° is plotted in figures 2 to 5 as a function of the molality of potassium chloride. The data for the acid solutions are shown in figure 2, for the carbonate buffers in figure 3, for the solutions of sodium carbonate in figure 4, and for sodium hydroxide and trisodium phosphate in figure 5. The solutions are identified by number and by circles and dots, the significance of which is noted in the accompanying legends. The intercepts at zero chloride, pwH°, were read from large-scale plots similar to figures 2, 3, 4, and 5. Tables 6 and 7 summarize pwH° and include similar data from the literature, where available, for solutions included in this study. The source of pwH° or the emf data from which it was computed is indicated in the last column of table 6. The pwH of 0.05–*M* sodium hydroxide solution was obtained by adding 0.017, the value of log (0.05/0.04809), to pwH for the 0.04809–*M* solution actually studied. This correction is based on the assumption that the ratio of the activity coefficients of chloride and hydroxide ions is substantially the same at these two concentrations.

907877—50——6

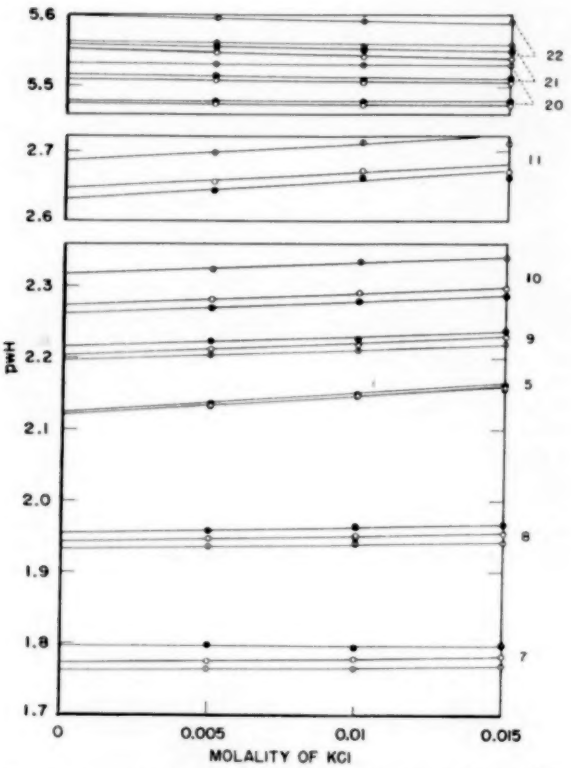

FIGURE 2. pwH *of acid solutions as a function of the molality of added potassium chloride.*

Marked circles, 0°; open circles, 25°; dots, 38°. Solution numbers appear at the right.

TABLE 4. *Electromotive force of cell* III *at 0°, 10°, 25°, and 38°*

(Acid solutions)

No.	Solution	KCl	Electromotive force at—			
			0°	10°	25°	38°
		m	*E*	*E*	*E*	*E*
5	Sulfamic acid, 0.01 *M*	0.015	0.45259	0.45519	0.45810	0.45972
		.01	.46160	.46442	.46789	.46969
		.005	.47703	.48060	.48480	.48746
		.015	.43125	.43340	.43581	.43721
7	$KH_3(C_2O_4)_2$, 0.05 *M*	.01	.44064	.44320	.44603	.44792
		.005	.45687	.46009	.46361	.46667
		.015	.44062	.44309	.44597	.44762
8	$KH_3(C_2O_4)_2$, 0.025 *M*	.01	.44999	.45291	.45622	.45834
			.45007	.45268	.45615	.45831
		.005	.46615	.46957	.47374	.47655
		.015	.45579	.45889	.46228	.46441
9	$KH(C_2O_4)_2$, 0.01 *M*	.01	.46476	.46812	.47206	.47464
		.005	.48072	.48472	.48944	.49292
		.015	.46222	.46419	.46631	.46743
10	Citric acid, 0.05 *M*	.01	.47151	.47374	.47635	.47781
		.005	.48721	.49007	.49354	.49577
		.015	.48226	.48501	.48832	.49064
11	Citric acid, 0.01 *M*	.01	.49196	.49501	.49889	.50149
		.005	.50741	.51104	.51577	.51836
		.015	.63504	.64263	.65415	.66436
20	NaHsuccinate, 0.05*M*; Na_2Suc, 0.05 *M*	.01	.64465	.65252	.66458	.67522
		.005	.66099	.66951	.68241	.69382
21	NaHSuc, 0.025 *M*; Na_2Suc, 0.025 *M*	.015	.63659	.64431	.65599	.66644
		.01	.64606	.65411	.66638	.67712
		.005	.66256	.67123	.68440	.69611
22	NaHSuc, 0.01 *M*; Na_2Suc, 0.01 M	.015	.63835	.64619	.65802	.66875
		.01	.64794	.65614	.66858	.67974
		.005	.66455	.67336	.68671	.69861

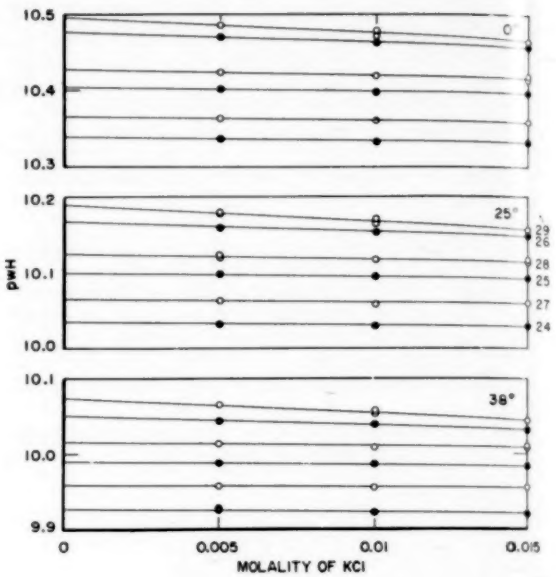

FIGURE 3. pwH *of bicarbonate-carbonate buffers as a function of the molality of added potassium chloride.*

Dots, $KHCO_3$-Li_2CO_3 mixtures; circles, $NaHCO_3$-Na_2CO_3 mixtures. Solution numbers appear at the right.

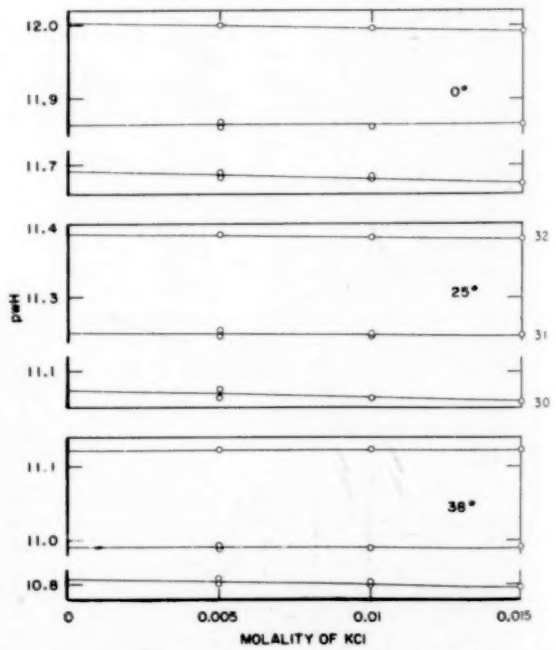

FIGURE 4. pwH *of sodium carbonate solutions as a function of the molality of added potassium chloride.*

Solution numbers appear at the right.

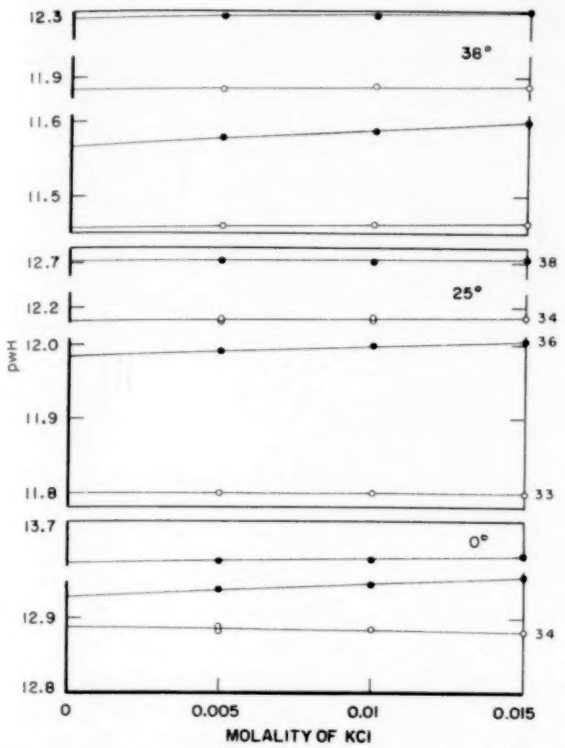

FIGURE 5. pwH *of trisodium phosphate and sodium hydroxide solutions as a function of the molality of added potassium chloride.*

Circles, Na_3PO_4 solutions; dots, NaOH solutions. Solution numbers appear at the right.

TABLE 5. *Electromotive force of cell* III *at 0°, 10°, 25°, and 38°*

[Alkaline solutions]

No.	Solution	KCl	Electromotive force at—			
			0°	10°	25°	38°
		m	v	v	v	v
24	$KHCO_3$, 0.05 *M*; Li_2CO_3, 0.05 *M*	0.015	0.89535	0.90651	0.92358	0.93859
		.01	.90493	.91643	.93404	.94957
		.005	.92142	.93356	.95199	.96845
25	$KHCO_3$, 0.025 *M*; Li_2CO_3, 0.025 *M*	.015	.92139	.93349	.95201	.96832
		.01	.89881	.91006	.92733	.94250
		.005	.90845	.92004	.93784	.95349
26	$KHCO_3$, 0.01 *M*; Li_2CO_3, 0.01 *M*	.015	.92495	.93709	.95586	.97224
		.01	.90212	.91345	.93062	.94550
		.005	.91195	.92362	.94136	.95678
27	$NaHCO_3$, 0.05 *M*; Na_2CO_3, 0.05 *M*	.015	.92865	.94087	.95952	.97571
		.01	.89676	.90810	.92542	.94072
		.005	.90639	.91794	.93581	.95160
28	$NaHCO_3$, 0.025 *M*; Na_2CO_3, 0.025 *M*	.015	.92283	.93513	.95386	.97030
		.01	.90000	.91140	.92883	.94414
		.005	.89972	.91113	.92858	.94389
29	$NaHCO_3$, 0.01 *M*; Na_2CO_3 0.01 *M*	.015	.89959	.91143	.92881	.94411
		.01	.90953	.92131	.93923	.95496
		.005	.92606	.93842	.95717	.97375
30	Na_2CO_3, 0.01 *M*	.015	.92614	.93848	.95738	.97389
		.01	.90252	.91384	.93116	.94626
		.005	.91282	.92460	.94243	.95793
		.015	.91266	.92455	.94236	.95785
		.01	.91281	.92462	.94235	.95780
		.005	.91238	.92414	.94202	.95760
		.015	.92951	.94188	.96071	.97697
		.01	.92947	.94182	.96059	.97698
		.005	.96805	.97452	.98446	.99271
		.015	.97797	.98474	.99516	1.00369
		.01	.97815	.98496	.99516	1.00392
		.005	.99432	1.00174	1.01302	1.02239
			.99474	1.00204	1.01370	1.02285

TABLE 5. *Electromotive force of cell* III *at 0°, 10°, 25°, and 38°*—Continued

[Alkaline solutions]

No.	Solution	KCl	Electromotive force at—			
			0°	10°	25°	38°
		m	v	v	v	v
31	Na_2CO_3, 0.025 *M*	.015	.97835	.98519	.99573	1.00463
		.01	.98775	.99493	1.00607	1.01545
			.98773	.99494	1.00623	1.01535
		.005	1.00400	1.01185	1.02380	1.03387
			1.00436	1.01212	1.02434	1.03429
32	Na_2CO_3, 0.05 *M*	.015	.98527	.99239	1.00349	1.01284
		.01	.99499	1.00251	1.01402	1.02376
		.005	1.01152	1.01951	1.03205	1.04228
33	Na_3PO_4, 0.01 *M*	.015			1.02832	1.03381
		.01			1.03876	1.04467
		.005			1.05656	1.06310
34	Na_3PO_4, 0.05 *M*	.015	1.03351	1.04075	1.05120	1.06004
			1.03350	1.04059	1.05115	1.06007
		.01	1.04328	1.05059	1.06165	1.07097
			1.04316	1.05049	1.06156	1.07092
					1.06143	
		.005	1.05973	1.06751	1.07930	1.08934
			1.05938	1.06720	1.07915	1.08923
36	NaOH, 0.01 *M*	.015	1.03749	1.03842	1.04050	1.04229
		.01	1.04643	1.04775	1.05053	1.05234
		.005	1.06237	1.06419	1.06786	1.07042
38	NaOH, 0.04809 *M*	.015	1.07448	1.07685	1.08090	1.08440
		.01	1.08369	1.08635	1.09116	1.09492
		.005	1.09993	1.10317	1.10900	1.11350

TABLE 6. pwH° *at 0°, 10°, 25°, and 38°*

[Acid solutions]

No.	Solution	pwH° at—				Reference
		0°	10°	25°	38°	
1	HCl, 0.1 *M*	1.190	1.192	1.198	1.204	[7]
2	HCl, 0.01 *M*; KCl, 0.09 *M*	2.203	2.205	2.208	2.212	[26, 27]
5	Sulfamic acid, 0.01 *M*	2.124	2.122	2.122	2.123	
6	$KH_3(C_2O_4)_2$, 0.1 *M*			1.626	1.635	[6]
7	$KH_3(C_2O_4)_2$, 0.05 *M*	1.763	1.768	1.773	1.797	
8	$KH_3(C_2O_4)_2$, 0.025 *M*	1.933	1.936	1.943	1.955	
9	$KH_3(C_2O_4)_2$, 0.01 *M*	2.197	2.200	2.203	2.215	
10	Citric acid, 0.05 *M*	2.318	2.296	2.274	2.261	
11	Citric acid, 0.01 *M*	2.687	2.667	2.648	2.634	
13	KH tartrate, 0.03 *M*			3.645	3.634	[6]
14	KH_2 citrate, 0.1 *M*	3.925		3.828	3.808	[6]
15	KH_2 citrate, 0.02 *M*	3.986		3.899	3.883	[6]
16	KH phthalate, 0.05 *M*	4.090	4.083	4.093	4.121	[28]
17	Acetic acid, 0.1 *M*; NaAc, 0.1 *M*	4.790		4.762	4.769	[6]
18	Acetic acid, 0.05 *M*; NaAc, 0.05 *M*	4.789		4.762	4.770	Interpolated
19	Acetic acid, 0.01 *M*; NaAc, 0.01 *M*	4.780		4.762	4.771	[6]
20	NaHsuccinate, 0.05 *M*; Na_2Suc, 0.05 *M*	5.532	5.498	5.475	5.478	
21	NaHSuc, 0.025 *M*. Na_2Suc, 0.025 *M*	5.561	5.528	5.503	5.516	
22	NaHSuc, 0.01 *M*; Na_2Suc, 0.01 *M*	5.600	5.569	5.551	5.559	

TABLE 7. pwH° *at 0°, 10°, 25°, and 38°*

[Alkaline solutions]

No.	Solution	pwH° at—			
		0°	10°	25°	38°
23	$Na_2B_4O_7$, 0.01 *M* [a]	9.322	9.388	9.240	9.145
24	$KHCO_3$, 0.05 *M*; Li_2CO_3, 0.05 *M*	10.339	10.199	10.034	9.927
25	$KHCO_3$, 0.025 *M*; Li_2CO_3, 0.025 *M*	10.404	10.263	10.099	9.990
26	$KHCO_3$, 0.01 *M*; Li_2CO_3, 0.01 *M*	10.476	10.333	10.165	10.050
27	$NaHCO_3$, 0.05 *M*; Na_2CO_3, 0.05 *M*	10.365	10.227	10.065	9.958
28	$NaHCO_3$, 0.025 *M*; Na_2CO_3, 0.025 *M*	10.427	10.288	10.124	10.015
29	$NaHCO_3$, 0.01 *M*; Na_2CO_3, 0.01 *M*	10.495	10.355	10.189	10.074
30	Na_2CO_3, 0.01 *M*	11.692	11.422	11.074	10.807
31	Na_2CO_3, 0.025 *M*	11.864	11.594	11.251	10.990
32	Na_2CO_3, 0.05 *M*	12.003	11.730	11.386	11.122
33	Na_3PO_4, 0.01 *M*			11.800	11.458
34	Na_3PO_4, 0.05 *M*	12.888	12.580	12.182	11.884
36	NaOH, 0.01 *M*	12.928	12.514	11.983	11.567
38	NaOH, 0.05 *M*	13.645	13.229	12.702	12.290

[a] Values for borax calculated from data of [29].

V. Calculations and Discussion

The Brønsted theory of specific ionic interaction [30] is founded upon the hypothesis that the activity coefficients of ions are influenced differently by the specific characteristics of the ions of opposite sign composing the medium and in a like manner by other ions of like charge which, through repulsion, are presumed beyond the reach of short range forces. Although the studies of Güntelberg [31], Scatchard and Prentiss [32], Harned [27], and others indicate that Brønsted's treatment is somewhat oversimplified, they serve to confirm this primary postulate. Hence, the activity coefficient of chloride ion needed to compute a pH value from pwH is probably influenced not only by the ionic strength but to some extent by the kinds of cations present.

When hydrochloric acid is replaced either partially or completely by alkali chloride at constant ionic strength, the activity coefficient of the acid decreases [27]. This means that the ion-size parameter of eq 4 also decreases. Inasmuch as no change has taken place in the anionic composition of the medium, it is not unreasonable to assume that the replacement of hydrogen ion by alkali metal ion results in a decrease of a_i for the acid. The activity coefficient of chloride ion in a pure dilute solution of hydrochloric acid is believed to approximate the mean activity coefficient of the acid. Furthermore, the ion-size parameter for the latter ranges from 6, for pure hydrochloric acid, to 5.0 to 5.4, for hydrochloric acid in pure sodium chloride and pure potassium chloride.[2] Hence, if a_i for chloride ion in mixtures containing sodium and potassium ions is assumed to be approximately the same as the ion-size parameter for hydrochloric acid in the mixtures, a choice of 4 to 6 can be justified. The uncertainty in f°_{Cl} and in the pH_s computed by eq 3a must be at least as great as the difference between the results furnished by these two reasonable values of a_i.

The pH_s values given in tables 8 and 9 were computed from pwH° by eq 3a. At each of the four temperatures, f°_{Cl} was estimated by eq 4 with a_i equal to 5. The approximate ionic strengths, μ, were obtained with the aid of the concentrations of hydrogen and hydroxyl ions derived from the pH given in table 2. For the acid salts, the ratio of constants for the overlapping equilibria was used, together with m_H. The formula for the calculation appears in an earlier contribution [34]. In order to indicate the uncertainty of the values given in the tables, the difference, δpH, between the pH_s furnished by $a_i=4$ and $a_i=6$ at 25° is listed in the last column of each table.

[2] Cesium chloride lowers the parameter still more [33].

TABLE 8. pH_s *from cells without liquid junction (type II)*

Acid solutions

No.	Solution	μ	pH_s at—				δpH
			0°	10°	25°	38°	
1	HCl, 0.1 *M*	0.1	1.088	1.088	1.092	1.096	0.014
2	HCl, 0.01 *M*; KCl, 0.09 *M*	.1	2.101	2.101	2.102	2.104	.014
3	Sulfamic acid, 0.01 *M*	.0078	2.086	2.084	2.083	2.083	.002
4	$KH_3(C_2O_4)_2$, 0.1 *M*	.144	.....	.....	1.507	1.514	.019
5	$KH_3(C_2O_4)_2$, 0.05 *M*	.077	1.670	1.673	1.676	1.698	.012
6	$KH_3(C_2O_4)_2$, 0.025 *M*	.042	1.858	1.860	1.865	1.875	.008
7	$KH_3(C_2O_4)_2$, 0.01 *M*	.018	2.143	2.145	2.147	2.158	.004
8	Citric acid, 0.05 *M*	.0063	2.284	2.261	2.238	2.224	.001
9	Citric acid, 0.01 *M*	.0025	2.664	2.644	2.624	2.610	.000
10	KH tartrate, 0.03 *M*	.036	.....	.....	3.571	3.559	.007
11	KH_2 citrate, 0.1 *M*	.115	3.818	.....	3.717	3.695	.016
12	KH_2 citrate, 0.02 *M*	.024	3.926	.....	3.836	3.819	.005
13	KH phthalate, 0.05 *M*	.053	4.008	4.000	4.008	4.034	.009
14	Acetic acid, 0.1 *M*; NaAc, 0.1 *M*	.1	4.688	.....	4.656	4.661	.014
15	Acetic acid, 0.05 *M*; NaAc, 0.05 *M*	.05	4.709	.....	4.679	4.685	.009
16	Acetic acid, 0.01 *M*; NaAc, 0.01 *M*	.01	4.747	.....	4.718	4.726	.003
17	NaHsuccinate, 0.05 *M*; Na_2Suc, 0.05 *M*	.202	5.405	5.369	5.343	5.344	.023
18	NaHSuc, 0.025 *M*; Na_2Suc, 0.025 *M*	.101	5.459	5.424	5.403	5.408	.015
19	NaHSuc, 0.01 *M*; Na_2Suc, 0.01 *M*	.041	5.526	5.494	5.474	5.480	.007

TABLE 9.—pH_s *from cells without liquid junction (type III)*

(Alkaline solutions)

No.	Solutions	μ	pH_s at—				δpH
			0°	10°	25°	38°	
23	$Na_2B_4O_7$, 0.01 *M*	0.02	9.466	9.331	9.181	9.085	0.005
24	$KHCO_3$, 0.05 *M*; Li_2CO_3, 0.05 *M*	.2	10.212	10.070	9.902	9.793	.022
25	$KHCO_3$, 0.025 *M*; Li_2CO_3, 0.025 *M*	.1	10.302	10.159	9.993	9.882	.014
26	$KHCO_3$, 0.01 *M*; Li_2CO_3, 0.01 *M*	.04	10.402	10.258	9.088	9.972	.008
27	$NaHCO_3$, 0.05 *M*; Na_2CO_3, 0.05 *M*	.2	10.238	10.098	9.933	9.824	.022
28	$NaHCO_3$, 0.025 *M*; Na_2CO_3, 0.025 *M*	.1	10.325	10.184	10.018	9.907	.014
29	$NaHCO_3$, 0.01 *M*; Na_2CO_3, 0.01 *M*	.04	10.421	10.280	10.112	9.996	.008
30	Na_2CO_3, 0.01 *M*	.029	11.627	11.356	11.006	10.738	.006
31	Na_2CO_3, 0.025 *M*	.074	11.772	11.500	11.155	10.892	.012
32	Na_2CO_3, 0.05 *M*	.148	11.887	11.612	11.266	11.000	.019
33	Na_3PO_4, 0.01 *M*	.047	.....	.....	11.719	11.375	.009
34	Na_3PO_4, 0.05 *M*	.27	12.750	12.440	12.039	11.739	.026
36	NaOH, 0.01 *M*	.01	12.886	12.471	11.939	11.522	±.003
38	NaOH, 0.05 *M*	.05	13.565	13.148	12.616	12.205	.009

1. Nature of the practical pH scale

The practical pH scale is defined in terms of the emf of cells of type II. In the pH meter, the emf of cell II is obtained as the difference between two measurements, one of which is the standardization with a solution of known pH. Saturated potassium chloride is interposed between the unknown and the standard buffer solution in an attempt to lower the liquid-junction potentials to a small constant value. Although these potentials at the boundaries between

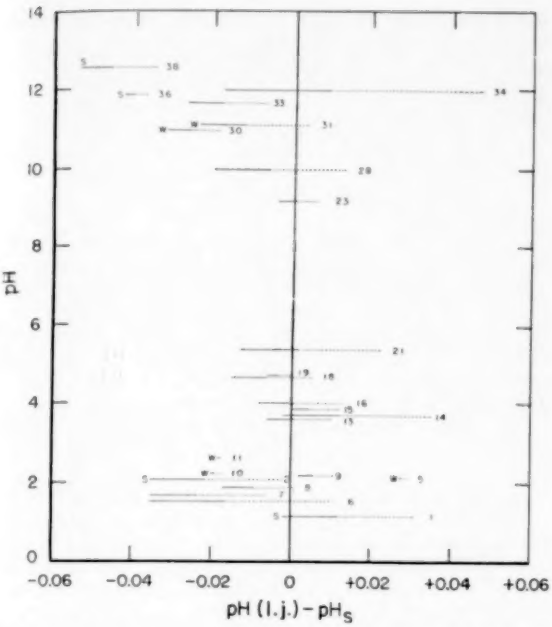

FIGURE 6. *Liquid-junction error of the practical* pH *scale.*

Solid line corresponds to the most probable range, 4 to 6, for the ion-size parameter. Broken line represents values from 2 to 4. Solution numbers appear beside the lines. S and W identify solutions of strong and weak electrolytes, respectively; the remainder are buffer solutions.

the saturated solution of potassium chloride and the unknown and standard solutions cannot be eliminated, it is hopefully assumed that their difference is small or zero, and no correction for residual liquid-junction potentials is made.

Figure 6 compares the pH furnished by the practical measurement of cells of type II (phosphate standard) with the value (designated pH$_s$) computed from the cell without liquid junction. The uncertainty in a_i is indicated by the length of the lines. The solid lines represent pH (l. j.)$-$pH$_s$ for a_i between 4 and 6 and the broken lines between 2 and 4. It is considered likely that the proper value lies between 4 and 6. The solution number appears beside each line. S identifies solutions containing strong acid or base, and W identifies solutions of weak acids and sodium carbonate. The remainder are buffer solutions.

Hydrogen and hydroxyl have the highest mobilities of any of the ions. Hence, one would expect, from simple qualitative considerations, to find that pH (l. j.)$-$pH$_s$ is positive for strongly acid solutions and negative for strongly alkaline ones. However, as figure 6 shows, negative values were found for some acid solutions as well as for those of high pH. Such a result might be attributed to a transfer of anions, present in concentrations greatly exceeding that of the hydrogen ion, across the boundary.

The potential differences at the boundary between solutions such as those studied here cannot be measured or calculated with accuracy. Even when ideal behavior for each ionic species is assumed and activity set equal to molality, a particular distribution of the ions through the boundary must be assumed, and the transference number of each must be known in all of the transition layers formed by diffusion or mixing of the two end solutions. Nevertheless, a further examination of the liquid-junction errors apparent in figure 6 seemed worth while.

There are two liquid junctions in a cell of type II. Each can be represented by

$$\text{Solution} \mid \text{satd. KCl};\ E_j,$$

where E_j is the potential difference across the boundary represented by the vertical line. The resulting error in pH, ΔpH, at 25° is

$$\Delta\text{pH} = E_j/0.059154 - E_{j(s)}/0.059154, \qquad (5)$$

where $E_{j(s)}$ indicates the potential at the boundary between the standard phosphate solution and saturated potassium chloride.

If the boundary is of the "continuous mixture" type, the equation developed by Henderson [35] applies. These junctions actually correspond more closely to the "free diffusion" type. Although the diffusion junction is easily set up and reproducible, it is difficult to treat theoretically. The Henderson equation can be written

$$E_j/0.059154 = \frac{(U_1 - V_1) - (U_2 - V_2)}{(U_1' + V_1') - (U_2' + V_2')} \log \frac{(U_1' + V_1')}{(U_2' + V_2')}. \qquad (6)$$

If the ionic mobilities in each solution are taken equal to the mobilities at infinite dilution, $\lambda^\circ/\boldsymbol{F}$, where λ° is the limiting equivalent ionic conductance and $\boldsymbol{F}$ is the faraday, we have the following formulas:

$$U \equiv \Sigma c_+ \lambda_+^\circ, \qquad (7a)$$

$$V \equiv \Sigma c_- \lambda_-^\circ, \qquad (7b)$$

$$U' \equiv \Sigma c_+ \lambda_+^\circ \mid z_+ \mid, \qquad (7c)$$

$$V' \equiv \Sigma c_- \lambda_-^\circ \mid z_- \mid. \qquad (7d)$$

The subscript 1 refers to the standard phosphate buffer or other solution in question, and 2 refers in each case to the saturated solution of potassium chloride; c is the ionic concentration (g ions per liter) and $|z_+|$ and $|z_-|$ are the absolute values of the valences of the ions.

The error, ΔpH, computed from eq 5 and 6 is compared in table 10 with the corresponding "observed" difference, pH (l. j.)$-$pH$_s$. The ion-size parameter, a_i, was taken to be 4 for the calculation of pH$_s$ from pwH°. The limiting equivalent conductances of the ions were taken from the literature and from the list given in Harned and Owen's monograph [33]. The conductances of carbonate ion, secondary and tertiary phosphate ions, primary cit-

rate ion, and secondary phthalate ion were estimated from those of other ions of like charge and similar structure. Hydrolysis and dissociation were considered in computing the required ionic concentrations.

TABLE 10. *Liquid-junction error of the practical* pH *scale with the phosphate buffer as primary standard*

Comparison of "observed" pH (l. j.)—pH_s with ΔpH calculated by the Henderson equation

No.	Solution	Observed pH_s(l. j.)—pH_s	Calculated ΔpH
1	HCl, 0.1 *M*	+0.012	+0.038
2	HCl, 0.01 *M*; KCl, 0.09 *M*	−.021	−.004
6	$KH_3(C_2O_4)_2$, 0.1 *M*	−.016	+.024
7	$KH_3(C_2O_4)_2$, 0.05 *M*	−.023	+.013
8	$KH_3(C_2O_4)_2$, 0.025 *M*	−.009	+.012
9	$KH_3(C_2O_4)_2$, 0.01 *M*	+.006	+.010
10	Citric acid, 0.05 *M*	−.019	+.012
11	Citric acid, 0.01 *M*	−.018	+.016
14	KH_2 citrate, 0.1 *M*	+.012	+.005
15	KH_2 citrate, 0.02 *M*	+.005	+.009
16	KH phthalate, 0.05 *M*	+.001	+.001
18	Acetic acid, 0.05 *M*; NaAc, 0.05 *M*	−.006	.000
19	Acetic acid, 0.01 *M*; NaAc, 0.01 *M*	−.003	+.013
28	$NaHCO_3$, 0.025 *M*; Na_2CO_3, 0.025 *M*	−.006	−.003
30	Na_2CO_3, 0.01 *M*	−.026	+.004
31	Na_2CO_3, 0.025 *M*	−.012	−.001
33	Na_3PO_4, 0.01 *M*	−.018	−.003
34	Na_3PO_4, 0.05 *M*	+.009	−.013
36	NaOH, 0.01 *M*	−.040	−.018
38	NaOH, 0.05 *M*	−.046	−.029

In general, pH(l. j.)$-pH_s$ is less than the calculated error by 0.01 to 0.04 unit. A smaller a_i would compensate in some measure for the discrepancy. Nevertheless, the approximations made in the calculation, together with the assumptions involved in the use of the Henderson equation, are probably chiefly responsible. It is perhaps significant that the difference is large for solutions of potassium tetroxalate and solutions of citric acid, both of which contain appreciable amounts of molecular acid. The agreement is good for the most dilute (0.01-*M*) solution of potassium tetroxalate and for potassium dihydrogen citrate, potassium acid phthalate, the acetate buffers, and the 1:1 carbonate buffer. All of these are well-buffered solutions, and none has a pH value below 2 or above 10.1. The calculation appears to confirm the belief that the potential at the liquid junction between 0.01-*M* hydrochloric acid, 0.09-*M* potassium chloride and the saturated potassium chloride solution matches the corresponding potential for common buffer solutions much more closely than does that for 0.1-*M* hydrochloric acid. The observed pH difference, however, does not agree as well as might be desired.

Figure 6 demonstrates the consistency of the three NBS pH standards, namely the reference phosphate, the phthalate buffer (No. 16) and the borax buffer (No. 23). It also shows that low pH values are usually obtained from cells with liquid junction in strongly alkaline solutions, for the values of pH(l.j.)$-pH_s$ are too large in general to attribute to the uncertainty in pH_s. This error may amount to 0.05 unit or more and is in the same direction as the alkaline error of the glass electrode. The error in acid solutions may be as great as 0.03 unit and be either in the direction of too high or too low pH.

2. pH standards of high acidity and high alkalinity

There are two reasons why standards of low and high pH are needed. First, if pH at the ends of the practical scale is to be interpreted in terms of the activity of hydrogen ion, a means of rectifying the aberration apparent in figure 6 should be sought. Standards of which the assigned pH has significance in terms of hydrogen ion and whose liquid-junction errors match those of the majority of unknowns of comparable pH would provide a partial solution to the problem. It appears, for example, that measurements on the practical scale are approximately correct at pH 10, about 0.02 unit low at pH 11 to 12, and about 0.04 unit low at pH 13. Thus a standard of pH 11 to 12 might reduce the error of measurements in the range pH 10 to 13 to ± 0.02 unit. However, this procedure offers little help at pH values below 2.5, where the errors may be either positive or negative. Present standards are adequate between pH 2.5 and 10.5.

In the second place, new pH standards of high acidity and alkalinity would improve the accuracy of measurement in these regions by reducing the pH span between unknown and standard. In this way the errors caused by differences in temperature between the two solutions or failure to adjust the instrument to the proper emf/pH slope would be minimized. Glass-electrode errors would also be compensated to some extent.

A choice of suitable standards entails consideration of the purity and stability of the materials from which the standard solution is prepared, the stability of the solution itself, and the magnitude of the residual liquid-junction potential compared, as in figure 6, with other typical solutions in the same pH range. In general, buffer solutions form the sharpest, most reproducible junctions. The following paragraphs summarize the properties, desirable and undesirable, of the materials included in the present study.

Sulfamic acid did not appear to be appreciably hygroscopic, but its solution displayed an abnormal liquid-junction potential. Potassium tetroxalate dihydrate can be obtained as a pure solid, stable in air at ordinary temperatures and humidities. The pH of the 0.05-*M* solution increased only 0.01 unit in 90 days. The liquid-junction error of the 0.01-*M* solution is negligible.

Citric acid, potassium dihydrogen citrate, and potassium hydrogen tartrate can be obtained in pure form, but their solutions support mold growth. The saturated solution of potassium hydrogen tartrate (about 0.034 *M*) is a useful standard that is easily prepared [36]. However, it must be renewed every few days, for mold appears in from 1 to 4 weeks and is accompanied by an increase in pH of 0.02 to 0.1 unit [37]. The standard 0.05-*M* phthalate buffer solution was found to be mold-free after 130 days. The pH had increased only 0.005 unit.

Acetate buffer solutions are good standards but are difficult to prepare. The succinate salts have little tendency to absorb moisture [22], and their solutions are satisfactorily stable, as are those of sodium and potassium bicarbonates. Succinate

solutions may mold several weeks after preparation. Lithium and sodium carbonates have the distinct disadvantage of requiring ignition before use. Pure solid trisodium phosphate could not be prepared, but its solution was formed from equal molal amounts of solid disodium hydrogen phosphate and of sodium hydroxide (in aqueous solution). As a result of extensive hydrolysis, the buffer capacity of such solutions is high. The pH of a 0.025-*M* solution of trisodium phosphate was found to be altered less than 0.02 unit by addition of 4 mole percent of sodium hydroxide or an equal amount of disodium hydrogen phosphate. The pH of the 0.05-*M* solution, preserved in a paraffin-lined bottle which was occasionally opened, decreased only 0.004 unit in 90 days and 0.008 unit in 140 days.

The solution of trisodium phosphate can be used for the calibration of high-alkalinity glass electrodes. When an uncertainty of ± 0.05 unit is permissible, solutions of sodium hydroxide will also be found useful for this purpose. The pH at 25° computed from the ionization constant of water and the activity coefficient of hydroxide ion, assuming the latter to be the same as the mean activity coefficient of the solute, is 12.61 for the 0.05-*M* solution and 12.88 for the 0.1-*M* solution. This value for 0.05-*M* sodium hydroxide is in close agreement with 12.616 computed from the emf of cell III. However, the two calculations are not completely independent, inasmuch as the value for the ionization constant of water rests in part on measurements of cells of type III. Between 25° and 30°, the pH of these solutions of sodium hydroxide decreases about 0.03 unit for each degree increase in temperature.

Five buffer solutions are recommended:

Solution	pH, at—			
	0°	10°	25°	38°
Potassium tetroxalate, 0.01 *M*	2. 14	2. 15	2. 15	2. 16
Potassium hydrogen tartrate (satd. at room temperature)	-------	-------	3. 56	3. 55
Sodium acid succinate, 0.025 *M*; sodium succinate, 0.025 *M*	5. 46	5. 42	5. 40	5. 41
Sodium bicarbonate, 0.025 *M*; sodium carbonate, 0.025 *M*	10. 32	10. 18	10. 02	9. 91
Trisodium phosphate, 0.01 *M*	-------	-------	11. 72	11. 38

These values are probably reliable to about ± 0.01 unit. The pH of the acid standards is little affected by temperature changes. On the other hand, rather careful control of temperature is essential to accurate measurement of pH at high alkalinities.

VI. References

[1] W. M. Clark, The determination of hydrogen ions, 3d ed. (The Williams & Wilkins Co., Baltimore, Md., 1928).
[2] G. Kortüm, Z. Elektrochem. **48,** 145 (1942).
[3] D. A. MacInnes, Science **108,** 693 (1948).
[4] E. R. Smith and R. G. Bates, Compt. rend., p. 118 Quinzième Conférence, International Union of Pure and Applied Chemistry, Amsterdam (1949).
[5] J. W. M. Du Mond and E. R. Cohen, Rev. Modern Phys. **20,** 82 (1948).
[6] R. G. Bates, Chem. Revs. **42,** 1 (1948).
[7] H. S. Harned and R. W. Ehlers, J. Am. Chem. Soc. **55,** 2179 (1933).
[8] R. G. Bates and G. D. Pinching, J. Research NBS **42,** 419 (1949) RP1982.
[9] R. G. Bates and E. R. Smith, J. Wash. Acad. Sci. **38,** 61 (1948).
[10] M. Kilpatrick and E. F. Chase, J. Am. Chem. Soc. **53,** 1732 (1931).
[11] M. Kilpatrick, E. F. Chase, and L. C. Riesch, J. Am. Chem. Soc. **56,** 2051 (1934).
[12] D. I. Hitchcock and R. Peters, J. Am. Chem. Soc. **68,** 1753 (1946).
[13] P. Debye and E. Hückel, Physik. Z. **24,** 185 (1923).
[14] N. Bjerrum, Kgl. Danske Videnskab. Selskab., Math.-fys. Medd. **7,** No. 9 (1926).
[15] E. Hückel, Physik. Z. **26,** 93 (1925).
[16] D. I. Hitchcock and A. C. Taylor, J. Am. Chem. Soc. **59,** 1812 (1937); **60,** 2710 (1938).
[17] D. A. MacInnes, D. Belcher, and T. Shedlovsky, J. Am. Chem. Soc. **60,** 1094 (1938).
[18] G. D. Pinching and R. G. Bates, J. Research NBS **37,** 311 (1946) RP1749.
[19] W. J. Hamer and S. F. Acree, J. Research NBS **33,** 87 (1944) RP1598.
[20] R. G. Bates and S. F. Acree, J. Research NBS **30,** 129 (1943) RP1524.
[21] R. G. Bates and G. D. Pinching, J. Am. Chem. Soc. **71,** 1274 (1949).
[22] G. D. Pinching and R. G. Bates, J. Research NBS **45,** (1950) RP2142.
[23] I. M. Kolthoff and E. B. Sandell, Textbook of quantitative inorganic analysis, p. 519, 524 (The Macmillan Co., New York, N. Y., 1937).
[24] S. J. Kiehl and R. D. Loucks, Trans. Electrochem. Soc. **67,** 81 (1935).
[25] R. G. Bates and S. F. Acree, J. Research NBS **34,** 373 (1945) RP1648.
[26] H. S. Harned and W. J. Hamer, J. Am. Chem. Soc. **55,** 2194 (1933).
[27] H. S. Harned, J. Am. Chem. Soc. **57,** 1865 (1935).
[28] W. J. Hamer and S. F. Acree, J. Research NBS **32,** 215 (1944) RP1586.
[29] G. G. Manov, N. J. De Lollis, P. W. Lindvall, and S. F. Acree, J. Research NBS **36,** 543 (1946) RP1721.
[30] J. N. Brønsted, J. Am. Chem. Soc. **44,** 877 (1922); **45,** 2898 (1923).
[31] E. Güntelberg, Z. physik. Chem. **123,** 199 (1926).
[32] G. Scatchard and S. S. Prentiss, J. Am. Chem. Soc. **56,** 2320 (1924).
[33] H. S. Harned and B. B. Owen, The physical chemistry of electrolytic solutions, chapter 14 and appendix (Reinhold Publishing Corp., New York, N. Y., 1943).
[34] R. G. Bates, J. Am. Chem. Soc. **70,** 1579 (1948).
[35] P. Henderson, Z. physik. Chem. **59,** 118 (1907); **63,** 325 (1908).
[36] J. J. Lingane, Anal. Chem. **19,** 810 (1947).
[37] R. G. Bates, Anal. chem. (publication pending).

WASHINGTON, July 6, 1950.

Journal of Research of the National Bureau of Standards Vol. 45, No. 5, November 1950 Research Paper 154

Electrode Function (pH Response), Hygroscopicity, and Chemical Durability of Soda-Lead Oxide-Silica Glasses

By Donald Hubbard, Mason H. Black, and Gerald F. Rynders

The pH response, hygroscopicity, and chemical durability of a series of Na_2O–PbO–SiO_2 (soda-lead oxide-silica) glasses have been investigated. The results obtained are in complete accord with the data previously published for a series of Na_2O–CaO–SiO_2 glasses and show that: 1. Glasses of very low hygroscopicity yield electrodes whose pH responses fall appreciably below the theoretical 59 millivolts per pH at 25° C; 2. electrodes prepared from glasses of poor chemical durability also fail to develop the full theoretical voltage.

When the approximate compositions at which changes in the primary phase appear for the Na_2O–PbO–SiO_2 system are superimposed upon the pH response and chemical durability curves, the marked changes in these properties appear to reflect some of the critical compositions of the phase equilibrium diagram.

The chemical durability data obtained by the interferometer procedure indicate that the property of swelling in acid solutions is much more universal for silicate glasses than previously realized.

I. Introduction

All glasses, when immersed in aqueous solutions, develop an electromotive force [1 to 6],[1] which in some cases serves as a reliable indicator of the hydrogen ion activity of the solution in quantitative accord with the prediction of the Nernst equation, $\Delta E = 0.000198\ T\ \Delta$ pH [7, 8]. Nevertheless, many glasses, show little or no pH response, whereas still others give the theoretical increment of voltage over only a limited pH range [1, 9 to 11]. From this apparent chaotic pH performance of glasses of different compositions have emerged certain definite characteristics of behavior, as follows:

1. Glasses of very low hygroscopicity or low water content produce electrodes that fail to develop the theoretical 59 mv per pH at 25° C [1, 6, 12, 13].

2. Electrodes prepared from glasses of very poor chemical durability also fail to develop the full theoretical voltage [13, 14].

3. Only those glasses having both adequate hygroscopicity and uniform chemical durability over an extended pH range produce electrodes that approximate the correct pH response [7, 12, 13, 15].

4. Voltage departures (errors) for electrodes prepared from pH responsive glasses occur in those solutions that cause an appreciable change in the attack on the glass, such as strong alkaline and hydrofluoric acid solutions [5, 13, 15, 17].

5. Voltage departures that appear in solutions of a dehydrating nature, such as strong H_2SO_4 and acetic acid [11], as well as in nonaqueous solutions such as ethanol, are accompanied by detectable changes in the surface of the glass, notably the repression of swelling [6 (p. 81), 16, 17].

In the present investigation, the hygroscopicity, chemical durability, and pH response of a series of Na_2O-PbO-SiO_2 glasses were studied for the purpose of determining if the above generalizations are valid for this series, and also to observe if the above properties reflect any of the critical compositions of the phase equilibrium diagram.

[1] Figures in brackets indicate the literature references at the end of this paper.

II. Experimental Procedure

The hygroscopicity data were obtained by weighing the water "sorbed" [18] by powdered samples of the glasses exposed for 1- and 2-hr periods, to the high humidity maintained by a saturated solution of $CaSO_4.2H_2O$ at 25° C [12, 13]. The samples consisted of approximately 1.5 g of the powdered glass that passed through a Tyler standard 150 mesh sieve.[2] In order to make a legitimate comparison between glasses differing greatly in density, the hygroscopicity values are reported as milligrams of water sorbed per cubic centimeter, that is, water sorbed times the density of the glass divided by the weight of the sample.

The chemical durability determinations were made by the interferometer procedure [15, 19, 20], which consists of determining the displacement of fringes by the alteration of the surface of the experimental glass after partial immersion in the test solution. Swelling is plotted in all figures as negative attack. To make the results comparable with previous publications [13, 14, 15, 17, 21, 22] the exposures were made at 80°±0.2° C to Britton-Robinson universal buffer solutions [23] ranging from pH 2 to 11.8. All values are reported for a 6-hr period, although the durabilities for many of the glasses were so poor that exposure times had to be reduced in order to keep the attack values within the limitations of the interferometer and preserve the optical quality of the surfaces. In one extreme case it was necessary to reduce the time of exposure to 5 secs.

The experimental electrodes were made by blowing a small thin-walled bulb on the end of tubing, which was drawn from the melts at the time of pouring. The inner electrical connection was established by filling the bulb and a portion of the stem with mercury [2, 24]. The emf measurements were made at room temperature with a Beckman pH meter, model G, using a well-conditioned Beckman glass electrode

[2] No. 140 sieve of U. S. Standard Sieve Series.

a reference electrode. The voltage difference between the reference and experimental electrodes obtained in the buffer of pH 2 was taken as the zero departure. This reference point, for some of the glasses, proved to be an unfortunate choice, as the readings were more unsteady in this buffer than at other acid pH values.[3] The data for pH response (mv per pH) were calculated from the voltage readings at pH 4.1 and 8.2.

The voltage data presented in this paper generally represent the best performance recorded for an electrode from a given glass. These optimum values were obtained for periods ranging from a few minutes after the electrodes were prepared, for some glasses, to several days for others, depending on the life span of the electrodes as dictated by the chemical durability of the glasses.

The glasses investigated were from a series furnished by F. W. Glaze and J. M. Florence as a part of their general study of infrared transmittance of glasses [25, 26]. The compositions of these glasses were computed from the batch and are identified throughout the text of this paper as weight percent in the ratio of Na_2O:PbO:SiO_2.

[3] This unsteady "zero" voltage feature was undoubtedly associated with the chemical durability of the glass. Differences in appearance of the specimens and tarnishing of the surface upon exposure to the acid buffers were evident, although surface alteration could not be definitely demonstrated by the interferometer.

III. Results and Discussion

Typical data for hygroscopicity, chemical durability, voltage departure, and pH response for the Na_2O-PbO-SiO_2 glasses are listed in table 1.

TABLE 1. *Hygroscopicity (water sorbed), pH response and chemical durability of some* Na_2O-PbO-SiO_2 *glasses*

No.	Glasses			Water sorbed for—		Voltage departure at pH—						pH response, pH 4.1 to 8.1	Chemical durability (attack) at pH—					
	Na_2O	PbO	SiO_2	1 hr	2 hr	2.0	4.1	6.0	8.2	10.2	11.8		2.0	4.1	6.0	8.2	10.2	11.8
	%	%	%	mg/cm²	mg/cm²	mv	mv	mv	mv	mv	mv	mv per pH	Fringes	Fringes	Fringes	Fringes	Fringes	Fringes
1	10	10	80	37	69	0	2	4	9	20	46	57+	[a]ND	ND	ND	ND	(?)	2
2	15	5	80	62	105	0	0	0	0	0	−8	59	1/10 swell	1/10 swell	1/10 swell	D swell	D swell	3−
3	20	0	80	108	256	0	10	17	25	37	49	55	1½ swell	2 swell	2+swell	2 swell	1 swell	3+
4	10	20	70	30	62	0	0	2	12	26	56	56	ND	ND	ND	ND	1/10+	2½
5	15	15	70	52	99	0	0	1	2	5	11	58+	3/10 swell	D swell	D+swell	D	D	3
6	20	10	70	81	189	0	2	5	15	26	37	56	1+swell	1+swell	1+swell	1+swell	D	4½
7	25	5	70	120	250	0	5	18	30	45	52	53−	18 swell	18 swell	18 swell	12 swell		96
8	30	0	70	186		0	35	117	221	315	395	13	72 swell	72 swell	72 swell	72 swell	18 swell	252
9	5	35	60	20	29	[b]	[b]	[b]	[b]	[b]	[b]		ND	ND	ND	ND	1/10	2+
10	10	30	60	33	59	0	0	3	12	22	58	56	ND	ND	ND	ND	2/10	4+
11	15	25	60	51	95	0	0	0	0	5	17	59	1/10 swell	2/10 swell	1/10+swell		¼+	6−
12	20	20	60	75	163	0	0	0	1	15	40	59−	1¼ swell	1¼ swell	1¼ swell	1¼ swell	D+	7
13	25	15	60	113	228	0	−3	15	45	90	150	49	15 swell	18 swell	18 swell	18 swell	[c]SC, swell	12
14	30	10	60	208	300	0	−46	22	111	186	282	20	180 swell	180 swell	180 swell	(?)	(?)	50
15	40		60	>300		0	95	180	282	365	460	13			Failed to maintain polish.			
16	5	45	50	20	32	[b]	[b]	[b]	[b]	[b]	[b]		D	ND	ND	D	2/10+	3−
17	10	40	50	34	59	0	0	1	1	43	68	57	D swell	2/10 swell	¼swell	1½	¾	5+
18	15	35	50	50	102	0	0	5	13	41	62	56	¼−swell	¼+swell	½ swell	2	½	7+
19	20	30	50	72	154	0	2	7	24	68	126	54	15 swell	15 swell	10 swell	1 swell	¾	10
20	25	25	50	118	228	0	−33	−2	33	85	156	42	72 swell	72 swell	60 swell	50 swell	10 swell	48
21	30	20	50	219	320	0	−25	51	149	240		15	450 swell	720 swell		720 swell		360
22	5	55	40	20	39	[b]	[b]	[b]	[b]	[b]	[b]		2/10 swell	1/10 swell	1/10 swell	2−	¾	6½
23	10	50	40	33	68	0	0	3	13	42	7	56	2/10	1/10	D	½ swell	1+	9½
24	15	45	40	49	108	0	0	8	20	54	96	54	1	½+	½	4	1¾	15
25	20	40	40	75	156	0	−18	−14	16	89	187	51	4½ swell	9 swell	1½	9	2½+	24
26	25	35	40	127	280	0	−27	38	132	236	358	20	180 swell			54 swell		>50
27	30	30	40	300	515	[d]	[d]	[d]	[d]	[d]	[d]	<15	4,320 swell	4,320 swell	4,320 swell	>2,160 swell	2,160	(?)
28	0	70	30	14	17	[b]	[b]	[b]	[b]	[b]	[b]		2/10	¼+swell	½ swell	4	3−	9+
29	5	65	30	22	50	[b]	[b]	[b]	[b]	[b]	[b]		2−	¾−	1½ swell	3+	D+	12
30	10	60	30	37	92	0	0	2	18	29	7	55	3+	3− swell	3− swell	15−	15	18
31	15	55	30	65	130	0	27	58	78	107	67	47	1½	3	3 swell	15	15	18
32	0	80	20	13	16	[b]	[b]	[b]	[b]	[b]	[b]	0	3−	3+swell	3 swell	6 swell	3−swell	24−
33	5	75	20	30	68	0	−26	−28	13	53	107	49	3−	3 swell	3 swell	3−swell	3	54
34	12	0	88	52	104	0	10	18	32	45	54	55	D swell	D swell	D		(?)	3
35	14	0	86	61	124	0	2	4	6	8	10	58	2/10 swell	2/10− swell	2/10 swell		D	2−
36	16	0	84	83	178	0	3	7	7	9	11	58	¼+ swell	¼+ swell	¼+ swell	2/10 swell	(?)	1¼
37	18	0	82	96	220	0	10	18	18	26	34	57	½ swell	½ swell	½ swell	½−swell	(?)	2½
38	20	0	80	108	276	0	10	17	25	37	49	55	1½ swell	2 swell	2+swell	2 swell	1 swell	3+
39	22	0	78	112	265	0	10	18	28	39	49	55	2½ swell	6-swell	6 swell	6−swell	(?)	6
40	24	0	76	127	270	0	9	24	32	49	52	53	12 swell	12 swell	12 swell	6−swell	2½ swell	30−
40	0	65	35	14	21	[b]	[b]	[b]	[b]	[b]	[b]		1/10 swell	3 swell	1/10 swell	3−swell	D	9−
41	0	70	30	14	17	[b]	[b]	[b]	[b]	[b]	[b]		¼	¼+swell	½ swell	SC	3−	9+
42	0	75	25	12	14	[b]	[b]	[b]	[b]	[b]	[b]		3−	18 swell	3−swell	3−swell	6	18
43	0	78.8	21.2	12	15	[b]	[b]	[b]	[b]	[b]	[b]		9	9 swell	3−swell	3−swell	3−	21
44	0	80	20	13	16	[b]	[b]	[b]	[b]	[b]	[b]		3−	3+swell	3 swell	6 swell	3−swell	24
45	0	84.6	15.4	12	15	[b]	[b]	[b]	[b]	[b]	[b]		3−	3−swell	3 swell	3 swell	3−swell	60
46	0	88.1	11.9	13	22	[b]	[b]	[b]	[b]	[b]	[b]		White and gelatinous.	3−swell	3−swell	2 swell	3−	72
47	Corning 015			59	138	0	0	0	0	0	3	59	2/10−swell	2/10−swell	2/10−swell	SC	¼+	2

[a] D, Detectable; ND, not detectable.
[b] No definite pH response.
[c] SC, Surface cut.
[d] Tube disintegrated.
[e] The voltage departure and pH response of electrodes prepared from glass 12:0:88 are not in accord with the hygroscopicity and chemical durability values of this glass. However, difficulty was encountered in melting the batch, and the tubes obtained consisted of stringy glass, indicating incipient devitrification.

1. Hygroscopicity and pH Response

Figure 1 illustrates the results obtained upon plotting the pH response of these glasses against the hygroscopicity. As was the case for the Na_2O-CaO-SiO_2 series [13], these glasses also fall into distinct family groups of equal percentage of SiO_2. The curves for each family in which sufficient members could be prepared without devitrification passed through a region of optimum performance. Electrodes from the glasses of very low hygroscopicity gave little or no pH response, while those of intermediate hygroscopicity more nearly approached the theoretical. All glasses to the right of the optimum showed a falling off in pH function, which was accompanied by a progressive decrease in chemical durability (table 1, figs. 2 to 15, incl.) with increasing hygroscopicity. Thus, the suggestion that a low pH response might be used as an indicator of serviceability of optical glasses [27] must be accepted with reservations, because only the glasses of low pH response and low hygroscopicity possess any degree of acceptable serviceability, whereas those of low pH response and high hygroscopicity are accompanied by poor chemical durability and poor serviceability.

2. Chemical Durability and Voltage Departure

A visual comparison of the chemical durability and voltage departure characteristics of those family groups of glasses having like SiO_2 content shown in figure 1 can be obtained from inspection of figures 2 to 8 in which the above properties have been plotted over an extended pH range. In some cases the correlation of voltage departure with the chemical durability may be confusing or even appear contradictory, but if one keeps in mind that low hygroscopicity as well as poor chemical durability contributes to voltage departures from the theoretical, order is established from the apparent chaos. For example, in the family for 80 percent of SiO_2 (fig. 2) the member 15:5:80 [4] more nearly approaches the hygroscopicity and chemical durability characteristics of Corning 015 [6, 29] than any of the others, and at the same time its voltage characteristics are the best of the 80 percent SiO_2 group. The large voltage departures for glass 20:0:80 is due to the inferior durability compared to 015, whereas the large departures for glass 10:10:80 results from its low hygroscopicity.

For the family of 70 percent of SiO_2 (fig. 3), the glass 15:15:70 has the best voltage characteristics of the group. Its hygroscopicity and chemical durability characteristics also more nearly duplicate 015 than do any of the other members studied. Glass 10:20:70 has much lower hydroscopicity than 015, while the remaining members have poorer chemical durabilities over the entire pH range.

The same qualitative conditions prevail for the 60 percent SiO_2 family (fig. 4), in which glass 15:25:60 has the least votage departure and at the same time, its hygroscopicity and chemical durability characteristics more nearly approach 015 than do any of the other members of this group. The members with low hygroscopicity have voltage departures in accord with their respective water-sorbing capacities. The other members having poorer chemical durabilities than 015 have voltage departures that are qualitatively in the same order as their durabilities.

None of the glasses from the 50 percent SiO_2 (fig. 5) family gave satisfactory voltages, but their relative order of performance can be readily ascertained by a glance at their hydroscopicity and chemical durability characteristics. Some of the chemical durability curves for this family group exhibited an abnormal attack at pH 8 with some improvement at pH 10, followed in turn by vigorous attack at pH 11.8. The same feature is exhibited to a more exaggerated degree for the 40 percent SiO_2 series (fig. 6). For the 30 percent SiO_2 group, the same durability characteristics persist, although in a somewhat confused fashion (fig. 7) This particular type of chemical durability curve has been previously reported for some optical glasses [28].

Several of the electrodes whose voltage departure curves are shown in figures 4, 5, 6, and 8 exhibited large negative departures in the acid range [11].

The emf behavior of the glasses for the families 40 percent, 30 percent, and 20 percent of SiO_2 is in no case in accord with the straight-line relation of the Nernst equation. The glasses of very low hygroscopicity 5:55:40, 0:70:30, 5:65:30, and 0:80:20 failed to develop any definite pH response. The remaining glasses gave erratic electrode performance to accompany their erratic chemical durability curves. The dashed lines for the voltage departure for glasses such as 5:55:40 and 30:30:40 in figure 6 and for other glasses in figures 4, 5, 7, and 8 are included merely to emphasize that glasses having very low hygroscopicity and those at the other extreme having such high hygroscopicity values and poor chemical durability as to behave as punctured electrodes, approach the theoretical limiting voltage for an electrode possessing no hydrogen electrode function [14].

Such glasses as 5:65:30 and 5:75:20 (table 1, and figs. 7 and 8) serve well to illustrate that low hygroscopicity is not an indicator of good chemical durability. These glasses of low hygroscopicity and poor chemical durability maintain clear surfaces in air, but tarnish rapidly in the buffer solutions.

None of the glasses containing only lead oxide and silica had sufficient hygroscopicity to produce electrodes showing any pH function (table 1).

The behavior of a limited number of glasses with 0 percent of lead oxide is included in table 1 for comparison. However, as but two of these (20:0:80 and 30:0:70) fit into the family groups, a discussion of these glasses will be postponed to a later publication on the Na_2O-K_2O-SiO_2 system. It is of interest to note that the pH response of electrodes prepared from glass 12:0:88 was less than that expected from the hygroscopicity and chemical durability values. This is not surprising, as difficulty was encountered

[4] A glance at fig. 2 shows an apparent discrepancy between the voltage departure and the chemical durability value at pH 11.8 for glasses 15:5:80 and 015. However, there is no reason to suppose that the increment of voltage departure per unit of attack for the soda-lead-silica glasses would be the same as for that of the soda-lime-silica system.

in melting the batch, and the tubes obtained consisted of stringy, partially crystallized glass [29].

3. Effect of Composition on Hygroscopicity, Chemical Durability, and pH Response

To further emphasize the orderly interrelation between the hygroscopicity, chemical durability, and voltage performance of the Na_2O-PbO-SiO_2 glasses, these properties were plotted against the PbO content for each family in figures 9 to 15. From the hygroscopicity curves, it is evident that all glasses having low water "sorption" properties fail to develop the full theoretical pH response.

The chemical durability curves presented are for the extremes of pH studied, namely pH 2 and 11.8. These curves illustrate the marked difference in chemical durability behavior for glasses in acid and basic solutions, with swelling predominating in the acid pH range and solution occurring at high alkalinity. The divergence of these curves serves to emphasize the compositions at which marked durability differences appear. Further, a glance at the pH response curves reveals that the hydrogen electrode function of the glasses starts declining at the same compositions at which the chemical durabilities show a marked change.

The question always arises, do the chemical or physical properties of a series of glasses reflect any of the critical compositions of the phase-equilibrium diagram? In figures 9 to 14, dashed lines are drawn near the compositions at which a change of primary phase occurs [30]. In figure 10 a sharp change in the chemical durability of the series appears between the successive glass members, one of which falls in the composition range where $Na_2O.2SiO_2$ is the primary phase, and the other in which SiO_2 becomes the primary phase. A similar correspondence appears for the pH response-composition curve in figure 10. The same features seem to be indicated in figures 11 and 12. The pH response of the electrode prepared from the glass of 20 percent of PbO in figure 11 appears to be "too good" for convincing agreement. A comparison of the durability data for this glass with other glasses of table 1 implies that a lower pH response from this glass might well be expected. The cross sections of the phase-equilibrium diagram for the data presented in figures 13 and 14 are complicated and the experimental data inadequate for specific conclusions, yet the over-all picture is one of correspondence to the major composition changes. Figure 15 indicates that the region of high percentages of PbO is not a good one to explore for glasses having satisfactory pH response characteristics.

An over-all picture of the hygroscopicity versus composition for the Na_2O-PbO-SiO_2 glasses is presented in the ternary diagram, figure 16. The compositions of equal hygroscopicity (isosorbs) were obtained by interpolation of the observed data. The glass compositions that gave electrodes that developed pH functions as high as 56 mv/pH between pH 4 and 8 are included in the shaded area, while those glasses that produced electrodes developing the full 59 mv/pH are connected by a heavy dashed line. The glasses of higher Na_2O content and higher hygroscopicity gave electrodes that fell appreciably below the theoretical voltage and were also short-lived. It appears that the Na_2O-PbO-SiO_2 glasses fall into the same three groups that were characteristic of the $Na_2O.CaO.SiO_2$ series [13]: A, glasses that are too "dry" for successful electrodes; B, glasses that produce successful electrodes; and C, glasses having poor chemical durability, which are too "wet". Actually, the area B is also very much reduced because of poor durability of its members.

IV. Conclusions

The Na_2O-PbO-SiO_2 series of glasses appear to follow the generalizations for the hydrogen electrode behavior of glasses as outlined in the introduction of this report. All the members having very low hygroscopicity gave electrodes that failed to develop the theoretical voltage predictable from the Nernst equation at room temperatures. Likewise, the electrodes from glasses of very poor chemical durability failed to develop the full theoretical voltage. Although it is improbable that the best possible of the Na_2O-PbO-SiO_2 glasses for pH measurement were included in this series, it is obvious that those members that most nearly approached the hydgroscopicity and chemical durability characteristics of Corning 015 most nearly approached the ideal hydrogen electrode performance at 25° C. Poor chemical durability in the alkaline range, even for the best glasses produced, is one of the major factors limiting their usefulness.

Most of the durability measurements reported are qualitative. They are of interest in demonstrating the initial alteration of glass surfaces during attack by aqueous solutions, especially for the acid buffers in which many of the glasses exhibited a rapid rate of swelling. The pH-response and chemical-durability curves appear to reflect some of the critical compositions of the phase equilibrium diagram for the Na_2O-PbO-SiO_2 system.

V. References

[1] M. Cremer, On the causes of the electromotive properties of tissue and a discussion of polyphase electric cells, Z. Biol. **47,** 562 (1906).

[2] F. Haber and Z. Klemensiewicz, On electrical interfacial potentials, Z. physik. Chem. **67,** 385 (1909).

[3] G. Borelius, Interfacial potentials of solutions in contact with insulators, Ann. physik. [4] **45,** 929 (1914).

[4] H. Freundlick and Rona, The relation between electrokinetic potential pressure and the electric force at phase interfaces, Sitz. preuss. Akad. Wiss. **20,** 397 (1920).

[5] W. S. Hughes, The potential difference between glass and electrolytes in contact with glass, J. Am. Chem. Soc. **44,** 2860 (1922).

[6] M. Dole, Glass electrode (John Wiley & Sons, Inc., New York, N. Y., 1941).

[7] D. A. MacInnes and M. Dole, The behavior of glass electrodes of different compositions, J. Am. Chem. Soc. **52,** 29 (1930).

[8] George A. Perley, Glasses for measurement of pH, Anal. Chem. **21,** 394 (1949); U. S. Patent 2,444,845 (1948).
[9] B. Lengyel and E. Blum, The behavior of the glass electrode in connection with its chemical composition, Trans. Faraday Soc. **30,** 461 (1934).
[10] W. E. L. Brown, The measurement of hydrogen-ion concentration with glass electrodes, J. Sci. Instr. **2,** 12 (1924).
[11] D. A. MacInnes and D. Belcher, Further studies of the glass electrode, J. Am. Chem. Soc. **53,** 3315 (1931).
[12] Donald Hubbard, Hygroscopicity of optical glasses as an indicator of serviceability, J. Research NBS **36,** 365 (1946) RP1706.
[13] Donald Hubbard, Given W. Cleek, and Gerald F. Rynders, Electrode Function (pH response), hygroscopicity, and chemical durability of Na_2O-CaO-SiO_2 glasses, J. Research NBS **45,** 247 (1950) RP2076.
[14] Gerald F. Rynders, Oscar H. Grauer and Donald Hubbard, Electrode Function (pH response) of soda-silica glasses, J. Research NBS **41,** 273 (1948) RP1923.
[15] Donald Hubbard, Edgar H. Hamilton and A. N. Finn, Effect of the solubility of glass on the behavior of the glass electrode, J. Research NBS **22,** 339 (1939) RP1187.
[16] G. Buchbock, A property of the glass electrode, Z. physik. Chem. **156A** 232 (1931).
[17] Donald Hubbard and Gerald F. Rynders, Voltage anomalies of the glass electrode and the chemical durability of the glass, J. Research NBS **39,** 561 (1947) RP1848.
[18] James W. McBain, The mechanism of the adsorption ("sorption") of hydrogen on carbon, Phil. Mag. **18,** 916 (1909); Z. physik. chem. **68,** 471 (1909).
[19] Relative durability of optical glass, NBS Technical News Bulletin No. 221, 88 (1935).
[20] E. Berger, Grundsatzliches uber die chemische ar reifbarkeit von glasen I, Glastech. Ber. **14,** 351 (19
[21] Donald Hubbard and Gerald F. Rynders, Effect of annealing and other heat treatments on the pH response of the glass electrode, J. Research NBS **40,** 105 (1948) RP1859.
[22] Donald Hubbard and Gerald F. Rynders, Thickness of inhibiting films on glass electrode surfaces, J. Research NBS **41,** 163 (1948) RP1915.
[23] H. T. S. Britton, Hydrogen ions, **1,** 3d ed., 88C, p. 313 (D. Van Nostrand Co., Inc., New York, N. Y., 1943).
[24] M. R. Thompson, A metal-connected glass electrode, BS J. Research **9,** 833 (1932) RP 511.
[25] Jack M. Florence, Francis W. Glaze, Clarence H. Hahner, and Ralph Stair, Transmittance of near infra red energy by binary glasses, J. Research NBS **41,** 623 (1948) RP1945.
[26] J. M. Florence, C. C. Allshouse, F. W. Glaze, C. H. Hahner. The absorptance of near-infrared energy by certain glasses, J. Research NBS **45,** 121 (1950) RP2118.
[27] Donald Hubbard, Hygroscopicity and electrode function (pH response) of glasses as a measure of serviceability, J. Research NBS **36,** 511 (1946) RP1719.
[28] Donald Hubbard and Edgar H. Hamilton, Studies of the chemical durability of glass by an interferometer method, J. Research NBS **27,** 143 (1941) RP1409.
[29] W. S Hughes, On Haber's glass cell, J. Chem. Soc. 491 (1928).
[30] K. A. Krakou, E. J. Mukhin, and M. S. Heinrich, Equilibrium diagram of the ternary system Na_2SiO_3-$PbSiO_3$-SiO_2, Compt. rend. acad. sci. URSS **14,** 281 (1937).

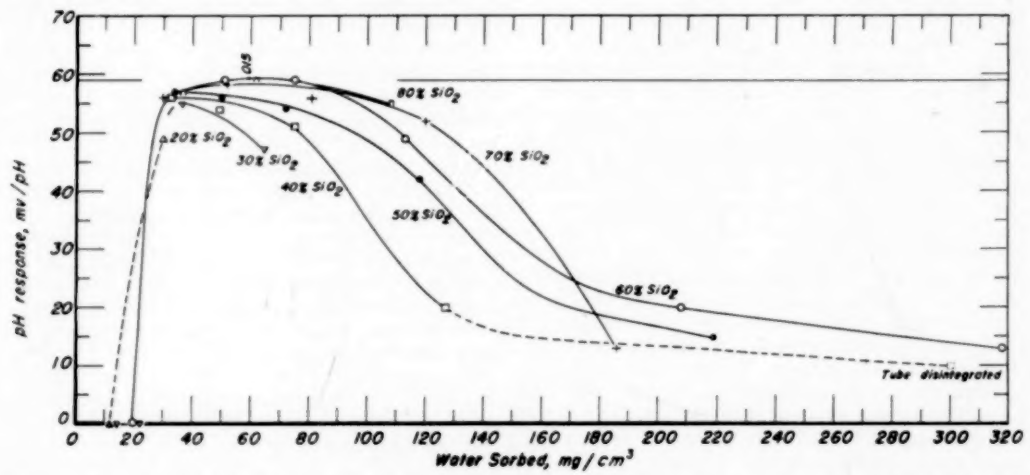

FIGURE 1. *Comparison of the hygroscopicity (water sorbed, 1 hr) and* pH *response of a series of* Na_2O-PbO-SiO_2 *glasses.*

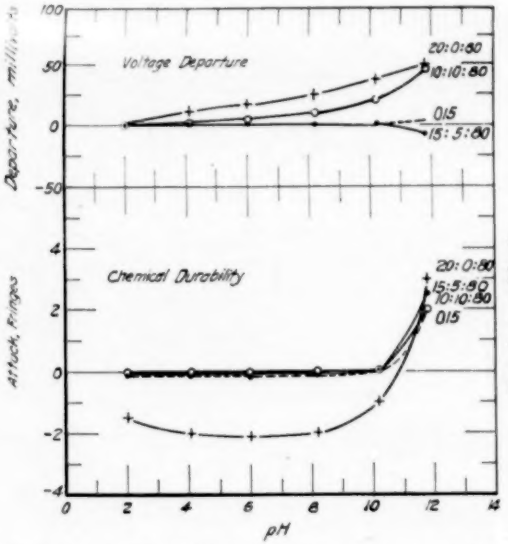

FIGURE 2. *The* pH*-voltage departure curves for electrodes prepared from* Na_2O-PbO-SiO_2 *glasses containing 80 percent of* SiO_2 *compared with the chemical durability curves of the glasses.*

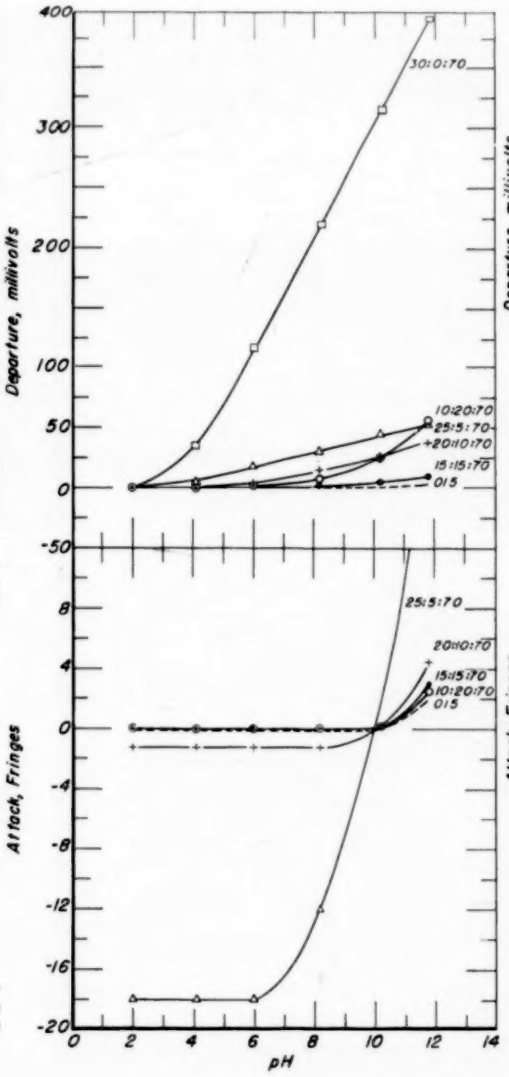

FIGURE 3. *The* pH*-voltage departure curves for electrodes prepared from* Na_2O-PbO-SiO_2 *glasses containing 70 percent of* SiO_2 *compared with the chemical durability curves of the glasses.*

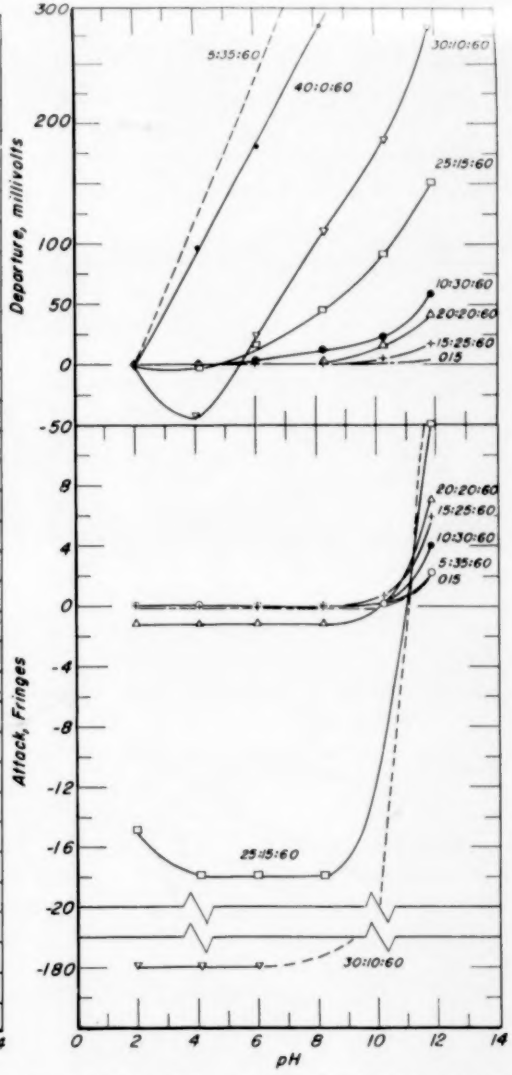

FIGURE 4. pH*-voltage departure curves for electrodes prepared from* Na_2O-PbO-SiO_2 *glasses containing 60% of* SiO_2 *compared with chemical durability curves of the glasses.*

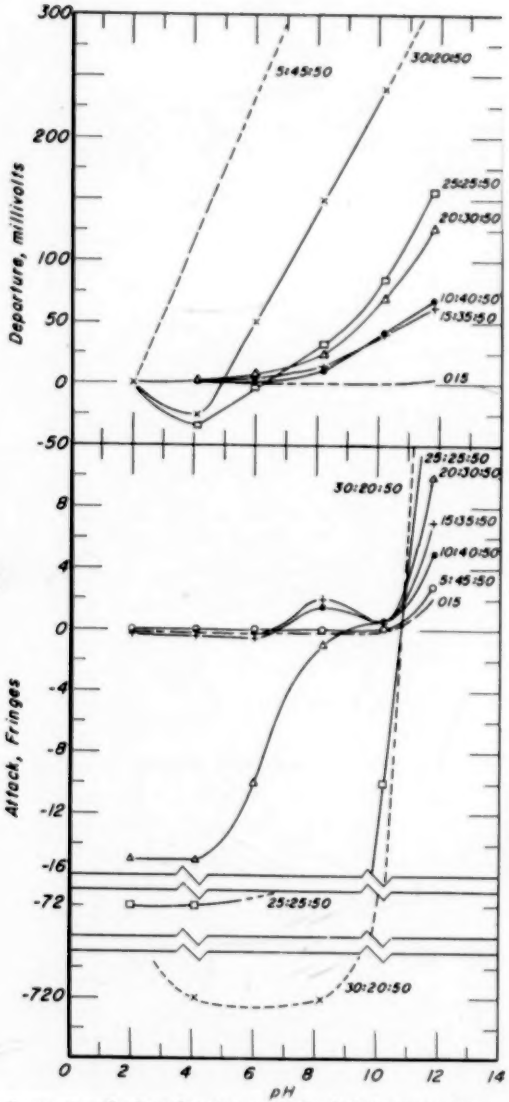

FIGURE 5. *pH-voltage departure curves for electrodes prepared from Na_2O-PbO-SiO_2 glasses containing 50% of SiO_2 compared with chemical durability curves of the glasses.*

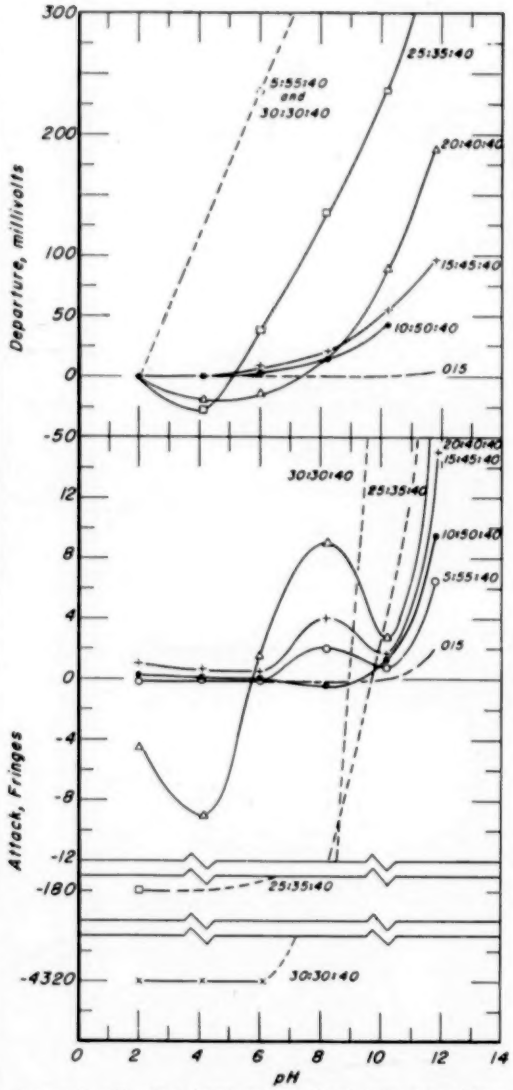

FIGURE 6. *pH voltage departure curves for electrodes prepared from Na_2O-PbO-SiO_2 glasses containing 40% of SiO_2 compared with chemical durability curves of the glasses.*

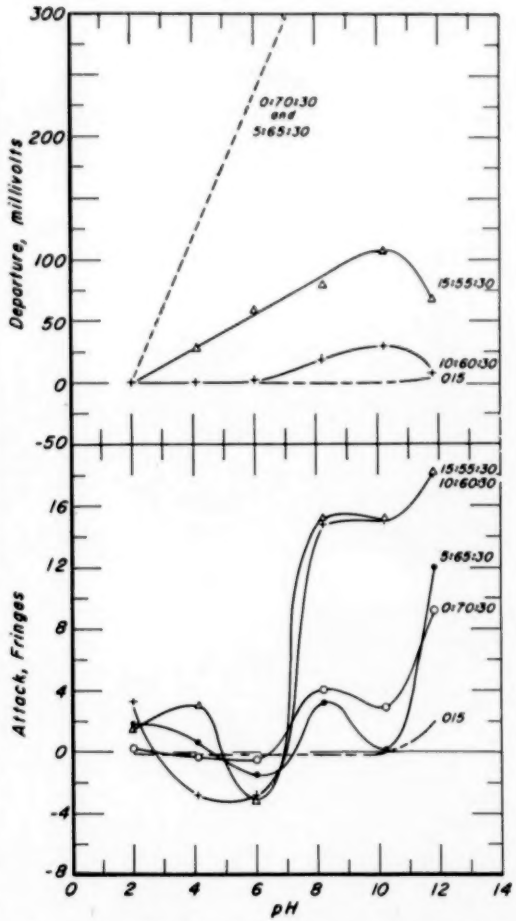

FIGURE 7. *The pH-voltage departure curves for electrodes prepared from Na_2O-Pb-SiO_2 glasses containing 30 percent of SiO_2 compared with the chemical durability curves for the glasses.*

pH

FIGURE 5. pH-voltage departure curves for electrodes prepared from Na_2O-PbO-SiO_2 glasses containing 50% of SiO_2 compared with chemical durability curves of the glasses.

FIGURE 6. pH voltage departure curves for electrodes prepared from Na_2O-PbO-SiO_2 glasses containing 40% of SiO_2 compared with chemical durability curves of the glasses.

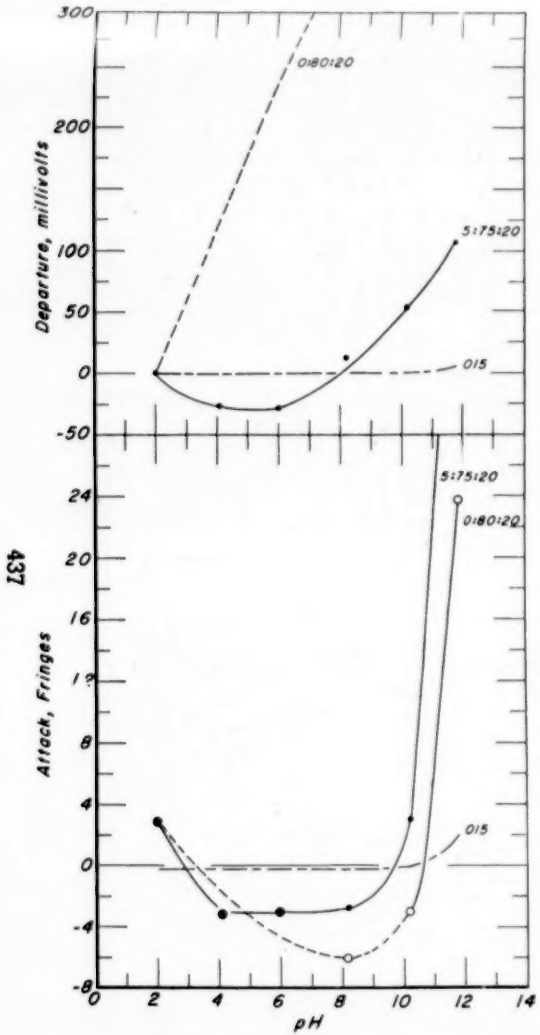

FIGURE 8. *The* pH-*voltage departure curves for electrodes prepared from* Na_2O-PbO-SiO_2 *glasses containing 20 percent of* SiO_2 *compared with the chemical durability curves of the glasses.*

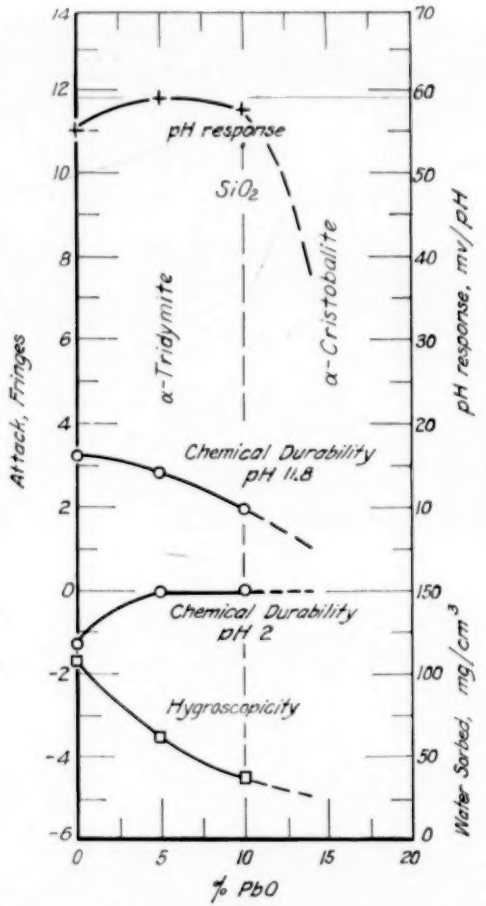

FIGURE 9. *Values for* pH-*response, hygroscopicity, and chemical durability at* pH *2 and 11.8 plotted against the percentage of* PbO *for* Na_2O-PbO-SiO_2 *glasses containing 80 percent of* SiO_2.

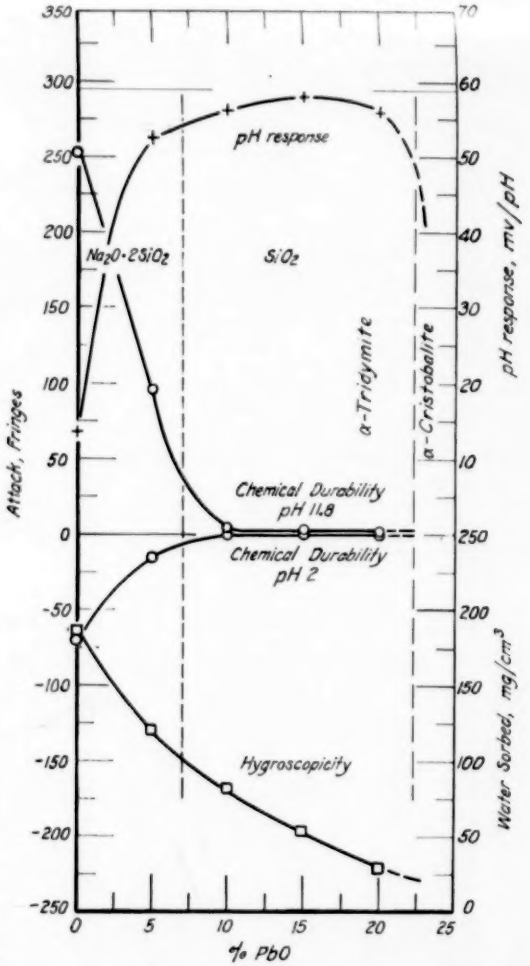

FIGURE 10. *Values for* pH-*response, hygroscopicity, and chemical durability at* pH *2 and 11.8 plotted against the percentage of* PbO *for* Na_2O-PbO-SiO_2 *glasses containing 70 percent of* SiO_2.

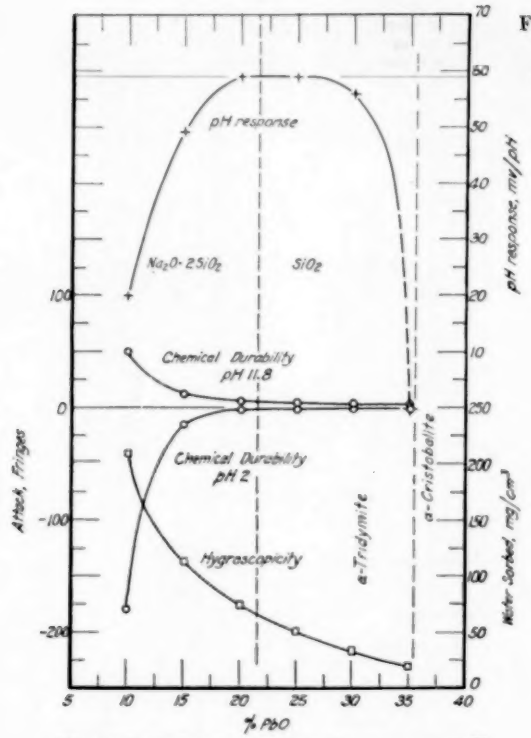

FIGURE 11. *Values for* pH*-response, hygroscopicity, and chemical durability at* pH *2 and 11.8 plotted against the percentage of* PbO *for* Na_2O-PbO-SiO_2 *glasses containing 60 percent of* SiO_2.

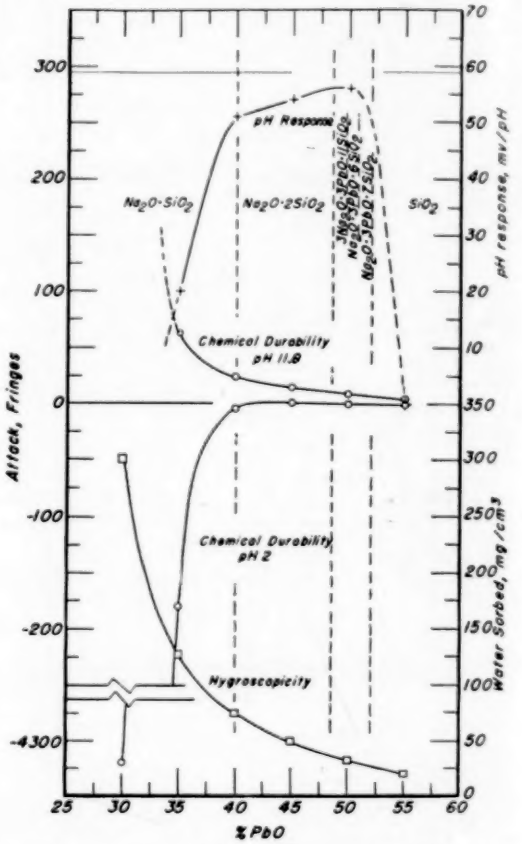

FIGURE 13. *Values for* pH*-response, hygroscopicity, and chemical durability at* pH *2 and 11.8 plotted against the percentage of* PbO *for* Na_2O-PbO-SiO_2 *glasses containing 40 percent of* SiO_2.

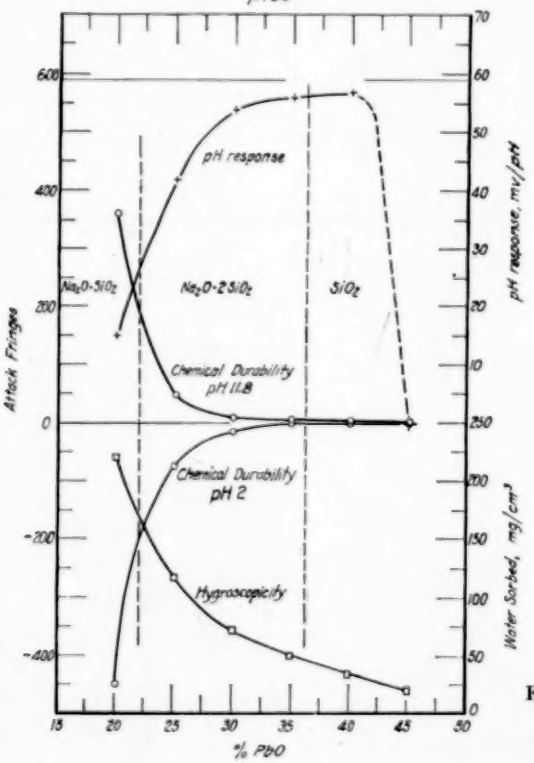

FIGURE 12. *Values for* pH*-response, hygroscopicity, and chemical durability at* pH *2 and 11.8 plotted against the percentage of* PbO *for* Na_2O-PbO-SiO_2 *glasses containing 50 percent of* SiO_2.

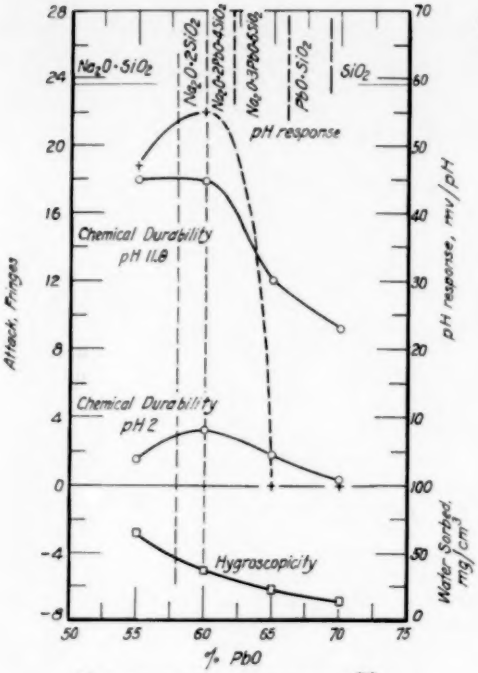

FIGURE 14. *Values for* pH*-response, hygroscopicity, and chemical durability at* pH *2 and 11.8 plotted against the percentage of* PbO *for* Na_2O-PbO-SiO_2 *glasses containing 30 percent of* SiO_2.

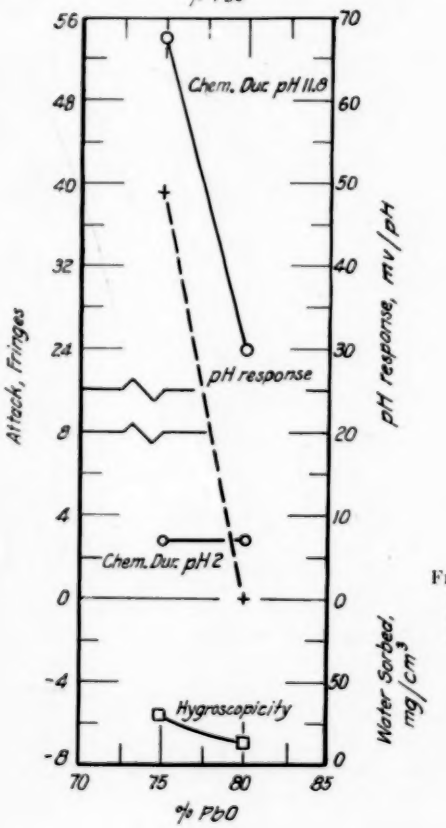

FIGURE 15. *Values for* pH*-response, hygroscopicity, and chemical durability at* pH *2 and 11.8 plotted against the percentage of* PbO *for* Na_2O-PbO-SiO_2 *glasses containing 20 percent of* SiO_2.

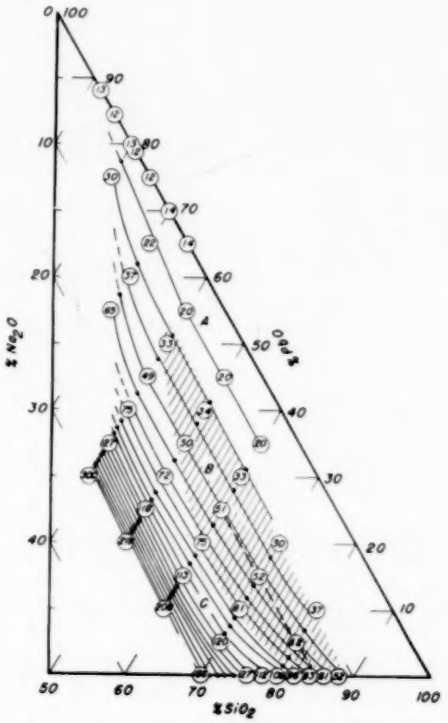

FIGURE 16. *Hygroscopicity of* Na_2O-PbO-SiO_2 *glasses for 1-hr exposure showing lines of equal hygroscopicity (iso-sorbs for intervals of 10 mg/cm²) and the shaded area over which electrodes prepared from these glasses developed as high as 56 mv/pH.*

The heavy dashed line links the only three glasses of the series that developed the theoretical 59 mv/pH at 25° C.

WASHINGTON, MAY 24, 1950.